

Two particle correlations with identified trigger
particles (pions and protons) in p-Pb and p-p collisions
at the Large Hadron Collider (LHC) energies.

By

Debojit Sarkar

Enrollment No. PHYS04201104004

Variable Energy Cyclotron Centre, Kolkata

A thesis submitted to

The Board of Studies in Physical Sciences

In partial fulfillment of requirements for the Degree of

DOCTOR OF PHILOSOPHY

of

HOMI BHABHA NATIONAL INSTITUTE

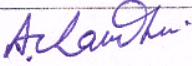
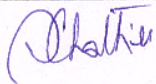
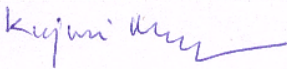
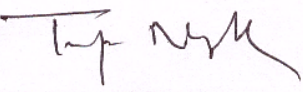
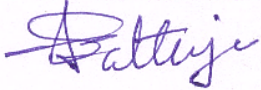


November, 2017

Homi Bhabha National Institute¹

Recommendations of the Viva Voce Committee

As members of the Viva Voce Committee, we certify that we have read the dissertation prepared by **Debojit Sarkar** entitled “Two particle correlations with identified trigger particles in p-Pb and pp collisions at Large Hadron Collider (LHC) energy” and recommend that it may be accepted as fulfilling the thesis requirement for the award of Degree of Doctor of Philosophy.

Chairman – Dr. Asis Kumar Chaudhury		Date: 01/11/2017
Guide / Convener – Dr. Subhasis Chattopadhyay		Date: 01/11/2017
Examiner – Dr. Kajari Mazumdar		Date: 01/11/2017
Member 1- Dr. Tapan Kumar Nayak		Date: 01/11/2017
Member 2- Dr. Sukalyan Chattopadhyay		Date: 01/11/2017

Final approval and acceptance of this thesis is contingent upon the candidate's submission of the final copies of the thesis to HBNI.

I/~~we~~ hereby certify that I/~~we~~ have read this thesis prepared under my/~~our~~ direction and recommend that it may be accepted as fulfilling the thesis requirement.

Date: 01/11/2017

Place: VEC, Kolkata


<Signature>

Guide

¹ This page is to be included only for final submission after successful completion of viva voce.

STATEMENT BY AUTHOR

This dissertation has been submitted in partial fulfilment of requirements for an advanced degree at Homi Bhabha National Institute (HBNI) and is deposited in the Library to be made available to borrowers under rules of the HBNI.

Brief quotations from this dissertation are allowable without special permission, provided that accurate acknowledgement of source is made. Requests for permission for extended quotation from or reproduction of this manuscript in whole or in part may be granted by the Competent Authority of HBNI when in his or her judgment the proposed use of the material is in the interests of scholarship. In all other instances, however, permission must be obtained from the author.

Debojit Sarkar

Debojit Sarkar

DECLARATION

I, hereby declare that the investigation presented in the thesis has been carried out by me. The work is original and has not been submitted earlier as a whole or in part for a degree/diploma at this or any other Institution/University.

Debojit Sarkar
Debojit sarkar

List of publications arising from the thesis

a) Published

1. "Effect of radial flow on two particle correlations with identified triggers at intermediate p_T in p-Pb collisions at $\sqrt{s_{NN}} = 5.02$ TeV"
Debojit Sarkar, Subikash Choudhury, Subhasis Chattopadhyay
Physics Letters B 760 (2016) 763 - 768
2. "Two particle correlations with identified triggers in p-Pb collisions at LHC energy using A multi phase transport model"
Debojit Sarkar, Subikash Choudhury, Subhasis Chattopadhyay
Phys. Rev. C 94, 044909 (2016)
3. "Investigating the role of partonic and hadronic dynamics in mass splitting of elliptic anisotropy in p-Pb collisions at LHC energy"
Debojit Sarkar, Subikash Choudhury, Subhasis Chattopadhyay
Phys. Rev. C 94, 044919 (2016)
4. "Ridge from jet-medium interaction in p-Pb collisions at $\sqrt{s_{NN}} = 5.02$ TeV"
Debojit Sarkar, Subhasis Chattopadhyay
Phys. Rev. C 95, 044906 (2017)
5. "Testing of the coalescence mechanism in high energy heavy ion collisions using two-particle correlations with identified particle trigger"
Subikash Choudhury, **Debojit Sarkar**, Subhasis Chattopadhyay
Phys. Rev. C 93, 054902 (2016)
6. "Elliptic flow of ϕ mesons at intermediate p_T : Influence of mass versus quark number"
Subikash Choudhury, **Debojit Sarkar**, Subhasis Chattopadhyay
Phys. Rev. C 95, 024904 (2017)

b) Communicated

1. "Investigating the radial flow like effects in pp collisions at $\sqrt{s} = 7$ TeV"
Debojit Sarkar, Subhasis Chattopadhyay
arXiv:1710.09785 [hep-ph] (submitted to Phys. Rev. C)
2. "Energy independent scaling of ridge and final state description of high multiplicity p+p collisions at $\sqrt{s} = 7$ and 13 TeV"
Debojit Sarkar
arXiv:1710.09774 [hep-ph] (submitted to Phys. Rev. D. (Rapid Communication))
3. "Violation of quark number scaling (NCQ) of elliptic flow (v_2) at LHC energy"
Subikash Choudhury, **Debojit Sarkar**, Subhasis Chattopadhyay
submitted to Journal. Phys. G.

Other Publications

Conference / Symposium

1. "Investigating the role of partonic and hadronic interactions towards collective dynamics in small systems"
Debojit Sarkar , Subikash Choudhury, Subhasis Chattopadhyay
Proceedings of the DAE-BRNS Symp. on Nucl. Phys. 60 (2015)
<https://www.sympnp.org/proceedings/> (Vol-60, E54)
2. "Probing the particle production mechanism at intermediate p_T through identified triggered correlations in p-Pb collisions at $\sqrt{s_{NN}} = 5.02$ TeV"
Debojit Sarkar , Subikash Choudhury, Subhasis Chattopadhyay
Proceedings of the 61st DAE-BRNS Symposium on Nuclear Physics (2016)
<http://sympnp.org/snp2016/> (E4)
3. "Contribution from fluid-jet interaction towards ridge in p-Pb collisions at $\sqrt{s_{NN}} = 5.02$ TeV"
Debojit Sarkar , Subikash Choudhury, Subhasis Chattopadhyay
Proceedings of the 61st DAE-BRNS Symposium on Nuclear Physics (2016)
<http://sympnp.org/snp2016/> (E11)
4. "Study of mass ordering of v_2^{hadron} from hadronic interactions in AMPT in p-Pb collisions at LHC energy"
Debojit Sarkar , Subikash Choudhury, Subhasis Chattopadhyay
Proceedings of the 61st DAE-BRNS Symposium on Nuclear Physics (2016)
<http://sympnp.org/snp2016/> (E60)
5. "Present and future of QGP research in high energy heavy ion collision experiments"
Subhasis Chattopadhyay, Subikash Choudhury, Debojit Sarkar
Indian Natn Sci Acad 81(2015)321-335
6. "Two particle correlations at intermediate p_T with identified leading hadrons at the LHC energy using AMPT model"
Subikash Choudhury, Debojit Sarkar, Subhasis Chattopadhyay
Springer Proceedings in Physics, XXI DAE-BRNS, High Energy Physics Symposium Proceedings, DOI:10.1007/978-3-319-25619-1 – 29

Debojit Sarkar

Debojit Sarkar

Acknowledgement

I am extremely thankful to my supervisor Prof. Subhasis Chattopadhyay for his constant supervision and training and very much appreciate his encouragement towards independent thinking. Special thank goes to my collaborator Subikash Choudhury whose support helped me to make this journey memorable. I convey my deepest gratitude to Dr. Prithwish Tribedy for all the interesting discussion sessions. Words are inadequate for his efforts to enrich my knowledge and to grow my interest towards various open problems through countless number of discussions. I sincerely thank Prof. Tapan Nayak for all his help and support throughout these years. A special note of thanks goes to Prof. Federico Antinori whose valuable suggestions have enriched my understanding on this topic and help me to make some interesting publications. I thank the members of my thesis committee and referees for their constructive suggestions. I am grateful to Prof. Jane Alam, Prof. Asis Kumar Choudhuri, Prof. Sourav Sarkar, Prof. Dinesh K Srivastava for their teachings, valuable suggestions and encouragements. I would like to convey my heartfelt thanks to my senior colleagues and collaborators Sidharth K Prasad, Sumit Basu, Rajesh Ganai, Arindam Roy, Sanjib Muhuri for sharing their experience and insights with me. A warm affection and gratitude is extended towards my friends and juniors, Somnath Kar, Tanmoy Roy, Avirup Choudhury, Ashik Iqbal, Arghya Chatterjee, Noor Alam, Snigdha Ghosh, Golam Sarwar, Rajendra Patra, Shreyashi Acharya, Mitali Mondal who have provided me a friendly environment all these years. I thank all my fellow collaborators of the ALICE experiment at LHC, particularly Panos Christakoglou, Leonardo Milano, Michael Weber, Alice Ohlson, Anthony Robert Timmins, Emilia Leogrande, Alis Rodriguez Manso who have helped me in many ways to perform the data analysis. I thank everyone from the PMD collaboration of India. I also thank all the members of the VECC grid computing facility for their constant effort to keep the facility running and for helping with Monte Carlo data generation.

I am very lucky to have a wonderful family that has been the source of endless love and support. I am grateful to my parents, Dipak Kumar Sarkar and Chaitali Sarkar and also my sister Deborupa Sarkar for their constant inspiration to pursue a career in research.

Contents

List of Figures	11
List of Tables	23
Synopsis	24
0.1 Introduction:	25
0.2 Data Analysis:	26
0.3 Model based analysis (Phenomenological study):	27
1 Introduction	32
1.1 New form of matter under extreme conditions	32
1.2 The QCD phase diagram	35
1.3 Formation and evolution of QGP in heavy ion collisions	38
1.4 Experimental Observations	44
1.4.1 Energy density in heavy ion collisions	44
1.4.2 Soft probes for QGP	46
1.4.3 Hard probes for QGP	53
1.5 Collectivity in small collision systems?	60
2 Effect of radial flow and hadronization by coalescence on two particle correlations with identified triggers at intermediate p_T in p-Pb collisions at $\sqrt{s_{NN}} = 5.02$ TeV	77
2.1 Introduction	77
2.2 The EPOS3 Model	82
2.3 The AMPT Model	83
2.4 Analysis Method	85
2.5 Results from EPOS3	87
2.6 Results from AMPT	93
3 The ALICE Experiment at the LHC	103
3.1 Introduction	103
3.2 The Large Hadron Collider (LHC)	104
3.3 The ALICE Experiment	105
3.3.1 Inner Tracking System -ITS	107

3.3.2	Time Projection Chamber -TPC	109
3.3.3	Time of Flight -TOF	111
3.3.4	VZERO (V0)	113
3.4	The Forward Detectors	114
3.5	Event Reconstruction - Vertexing and Tracking	116
4	Two particle correlations with identified trigger particles in p-Pb collisions at $\sqrt{s_{NN}} = 5.02$ TeV (Data analysis in ALICE)	121
4.1	Introduction	121
4.2	Datasets	122
4.3	Event Selection	123
4.4	Multiplicity class selection	124
4.5	Track Selection	126
4.6	Correlation Function	128
4.7	Particle Identification	132
4.7.1	Misidentification rate	135
4.8	Analysis and Corrections	137
4.9	Bulk Subtraction Procedure	138
4.10	YIELD DETERMINATION	139
4.11	Systematics	141
4.11.1	ZYAM procedure vs Fit	142
4.11.2	Tracking efficiency	142
4.11.3	Track selection	144
4.11.4	PID selection	144
4.11.5	DCA cut variation	144
4.11.6	Pile-up	146
4.11.7	MC-closure	146
4.12	Results and Discussion	148
5	Investigating the radial flow like effects in pp collisions at $\sqrt{s} = 7$ TeV using two particle correlations with identified triggers	155
5.1	Introduction	155
5.2	The EPOS 3 model	158
5.3	The PYTHIA 8 model	158
5.4	Analysis Method	159
5.5	Results and Discussion	160
6	Ridge from jet-medium interaction in p-Pb collisions at $\sqrt{s_{NN}} = 5.02$ TeV	168
6.1	Introduction	168
6.2	Analysis Method	172
6.3	Results and Discussion	173

7	Investigating the role of partonic and hadronic dynamics in mass splitting of elliptic anisotropy in p-Pb collisions at $\sqrt{s_{NN}} = 5.02$ TeV using a multi phase transport model (AMPT)	181
7.1	Introduction	181
7.2	The AMPT Model	183
7.3	\mathbf{v}_2 extraction	183
7.4	Results and Discussion	186
8	Summary and Outlook	196

List of Figures

1.1	[Color online] The measurements of α_S as a function of the respective energy scale Q [11].	34
1.2	[Color online] Static quark potential from Lattice QCD as a function of the distance between the quarks R . The different symbols indicate the direction of R in terms of points of the lattice [25].	34
1.3	[Color online] QCD phase diagram scheme in terms of temperature T (in the y -axis) as a function of baryochemical potential μ_B [27].	36
1.4	[Color online] Equation of State from Lattice QCD at zero baryon density [32]. . .	37
1.5	[Color online] Schematic representation of the evolution of a relativistic heavy-ion collision. [40]	38
1.6	[Color online] Wounded nucleon distributions in the plane perpendicular to the beam axis with same number of wounded nucleons. ($N_W = 100$) [46, 47]	40
1.7	[Color online] A schematic diagram showing the location of the reaction plane relative to the incoming nuclei [48].	41
1.8	[Color online] Schematic diagram showing the formation of azimuthal anisotropy from the initial state anisotropy [49].	42
1.9	[Color online] Top: $\sqrt{s_{NN}}$ dependence of Bjorken energy density for Au-Au, Cu-Au, and Cu-Cu collisions at $\sqrt{s_{NN}} = 200$ and 62.4 GeV [68]. Bottom: The values of Bjorken energy density are shown for Pb-Pb collisions at LHC energy ($\sqrt{s_{NN}} = 2.76$ TeV), together with energies available for Au-Au collisions at RHIC [69]. .	45

1.10	[Color online] The transverse momentum (p_T) dependence v_2 of identified particles in Pb-Pb collisions at $\sqrt{s_{NN}} = 2.76$ TeV [70].	47
1.11	[Color online] Particle species dependence of v_2 versus p_T (left), v_2 versus m_T -m (middle) and v_2/n_q versus $(m_T - m)/n_q$ (right) in Au-Au collisions at $\sqrt{s_{NN}} = 200$ GeV. [78–80].	49
1.12	[Color online] Top The inclusive $p(\bar{p})/\pi^\pm$ ratio from d-Au and Au-Au collisions at $\sqrt{s_{NN}} = 200$ GeV. The dotted-dashed lines shows the inclusive $p(\bar{p})/\pi^\pm$ ratio from light quark jets in e+ e- collisions at 91.2 GeV. Comparisions with different model calculations are also shown [81, 82]. Bottom: p_T -dependence of particle ratios measured in pp and 0-5% most central Pb-Pb collisions at 2.76 TeV. Comparison with different model predictions for 0-5% Pb-Pb collisions are also shown [83–86].	50
1.13	[Color online] A schematic diagram showing the idea of hadronization through coalescence model of hadronization. [87]	50
1.14	[Color online] The pion and proton spectra as measured by the ALICE collaboration and the comparison made using the recombination model [93].	51
1.15	[Color online] Top: NCQ scaling of v_2 for different hadron species as measured in 10-20% centrality class of Pb-Pb collisions at $\sqrt{s_{NN}} = 2.76$ TeV. Bottom: Double ratio of v_2/n_q as a function of p_T relative to the seventh order polynomial fit to v_2/n_q of (anti) protons in 10-20% centrality class of Pb-Pb collisions at $\sqrt{s_{NN}} = 2.76$ TeV [70].	52
1.16	[Color online] A schematic presentation of two quarks originating from a hard scattering near the surface of the medium. One of the quarks going out directly to the vacuum, radiating gluons and hadronize. The other quark going through the dense plasma formed in the collision, suffering energy loss by both radiational and collisional processes and finally fragmenting into a quenched jet.	54

1.17	[Color online] Nuclear modification factor versus transverse momentum as measured by the ALICE, STAR and PHENIX collaborations in heavy ion collisions [110].	55
1.18	[Color online] The nuclear modification factor R_{AA} as a function of p_T for different hadron species for different collision centralities in Pb-Pb collisions at 2.76 TeV [111].	56
1.19	[Color online] Di-hadron correlations from p + p, d + Au, and Au + Au collisions at $\sqrt{s_{NN}} = 200\text{GeV}$ with trigger particles with $4.0 < p_T < 6.0\text{ GeV/c}$ and associated particles with $2.0 < p_T < 4.0\text{ GeV/c}$ [114].(a)Correlations for p+p,minimumbias d+Au,and central d + Au collisions with no background subtraction. (b) Correlations for p + p, d + Au, and 0-10% central Au + Au collisions after background subtraction.	57
1.20	[Color online] Two particle correlation functions with trigger particles with $3.0 < p_T < 4.0\text{ GeV/c}$ and associated particles with $2.0 < p_T < 2.5\text{ GeV/c}$ in 0-10% central Pb-Pb collisions at 2.76 TeV [118].	58
1.21	[Color online] Leftpanel: I_{AA} of the near-side jet yield ($\Delta\phi < \pi/2$) for two centralities Rightpanel: I_{AA} of the away-side yield ($\Delta\phi > \pi/2$) for two centralities [119].	59
1.22	(Color online) Double ridge from two-particle correlations in high multiplicity events after subtraction of two-particle correlations in low multiplicity events in p-Pb collisions at $\sqrt{s_{NN}} = 5.02\text{ TeV}$ [122].	60
1.23	(Color online) Elliptic flow v_2 as a function of p_T for pions, kaons and protons in p-Pb collisions at 5.02 TeV [123].	61
1.24	(Color online) The baryon to meson enhancement with multiplicity in pp, p-Pb and Pb-Pb collisions at LHC energies [135].	62

1.25	(Color online) Top: The nuclear modification factor as measured in p-Pb collisions at 5.02 TeV for minimum bias p-Pb collisions and compared with the same as measured in central heavy ion collisions at RHIC and LHC energies [128]. bottom: Multiplicity dependence of the nuclear modification factor in p-Pb collisions at 5.02 TeV [129].	63
2.1	[Color online] Inclusive proton over pion ratio as obtained from (a) EPOS 3.107 and (b) AMPT SM version (right) in 0-10% and 60-100% event classes of p-Pb collisions at 5.02 TeV.	80
2.2	[Color online] Two particle $\Delta\eta$ - $\Delta\phi$ correlation function in 0-10 % event class of p-Pb collisions at $\sqrt{s_{NN}} = 5.02$ TeV from EPOS 3 with (a) pion and (b) proton as trigger particles.	86
2.3	[Color online] Two Particle $\Delta\eta$ - $\Delta\phi$ correlation function in 0-10 % event class of p-Pb collisions at $\sqrt{s_{NN}} = 5.02$ TeV from AMPT SM (with ART) with (a) pion and (b) proton as trigger particles.	86
2.4	[Color online] (a) The $\Delta\phi$ projected correlation function for pion triggered correlation in 0-10% event class in EPOS 3 for two $\Delta\eta$ regions referred to as jet (blue) and bulk (red). (b) The $\Delta\phi$ projected correlation function after bulk subtraction as discussed in the text.	87
2.5	[Color online] (a) The $\Delta\phi$ projected correlation function for proton triggered correlation in 0-10% event class in AMPT SM for two $\Delta\eta$ regions referred to as jet (blue) and bulk (red). (b) The $\Delta\phi$ projected correlation function after bulk subtraction as discussed in the text.	88
2.6	[Color online] Two particle $\Delta\eta$ - $\Delta\phi$ correlation function in 0-10 % event class of p-Pb collisions at $\sqrt{s_{NN}} = 5.02$ TeV in case of corona-corona correlation from EPOS 3 with (a) pion and (b) proton as trigger particles.	88

2.7	[Color online] (a) Multiplicity dependence of the near-side jet-like per trigger yield associated with pion and proton triggers in case of corona - corona correlation in p-Pb collisions at $\sqrt{s_{NN}} = 5.02$ TeV from EPOS 3.107 with hadronic cascade off. (b) Multiplicity dependence of the ratio of the near-side jet-like per trigger yield associated with proton and pion triggers in case of corona - corona correlation in p-Pb collisions at $\sqrt{s_{NN}} = 5.02$ TeV from EPOS 3.107 with hadronic cascade off.	89
2.8	[Color online] (a) Multiplicity dependence of the near-side jet-like per trigger yield (bulk subtracted) associated with pion and proton triggers (particles from both core and corona are considered) in p-Pb collisions at $\sqrt{s_{NN}} = 5.02$ TeV from EPOS 3.107 without hadronic cascade. (b) Multiplicity dependence of the ratio of the near-side jet like per trigger yield (bulk subtracted) associated with proton and pion triggers (particles from both core and corona are considered) in p-Pb collisions at $\sqrt{s_{NN}} = 5.02$ TeV from EPOS 3.107 without hadronic cascade. . . .	91
2.9	[Color online] (a) Multiplicity dependence of the near-side jet-like per trigger yield (bulk subtracted) associated with pion and proton triggers (particles from both core and corona are considered) in p-Pb collisions at $\sqrt{s_{NN}} = 5.02$ TeV from EPOS 3.107 with hadronic cascade on. (b) Multiplicity dependence of the ratio of the near-side jet like per trigger yield (bulk subtracted) associated with proton and pion triggers (particles from both core and corona are considered) in p-Pb collisions at $\sqrt{s_{NN}} = 5.02$ TeV from EPOS 3.107 with hadronic cascade on. . . .	92
2.10	[Color online] N_{part} dependence of the near-side jet like yield associated with baryon and meson triggers in Au-Au collisions at $\sqrt{s_{NN}} = 200$ GeV [32] and it's comparison with the minimum bias d-Au collisions at $\sqrt{s_{NN}} = 200$ GeV.	92

2.11	[Color online] (a) Multiplicity dependence of the near-side jet-like per trigger yield (bulk subtracted) associated with pion and proton triggers in p-Pb collisions at $\sqrt{s_{NN}} = 5.02$ TeV from HIJING. (b) Multiplicity dependence of the ratio of the near-side jet like per trigger yield (bulk subtracted) associated with proton and pion triggers.	94
2.12	[Color online] (a) Multiplicity dependence of the near-side jet like per trigger yield (bulk subtracted) associated with pion and proton triggers in p-Pb collisions at $\sqrt{s_{NN}} = 5.02$ TeV from AMPT SM without hadronic cascade. (b) Multiplicity dependence of the ratio of the near-side jet like per trigger yield (bulk subtracted) associated with proton and pion triggers.	95
2.13	[Color online] (a) Multiplicity dependence of the near-side jet like per trigger yield (bulk subtracted) associated with pion and proton triggers in p-Pb collisions at $\sqrt{s_{NN}} = 5.02$ TeV from AMPT SM with hadronic cascade on. (b) Multiplicity dependence of the ratio of the near-side jet like per trigger yield (bulk subtracted) associated with proton and pion triggers.	95
2.14	[Color online] Centrality dependence of the near-side yield from the background subtracted correlation function. The yields from default version of AMPT have been multiplied by 1.5 for better visualization [47].	96
2.15	[Color online] (a) Multiplicity dependence of the near-side jet-like per trigger yield (bulk subtracted) associated with pion and proton triggers in p-Pb collisions at $\sqrt{s_{NN}} = 5.02$ TeV from (a) AMPT SM and (b) EPOS 3 without hadronic cascade.	98
2.16	[Color online] Multiplicity dependence of the ratio of the near-side jet-like per trigger yield (bulk subtracted) associated with proton and pion triggers in p-Pb collisions at $\sqrt{s_{NN}} = 5.02$ TeV from (a) AMPT SM and (b) EPOS 3 without hadronic cascade.	98
3.1	(Color online) Schematic view of the LHC acceleration stages and collision schemes [3]	104

3.2	(Color online) Schematic view of the ALICE experiment, with its subdetectors. Photo Courtesy: CERN Document Server (ALICE-PHO-GEN-2012-001-12) . . .	106
3.3	(Color online) A schematic view of ALICE-Inner Tracking Chamber with different sub-layers: SPD, SDD and SSD.	107
3.4	(Color online) Schematic view of the ALICE-TPC [8]	109
3.5	(Color online) $\frac{dE}{dx}$ versus momentum (p) curve in the TPC active volume for p-Pb collisions at $\sqrt{s_{NN}} = 5.02$ TeV. For each particle there is a distinctly separated band below $p_T < 1$ GeV/c which merges at higher p_T	110
3.6	(Color online) Photograph of the 10-gap glass-MRPC used to fabricate ALICE- TOF [13].	112
3.7	(Color online) TOF $\beta = v/c = L/tc$ distribution as measured by ALICE-TOF detector as a function of momentum in p-Pb collisions at $\sqrt{s_{NN}} = 5.02$ TeV. . .	113
3.8	(Color online) V0 detector modules [17]	114
4.1	p_T -differential p/pi ratio for different multiplicity classes/centralities in pp at 7 TeV (left panel), p-Pb at 5.02 TeV (central panel) and Pb-Pb at 2.76 TeV (right panel).	122
4.2	Number of events after each selection step.	123
4.3	Distribution of the sum of amplitudes in the V0A hodoscopes (Pb-going direction for p-Pb collisions at 5.02 TeV), as well as the NBD-Glauber fit (explained in the text) of the data points. Figure taken from [8]	124
4.4	V0A multiplicity as a function of N_{part} from Glauber Monte Carlo for p-Pb collisions at 5.02 TeV (left) and Pb-Pb collisions at 2.76 TeV (right). Figure taken from [8].	125
4.5	ϕ (top) and η (bottom) distribution of particles as obtained from filterbit 768.	127
4.6	Pion triggered correlation functions (efficiency corrected) for five multiplicity classes used in this analysis.	129
4.7	Proton triggered correlation functions (efficiency corrected) for five multiplicity classes used in this analysis.	130

4.8	Normalized mixed event distribution function for trigger pions having $2.0 < p_T < 4.0$ GeV/c and unidentified associated particles having $1.0 < p_T < 4.0$ GeV/c in 0-10% multiplicity class of p-Pb collisions at $\sqrt{s_{NN}} = 5.02$ TeV (This Thesis).	132
4.9	Left: Specific energy loss dE/dx in the tPC together with Bethe-Bloch curves for the different particle species. Right: TOF β (velocity) vs particle momentum (measured with TPC) curve.	133
4.10	$n\sigma$ distribution for the different detectors in pion mass hypothesis for p-Pb collisions ($\sqrt{s_{NN}} = 5.02$ TeV) data sample.	133
4.11	$n_{\sigma,TPC}-n_{\sigma,TOF}$ plot for $1.5 < p_T < 1.6$ GeV/c in pion mass hypothesis for p-Pb collisions at $\sqrt{s_{NN}} = 5.02$ TeV	135
4.12	Misidentification rate for $2.0 < p_T < 4.0$ GeV/C for p-Pb collisions at $\sqrt{s_{NN}} = 5.02$ TeV (using DPMJET) (This Thesis).	136
4.13	The correction factor(defined in Eq. 4.7) as a function of p_T for different η ranges and particle species (This Thesis).	137
4.14	$\Delta\varphi$ distributions of the jet ($\Delta\eta < 1.2$) and bulk ($\Delta\eta > 1.2$) region for pion triggered (left) and proton triggered (right) correlation function in 0-10% V0A multiplicity class (This Thesis).	138
4.15	The bulk subtracted $\Delta\varphi$ distributions for pion triggered (left) and proton triggered (right) correlation functions in 0-10% V0A multiplicity class. The flattish away side is fitted with zero-degree-polynomial function for residual baseline determination (This Thesis). . . .	139
4.16	a) Pion triggered and b) proton triggered correlation function ($\Delta\phi$ projection) fitted with 2 gaussians and a flat baseline in 0-10% V0A multiplicity class (This Thesis). . . .	140
4.17	χ^2/Ndf values of 1-D fit to a) pion and b) proton triggered correlation function for different multiplicity classes (This Thesis).	141
4.18	Near side yield associated with a) pion and b) proton triggered correlation calculated from bin counting and fit. The lower panel shows the relative difference w.r.t to bin counting method in both cases (This Thesis).	142

4.19	Near side yields of a) pion and b) proton triggered correlation in 0-40% and 40-100% V0A multiplicity classes for different track selection cuts .The lower panel shows the relative difference w.r.t default track cut (Filterbit- 768 which is discussed in detail in section 4.5) (This Thesis).	143
4.20	Near side yields of a) pion and b) proton triggered correlation in 0-40% and 40-100% V0A multiplicity classes for different PID selection cuts .The lower panel shows the relative difference w.r.t default 3σ PID cut (This Thesis).	143
4.21	Near side yields of a) pion and b) proton triggered correlation in 0-40% and 40-100% V0A multiplicity classes for different DCA cut values. The lower panel shows the relative difference w.r.t default 7σ DCA cut (This Thesis).	145
4.22	Near side yields of a) pion and b) proton triggered correlation in 0-40% and 40-100% V0A multiplicity classes with and without pile up correction. The lower panel shows the relative difference w.r.t without correction (This Thesis).	145
4.23	$\Delta\varphi$ distribution of the MC TRUTH and MC RECO (efficiency corrected) a) pion and b) proton triggered correlation function in 0-10% V0A multiplicity class (This Thesis). . .	146
4.24	Ratio of $\Delta\varphi$ distribution of the MC TRUTH and MC RECO (efficiency corrected) a) pion and b) proton triggered correlation function in 0-10% V0A multiplicity class (This Thesis).	147
4.25	Near side yields of a) pion and b) proton triggered correlation for different multiplicity classes of p-Pb collisions at 5.02 TeV, with and without bulk subtraction (This Thesis). .	149
4.26	a) Near side yields of pion and proton triggered correlation for different V0A multiplicity classes of p-Pb collisions at 5.02 TeV, with bulk subtraction (This Thesis). b) Ratio of the near side jet-like yields associated with proton and pion triggers.	149
4.27	Near side yield from pion and proton triggered correlation in DATA (left), EPOS 3 (middle) and AMPT string melting (right).	150

5.1	[Color online] Inclusive proton over pion ratio as obtained from PYTHIA 8 (left) and EPOS 3 (right) in 0-10% and 60-100% event classes of pp collisions at $\sqrt{s} = 7$ TeV.	157
5.2	[Color online] Two particle $\Delta\eta$ - $\Delta\phi$ correlation function in 0-10 % event class of pp collisions at $\sqrt{s} = 7$ TeV with proton as trigger particles from (a) PYTHIA 8 and (b) EPOS 3.	159
5.3	[Color online] The $\Delta\phi$ projected correlation function for two $\Delta\eta$ regions referred to as jet (blue) and bulk (red).	160
5.4	[Color online] The $\Delta\phi$ projected correlation function after bulk subtraction as discussed in the text.	161
5.5	[Color online]a) Multiplicity dependence of the near-side jet-like per trigger yield (bulk subtracted) associated with proton and pion triggers in pp collisions at $\sqrt{s} = 7$ TeV from EPOS 3.107. b) Multiplicity dependence of the ratio of the proton to pion triggered yield in pp collisions at $\sqrt{s} = 7$ TeV from EPOS 3.107.	162
5.6	[Color online]a) Multiplicity dependence of the near-side jet-like per trigger yield (bulk subtracted) associated with proton and pion triggers in pp collisions at $\sqrt{s} = 7$ TeV from PYTHIA 8 (CR on). b) Multiplicity dependence of the ratio of the proton to pion triggered yield in pp collisions at $\sqrt{s} = 7$ TeV from PYTHIA 8 (CR on).	163
6.1	[Color online] Left: Flux tube breaking via $q\bar{q}$ production, which screens the color field (Schwinger mechanism). Right: Escaping string segment, getting its endpoint partons from the fluid. We show the case of a quark and an antiquark (a) and of a quark and a diquark (b). The rest of the string dissolves in matter. [12]170	
6.2	[Color online] Two Particle $\Delta\eta$ - $\Delta\phi$ correlation function in the 0-20 % event class of p-Pb collisions at $\sqrt{s_{NN}} = 5.02$ TeV from EPOS 3 for a) core-core , b) core-corona, c) corona-core, d) corona-corona correlations	174

6.3	[Color online] Multiplicity dependence of the near-side ridge (pedestal subtracted) obtained from a) core-core , b) core-corona, c) corona-core, d) corona-corona correlations. In each case ridges from 0-20% and 60-100% event class have been compared.	175
6.4	[Color online] Two Particle $\Delta\eta$ - $\Delta\phi$ correlation function in the 0-20 % event class of p-Pb collisions at $\sqrt{s_{NN}} = 5.02$ TeV from EPOS 3 considering all particles from core and corona.	176
6.5	[Color online] Relative contribution of ridges from different origins towards the total ridge in the 0-20% event class of p-Pb collisions at $\sqrt{s_{NN}} = 5.02$ TeV. . . .	177
6.6	[Color online] Relative contribution of ridges from different origins towards the total ridge in the 60-100% event class of p-Pb collisions at $\sqrt{s_{NN}} = 5.02$ TeV. . .	177
7.1	[Color online] Multiplicity dependence of p_T -differential v_2^{parton} in p-Pb collisions at $\sqrt{s_{NN}} = 5.02$ TeV from AMPT-SM with parton scattering cross-section of 3 mb.	186
7.2	[Color online] Coordinate space distribution of freezeout partons in a single event in a) 60-100% (top) and b) 0-20% (bottom) event class of p-Pb collisions at $\sqrt{s_{NN}} = 5.02$ TeV.	187
7.3	[Color online] v_2^{parton} plotted as a function of p_T in the highest multiplicity event class (0-20%) of p-Pb collisions at $\sqrt{s_{NN}} = 5.02$ TeV for parton scattering cross-section of 0 mb (red) and 3 mb (blue) from AMPT-SM version.	188
7.4	[Color online] Multiplicity evolution of $v_2(p_T)$ of pion and proton for 3 mb parton scattering cross-section in p-Pb collisions at $\sqrt{s} = 5.02$ TeV (a) without hadronic-rescattering (NO ART) and (b) with hadronic-rescattering ON (ART).	189
7.5	[Color online] $v_2(p_T)$ of pion and proton for most central (0-20%) event class in p-Pb collision at $\sqrt{s_{NN}} = 5.02$ TeV for different configurations: a) Default 3 mb without ART , b) 0 mb String Melting without ART and c) 3 mb String Melting without ART	191

7.6	[Color online] $v_2(p_T)$ of pion and proton in a) 60-100% (left) and b) 0-20% (right)	
	event class of p-Pb collisions at $\sqrt{s_{NN}} = 5.02$ TeV in string melting version of	
	AMPT with ART on and ZPC off.	192

List of Tables

1.1	The fundamental particles, forces and their basic properties [13].	33
4.1	Summary of Systematics	147

Synopsis

This thesis work is divided into two broad categories :

- **Analysis of data from the ALICE experiment at LHC :-**

Analysis of the ALICE data (p-Pb collisions at $\sqrt{s_{NN}} = 5.02$ TeV) for two particle correlations study with identified trigger particles at intermediate p_T where inclusive baryon to meson enhancement has been observed.

- **Phenomenological study on collectivity in small collision systems (p-Pb and pp) at Large Hadron Collider energy :-**

a) Two particle correlation analysis with identified trigger particles at intermediate p_T using EPOS 3 and AMPT event generators for p-Pb collisions at $\sqrt{s_{NN}} = 5.02$ TeV.

b) Investigating the role of partonic and hadronic dynamics in mass splitting of elliptic anisotropy in p-Pb collisions at $\sqrt{s_{NN}} = 5.02$ TeV.

c) Study of ridge structure originating from the jet-medium interaction in EPOS 3 event generator in p-Pb collisions at $\sqrt{s_{NN}} = 5.02$ TeV.

d) Investigating the effect of color reconnection and hydrodynamical flow on the identified triggered correlation in pp collisions at $\sqrt{s} = 7$ TeV.

0.1 Introduction:

A wealth of data collected during the decades of operation at the BNL Relativistic Heavy Ion Collider (RHIC) and first few years at the CERN Large Hadron Collider (LHC) provide compelling evidence that a strongly interacting and nearly perfect fluid of quarks and gluons are produced in Au-Au/Pb-Pb collisions at ultra-relativistic energies. Long-range ridge structures, elliptic anisotropy (v_2), mass ordering of v_2 , baryon to meson enhancement at intermediate p_T etc which were once attributed to the hydrodynamical evolution of a strongly interacting system of large dimensions found to be challenged when analogous measurements in small collision systems produced similar outcome [1–6]. Even hydro-based models [7–9] found to be in reasonable agreement with experimental results indicating that local thermal equilibration might be achieved even for a small system size.

However striking anomaly has been observed in the measurements sensitive to the energy loss. Absence of significant jet-quenching or negligible modification of the hadron yield (R_{pPb}) at high p_T [10] indicates that the medium may be transparent to the hard-QCD process.

However, the emergence of the near side ridge in high-multiplicity event classes of small collision systems (pp and p-Pb) [1] [3] still lacks un-ambiguous understanding. Several theoretical propositions have been made based on correlated emission from glasma flux tubes (CGC approach) [11], collective flow due to hydro-dynamical effects [7] [8] or incoherent parton scatterings [12] [13], but no general agreement could be reached.

In this thesis I have adopted the two-particle correlation technique to calculate the near-side jet like yield between identified triggers (pions and (anti) protons having $2.0 < p_T < 4.0$ GeV/ c) and un-identified associated charged particles ($1.0 < p_T < 4.0$ GeV/ c) as a function of event multiplicity using the data collected by the ALICE detector at CERN in p-Pb collisions at 5.02 TeV. An inclusive baryon to meson enhancement has been observed in this trigger p_T range in p-Pb collisions at 5.02 TeV [5], similar to that found in heavy ion collisions [14] [15], where it has been discussed in terms of radial flow and/or quark coalescence model of hadronization. Radial boost, generated during the hydrodynamical evolution, pushes the massive hadrons more to

higher p_T and provide a natural explanation to the enhanced baryon generation at intermediate p_T [9]. On the other hand, in conventional coalescence approach [16] [17], partons close in phase space recombine into hadrons. Since the p_T spectra of the hard partons (coming from initial hard scatterings) follow power law behaviour, an exponential thermal spectrum of soft partons is therefore imperative for the baryon to meson enhancement.

In this analysis, pion and proton triggered jetlike yield have been calculated as a function of event multiplicity after subtracting the flow-modulated back-ground estimated from large $|\Delta\eta|$ region. Hadrons pushed from lower p_T by radial flow or formed by coalescence of partons are expected not to have short range collimated jetlike correlation beyond the expected flow (ridge) like correlation. As a result, with an increase in multiplicity, a relatively higher suppression in the proton triggered jetlike yield is expected compared to the pion triggered case as triggers are selected from the intermediate p_T range where inclusive proton to pion enhancement has been observed [9]. This effect of higher suppression for proton triggered jetlike yield is commonly referred to as "trigger dilution" [18–22]. The sensitivity of the near side proton and pion triggered jetlike yield towards radial flow and coalescence model of hadronization has been tested using EPOS 3 and AMPT (string melting version) event generator [20, 21]. A comparison between the data and different model predictions has been made to constrain the underlying dynamics of small collision systems as well as the hadronization at intermediate p_T in a better way.

0.2 Data Analysis:

Two particle correlation is a widely used technique in high-energy physics for extracting the properties of the system produced in the ultra relativistic high energy collisions. In the present analysis the correlation function is obtained among two sets of charged particles classified as *trigger* and *associated*. The p_T ranges of trigger and associated particles are $2.0 < p_T < 4.0$ GeV/ c and $1.0 < p_T < 4.0$ GeV/ c respectively and the correlation function has been constructed with a p_T ordering ($p_T^{assoc} < p_T^{Trigger}$). The pseudo-rapidity of the particles are restricted within $-0.8 < \eta < 0.8$. This analysis has been performed by dividing the entire minimum bias events into 5

multiplicity classes based on the total number of charged particles detected within the acceptance range of the ALICE VZERO-A detector ($2.8 < \eta < 5.1$) positioned in the Pb going direction in case of p-Pb collisions [2],[3]. For each multiplicity class, the number of pairs between the triggers (identified as pions or protons) and associated charged hadrons is measured as a function of the azimuthal angle difference $\Delta\phi$ and pseudorapidity difference $\Delta\eta$. The correlation function thus obtained is corrected for pair acceptance and pair efficiency using the mixed event technique. Particle identification at the trigger p_T region has been done using the information obtained from the ALICE Time Projection Chamber (TPC) and ALICE Time Of Flight (TOF) detectors. The efficiency and contamination factors are estimated from the Monte-Carlo productions passed through GEANT simulated detector environment. The final correlation functions are corrected with all the correction factors discussed above and detailed description of the procedures will be discussed in the thesis.

This analysis concentrates only on the near side ($|\Delta\phi| < \pi/2$) of the correlation function. The particles originating from jet fragmentation are expected to be confined in a small angular region. To isolate the near side jetlike correlation, the flow modulated background is estimated from large $|\Delta\eta|$ ($|\Delta\eta| \geq 1.2$) and subtracted from the near side jet peak ($|\Delta\eta| < 1.2$). After bulk subtraction, the event averaged near side jetlike per trigger yield is calculated integrating the $\Delta\phi$ projection in the range $|\Delta\phi| < \pi/2$. The multiplicity evolution of the pion and proton triggered jetlike yield has been studied and a trigger dilution pattern has been observed.

0.3 Model based analysis (Phenomenological study):

a) Two particle correlation analysis with identified trigger particles at intermediate p_T using EPOS 3 and AMPT event generators for p-Pb collisions at $\sqrt{s_{NN}} = 5.02$ TeV.

The results obtained from the two particle correlation analysis using ALICE data has been compared with the outcome of the model based study using EPOS 3 and AMPT event generators for p-Pb collisions at $\sqrt{s_{NN}} = 5.02$ TeV [20, 21]. The sensitivity of the multiplicity evolution of the

individual pion and proton triggered jetlike yield towards radial flow (in EPOS 3) and coalescence model of hadronization (in AMPT string melting model) has been investigated in detail in this thesis.

b) Investigating the role of partonic and hadronic dynamics in mass splitting of elliptic anisotropy in p-Pb collisions at $\sqrt{s_{NN}} = 5.02$ TeV.

The mass ordering of elliptic flow (v_2^{hadron}) is considered as one of the key signatures of the presence of collectivity in the system formed in ultra relativistically high energetic collisions. The mass splitting of v_2^{hadron} has been experimentally observed in small collision systems like p-Pb collisions at 5.02 TeV where applicability of hydrodynamics is not so intuitive. Recent studies suggest that elliptic or triangular anisotropy in a multi phase transport model (AMPT) is primarily due to escape mechanism of partons rather than hydro like collectivity in the system [23]. In this thesis, I have shown that the mass splitting of v_2^{hadron} can originate independently both at the partonic and hadronic level in the string melting version of the AMPT model and not necessarily associated with the presence hydro like collectivity in the system [24].

c) Study of ridge originating from the jet-medium interaction in p-Pb collisions at $\sqrt{s_{NN}} = 5.02$ TeV using EPOS 3 event generator.

EPOS 3 is an event by event 3+1 D hydrodynamical model that takes into account hydrodynamically expanding bulk matter (core), jets (corona) and the jet-medium (core-corona) interaction [25, 26]. In this work, it has been shown that the jet-medium interaction contributes towards the ridge like structure observed in high multiplicity p-Pb collisions at 5.02 TeV. The relative contributions of the core-core, core-corona, corona-core and corona-corona correlations towards the ridge in the high multiplicity p-Pb collisions at $\sqrt{s_{NN}} = 5.02$ TeV have been studied using the data generated by EPOS 3. The multiplicity evolution of the ridges in all the cases has also been investigated.

d) Investigating the effect of color reconnection and hydrodynamical flow on the identified triggered correlation in pp collisions at $\sqrt{s_{NN}} = 7$ TeV.

The observation of collective-like behaviors in pp collisions at LHC energy can be qualitatively (at least) explained by both hydro based models (e.g. EPOS 3) and other mechanisms like multiparton interactions (MPI) with color reconnection as implemented in PYTHIA 8 - making it difficult to pinpoint the underlying mechanism responsible for the observed collective like effects in high multiplicity pp collisions [27]. In this thesis, using the two particle correlation technique, I have demonstrated that the multiplicity evolution of the near side jet-like yield associated with pion and proton triggers selected from intermediate p_T (where inclusive baryon to meson enhancement has been observed) can disentangle the effect of hydrodynamical flow from the effect of MPI based color reconnection in a straightforward way.

Bibliography

- [1] CMS Collaboration, Phys. Lett. B 718 (2013) 795-814
- [2] B. Abelev et al. (ALICE Collaboration), Physics Letters B 719 (2013) 29-41
- [3] B. Abelev et al. (ALICE Collaboration), Phys. Lett. B 726 (2013) 164 - 177
- [4] B. Abelev et al. (ALICE Collaboration), Phys. Rev. C 90 (2014) 054901
- [5] B. Abelev et al. (ALICE Collaboration), Phys. Lett. B 728 (2014) 25-38
- [6] A. Adare et al. (PHENIX Collaboration) , Phys. Rev. Lett. 114, 192301 (2015)
- [7] K. Werner et al., Phys.Rev.Lett. 112 (2014) 23, 232301.
- [8] K. Werner, Iu. Karpenko, T. Pierog., Phys.Rev.Lett. 106 (2011) 122004.
- [9] K. Werner et al., Phys.Rev. C89 (2014) 6, 064903.
- [10] B. Abelev et al. (ALICE Collaboration), Phys. Rev. Lett. 110, 082302 (2013)
- [11] Kevin Dusling and Raju Venugopalan, Phys. Rev. D 87 (2013), 094034
- [12] Guo-Liang Ma and Adam Bzdak, Phys. Lett. B 739 (2014) 209-213
- [13] Adam Bzdak and Guo-Liang Ma, Phys. Rev. Lett. 113, 252301(2014)
- [14] S. S. Adler, et al. PHENIX Collaboration), Phys. Rev. C 69 (2004) 034909
- [15] B. Abelev et al. (ALICE Collaboration), Phys. Lett. B 736 (2014) 196-207

- [16] R. Fries, B. Muller, C. Nonaka, and S. Bass, Phys. Rev. Lett. 90 (2003) 202303.
- [17] V. Greco, C. Ko, and P. Levai, Phys. Rev. Lett. 90 (2003) 202302.
- [18] N. M. Abdelwahab et. al (STAR Collaboration) Phys. Lett. B 751 (2015) 233-240
- [19] S.S. Adler et. al (PHENIX Collaboration) Phys. Rev. C 71 (2005) 051902
- [20] D. Sarkar, S. Choudhury, S. Chattopadhyay, Physics Letters B 760 (2016) 763 - 768
- [21] D. Sarkar, S. Choudhury, S. Chattopadhyay, Phys. Rev. C 94, 044909 (2016)
- [22] S. Choudhury, D. sarkar, S. Chattopadhyay, Phys. Rev. C 93, 054902 (2016)
- [23] Liang He, Terrence Edmonds, Zi-Wei Lin, Feng Liu, Denes Molnar, Fuqiang Wang, Phys. Lett. B 753 (2016) 506-510
- [24] D. Sarkar, S. Choudhury, S. Chattopadhyay, Phys. Rev. C 94, 044919 (2016)
- [25] K. Werner et al., Phys.Rev. C82 (2010) 044904.
- [26] K. Werner, Phys.Rev.Lett. 98 (2007) 152301
- [27] A. Ortiz, G. Bencedia,1,3, H . Bello, arXiv:1608.04784

Chapter 1

Introduction

1.1 New form of matter under extreme conditions

The basic goal of ultra relativistic heavy ion collision programme at Relativistic Heavy Ion Collider (RHIC) at BNL and Large Hadron Collider (LHC) at CERN is to create a deconfined state of quarks and gluons namely Quark Gluon Plasma (QGP) which is believed to have existed a few microseconds after the Big Bang [1–3]. The quarks interact strongly with gluons as mediators as described by Quantum Chromodynamics (QCD), the theory of strong interaction, a building block of the Standard Model (SM) [4–7]. The quarks are fermions with spin one-half whereas the gluons are bosons with spin one and both carry color charge responsible for the strong interaction among them [8–10]. The quarks and gluons are always found to be confined within a dimension smaller than the characteristic QCD scale ($\Lambda_{QCD} \approx 200$ MeV) [11], forming colorless states called hadrons [12]. The quantum numbers of baryons(mesons) are determined by 3(2) valence quarks inside the hadrons. Apart from these, a hadron also contains an indefinite number of virtual (or sea) quarks, antiquarks, gluons which do not contribute to its quantum numbers. They are off-shell particles popping up as an effect of quantum fluctuations. The electric charge and the masses of the six types of quarks are shown in table 1.1 [13].

The two fundamental properties of QCD relevant for the formation of QGP in ultra-relativistic

high energetic collisions are : confinement and asymptotic freedom [14–19]. These two features of strong interaction are related to the variation of the coupling strength (α_S) between partons with momentum transfer during scattering or equivalently the probed length scale. This variation is described by the DGALP (Dokshitzer - Gribov - Lipatov - Altarelli - Parisi) equations [20] as shown in Fig 1.1.

Table 1.1: The fundamental particles, forces and their basic properties [13].

Quarks	Mass (GeV)	Charge	Leptons	Mass (GeV)	Charge	Carriers	Force
up (u)	0.003	2/3	electron (e)	0.00051111	-1	gluon (g)	strong
down (d)	0.006	-1/3	e- neutrino (ν_e)	$< 10^{-8}$	0	photon (γ)	electromagnetic
charm (c)	1.3	2/3	muon (μ)	0.106	-1	Z^0	weak
strange(s) (s)	0.1	-1/3	μ neutrino (ν_μ)	> 0.0002	0	W^\pm	weak
top(t) (t)	175	2/3	tau (τ)	1.7771	-1	H	weak
bottom (b)	4.3	-1/3	τ neutrino (ν_τ)	< 0.02	0	graviton ?	gravity

The partons have never been observed in free state and this experimental observation leads to the concept of confinement in QCD. As the equations of motion of QCD have not been solved exactly, no analytical proof of quark confinement exists. For a better understanding of the mechanism responsible for confinement, Lattice QCD [21–24] is used to study a discretized version of QCD matter using Monte Carlo techniques. Lattice QCD is a computational technique which discretizes the space-time by placing quarks in lattice structures with a fixed finite distance to calculate numerical integrals, cross sections, potential between quarks, and the equation of state (EoS) etc. The potential between a quark and an anti-quark $V(R)$ [25] (where R is the distance between the two quarks) as measured from Lattice QCD shown in Fig 1.2.

At large probed length (R) or equivalently small momentum transfer (Q), the potential energy

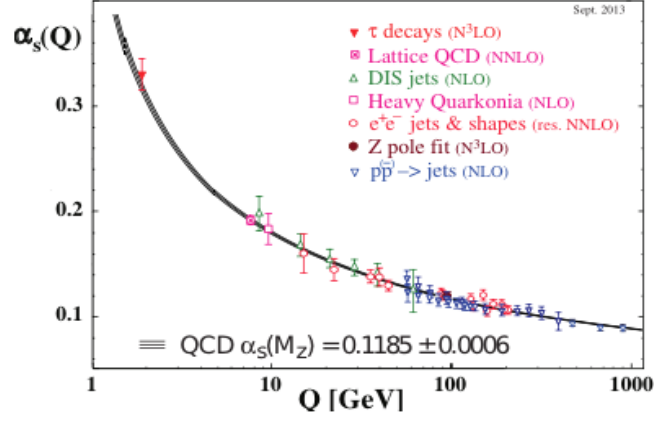


Figure 1.1: [Color online] The measurements of α_s as a function of the respective energy scale Q [11].

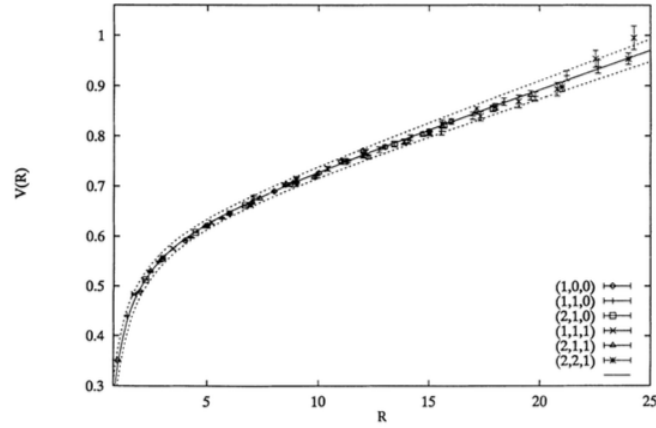


Figure 1.2: [Color online] Static quark potential from Lattice QCD as a function of the distance between the quarks R . The different symbols indicate the direction of R in terms of points of the lattice [25].

between partons increases linearly with the distance - leading to the confinement of the partons within the hadrons observed in nature. This can be explained using the string model [26] in which the partons are connected by color tubes/strings (basically the strong gluon field between them). The energy of a string is proportional to its length and it increases with the distance between the partons i.e when the strings are stretched. With increase in the length of the strings (equivalently the energy of strings), at some point it will be energetically more favourable to create a new quark-antiquark pair connected by shorter (i.e less energetic) color string to create another hadron (in this case a meson). On the other hand, the QCD coupling constant decreases at smaller probed length or large momentum transfer - making the interaction among partons asymptotically small (not zero). This leads to the possibility of creation of state where the quarks and gluons are asymptotically deconfined. This type of matter of deconfined partons can be formed at high temperature and/or very high density and is termed as Quark-Gluon Plasma (QGP) [14].

1.2 The QCD phase diagram

The possible scenario for hadronic to partonic phase transition can be described using the famous QCD phase diagram defined in the temperature- baryochemical potential plane (i.e. T, μ_B), as shown in Fig 1.3 [27]. The baryochemical potential is defined as the amount of energy needed to add a baryon to the system. In the phase diagram, the lower T and a baryochemical potential of $\mu_B \approx 940$ MeV correspond to ordinary matter where the partons are bound into colorless hadrons. At higher temperature ($T \gg \Lambda^{QCD}$), due to asymptotic freedom, quarks and gluons may be in deconfined state. The heavy-ion collision experiments at RHIC (Relativistic Heavy Ion Collision) and LHC (Large Hadron Collider) cover the low μ_B and high T region- a condition suitable for the formation of a baryon less or low baryon density QGP which is thought to be similar to the one formed in the early universe at a few microseconds after the Big Bang . Lattice QCD calculations suggest that at low μ_B , a cross-over transition occurs between the hadronic and the partonic phase [24, 28]. In a cross over, the system gradually changes from

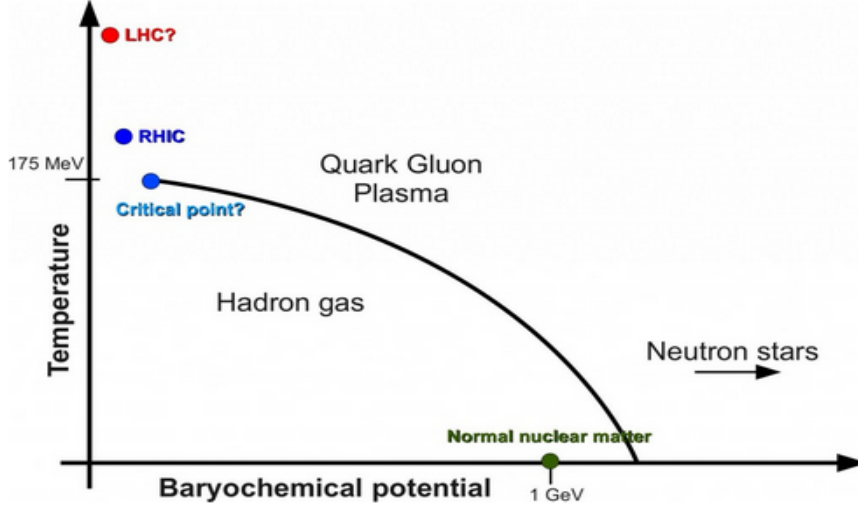


Figure 1.3: [Color online] QCD phase diagram scheme in terms of temperature T (in the y-axis) as a function of baryochemical potential μ_B [27].

a system of hadrons to a deconfined state of partons without having any discontinuities in the thermodynamical entities of the system or in other words without having a specific transition point. But at large μ_B , a first order transition [29] is expected in which a discontinuity in the first order derivative of the thermodynamic potentials of the system takes place which leads to large fluctuations around the transition region. The point of the transition curve at which the nature of the phase transition changes from first order to crossover is termed as the critical end point. The exact location of the critical point is debatable as Lattice QCD calculations are only approximate at non-zero baryon density [30]. However, at low μ_B ($\mu_B \approx 0$), Lattice QCD provides reliable results for the Equation of State (EoS) of the QCD matter. For a zero baryon density system, the variation of the energy density ϵ (scaled with T^4) and the specific heat C_v (scaled with T^3) with temperature T is shown in Fig 1.4. For an ideal, non-interacting gas of quarks and gluons at zero chemical potential ($\mu_B \approx 0$), the energy density is found to be proportional to [31] $g_{\text{QGP}}(\pi^2/30)T^4$, where g_{QGP} is 37 for two and 47.5 for three flavors. The energy density ϵ and the specific heat C_v (normalized to T^4 and T^3 respectively) exhibit a steep increase around $T \approx 160$ MeV which indicates a change in the effective degrees of freedom [32].

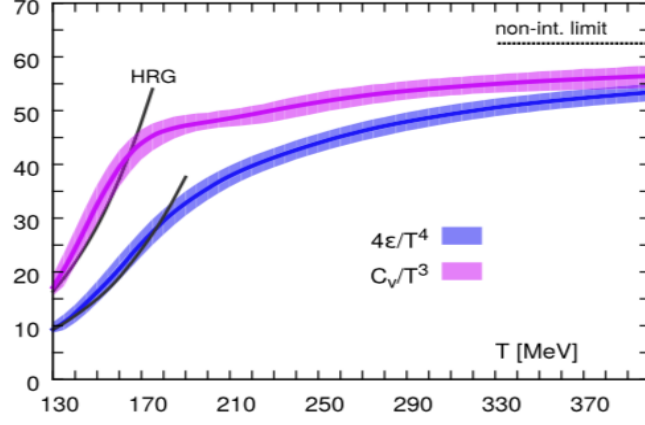


Figure 1.4: [Color online]Equation of State from Lattice QCD at zero baryon density [32].

This indicates towards the phase transition between the confined and the deconfined state. At higher temperature the lattice QCD equation of state (EoS) approaches the non interacting limit. The Lattice QCD EoS can be parameterized and used as an input required for hydrodynamical evolution of the system.

As shown in Fig 1.3, at higher μ_B , the confinement-deconfinement transition can also occur at lower temperatures. This is possible by increasing the density to 5 - 10 times the normal nuclear density ($\approx 0.15 \text{ fm}^{-3}$) using a process usually referred to as "cold compression" [33]. The region of very low temperature and high baryon density QGP is believed to exist in the core of neutron stars [34–36].

The matter created at high energy experiments at RHIC and LHC energies provide a tool for characterization of the properties of the matter under extreme conditions. Heavy-ion collisions at Brookhaven was initially performed in AGS (Alternating Gradient Synchrotron) with Au-Au collisions up to $\sqrt{s_{NN}} = 11.5 \text{ GeV}$ and later by RHIC (Relativistic Heavy Ion Collider) with $\sqrt{s_{NN}}$ ranging from 7.7 to 200 GeV [37]. At CERN, the SPS (Super Proton Synchrotron) was first used to perform heavy-ion collisions at $E_{\text{lab}} = 158 \text{ GeV}$. At LHC, the Pb-Pb collisions took place at $\sqrt{s_{NN}} = 2.76 \text{ TeV}$ in Run I [38] and $\sqrt{s_{NN}} = 5.02 \text{ TeV}$ in Run II [39]. Also, pp collisions are performed with center-of-mass energies upto $\sqrt{s_{NN}} = 14 \text{ TeV}$ and p-Pb collisions at $\sqrt{s_{NN}} =$

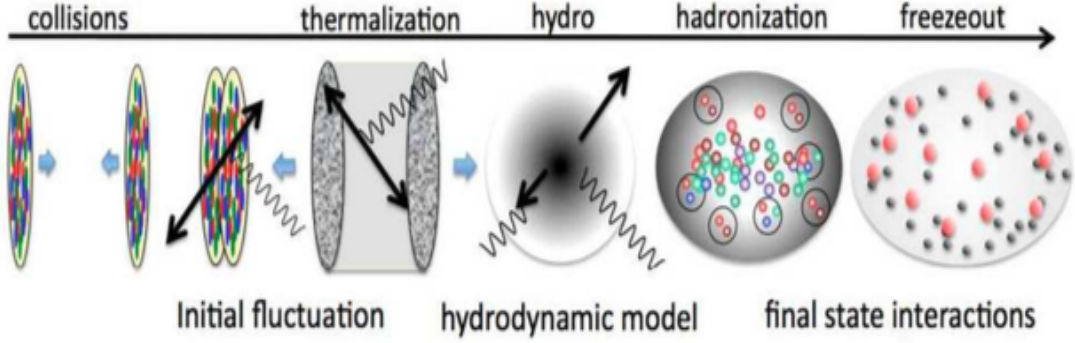


Figure 1.5: [Color online] Schematic representation of the evolution of a relativistic heavy-ion collision. [40]

5.02 TeV.

For low collision energies (5 - 10 GeV per nucleon), the colliding nuclei stop each other in the interaction zone and form a system of high baryon density. At very high energies (≈ 200 GeV per nucleon or higher), the participant nucleons interact and escape from the collision zone after depositing a large amount of energy in a small volume. This creates a high energy density matter with low net baryon content - a condition suitable to create low/zero baryon density QGP in such high energy colliders [41].

1.3 Formation and evolution of QGP in heavy ion collisions

In ultra-relativistically high energetic collisions at LHC or RHIC energies, two heavy nuclei are accelerated upto the speed of light (almost) and the partonic degrees of freedom become relevant. In that case, two bunches of partons in the Lorentz-contracted nuclei approach and collide with each other. Initially the partons inside nuclei have predominantly longitudinal momenta and transverse momenta, if any, are distributed isotropically. Now, if the partons from two nuclei do not interact with each other in the interaction zone, the final azimuthal distribution of the particles will be isotropic. But if the partons interact with each other frequently with a non zero cross section, then these partonic interactions will generate random motion among the

constituents (partons). Thermal energy is associated with random motion of the constituents of the system and during the interaction among the partons a portion of the initial kinetic energy (pumped into the nuclei by the accelerator) converts into thermal energy of the system. If the system size is large compared to the mean free path of the scattering and the density of the partons is high - the probability of large number of interactions among the partons becomes high and it may be sufficient to achieve a local thermal equilibrium of the system. But thermalization is always an assumption in this field and there is no direct experimental method to confirm this. The ability of different fluid models with the assumption of thermalization to reasonably explain the experimental data validates this idea [42]. Once thermalization of the system is assumed, it can be described in terms of thermodynamic variables like temperature, pressure etc and the system expands collectively as a response to the developed pressure. A schematic overview of the different stages of the heavy ion collisions is shown in Fig 1.5. The amount of energy deposited in such a collision can be characterized by the variable called "impact parameter" - which is defined as the distance between the centres of the two colliding nuclei. If the impact parameter is small, the overlap region is large and large number of nucleons from two nuclei interact with each other. The nucleons in the overlap zone are termed as participants and the nucleons outside the interaction zone are termed as spectators. The number of spectators and participants depend on the impact parameter of the collision. The events with small impact parameter (large overlap zone) are called central events whereas, the events with larger impact parameter (small overlap zone) are called peripheral ones.

The collisions with non zero impact parameter have an almond shaped initial geometry which also has a contribution from the density fluctuations in the system. The positions of the nucleons inside the nuclei just before the collision defines the initial state and it fluctuates from event to event. The simplest model to quantify these initial density fluctuations is the Glauber Model [43, 44] in which the colliding nuclei are characterized by a distribution function for the nucleons. For large nuclei, the Woods-Saxon function [45] is found to agree well with experimental results

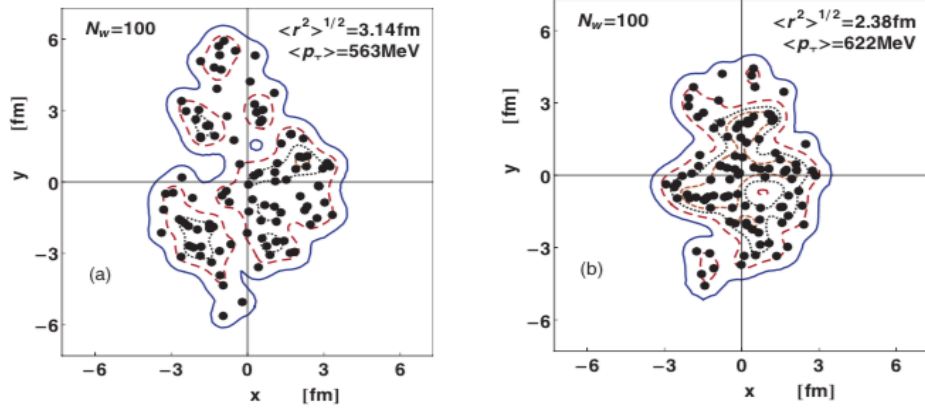


Figure 1.6: [Color online] Wounded nucleon distributions in the plane perpendicular to the beam axis with same number of wounded nucleons. ($N_W = 100$) [46, 47]

and is defined as:

$$\rho_A(r) = \frac{\rho_0}{A(1 + \exp[(r - r_0)/a])} \quad (1.1)$$

where A , a , ρ_0 and r_0 are parameters whose values are fixed from experiment. For a given impact parameter, to calculate the probability for a nucleon to interact at least one time inelastically, Monte Carlo methods are used (using the nucleon-nucleon inelastic cross section). These nucleons are referred to as participants /wounded nucleons and responsible for the deposition of energy in the interaction zone. In Fig 1.6, the density profiles of the wounded nucleons for same collision centrality (i.e equal number of wounded nucleons) are shown [46, 47]. Even for same number of wounded nucleons, the density profiles are quite different from each other due to the density fluctuations. This fluctuations in the the initial state along with the initial geometry of the overlap zone, lead to geometrical eccentricities of the system [48, 49]. If the local thermal equilibrium of the system is assumed, this initial spatial anisotropy leads to the anisotropic pressure gradients in the transverse plane as shown in Fig 1.7 and Fig 1.8. This anisotropy develops relative to a common plane defined by the impact parameter and the beam axis and referred to as "reaction plane" in case of heavy ion collisions as shown in Fig 1.7. The pressure gradients push particles outward and more matter is transported in the direction of the steepest

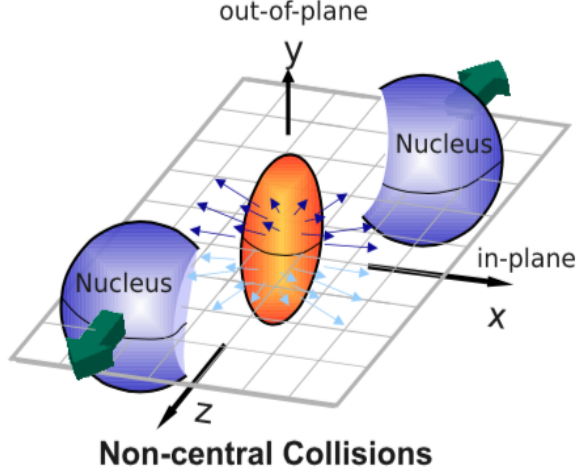


Figure 1.7: [Color online] A schematic diagram showing the location of the reaction plane relative to the incoming nuclei [48].

pressure gradient (in-plane) compared to the direction of the lower pressure gradient (out-of-plane) and therefore generate an anisotropic azimuthal distribution of particles as shown in Fig 1.8 [50–54]. The triple differential invariant distribution of the final state particles in relativistic heavy ion collisions is a periodic (period of 2π), even function of azimuthal angle ϕ (i.e. reflection symmetric with respect to the reaction plane) and can be expressed using a Fourier expansion [55, 56]:

$$E \frac{d^3N}{d^3p} = \frac{1}{2\pi} \frac{d^2N}{p_T dp_T dy} \left[1 + 2 \sum_{n=1}^{\infty} v_n \cos [n (\phi - \Psi_{RP})] \right] \quad (1.2)$$

where,

$$v_n(p_T, y) = \langle \cos [n (\phi - \Psi_{RP})] \rangle \quad (1.3)$$

Where E represents the energy of the particle, p the momentum, p_T the transverse momentum, y the rapidity, ϕ the azimuthal angle, Ψ_{RP} the reaction plane angle and the v_n are the Fourier coefficients of order n . The leading term in the bracket represents the azimuthally symmetric

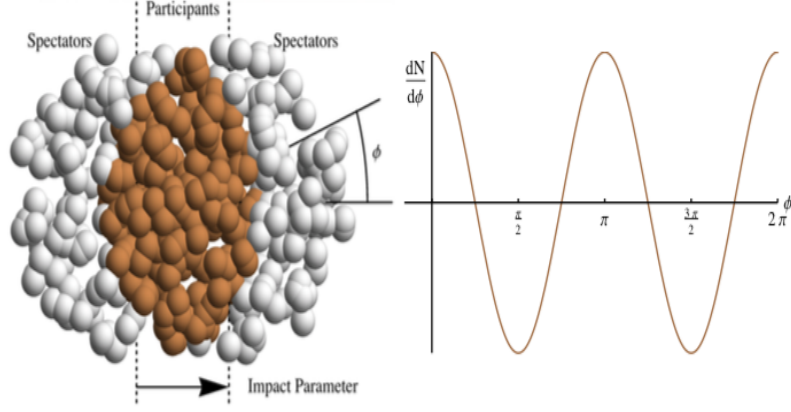


Figure 1.8: [Color online] Schematic diagram showing the formation of azimuthal anisotropy from the initial state anisotropy [49].

radial flow, v_1 : directed flow which illustrates the preference for particles to move in the direction along the beam axis. v_2 is defined as elliptic flow and it is a measure of anisotropic pressure gradient created in the system and has been studied most extensively in experiments. For higher values of n (> 2), the v_n decreases with increase in n and these higher harmonics are mainly sensitive to the initial density fluctuations in the system as discussed above. The fireball produced in such high energetic collisions expands rapidly due to the initial pressure and cools down i.e. the temperature of the system decreases. Now, due to expansion, the spatial anisotropy of the source gradually diminishes and this is termed as "self quenching". That's why the flow (v_n) develops early when the spatial anisotropy of the system is significant and it saturates as the spatial anisotropy continues to decrease with time. Thus, v_n is a measure of degree of thermalization of the matter produced early in the collision [50]. It is important to note that radial flow (isotropic transverse expansion) originates from early stage and continues to grow until the system freezes out.

The formation of QGP is associated with the idea of deconfinement (i.e. $\alpha_s \approx 0$) and that's why the QGP was initially thought to be a weakly coupled system. However, different experimental observations (e.g large v_2 , jet quenching in heavy ion collisions at different RHIC and LHC

energies - to be discussed later) indicate that QGP evolves as a strongly coupled one. Now, the deconfined state lasts for a very short time after the collision and if the interaction among the partons are not frequent then it is unlikely for the system to reach a thermally equilibrated state. But, it is found that at the top RHIC and LHC energies, the energy density of the system is high enough [37] such that the mean free path of interaction is much smaller than the system size. This increases the probability of a large number of interactions among the partons before the system freezes out and it behaves like a strongly coupled fluid. The time required to establish the initial local thermal equilibrium is called the thermalization time and there is no experimental technique to directly measure that. Different hydrodynamical models with Lattice-QCD equation of state (EoS) which assume a very short thermalization time (≈ 1 fm/c) [42] explains the experimentally observed data reasonably well. This data-model comparison favors the idea of such a short thermalization time in relativistic heavy ion collisions. The early measurements at RHIC [57] indicated that the strongly interacting QGP behaves like an ideal fluid but recent LHC measurements [58] point out towards the presence of small but non negligible viscous effects in the medium. Different types of viscosities namely *bulk* and *shear* viscosities resist the conversion of the initial spatial anisotropies into final state momentum anisotropies. Bulk viscosity opposes the radial expansion of the fireball, reducing the radial expansion rate of the system. Whereas, the shear viscosity tries to decrease the anisotropy in the pressure gradients and even the expansion rates along different directions. The effect of initial anisotropic pressure gradients will be reflected in terms of the anisotropic azimuthal distribution of final state hadrons only when the shear viscosity is small [59].

The QGP gradually expands, cools down and below a critical temperature ($T_C=150-160$ MeV) the phase transition occurs when the deconfined state of partons turns into hadrons. The initial hard scattered partons traverse through the medium and strongly interacts with the partons in the medium to produce shower partons and finally generate a collimated shower of hadrons termed as jets. The low momentum partons (thermal or shower) close in phase space recombine into hadrons and this process is known as recombination or coalescence model of hadronization. Hadronization

is basically a non perturbative process and mainly depends on different phenomenological models. The produced hadrons interact among themselves by both elastic and inelastic processes and the system keep on expanding and further cools down. The rate of inelastic processes decrease faster than the elastic one [31] and after a certain time, the relative abundances of the different particle species become fixed (except for decays of resonances)- this is known as chemical freeze-out (τ_{ch}) [60–63]. The hadrons still undergo elastic collisions which can change the momentum distributions of the individual hadron species (i.e. building up the hadronic radial flow). The elastic processes continue until the system further expands and the average distance between the constituents become larger than the strong interaction range - this is termed as kinetic freeze-out. At this point elastic collisions among the hadrons stop and hadrons decouple from the medium and stream freely to the detectors.

The hot QCD matter created in high energy heavy ion collisions mainly consists of hard and soft components. The hard part is the high momentum partons originate from initial hard scatterings. The soft or low momentum partons make the dominant contribution to the system and behaves as a relativistic fluid. All these partons hadronize to create high and low momentum hadrons and used to measure final state observables to probe the properties of the system. The interactions between the final hadrons produced in a heavy-ion collision are known as final state interactions (FSI) [64, 65] and it affects the final state observables calculated from these hadrons. So, in order to extract information about the deconfined phase (QGP), it is also important to understand the impact of FSI on the produced hadrons and on the different observables calculated using them.

1.4 Experimental Observations

1.4.1 Energy density in heavy ion collisions

Analysis of the wealth of data collected at the SPS, RHIC and LHC contributed significantly to enrich our understanding of the nature of the produced system in ultra-relativistically high energetic collisions. The two important observations are the measurements of elliptic flow and

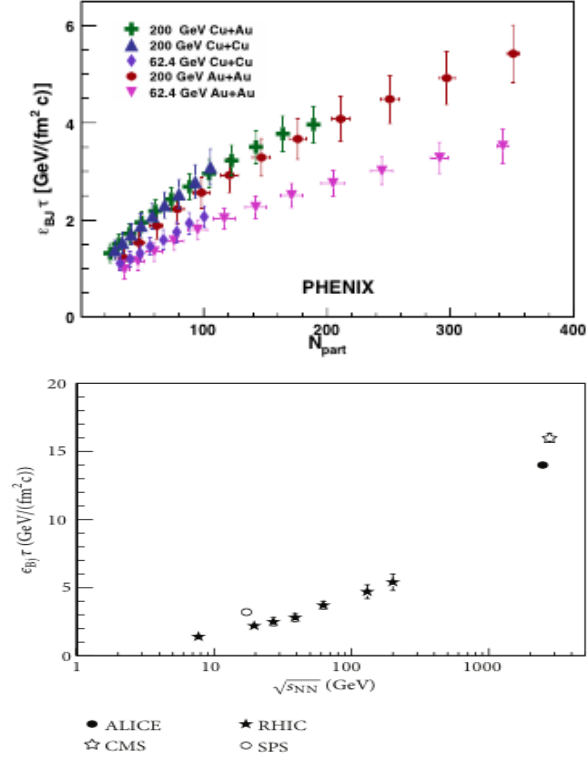


Figure 1.9: [Color online] **Top:** $\sqrt{s_{NN}}$ dependence of Bjorken energy density for Au-Au, Cu-Au, and Cu-Cu collisions at $\sqrt{s_{NN}} = 200$ and 62.4 GeV [68]. **Bottom:** The values of Bjorken energy density are shown for Pb-Pb collisions at LHC energy ($\sqrt{s_{NN}} = 2.76$ TeV), together with energies available for Au-Au collisions at RHIC [69].

jet quenching as these allow to study different properties (e.g the value of shear viscosity over entropy density and the energy density) of the system. As already discussed, the evolution of the thermalized medium is described by relativistic hydrodynamics. Modern hydrodynamic calculations are performed numerically with a finite viscosity and using an equation of state taken from Lattice QCD without assuming boost-invariance [31, 59]. These models work well in explaining identified particle spectra up to ($p_T < 2.0$ GeV/ c). But a simplistic approach of this idea is implemented in Bjorken model [42]. This model takes into account several approximations for the equation of state and the equations of motion such as perfect fluid, one dimensional expansion only, boost invariance, etc. These assumptions make it possible to find analytic

solutions. The estimate of the energy density provides an idea about the system produced in high energy heavy ion collisions. Using the Bjorken model [42], the spatial energy density of the system can be estimated using the following relation:

$$\epsilon = \frac{1}{c\tau_{th}A} \frac{dE_T}{dy} \quad (1.4)$$

where A is the transverse area of the over-lapped geometry of the incident nuclei and dE_T/dy denotes the transverse energy of the final state particles per unit of rapidity (y). The thermalization time (τ_{Th}) is considered to be ~ 1 fm/c. The $dE_T/d\eta$ was found to be 2 TeV by the CMS collaboration [66] for the most central Pb-Pb collisions at $\sqrt{s_{NN}} = 2.76$ TeV. Using these values and an overlap area of $A = \pi \times (7\text{fm})^2$, the initial energy density (ϵ) is found to be approximately $14 \text{ GeV}/\text{fm}^3$. This is much higher than the lattice-QCD predicted critical energy density of $1 \text{ GeV}/\text{fm}^3$ required for the formation of deconfinement state of quarks and gluons [67]. Using the same formalism, initial transverse energy density at SPS was estimated to be $3.0 \pm 0.6 \text{ GeV}/\text{fm}^3$ and in Au-Au collisions at $\sqrt{s_{NN}} = 200$ GeV it was estimated to be $6.0 \pm 1.0 \text{ GeV}/\text{fm}^3$ [68, 69]. All these estimations indicate towards satisfying the condition for the formation of QGP state in high energy heavy ion collisions at SPS, RHIC and LHC energies. The QGP finally cools down and produce hadrons which reach the detectors after the kinetic freeze out at (~ 10 fm/c) and carry information about the properties of the system.

1.4.2 Soft probes for QGP

The low p_T hadrons are used as soft probes of the system and carry the information of the deconfined state of partons which behave as fluid and described by the relativistic hydrodynamics. The anisotropy in the distribution of particles in the azimuthal plane (described by elliptic flow v_2) quantifies the response of the system towards the anisotropic pressure gradients due to the initial spatial anisotropy in the interaction zone [50–53]. The transverse momentum dependence of elliptic flow (v_2) for different particle species as measured in Pb-Pb collisions at $\sqrt{s_{NN}} = 2.76$

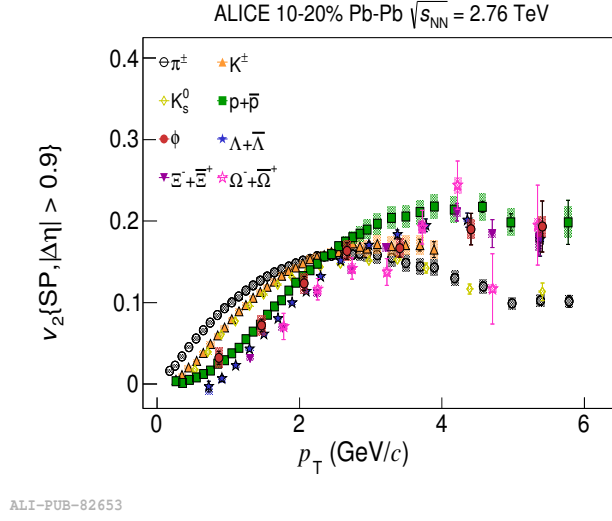


Figure 1.10: [Color online] The transverse momentum (p_T) dependence v_2 of identified particles in Pb-Pb collisions at $\sqrt{s_{NN}} = 2.76$ TeV [70].

TeV by ALICE [70] is shown in Fig 1.10. For $p_T < 3$ GeV/c there is an ordering of v_2 according to the mass of the particles. The heavier particles have lower v_2 compared to the lighter ones. This mass ordering is a combined effect of radial flow (isotropic transverse expansion) and elliptic flow. If the system is radially expanding with a velocity β , then a particle of mass m gets a momentum boost of $\gamma m \beta$ (where γ is the lorentz factor). The heavier particles (with higher values of m) get a higher boost compared to the lighter ones. So, radial flow pushes particles from lower to higher p_T (i.e flattens the p_T spectra) and the effect is more pronounced for heavier particles (higher values of m) and for larger average radial flow (i.e for higher values of β). As a result, the low p_T region gets depleted and that depletion is higher for heavier particles and also for in-plane particles (having a larger value of β due to larger pressure gradient) compared to the out-of-plane particles (with a lower value of β due to lower pressure gradient). This tends to reduce the anisotropy in the azimuthal distribution of low p_T particles and hence the value of v_2 . Since the protons are heavier than pions, their v_2 decrease more compared to the pions and generate the observed mass ordering in the low p_T region. The elliptic flow (v_2) measurements indicate that the QGP behaves as an almost perfect partonic fluid with very small values of

the shear viscosity to entropy density ratio (close to the AdS/CFT lower bound of $1/4\pi$ [71]). The success of different hydrodynamical models in the description of many aspects of RHIC and LHC data implies the thermalization of the deconfined medium when v_2 is formed. Also, as shown in Fig 1.10, hadrons containing strange quarks follow the same trends for v_2 , implying that strangeness is also thermalized. Furthermore, measurements of v_2 of electrons from decays of hadrons including charm quarks indicate that the charm quarks are also probably thermalized similar to that of light quarks [72].

At intermediate p_T ($2 < p_T < 5$ GeV/c), the hydrodynamic mass ordering switch over, with protons having higher v_2 than pions as shown in Fig 1.10. The baryon-meson splitting of identified particles $v_2(p_T)$ at intermediate p_T was first observed at RHIC and explained with the models invoking hadronization of a collectively expanding partonic medium via a mechanism of quark recombination or coalescence [73–77]. The basic assumption of this model is that the invariant spectrum of produced particles is proportional to the invariant spectra of the constituents i.e.

$$\frac{dN^h}{dp_T}(p_T) \propto \left[\frac{dN^q}{dp_T}\left(\frac{p_T}{n}\right) \right]^n \text{ which leads to}$$

$$1 + 2v_2^h(p_T)\cos(2\phi) = [1 + 2v_2^q\left(\frac{p_T}{n}\right)\cos(2\phi)]^n \text{ (using Eqn 1.2)}$$

$$\approx 1 + 2nv_2^q\left(\frac{p_T}{n}\right)\cos(2\phi) \text{ where } (v_2 \ll 1)$$

$$v_2^h(p_T) \approx nv_2^q\left(\frac{p_T}{n}\right)$$

Where "h" stands for hadron, "q" stands for parton and "n" is the number of constituent quarks in a hadron (2 for meson and 3 for baryon). Hence $v_2^h(p_T)/n$ vs p_T/n will be a universal curve representing the momentum-space anisotropy of the constituent quarks before hadronization. This is known as constituent quark number scaling (NCQ scaling) of hadron $v_2(p_T)$ and is an immediate consequence of the coalescence model of hadronization. The NCQ scaling of v_2 has been experimentally observed at RHIC energy as shown in Fig 1.11 and it indicates towards the

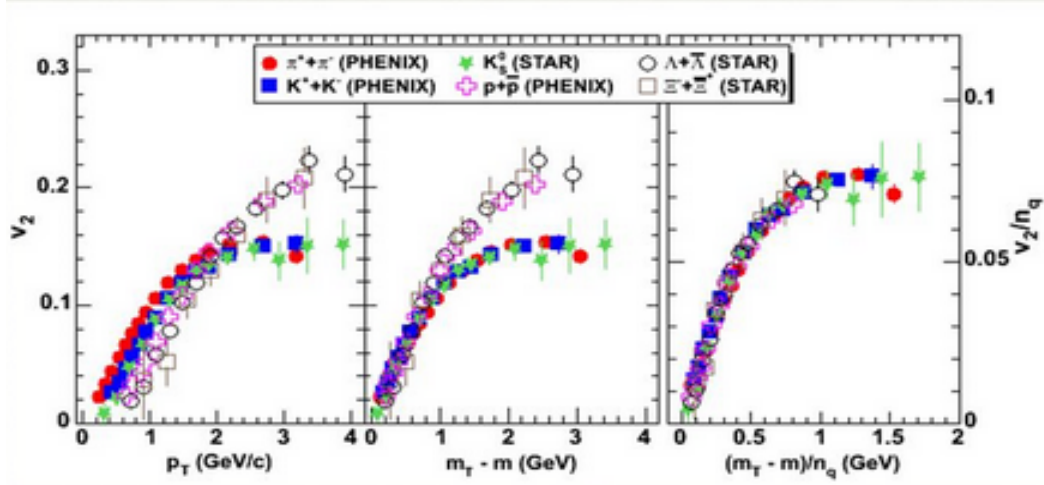


Figure 1.11: [Color online] Particle species dependence of v_2 versus p_T (left), v_2 versus $m_T - m$ (middle) and v_2/n_q versus $(m_T - m)/n_q$ (right) in Au-Au collisions at $\sqrt{s_{NN}} = 200$ GeV. [78–80].

dominance of partonic degrees of freedom [78–80] at the time of hadronization or in other words, the formation of deconfined state of quarks and gluons in the ultra relativistic high energy heavy ion collisions.

These models can also explain the large baryon-to-meson ratio found in heavy ion collisions [81, 82]. An anomalous enhancement in $p(\bar{p})/\pi^\pm$ ratio was observed as function of centrality in most central Au-Au/Pb-Pb collisions and the ratio was found to be 3/5 higher than in d-Au/pp collisions at same energy with a peak around 2-3 GeV/c as shown in Fig 1.12 [83–86]. In coalescence approach, in order to form a 3 GeV/c baryon, three 1 GeV/c quarks are required, whereas to form a 3 GeV/c meson, two 1.5 GeV/c quarks have to recombine. Assuming thermalized QGP medium (approximately following the Boltzmanian / exponential distribution), parton spectra falls off steeply with increasing p_T and the number of 1 GeV/c quarks are much more than 1.5 GeV/c ones (as illustrated in Fig 1.13). This leads to a relative increase in the baryon-to-meson ratio at intermediate p_T compared to the vacuum fragmentation case. There are different approaches of quark recombination as suggested by various groups. Each of them particularly differ in the way high p_T partons from the initial hard scatterings and the thermalized

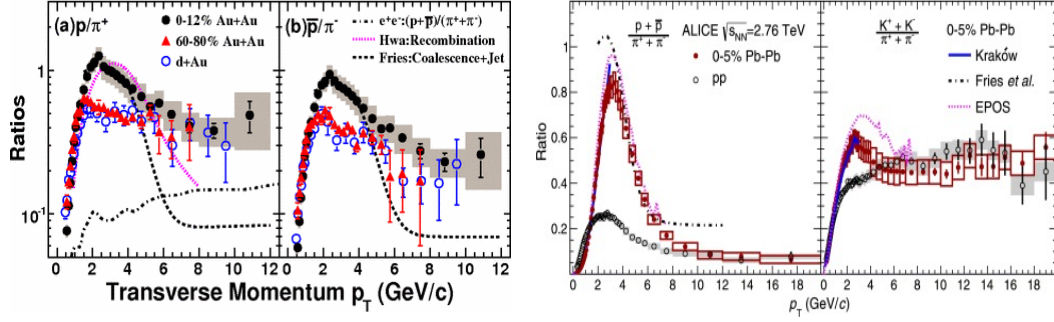


Figure 1.12: [Color online] **Top** The inclusive $p(\bar{p})/\pi^\pm$ ratio from d-Au and Au-Au collisions at $\sqrt{s_{NN}} = 200$ GeV. The dotted-dashed lines shows the inclusive $p(\bar{p})/\pi^\pm$ ratio from light quark jets in e+ e- collisions at 91.2 GeV. Comparisons with different model calculations are also shown [81, 82]. **Bottom:** p_T -dependence of particle ratios measured in pp and 0-5% most central Pb-Pb collisions at 2.76 TeV. Comparison with different model predictions for 0-5% Pb-Pb collisions are also shown [83–86].

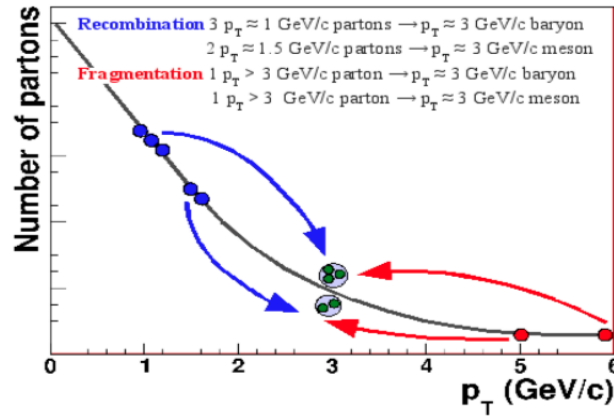


Figure 1.13: [Color online] A schematic diagram showing the idea of hadronization through coalescence model of hadronization. [87]

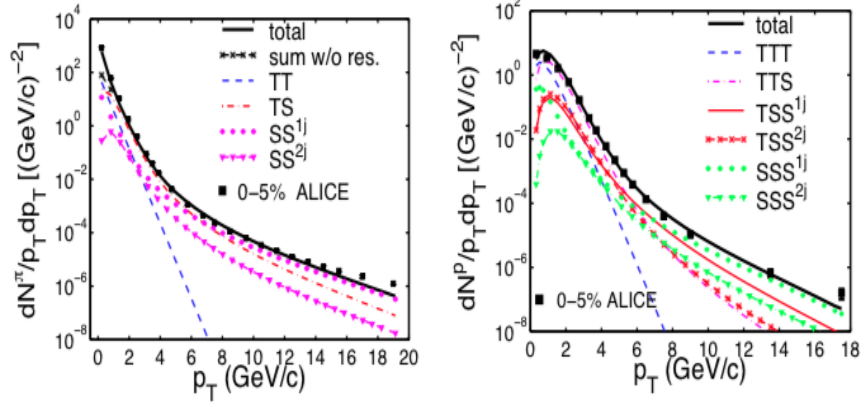


Figure 1.14: [Color online] The pion and proton spectra as measured by the ALICE collaboration and the comparison made using the recombination model [93].

soft partons are treated. While in some formalism, only coalescence among soft partons are considered and the hard partons are hadronized by fragmentation only [76, 88], others allow coalescence of both soft and hard minijet partons [89, 90]. As the p_T spectra of these hard partons show a power-law behavior, an exponential thermal spectrum of soft partons is therefore imperative for large baryon to meson enhancement. All these implementations with proper tuning of parameters describe the basic features at intermediate p_T - e.g., p_T spectra, NCQ scaling of v_2 reasonably well at RHIC energy. But at LHC, the NCQ scaling of v_2 has been found to be violated at the order of $\approx 20\%$ and can be explained using the soft-hard recombination formalism. In the recent versions of the recombination model, the thermal partons and shower partons (originated from jet-medium interaction) are allowed to recombine with each other irrespective of their origin [91–93]. This modified formalism explains the RHIC data at $\sqrt{s_{NN}} = 200$ GeV in a better way [93]. But the effect of shower partons become relatively more important at the LHC energy ($\sqrt{s_{NN}} = 2.76$ TeV) where recombination of shower partons originating from two separate showers [94] has to be considered to explain the observed spectra as shown in Fig 1.14. It is found that hadrons containing at least one shower parton contribute significantly to the spectra. This indicates towards the importance of the presence of shower partons in addition

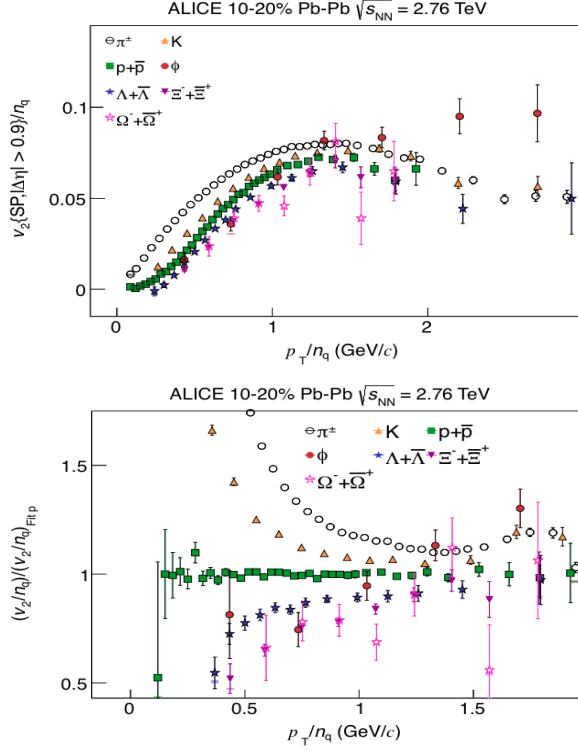


Figure 1.15: [Color online] **Top:** NCQ scaling of v_2 for different hadron species as measured in 10-20% centrality class of Pb-Pb collisions at $\sqrt{s_{NN}} = 2.76$ TeV. **Bottom:** Double ratio of v_2/n_q as a function of p_T relative to the seventh order polynomial fit to v_2/n_q of (anti) protons in 10-20% centrality class of Pb-Pb collisions at $\sqrt{s_{NN}} = 2.76$ TeV [70].

to the thermal ones in the medium produced in high energy heavy ion collisions where the jet-medium interaction has been found to be significant. Recombination models only suggest that QGP hadronization may occur by a different mechanism in heavy ion collisions and do not conflict with hydrodynamical models of the QGP. Indeed, hydrodynamical models which incorporates recombination model of hadronization are able to describe the data at RHIC reasonably well [95]. Also, recombination does not require complete thermalization of the medium [95].

Now, the radial flow which pushes heavier particles more from lower to higher p_T compared to the lighter ones can also describe this enhanced baryon production at intermediate p_T . The effect of radial flow has been found to be more dominant at LHC energy where the deviation in the NCQ scaling of v_2 has been found to be more prominent compared to the RHIC energy. Recent

measurements by ALICE have shown deviations in the NCQ scaling by the order of $\pm 20\%$ for $p_T > 3$ GeV/c [70] which indicate that mass of the particles plays more important role than that of constituent quark number (relevant in the coalescence formalism) at LHC energy. Now, the magnitude of radial flow and the p_T -integrated values of v_2 at LHC have increased by same amount (20-25%) than that of the RHIC. Also, as shown in Fig 1.15, v_2 of ϕ -meson (having 2 constituent quarks but with a mass similar to that of a proton $<\approx 1$ GeV $>$) at intermediate p_T region follow the baryon band rather than the band of mesons. All these observations indicate that the baryon-meson ordering of v_2 at LHC energy is predominantly determined by the mass of the particles than that of the constituent quark number [70].

1.4.3 Hard probes for QGP

Another experimental observation that leads towards the idea of formation of QGP in high energy heavy ion collisions is "jet quenching" [96–101]. Jets are basically high energetic partons produced from 2->2 scattering of partons from the incoming nuclei with large momentum transfer. Due to the momentum conservation, the scattered partons are separated by 180 degree in azimuth forming back-to-back di-jets as shown in Fig1.16. These jets are predominantly produced early in the collision and propagate through the dense partonic medium formed in heavy-ion collisions. The scattered partons finally hadronize into color-neutral hadrons and are detected in the detector. In hard scattering processes, the majority of the hadrons are produced roughly collinear to the fragmenting partons, resulting in a narrow cone of hadrons in the final state. The process of hadronization of jets is non-perturbative and it is described by fragmentation functions [102, 103]. The fragmentation function represents the probability for a parton to fragment into a particular hadron and can not be determined from first principles. It is usually parameterized as function of the parton energy and vacuum fragmentation functions are already well constrained using data from elementary collisions. In heavy ion collisions, the hard scattered partons produced early in the collision travel through the medium and interact strongly with the other partons of the medium and suffer energy loss through gluon radiations and multi- parton

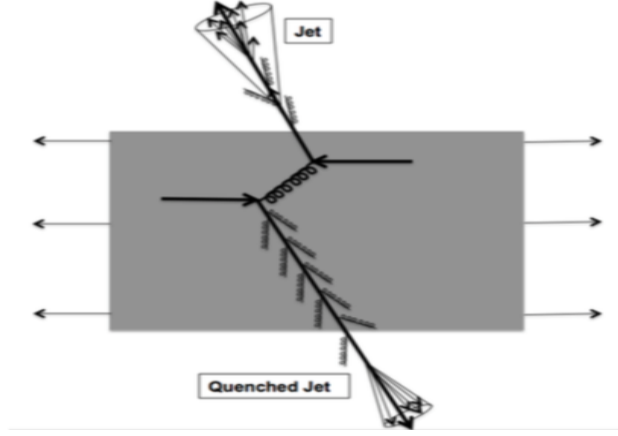


Figure 1.16: [Color online] A schematic presentation of two quarks originating from a hard scattering near the surface of the medium. One of the quarks going out directly to the vacuum, radiating gluons and hadronize. The other quark going through the dense plasma formed in the collision, suffering energy loss by both radiational and collisional processes and finally fragmenting into a quenched jet.

interactions. This leads to the suppression of the number of high p_T particles (produced mainly via jet fragmentation) compared to the vacuum fragmentation case (e.g. in minimum bias pp collisions where medium formation is not expected).

This in-medium energy loss by jets is estimated by the nuclear modification factor R_{AA} which is defined as the ratio between the particle yield in heavy-ion collisions divided by the same in pp collisions and normalized to the average number of binary nucleon-nucleon collisions (N_{coll}).

$$R_{AA}(p_T) = \frac{(1/N_{evt}^{AA}) d^2 N_{ch}^{AA} / d\eta dp_T}{\langle N_{coll} \rangle d^2 N_{ch}^{pp} / d\eta dp_T} \quad (1.5)$$

The number of binary collisions (N_{coll}) is determined by the Glauber model [43] using the Wood-Saxon nucleon density profile of the colliding nuclei. With the assumption of N_{coll} scaling of particle production at high p_T , $R_{AA} = 1$ would indicate that the heavy-ion collision is just a superposition of independent pp collisions without any thermalized and deconfined medium formation. However, any deviation in R_{AA} from unity would indicate a modification of the hadron yield due to the medium effects. The modification in R_{AA} can be attributed to the parton energy

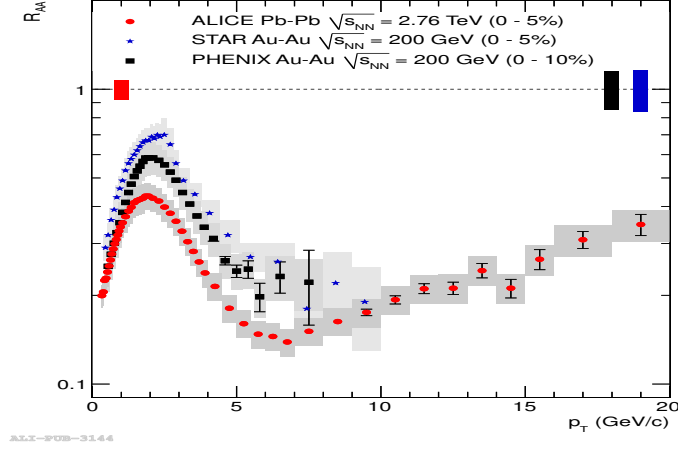


Figure 1.17: [Color online] Nuclear modification factor versus transverse momentum as measured by the ALICE, STAR and PHENIX collaborations in heavy ion collisions [110].

loss before fragmentation or modification of the fragmentation functions for partons that fragment in the medium. Also, the initial state effects like modification of the partonic distribution functions (PDFs) within the colliding nuclei may also contribute to the deviation of R_{AA} from unity. A large suppression in the yield of high p_T (i.e. $R_{AA} < 1$) hadrons has been observed in central Au-Au collisions at RHIC energies compared to the reference p-p or d-Au reactions at the same energy [104–106]. The observed suppression at RHIC energy has been reasonably reproduced by the models that consider the energy loss of partons in highly dense medium of initial gluon density $dN_g/dy \approx 1400$ [107].

The comparison of the nuclear modification factor as measured in central Pb-Pb collisions at LHC energy ($\sqrt{s_{NN}} = 2.76$ TeV) with the measurements in Au-Au collisions at $\sqrt{s_{NN}} = 200$ GeV (by the PHENIX and STAR experiments at RHIC) is shown in Fig 1.17. The R_{AA} at LHC has been found to be more suppressed than at RHIC in the p_T range of $5 < p_T < 10$ GeV/c. The energy loss (ΔE_{loss}) models predict that the energy loss is proportional to the mid-rapidity gluon density or dN_g/dy . As the mid rapidity gluon density exhibits a logarithmic increase with $\sqrt{s_{NN}}$, a larger suppression of R_{AA} is naturally expected for higher values of $\sqrt{s_{NN}}$. The higher suppression at LHC energy suggest that the formed medium is densely populated with

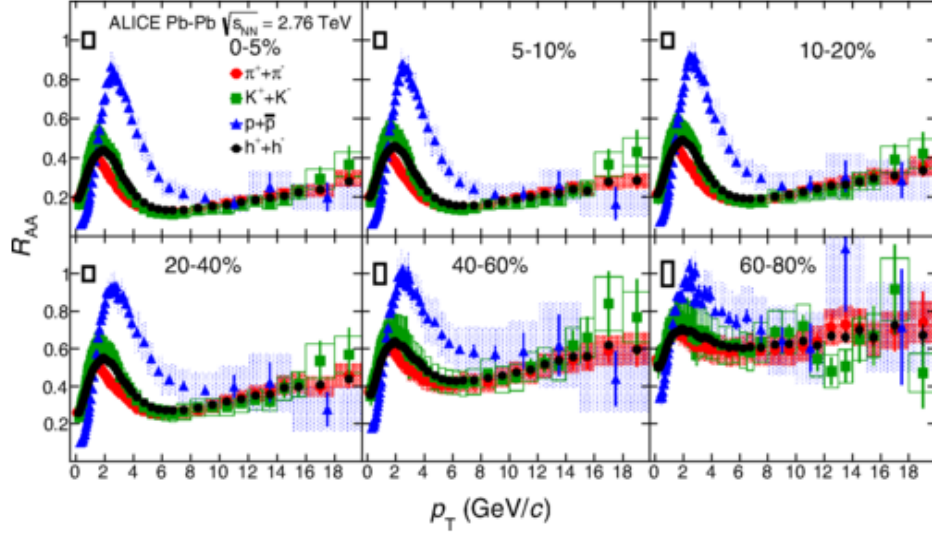


Figure 1.18: [Color online] The nuclear modification factor R_{AA} as a function of p_T for different hadron species for different collision centralities in Pb-Pb collisions at 2.76 TeV [111].

gluons ($dN_g/dy \approx 2000-4000$) and hard scattered partons lose energy in the dense and strongly interacting medium [108–110]. Using excellent particle identification capability of the ALICE detector, R_{AA} of identified particles (pions, kaons, protons) were measured up to a momentum range of 20 GeV/c as shown in Fig 1.18. The nuclear modification factor at high p_T was found to be independent of particle species and all particles exhibit equal suppression in the limit of the experimental uncertainties [111]. This suggests that jet-hadron chemistry of the high p_T particles (which mainly originate from the jet fragmentation) is independent of the vacuum or medium fragmentation.

The jets are being studied using mainly two methods. The first one is the jet-reconstruction in which a jet-finding algorithm is applied on the particles produced in a collision, that assigns every particle to a jet [112, 113]. This method is suitable for the cases where few jets are created and background (e.g. flow) is not significant (for example in pp collisions). It can recover the kinematics on the partonic level irrespective of the details of the hadronization. On the other hand, in head-on heavy-ion collisions where very many particles are created, due to large back-

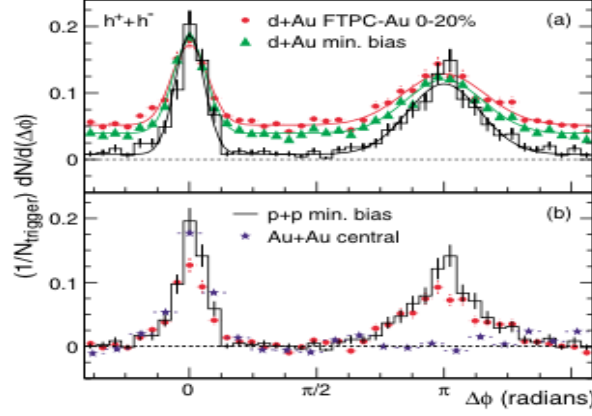


Figure 1.19: [Color online] Di-hadron correlations from $p + p$, $d + \text{Au}$, and $\text{Au} + \text{Au}$ collisions at $\sqrt{s_{NN}} = 200\text{GeV}$ with trigger particles with $4.0 < p_T < 6.0 \text{ GeV}/c$ and associated particles with $2.0 < p_T < 4.0 \text{ GeV}/c$ [114]. (a) Correlations for $p + p$, minimum bias $d + \text{Au}$, and central $d + \text{Au}$ collisions with no background subtraction. (b) Correlations for $p + p$, $d + \text{Au}$, and 0-10% central $\text{Au} + \text{Au}$ collisions after background subtraction.

ground (from flow, underlying event effects etc.) it is hard to disentangle the jet part from the background part and reconstruct the jet kinematics on the partonic level.

A second method to study jets is by using two particle correlations technique. In this method, a high momentum particle is selected as trigger particle and the angular distribution of the associated particles (in η and ϕ) relative to the trigger particle is determined. The primary criterion to determine trigger and associated particles is their momenta which determines the relative contributions of jets and background (e.g. anisotropic flow) in the correlation structure. In case both trigger and associated particles are selected at higher p_T , the contribution from background decreases. However, with decrease in trigger p_T a significant fraction of trigger particles may not come from jets and the background starts to contribute significantly to the correlation structure.

The two particle correlation has been studied extensively at RHIC and LHC energies. The jet-medium interaction was investigated in the angular correlation measurements that shows a disappearance of away side correlation structure of the two particle correlations in central A-A collisions [114–117] whereas no such quenching has been observed in minimum bias pp collisions

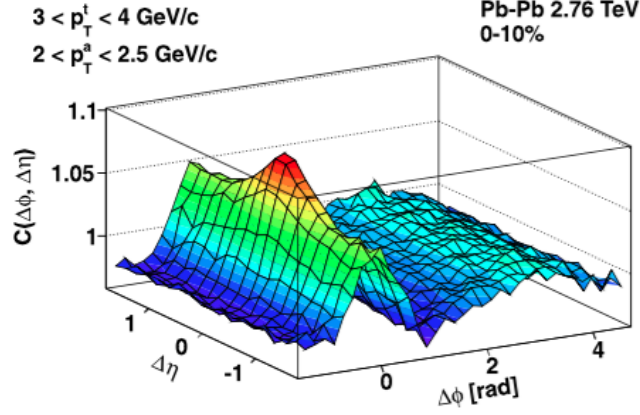


Figure 1.20: [Color online] Two particle correlation functions with trigger particles with $3.0 < p_T < 4.0$ GeV/c and associated particles with $2.0 < p_T < 2.5$ GeV/c in 0-10% central Pb-Pb collisions at 2.76 TeV [118].

as shown in Fig 1.19.

The two-dimensional correlation structure as obtained with trigger particles in the range ($3 < p_T < 4$ GeV/c) and associated particles in ($2 < p_T < 2.5$ GeV/c) [118] in Pb-Pb collisions at 2.76 TeV is shown in Fig 1.20. The peak-shaped structure around $(\Delta\eta, \Delta\phi \approx (0,0))$ represents the collimated shower of particles originate from the jet-fragmentation and termed as jet-peak. The origin of ridge-shaped (elongated structure along $|\Delta\eta|$) underneath the jet peak is explained using the collective motion or flow of the soft partons of the medium. On the away side ($\Delta\phi \approx \pi$), the ridge like structure comes from a momentum conserving jet opposite to the near-side jet ($\Delta\phi \approx 0$) and is termed as away-side jet. The anisotropic flow is entangled with the away side jet and it is hard to disentangle the two effects. Whereas, in near side ($|\Delta\phi| < \pi/2$), the jet is localized around $(\Delta\eta, \Delta\phi \approx (0,0))$ and it can be separated out from the anisotropic flow background using a $|\Delta\eta|$ cut. The details about bulk/flow subtraction from the near side of the correlation function will be discussed in the next chapter. After flow/background subtraction, the remaining jet peak can be studied to determine different jet properties such as jet-like yield, jet-peak shape, hadro-chemistry (yields of different identified particles inside the jet peak) etc.

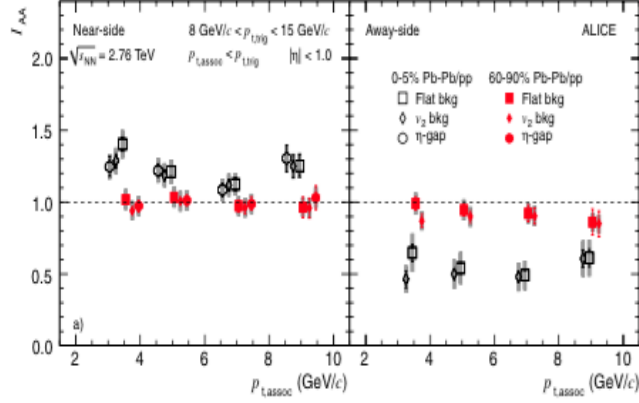


Figure 1.21: [Color online] **Leftpanel:** I_{AA} of the near-side jet yield ($\Delta\phi < \pi/2$) for two centralities **Rightpanel:** I_{AA} of the away-side yield ($\Delta\phi > \pi/2$) for two centralities [119].

The jet-medium interaction can be studied by comparing the multiplicity/centrality dependence of the near and away side jet yields with the same in pp collisions at the same collision energy using a variable named as I_{AA} [119]. The I_{AA} measurement as performed by the ALICE collaboration with trigger particles in the range $8 < p_T < 15$ GeV/c and $p_{T,assoc} < p_{T,trig}$ is shown in Fig 1.21. The jet yields are determined in the near ($|\Delta\phi| < \pi/2$) and away ($|\Delta\phi| > \pi/2$) side of the correlation function and the I_{AA} measurement is done for both central (0-10%) and peripheral (60-90%) Pb-Pb collisions at 2.76 TeV. The near and away side I_{AA} is close to unity is for peripheral events whereas for the most central events, it is more than unity in the near side and less than unity in the away side. The enhancement in the near side I_{AA} indicates towards the possible medium-modification of the fragmentation function and the suppression in the away side indicates the energy loss by the jet while traversing through the medium. Thus, using two particle correlation measurement, jet-quenching and medium modification of fragmentation can be studied and can complement the observations made using fully reconstructed jets [120].

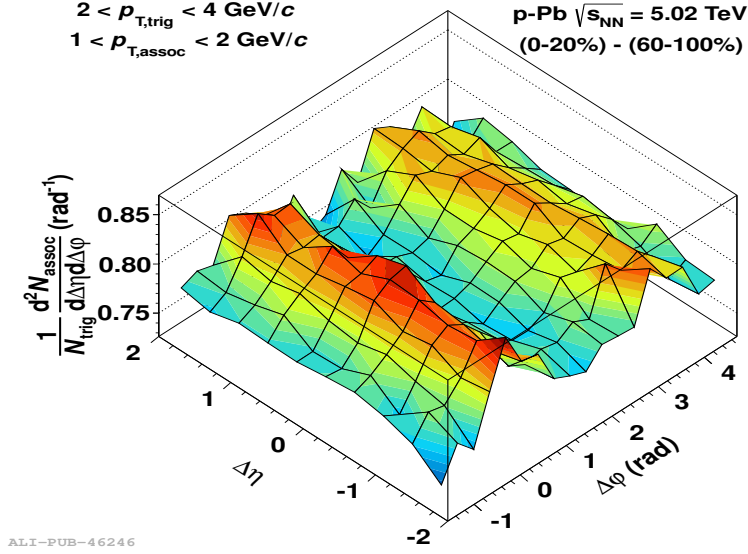


Figure 1.22: (Color online) Double ridge from two-particle correlations in high multiplicity events after subtraction of two-particle correlations in low multiplicity events in p-Pb collisions at $\sqrt{s_{NN}} = 5.02$ TeV [122].

1.5 Collectivity in small collision systems?

Collisions of small systems like pp [121], p-Pb [122–125] or d-Au [126] at LHC and RHIC energies have gained renewed interest following the discovery that the underlying collision dynamics might be analogous to that of the heavy-ions. Two-particle angular correlation measurements in pp [121], p-Pb [122] and d-Au [126] collisions have revealed existence of azimuthal correlations extended to a large pseudo-rapidity separation $|\Delta\eta|$, the effect popularly known as “ridge” as shown in Fig 1.22. In heavy-ion collisions, such structures have been attributed to the effect of the initial anisotropy in the overlap geometry of the colliding nuclei followed by the collective emission of particles. Several other observations, like, mass-ordering of the elliptic flow coefficient (v_2) of identified particles as shown in Fig 1.23 [123], quark-scaling of v_2 [127] and baryon-to-meson enhancement at intermediate p_T as shown in Fig 1.24 [125] suggest similarity between the systems formed in small and heavy-ion collisions.

However striking anomaly has been observed in the measurements sensitive to these energy loss. Absence of significant jet-quenching or negligible modification of the high p_T hadron yield in p-

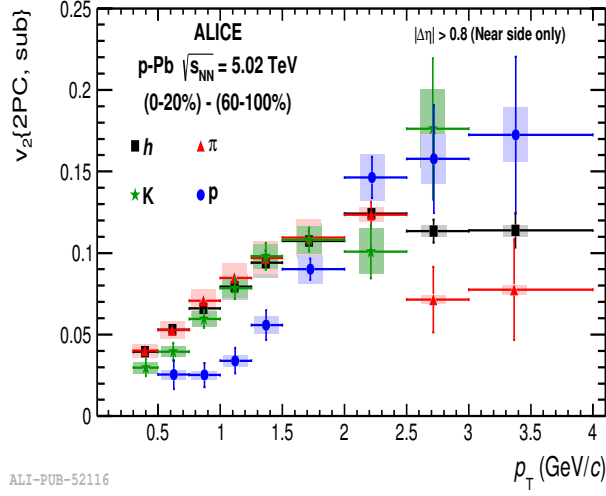


Figure 1.23: (Color online) Elliptic flow v_2 as a function of p_T for pions, kaons and protons in p-Pb collisions at 5.02 TeV [123].

Pb collisions (R_{pPb}) at 5.02 TeV as shown in Fig 1.25 [128, 129] indicates that the medium may be transparent to the hard-QCD processes. It has been argued that angular-correlations in small systems are dominated by jet-like processes. However, the emergence of the near side ridge in high-multiplicity event classes of pp and p-Pb collisions at LHC energies [121] [123] still lacks unambiguous understanding. Several theoretical propositions have been made based on correlated emission from glasma flux tubes (CGC approach) [130], collective flow due to hydrodynamical effects [131] [132] or incoherent parton scatterings [133] [134], but no general agreement could be reached.

In this thesis, the two-particle correlation technique has been adopted to calculate the near-side jet like yield between identified triggers ($2.0 < p_T < 4.0$ GeV/c) and un-identified associated particles ($0.5/1.0 < p_T < 4.0$ GeV/c) as a function of event multiplicity in p-Pb collisions at 5.02 TeV and pp collisions at 7 TeV. p_T ranges of trigger and associated particles are chosen in the region where the ridge structures have been prominently observed in the experimental results [122]. An inclusive baryon to meson enhancement has also been observed in this trigger p_T range in p-Pb collisions at 5.02 TeV [125] and pp collisions at 7 TeV [135] (as shown in Fig 1.24), similar to that found in heavy ion collisions [136] [137], where it has been discussed in terms of

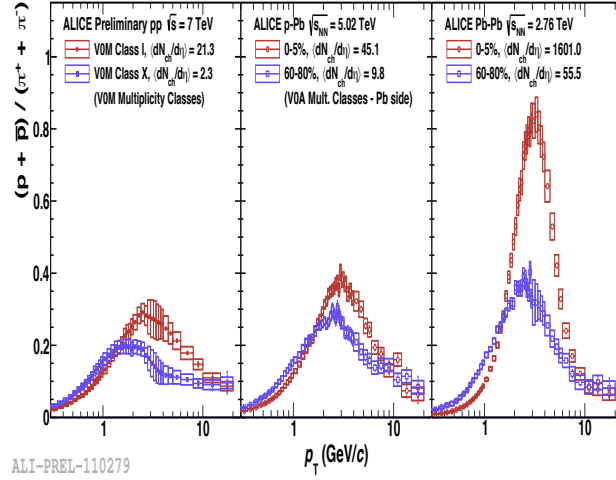


Figure 1.24: (Color online) The baryon to meson enhancement with multiplicity in pp, p-Pb and Pb-Pb collisions at LHC energies [135].

radial flow [138] and/or quark coalescence model of hadronization [139] [140]. The explanation of this baryon enhancement via coalescence model of hadronization has already been discussed. Radial boost, generated during the hydrodynamical evolution, pushes the massive hadrons more to higher p_T and also provide a explanation to the enhanced baryon generation at intermediate p_T . Assuming the applicability of the hydrodynamics in high multiplicity pp and p-Pb collisions, a larger radial flow has been suggested in high multiplicity classes of small collision systems compared to central Pb-Pb collisions [141] and supported by the experimental observation [125]. In this analysis the trigger particles are identified as pions or protons and the near side jet-like yields (per trigger) associated with these identified triggers are calculated as a function of event multiplicity after subtracting the flow-modulated back-ground estimated from large $|\Delta\eta|$ (will be discussed in detail in the next chapter). The anomalous baryon to meson enhancement is expected to alter the near-side jet yield associated with proton-triggers in a more significant way compared to the pion triggers. Hadrons pushed from lower to higher p_T by radial flow or generated by quark coalescence are expected not to exhibit a short range jet-like correlation beyond the expected flow (ridge) like correlation [142, 143]. Thus the bulk/flow subtracted near-side jet peak is dominated by the hard triggered (jet) correlation. Since the correlation functions

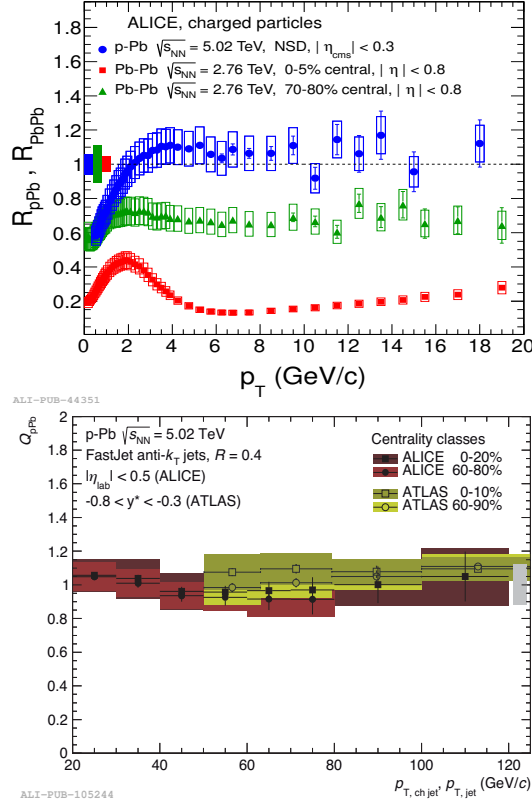


Figure 1.25: (Color online) **Top:** The nuclear modification factor as measured in p-Pb collisions at 5.02 TeV for minimum bias p-Pb collisions and compared with the same as measured in central heavy ion collisions at RHIC and LHC energies [128]. **bottom:** Multiplicity dependence of the nuclear modification factor in p-Pb collisions at 5.02 TeV [129].

are normalized by both hard and soft triggers, the soft triggers without any jet-like correlated partners are expected to cause a dilution in the per trigger jet-like yield. The proportion of soft triggers increase with multiplicity and the rate of increase has a species dependence as the soft processes like coalescence and/or radial flow favor proton production over the pion at intermediate p_T . So, the proton-triggered jet-like yield is expected to get diluted at a larger rate compared to the pion-triggered case with increase in multiplicity [142, 143] - an effect commonly referred to as "trigger dilution" [144] [145]. In absence of any significant jet-medium interplay in small systems, trigger species dependence of the associated jet-like yield may be attributed dominantly to the dynamics of quark coalescence and/or radial flow. Thus, this observable can be

used to probe the presence of collectivity in small collision systems and study the hadronization at intermediate p_T - this is the main motivation of this thesis.

In the next chapter, the construction of the two dimensional (2-D) $(\Delta\eta, \Delta\phi)$ angular correlation functions, background subtraction, near side jet-like yield calculations and interpretation of the results will be discussed using the two event generators AMPT (implements coalescence model of hadronization) and EPOS 3 (implements event by event 3+1 D hydrodynamical flow). In chapter 3, the different sub-components of the ALICE detector system will be discussed. The details of the analysis of the data taken by the ALICE collaboration for p-Pb collaboration at $\sqrt{s_{NN}} = 5.02$ TeV will be discussed in chapter 4. The comparison of the results obtained from the data analysis (in ALICE) with the model derived results (from EPOS 3 and AMPT string melting) will be made to achieve further insight on the underlying dynamics in small collision systems. In chapter 5, the prediction for the multiplicity dependence of near side jet-like yields associated with baryon and meson triggers at intermediate p_T for pp collisions at 7 TeV has been made using PYTHIA (with color reconnection) and EPOS 3. The effect jet-medium interaction as implemented in EPOS 3 on the ridge like structure as observed in p-Pb collisions at 5.02 TeV will be discussed in chapter 6. In chapter 7, the role of partonic and hadronic dynamics in mass splitting of elliptic anisotropy in p-Pb collisions at $\sqrt{s_{NN}} = 5.02$ TeV using a multi phase transport model (AMPT) will be investigated. The overview of this thesis will be discussed in chapter 8.

Bibliography

- [1] M. Riordan and W. A. Zajc, The first few microseconds, Sci. Am. 294N5, 24 (2006) [Spektrum Wiss. 2006 N11, 36 (2006)].
- [2] Coles, P., ed (2001). Routledge Critical Dictionary of the New Cosmology. Routledge. p. 202. ISBN 0-203-16457-1.
- [3] G. (1927) Expansion of the universe, A homogeneous universe of constant mass and increasing radius accounting for the radial velocity of extragalactic nebulae. Monthly Notices of the Royal Astronomical Society 91: 483-490, doi:10.1093/mnras/91.5.483
- [4] D.J. Gross, F. Wilczek, Phys. Rev. D 8, (1973).
- [5] H.D. Politzer, Phys. Rev. Lett. 30, (1973).
- [6] K.G. Wilson, Phys. Rev. D 10, 2445 (1974).
- [7] A. M. Polyakov, Nucl. Phys. B 120, 429 (1977) .
- [8] O.W. Greenberg: "Spin and Unitary Spin Independence in a Paraquark Model of Baryons and Mesons", Phys. Rev. Lett. 13, 598-602 (1964).
- [9] Y. Nambu: Preludes in Theoretical Physics, ed. A. de Shalit, H. Feshbach and L. Van Hove (North Holland, Amsterdam, 1966).
- [10] M.Y. Han and Y. Nambu: "Three-Triplet Model with Double SU(3) Symmetry", Phys. Rev. 139, B1006-B1010 (1965).

- [11] K. Olive et al. (Particle Data Group). Review of Particle Physics. Chin.Phys., C38:090001, 2014. <http://dx.doi.org/10.1088/1674-1137/38/9/090001>.
- [12] Rajan Gupta: Lectures given at the LXVIII Les Houches Summer School "Probing the Standard Model of Particle Interaction", July 28-Sept 5, 1997. arXiv:hep-lat/9807028.
- [13] K. Olive et al. (Particle Data Group). Review of Particle Physics. Chin.Phys., C38:090001, 2014. <http://dx.doi.org/10.1088/1674-1137/38/9/090001>.
- [14] J.C. Collins and M.J. Perry: "Superdense Matter: Neutrons or Asymptotically Free Quarks?", Phys. Rev. Lett. 34, 1353 (1975) 23.
- [15] E.V. Shuryak: "Quantum chromodynamics and the theory of superdense matter", Phys. Rep. 61, 71 (1980) 24.
- [16] B. Muller: "The Physics of the Quark-Gluon-Plasma", Lecture Notes in Physics, vol. 225, Springer, Heidelberg (1985).
- [17] L. McLerran: "The Physics of the Quark-Gluon Plasma", Rev. Mod. Phys. 58 1012 (1986) 24.
- [18] S. Weinberg: "The First Three Minutes", Basic Books, New York (1977) 23.
- [19] D. Gross, Asymptotic freedom and QCD: A historical perspective, Nucl.Phys.Proc.Suppl. 135 (2004) 193211.
- [20] Particle Data Group Collaboration, K. A. Olive et al., Review of Particle Physics, Chin. Phys. C38 (2014) 090001.
- [21] Z. Fodor and S.D. Katz: "Lattice determination of the critical point of QCD at finite T and μ ", JHEP 0203, 014 (2002) 24, 25, 29, 97, 99.
- [22] Ph. de Forcrand and O. Philipsen: "The QCD phase diagram for small densities from imaginary chemical potential", Nucl. Phys. B642, 290 (2002).

- [23] C.R. Allton et al.: "The Equation of state for two flavor QCD at nonzero chemical potential", Phys. Rev. D68, 014507 (2003) 97.
- [24] F. Karsch and E. Laermann: "Thermodynamics and In Medium Hadron Properties from Lattice QCD". In: R.C. Hwa and X.-N. Wang (eds.) Quark-Gluon Plasma 3, p. 1, World Scientific, Singapore (2004) 24, 25, 29, 99.
- [25] G. S. Bali and K. Schilling. Static quark-antiquark potential: Scaling behavior and finite-size effects in SU(3) lattice gauge theory. Physical Review D, 46: 2636-2646, September 1992.
- [26] B. Andersson, G. Gustafson, G. Ingelman, and T. Sjostrand, Parton Fragmentation and String Dynamics, Phys. Rept. 97 (1983) 31-145.
- [27] <http://www.quantumdiaries.org/2010/04/26/the-quark-gluon-plasma>.
- [28] A. Bazavov et al., The chiral and deconfinement aspects of the QCD transition, Phys. Rev. D85 (2012) 054503, arXiv:1111.1710 [hep-lat].
- [29] R. Rapp, T. Schafer and E.V. Shuryak: "High-density QCD and instantons", Ann. Phys. 280, 35 (2000) 25, 29.
- [30] M. A. Stephanov, QCD phase diagram: An Overview, PoS LAT2006 (2006) 024, arXiv:hep-lat/0701002 [hep-lat].
- [31] W. Florkowski. Phenomenology of Ultra-Relativistic Heavy-Ion Collisions. World Scientific, 2010.
- [32] HotQCD Collaboration, A. Bazavov et al., Equation of state in (2+1)-flavor QCD, Phys. Rev. D90 (2014) 094503, arXiv:1407.6387 [hep-lat].
- [33] Michael. K, Raghunath. S, Tim. S, and Reinhard. S: "Global Properties of Nucleus-Nucleus Collisions", Lect. Notes Phys. 785: 23-103, 2010.

- [34] S.L. Shapiro and S. Teukolsky: "Black Holes, White Dwarfs and Neutron Stars", Wiley, New York, (1983) 25.
- [35] F. Weber: "Pulsars as Astrophysical Laboratories", Institute of Physics Publishing, Bristol (1999).
- [36] R. Oechslin, H.T. Janka and A. Marek: "Relativistic neutron star merger simulations with non-zero temperature equations of state I. Variation of binary parameters and equation of state", astro-ph/ 0611047 25.
- [37] P. Steinberg, Relativistic heavy ion physics: Results from AGS to RHIC, eConf C020620 (2002) FRBT03, arXiv:nucl-ex/0210009 [nucl-ex]. [,168(2002)].
- [38] B. Muller, J. Schukraft, and B. Wyslouch, First Results from Pb+Pb collisions at the LHC, Ann. Rev. Nucl. Part. Sci. 62 (2012) 361-386, arXiv:1202.3233 [hep-ex].
- [39] ALICE Collaboration, J. Adam et al., Centrality dependence of the charged-particle multiplicity density at mid-rapidity in Pb-Pb collisions at $\sqrt{s_{NN}} = 5.02$ TeV, arXiv:1512.06104 [nucl-ex].
- [40] C. Nonaka and M. Asakawa, arXiv:1204.4795[nucl-th], (2012).
- [41] F. Prino, Study of the phase transition to QGP at the CERN SPS with the NA50 multiplicity detector. PhD thesis, Turin U., 2001.
- [42] J. D. Bjorken, Highly Relativistic Nucleus-Nucleus Collisions: The Central Rapidity Region, Phys. Rev. D27 (1983) 140-151.
- [43] M. L. Miller, K. Reygers, S. J. Sanders, and P. Steinberg. Glauber Modeling in High-Energy Nuclear Collisions. Annual Review of Nuclear and Particle Science, 57:205-243, 2007.
- [44] A. Biallas, M. Bleszynski, and W. Czyz. Multiplicity distributions in nucleus-nucleus collisions at high energies. Nuclear Physics B, 111:461-476, 1976.

- [45] R. D. Woods and D. S. Saxon. Diffuse surface optical model for nucleon-nuclei scattering. *Physical Review*, 95:577-578, July 1954.
- [46] W. Broniowski, M. Rybczynski, and P. Bozek. GLISSANDO: GLauber Initial-State Simulation AND mOre... *Computer Physics Communications*, 180(1):69-83, 2009.
- [47] P. Bozek and W. Broniowski. Transverse-momentum fluctuations in relativistic heavy-ion collisions from event-by-event viscous hydro- dynamics. *Physical Review C*, 85:044910, April 2012.
- [48] T. Ullrich, RHIC experimental overview - what we have learned, Talk at Colliders to Cosmic Rays 2007, 2007.
- [49] CERN-THESIS-2015-227, Rodriguez Manso, Alis (Utrecht U.), <http://cds.cern.ch/record/2109982?ln=en>
- [50] J.Y. Ollitrault: "Anisotropy as a signature of transverse collective flow", *Phys. Rev. D* 46, 229 (1992) 161.
- [51] STAR Collaboration: "Elliptic flow in Au+Au collisions at $\sqrt{s_{NN}} = 130$ GeV", *Phys. Rev. Lett.* 86, 402 (2001) 161.
- [52] H. Heiselberg and A.M. Levy: "Elliptic flow and Hanbury- Brown-Twiss correlations in noncentral nuclear collisions", *Phys. Rev. C* 59, 2716 (1999) 161.
- [53] H. Sorge: "Highly Sensitive Centrality Dependence of Elliptic Flow: A Novel Signature of the Phase Transition in QCD", *Phys. Rev. Lett.* 82, 2048 (1999).
- [54] S.A. Voloshin and A.M. Poskanzer: "The physics of the centrality dependence of elliptic flow", *Phys. Lett. B* 474, 27 (2000) 161.
- [55] S. Voloshin and Y. Zhang: "Flow Study in Relativistic Nuclear Collisions by Fourier Expansion of Azimuthal Particle Distributions", *Z.Phys.C* 70:665-672, 1996.

- [56] A.M. Poskanzer and S.A. Voloshin: "Methods for analyzing anisotropic flow in relativistic nuclear collisions", Phys. Rev. C 58, 1671 (1998) 160.
- [57] P. Steinberg, Relativistic heavy ion physics: Results from AGS to RHIC, eConf C020620 (2002) FRBT03, arXiv:nucl-ex/0210009 [nucl-ex]. [,168(2002)].
- [58] B. Muller, J. Schukraft, and B. Wyslouch, First Results from Pb+Pb collisions at the LHC, Ann. Rev. Nucl. Part. Sci. 62 (2012) 361-386, arXiv:1202.3233 [hep-ex].
- [59] U. Heinz and R. Snellings, Collective flow and viscosity in relativistic heavy-ion collisions, Ann. Rev. Nucl. Part. Sci. 63 (2013) 123-151, arXiv:1301.2826 [nucl-th].
- [60] A. Andronic, P. Braun-Munzinger, and J. Stachel, Phys. Lett. B 673, 142 (2009).
- [61] P. Braun-Munzinger, J. Stachel, and C. Wetterich, Phys. Lett. B 596, 61 (2004).
- [62] A. Andronic, P. Braun-Munzinger, K. Redlich, and J. Stachel, J.Phys.G G38, 124081 (2011).
- [63] R. Rapp and E. V. Shuryak, Phys. Rev. Lett. 86, 2980 (2001).
- [64] A. Andronic and P. Braun-Munzinger and K. Redlich and J. Stachel. The statistical model in Pb-Pb collisions at the LHC. Nuclear Physics A , 904-905(0):535c-538c, 2013.
- [65] J. Steinheimer, J. Aichelin, and M. Bleicher. Physical review letters, 110(4):042501, 2013.
- [66] CMS Collaboration. Measurement of the Pseudorapidity and Centrality Dependence of the Transverse Energy Density in Pb-Pb Collisions at $\sqrt{s_{NN}} = 2.76$ TeV. Physical Review Letters, 109:152303, October 2012.
- [67] E. V. Shuryak. Quantum chromodynamics and the theory of super- dense matter. Physics Reports, 61(2):71-158, May 1980.
- [68] J.T. Mitchell (for the PHENIX Collaboration), arXiv:1601.00904.

- [69] Ranbir Singh et al., Advances in High Energy Physics 761474, (2013).
- [70] B. Abelev et al.(ALICE Collaboration), JHEP 06 190, (2015) .
- [71] P. Kovtun, D. Son, and A. Starinets: "Viscosity in Strongly Interacting Quantum Field Theories from Black Hole Physics", Phys. Rev. Lett. 94, 111601 (2005).
- [72] A. Adare et al. (PHENIX Collaboration), Energy Loss and Flow of Heavy Quarks in Au+Au Collisions at $\sqrt{s_{NN}} = 200$ GeV, Phys. Rev. Lett. 98, 172301 (2007), nucl-ex/0611018.
- [73] Z.W. Lin and C. M. Ko, Phys. Rev. Lett. 89, 202302 (2002);
- [74] D. Molnar and S. A. Voloshin, Phys. Rev. Lett. 91, 092301 (2003);
- [75] R. C. Hwa and C. B. Yang, Phys. Rev. C 67, 064902 (2003);
- [76] R. J. Fries, B. Muller, C. Nonaka, and S. A. Bass, Phys. Rev. Lett. 90, 202303 (2003);
- [77] V. Greco, C. M. Ko, and P. Levai, Phys. Rev. Lett. 90, 202302 (2003).
- [78] S. A. Voloshin, A. M. Poskanzer, and R. Snellings, Collective phenomena in non-central nuclear collisions, (2008), 0809.2949.
- [79] M. L. Miller, K. Reygers, S. J. Sanders, and P. Steinberg, Glauber modeling in high energy nuclear collisions, Ann. Rev. Nucl. Part. Sci. 57, 205 (2007), nucl-ex/0701025.
- [80] A. Adare et al. (PHENIX Collaboration), Scaling properties of azimuthal anisotropy in Au + Au and Cu + Cu collisions at $\sqrt{s_{NN}} = 200$ -GeV, Phys. Rev. Lett. 98, 162301 (2007), nucl-ex/0608033.
- [81] STAR Collaboration. Identified Baryon and Meson Distributions at Large Transverse Momenta from Au + Au Collisions at $\sqrt{s_{NN}} = 200$ GeV. Physical Review Letters, 97:152301, October 2006.

- [82] PHENIX Collaboration. Scaling Properties of Proton and Antiproton Production in $\sqrt{s_{NN}} = \text{GeV}$ Au+Au Collisions. Physical Review Letters, 91:172301, October 2003.
- [83] ALICE Collaboration. Production of charged pions, kaons and protons at large transverse momenta in pp and Pb-Pb collisions at $\sqrt{s_{NN}} = 2.76 \text{ TeV}$. Physics Letters B, 736:196-207, September 2014.
- [84] P. Bozek and I. Wyskiel-Piekarska. Particle spectra in Pb-Pb collisions at $\sqrt{s_{NN}} = 2.76 \text{ TeV}$. Physical Review C, 85(6):064915, 2012.
- [85] R. J. Fries, B. Müller, C. Nonaka, and S. A. Bass. Hadron production in heavy ion collisions: Fragmentation and recombination from a dense parton phase. Physical Review C, 68(4):044902, 2003.
- [86] K. Werner, I. Karpenko, M. Bleicher, T. Pierog, and S. Porteboeuf-Houssais. Jets, bulk matter, and their interaction in heavy ion collisions at several TeV. Physical Review C, 85(6):064907, 2012.
- [87] Thesis of Christine Nattrass; nattrass.utk.edu/NattrassThesis.pdf
- [88] R. J. Fries, B. Muller, C. Nonaka, and S. A. Bass, Phys. Rev. C 68, 044902 (2003).
- [89] R. J. Fries, S. A. Bass, and B. Muller, Phys. Rev. Lett. 94, 122301 (2005).
- [90] R. C. Hwa and C. B. Yang. Recombination of shower partons in fragmentation processes. Physical Review C, 70:024904, August 2004.
- [91] R. C. Hwa and C. B. Yang. Recombination of shower partons at high pT in heavy-ion collisions. Physical Review C, 70:024905, August 2004.
- [92] R. C. Hwa. Hadron Correlations in Jets and Ridges Through parton Recombination. arXiv:0904.2159 [nucl-th], 2009.

- [93] L. Zhu and R. C. Hwa. Effects of Shower Partons on Soft and Semihard hadrons Produced in Pb-Pb Collisions at $\sqrt{s_{NN}} = 2.76\text{TeV}$. arXiv:1406.5733 [nucl-th], 2014.
- [94] ALICE Collaboration. Production of charged pions, kaons and protons at large transverse momenta in pp and Pb-Pb collisions at $\sqrt{s_{NN}} = 2.76\text{ TeV}$. Physics Letters B, 736:196-207, September 2014.
- [95] R. J. Fries, V. Greco, and P. Sorensen, Coalescence Models For Hadron Formation From Quark Gluon Plasma, (2008), 0807.4939.
- [96] ALICE Collaboration: "Measurement of charged jet suppression in Pb-Pb collisions at $\sqrt{s_{NN}} = 2.76\text{ TeV}$ ", JHEP 30 (2014) 013.
- [97] ALICE Collaboration: "Particle-Yield Modification in Jet- like Azimuthal Dihadron Correlations in Pb-Pb Collisions at $\sqrt{s_{NN}} = \text{TeV}$ ", Phys. Rev. Lett. 108, 092301 (2012).
- [98] C.A. Salgado and U.A. Wiedemann: "Medium Modification of Jet Shapes and Jet Multiplicities", Phys. Rev. Lett. 93, 042301 (2004) 294, 296, 331.
- [99] I. Vitev, S. Wicks and B.W. Zhang: "A theory of jet shapes and cross sections: from hadrons to nuclei", JHEP 0811: 093, 2008.
- [100] F. Arleo: "(medium-modified) Fragmentation Functions", Eur. Phys. J. C 61: 603-627, 2009.
- [101] ALICE Collaboration: "Suppression of Charged Particle Production at Large Transverse Momentum in Central Pb-Pb Collisions at $\sqrt{s_{NN}} = 2.76\text{ TeV}$ ", Phys. Lett. B 696 (2011) 30-39.
- [102] J. Binnewies, B. A. Kniehl, and G. Kramer. Pion and kaon production in e-e and e-p collisions at next-to-leading order. Physical Review D, 52: 4947-4960, November 1995.
- [103] B. A. Kniehl and G. Kramer and B. Potter. Fragmentation functions for pions, kaons, and protons at next-to-leading order. Nuclear Physics B, 582(1-3): 514-536, 2000.

- [104] A. Adare et al., (PHENIX Collaboration), Phys. Rev. Lett. 101, 232301 (2008).
- [105] J. Adams et al. (STAR Collaboration), Phys. Rev. Lett. 91, 172302 (2003).
- [106] B.I. Abelev et al. (STAR Collaboration), Phys. Rev. Lett. 97, 152301 (2006).
- [107] I. Vitev and M. Gyulassy, Phys. Rev. Lett. 89, 252301 (2002).
- [108] S. Chatrchyan et al. (CMS Collaboration), Eur. Phys. J. C 72, 1945 (2012).
- [109] B. B. Abelev et al. (ALICE Collaboration) Phys. Lett. B 720, 52 (2013).
- [110] ALICE Collaboration, K. Aamodt et al., Suppression of Charged Particle Production at Large Transverse Momentum in Central Pb-Pb Collisions at $\sqrt{s_{NN}} = 2.76$ TeV, Phys. Lett. B696 (2011) 30-39, arXiv:1012.1004 [nucl-ex].
- [111] J. Adam et. al (ALICE Collaboration), Phys. Rev. C 93, 034913 (2016).
- [112] M. Cacciari, G. P. Salam, and G. Soyez. The anti-kt jet clustering algorithm. Journal of High Energy Physics, 2008(04) April 2008.
- [113] S. Catani, Y. L. Dokshitzer, M. H. Seymour, and B. R. Webber. Nuclear Physics B, 406(1-2),187 - 224, September 1993.
- [114] J. Adams et al. (STAR Collaboration), Evidence from d + Au measurements for final-state suppression of high p_T hadrons in Au + Au collisions at RHIC, Phys. Rev. Lett. 91, 072304 (2003), nucl-ex/0306024. 166
- [115] C. Adler et al (STAR Collaboration), Phys. Rev. Lett. 90, 082302 (2003).
- [116] L. Adamczyk et al. (STAR Collaboration), Phys. Rev. Lett. 112, 122301 (2014).
- [117] K. Aamodt et al. (ALICE Collaboration), Phys. Rev. Lett. 108, 092301 (2012).
- [118] ALICE Collaboration. Harmonic decomposition of two particle angular correlations in Pb-Pb collisions at. Physics Letters B, 708(3- 5):249-264, February 2012.

- [119] ALICE Collaboration. Particle-yield modification in jetlike azimuthal dihadron correlations in Pb-Pb collisions at $\sqrt{s_{NN}} = 2.76$ TeV. Physical Review Letters, 108(March):1-11, 2012.
- [120] CERN-THESIS-2016-032, Veldhoen, Misha (Utrecht U.), <http://cds.cern.ch/record/2151947?ln=e>
- [121] CMS Collaboration, Phys. Lett. B 718 (2013) 795-814
- [122] B. Abelev et al. (ALICE Collaboration), Physics Letters B 719 (2013), pp. 29-41
- [123] B. Abelev et al. (ALICE Collaboration), Phys. Lett. B 726 (2013) 164-177
- [124] B. Abelev et al. (ALICE Collaboration), Phys. Rev. C 90 (2014) 054901
- [125] B. Abelev et al. (ALICE Collaboration), Phys. Lett. B 728 (2014) 25-38
- [126] A. Adare et al. (PHENIX Collaboration) , Phys. Rev. Lett. 114, 192301 (2015)
- [127] CMS Collaboration, Phys. Lett. B 742 (2015) 200-224
- [128] B. Abelev et al. (ALICE Collaboration), Phys. Rev. Lett. 110, 082302 (2013)
- [129] Centrality dependence of charged jet production in p-Pb collisions at $\sqrt{s_{NN}} = 5.02$ TeV., Eur. Phys. J. C 76 (2016) 271
- [130] Kevin Dusling and Raju Venugopalan, Phys. Rev. D 87 (2013), 094034
- [131] K. Werner et al., Phys.Rev.Lett. 112 (2014) 23, 232301.
- [132] K. Werner, Iu. Karpenko, T. Pierog., Phys.Rev.Lett. 106 (2011) 122004.
- [133] Guo-Liang Ma and Adam Bzdak, Phys. Lett. B 739 (2014) 209-213
- [134] Adam Bzdak and Guo-Liang Ma, Phys. Rev. Lett. 113, 252301(2014)
- [135] Identified particle production in pp collisions at 7 and 13 TeV measured with ALICE. (Rafael Derradi De Souza on behalf of the ALICE Collaboration, SQM2016) <https://indico.cern.ch/event/403913/contributions/2142003/>

- [136] S. S. Adler, et al. PHENIX Collaboration), Phys. Rev. C 69 (2004) 034909
- [137] B. Ablev et al. (ALICE Collaboration), Phys. Lett. B 736 (2014) 196-207
- [138] K. Werner et al., Phys.Rev. C89 (2014) 6, 064903.
- [139] R. Fries, B. Muller, C. Nonaka, and S. Bass, Phys. Rev. Lett. 90 (2003) 202303.
- [140] V. Greco, C. Ko, and P. Levai, Phys. Rev. Lett. 90 (2003) 202302.
- [141] E. Shuryak and I. Zahed, (2013), hep-ph/1301.4470.
- [142] Debojit Sarkar, Subikash Choudhury, Subhasis Chattopadhyay, Physics Letters B 760 (2016) 763768
- [143] Debojit Sarkar, Subikash Choudhury, Subhasis Chattopadhyay, Physical Review C 94, 044909 (2016)
- [144] N. M. Abdelwahab et. al (STAR Collaboration) Phys. Lett. B 751 (2015) 233-240
- [145] S.S. Adler et. al (PHENIX Collaboration) Phys. Rev. C 71 (2005) 051902

Chapter 2

Effect of radial flow and hadronization by coalescence on two particle correlations with identified triggers at intermediate p_T in p-Pb collisions at $\sqrt{s_{NN}} = 5.02$ TeV

2.1 Introduction

Recent two particle correlation measurements in pp [1] and p-Pb collisions at LHC energies [2–5] and d-Au collisions at RHIC energy [6] have revealed the existence of a near-side long-range structure over a large pseudo-rapidity(η) separation. The so-called “ridge” like structure was initially observed in two particle angular correlation measurements in heavy ion collisions where it has been attributed to the hydrodynamical expansion of the medium and can be reasonably described by the second and third order Fourier harmonics generally represented as elliptic (v_2)

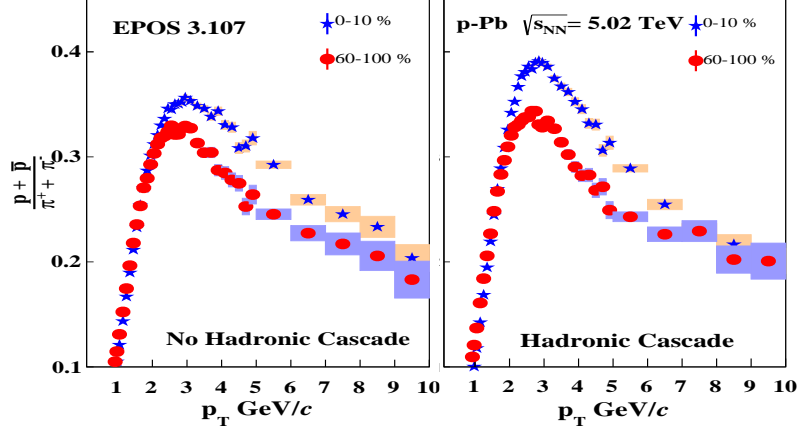
and triangular (v_3) flow [2, 3]. Other observations like mass-ordering of the elliptic flow coefficient (v_2) of identified particles [3], quark-scaling of v_2 [7] and the baryon-to-meson enhancement at intermediate p_T [5] which were once attributed to the hydrodynamical evolution of a strongly interacting system were also observed in small collision systems- indicating that the underlying dynamics in small collision systems might be analogous to that of heavy-ions. However measurements sensitive to the energy loss show a stark difference. In case of heavy ion collisions, the highly energetic partons (jets) are expected to lose energy in the medium prior to fragmentation. An immediate consequence is the suppression of the invariant yield of high- p_T particles when compared to the p-p collisions at the same collision energy referred to as “jet quenching” [8]. Earlier measurements at RHIC have revealed that the yield of high- p_T particles are strongly suppressed in central Au-Au collisions whereas no such suppression was reported for d-Au collisions at the same energy [9, 10]. At LHC energy, suppression in Pb-Pb collisions persist upto $p_{T,jet}$ of 100 GeV/c [11] but in p-Pb collisions, nuclear modification factor, R_{pPb} measurements do not show any deviation from unity [12]. This indicates that the system produced in pp or p-Pb collisions at LHC energies may be transparent to the hard-QCD processes. The experimental observations suggesting collectivity in small collision systems can be reasonably described by both hydro based models like EPOS-3 [13, 14] and transport models like AMPT [15, 16], but the hydrodynamical modelling of small systems like p-Pb is debatable [17]. Recently, a series of studies have shown that AMPT can reasonably explain the collective-like behaviors in p-Pb collisions through incoherent parton scatterings with a modest parton scattering cross-section [15, 16]. In [18], it has been shown that in the context of the AMPT model the elliptic flow (v_2) generated in Au-Au collisions at $\sqrt{s_{NN}} = 200$ GeV and p-Pb collisions $\sqrt{s_{NN}} = 5.02$ TeV is dominantly due to the anisotropic escape mechanism of partons and contribution from the hydrodynamic pressure gradient is negligible in that case. Also the mass ordering of v_2 in AMPT can be generated from the dynamics of coalescence [19, 20] and hadronic scattering only [21] and not necessarily associated with the hydro like collectivity in the system.

Now, EPOS-3 has also reasonably reproduced the double ridge and mass ordering of v_2 of iden-

tified particles in high multiplicity p-Pb collisions as observed by the ALICE collaboration at CERN [2] [3]. This model has successfully explained the nuclear modification factor R_{pPb} for NSD (non single-diffractive) p-Pb collisions at $\sqrt{s_{NN}} = 5.02$ TeV as measured by ALICE [14] [22]. In section VIII of [14], the multiplicity dependence of the identified particle spectra as measured by ALICE in p-Pb collisions at 5.02 TeV has been compared with different event generators (e.g. QGSJETII, AMPT and EPOS 3). Models like QGSJETII (contains no flow) and AMPT under predicts the spectra at intermediate p_T . The mismatch with the data is more prominent for heavier particles (proton, lambda) compared to the low mass ones (e.g. pion) indicating the need of flow like effect (mainly radial flow) to explain the spectra at intermediate p_T . Radial flow originated in EPOS-3 pushes heavier particles more compared to the lighter ones from lower to higher p_T , describing the spectra at the intermediate p_T in a better way [14].

In this thesis, the two-particle correlation technique has been adopted to obtain the near-side jet-like yield between the identified triggers ($1.5/2.0 < p_T < 4.0$ GeV/ c) and the un-identified associated charged particles ($1.0 < p_T < 4.0$ GeV/ c) as a function of event multiplicity in p-Pb collisions at 5.02 TeV. p_T ranges of trigger particles are chosen in the region where an inclusive baryon to meson enhancement has been observed in p-Pb collisions at 5.02 TeV [5]. It is similar to that found in heavy ion collisions [23] [24], where it has been discussed in terms of radial flow and/or quark coalescence mode of hadronization [25–27]. Radial boost, generated during the hydrodynamical evolution, pushes the massive hadrons more to higher p_T and provide a natural explanation to the enhanced baryon generation at intermediate p_T . Assuming the applicability of the hydrodynamics in high multiplicity p-Pb collisions, a larger radial flow has been suggested in high multiplicity p-Pb collisions compared to central Pb-Pb collisions [28] and supported by the experimental observation [5]. The rise in baryon-to-meson ratio at intermediate p_T with increase in multiplicity in p-Pb collisions at $\sqrt{s_{NN}} = 5.02$ TeV is qualitatively captured by both hydro based model EPOS 3 [14] and coalescence model of hadronization [29] [30] as implemented in the string melting version of AMPT. Therefore, the exact origin of baryon enhancement remains incomprehensible till date. Thus, it calls for more differential measurements which could possibly

a)



b)

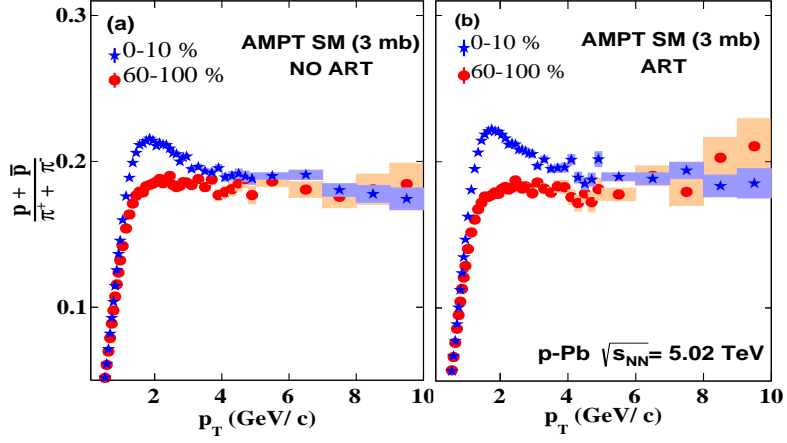


Figure 2.1: [Color online] Inclusive proton over pion ratio as obtained from (a) EPOS 3.107 and (b) AMPT SM version (right) in 0-10% and 60-100% event classes of p-Pb collisions at 5.02 TeV.

distinguish whether the enhanced baryon production is a natural consequence of the radial flow or a manifestation of particle production via quark recombination.

The inclusive proton to pion enhancement as obtained from EPOS 3 and AMPT is shown in Fig 2.1. Hadrons pushed from lower to higher p_T by radial flow or generated by quark coalescence are expected not to exhibit a short range jet-like correlation beyond the expected flow (ridge) like correlation [33, 34]. In this analysis pion and proton triggered jet-like yield (per trigger) is calculated as a function of event multiplicity after subtracting the flow-modulated back-ground estimated from large $|\Delta\eta|$. The bulk/flow subtracted near-side jet peak is dominated by the hard triggered (jet) correlation only. Since the correlation functions are normalized by both hard and soft triggers, the soft triggers without any jet-like correlated partners in the bulk subtracted jet peak are expected to cause a dilution in the per trigger jet-like yield. With increase in multiplicity, the proportion of soft triggers increase and the rate of increase has a species dependence as the soft processes like coalescence model of hadronization and/or radial flow favour proton production over the pion at intermediate p_T (trigger p_T range for this analysis). Thus once bulk is subtracted, the baryon-triggered jet like yield is expected to get suppressed more compared to the suppression in pion triggered correlation while going from low to high multiplicity event classes - an effect commonly referred to as "trigger dilution" [31] [32].

In this work, the effect of hydrodynamical flow and coalescence mode of hadronization on per-trigger yield associated with pion and proton triggers at intermediate p_T has been studied using EPOS 3 and AMPT string melting model. In absence of significant jet-medium interplay in small collision systems like p-Pb, any possible deviation in the multiplicity evolution of the near-side jet-like yield from AMPT string melting [33] compared to the same observable in EPOS [34] can be used to disentangle the effect of coalescence from the hydrodynamical flow and will be helpful to understand the underlying dynamics responsible for the observed collective like signatures in high multiplicity p-Pb collisions at LHC energy.

2.2 The EPOS3 Model

EPOS3 basically contains a hydrodynamical approach based on flux tube initial conditions [14] [35] [36]. This is a parton based model where the partons initially undergo multiple scatterings. Each scattering is composed of hard elementary scattering with initial and final state linear parton emission- forming parton ladder or "pomeron". Each parton ladder has it's own saturation scale Q_s^2 depending on the number of connected participants and it's center of mass energy and this will separate the soft processes from hard/p-QCD ones. This formalism is referred as "Parton based Gribov Regge Theory" and explained in detail in [13] [36]. In this formalism each ladder may be considered as a longitudinal colour field which can be treated as a relativistic string. After multiple scatterings the final state partonic system consists of mainly longitudinal colour flux tubes carrying transverse momentum of the hard scattered partons in transverse direction. Depending on the energy of the string segments and local string density - the high density areas form the "core"(containing string segments more than a critical value per unit area in given transverse slices) and the low density area form the "corona" [37]. The core part basically forms the bulk matter. The strings in the core thermalize and then undergo hydrodynamical expansion and finally hadronize. The strings in the corona hadronize by Schwinger's mechanism and basically constitutes the jet part (high p_T particles) of the system. The hadrons formed in the final stage can undergo scattering. EPOS3 introduces a theoretical scheme which takes into account event by event 3+1D viscous hydrodynamical evolution of the bulk matter, jets and their interactions [13]. In the context of this model , multiplicity of an event is proportional to the number of pomerons whose positions are generated randomly and may lead to an elliptical shape of the core part eventually creating a $\cos(2\Delta\phi)$ shaped correlation function [13]. The translational invariance of the structure finally generates a double ridge. In [13], EPOS3 has reasonably reproduced the double ridge and mass ordering of v_2 of identified particles in high multiplicity p-Pb collisions as observed by the ALICE collaboration at CERN [2] [3]. This model has also explained the nuclear modification factor R_{pPb} [14] [22], radial flow like effects on the identified particle spectra [14], baryon to meson enhancement at intermediate p_T [14] among

others in p-Pb collisions at $\sqrt{s_{NN}} = 5.02$ TeV.

In Fig 2.1. the inclusive proton to pion ratio as obtained from EPOS 3.107 is shown with hadronic scattering on and off. In both cases a clear p/π enhancement at intermediate p_T has been observed. The hadronic rescattering shows a slight enhancement in the ratio indicating the generation of mild radial flow during hadronic evolution. Two particle correlation analysis has been performed with trigger particles from intermediate p_T ($2.0 < p_T < 4.0$ GeV/ c) using the data generated by EPOS 3 event generator. The goal of this study is to evaluate how radial flow affects the jet like per trigger yield associated with proton and pion triggers in different multiplicity classes.

2.3 The AMPT Model

AMPT is a Monte-Carlo event generator [38] that has successfully modeled various bulk properties of matter produced in heavy ion collision at RHIC and LHC energies[39, 40]. Recent studies have shown that bulk phenomena like long range correlations and azimuthal anisotropy (v_2 and v_3) in small collision systems are also reasonably reproduced by AMPT [15, 16, 41]. If broadly classified, the model has two modes: default (minijets and strings) and string melting [42]. The spatial and momentum distributions of minijet partons and excited soft strings, obtained from the HIJING model [43] are used as initial conditions for subsequent modeling of partonic evolution.

In the default version, only minijet partons are subjected to partonic scattering modeled by Zhang Parton Cascade (ZPC) [44] scheme. Currently this model includes only 2-body elastic scatterings with scattering cross-section derived from the leading order p-QCD calculations as:

$$\sigma = \frac{9\pi\alpha_s^2}{2\mu^2} \quad (2.1)$$

where α_s is the QCD coupling constant for strong interactions and μ is the Debye screening mass of gluonic medium. Although, it is a function of temperature and density of the partonic medium but in ZPC it is parameterized to fix the magnitude of scattering cross-section. At the completion of the cascade, minijet partons are recombined with their parent strings and hadronized via the Lund string fragmentation, using the following fragmentation function [38]:

$$f(z) \propto z^{-1}(1-z)^a \exp(-bm_T^2/z), \quad (2.2)$$

Where z is the light-cone momentum fraction of the produced hadron with respect to that of the fragmenting string and m_T is the transverse mass of the hadron. The fragmentation parameters a and b are set to 0.5 and 0.9 GeV^{-1} for this analysis.

In string melting version, strings are first fragmented to hadrons followed by conversion of these hadrons to valance quarks/antiquarks preserving their flavor and spin quanta. Now the system comprises both minijets and string melted partons, which are further scattered using parton cascade model (ZPC) as discussed above. Once the interaction ceases, partons are re-confined to hadrons via an implementation of coalescence formalism that combines two or three partons nearest in coordinate space to mesons and/or baryons respectively. Mass and flavor of hadrons are determined from the invariant mass and respective flavors of the coalescing partons. Therefore a quark-antiquark pair will be recombined to pions provided di-quark invariant mass is in the proximity of pion mass. The post-hadronization stage is modeled by a relativistic transport model (ART) [45, 46], which guides the hadronic interactions until freeze-out. Detailed discussion on AMPT can be found in [38, 42, 47].

The present work has been carried out on the string melting version of AMPT with parton scattering cross-section of 3 mb ($\alpha_s = 0.4714$ and $\mu = 3.22 \text{ fm}^{-1}$). To study the effect hadronic interactions on the inclusive p/π ratio and the near-side jet-like yield, the analysis is performed with hadronic scatterings (ART) on and off. Events are also generated from HIJING [43] event generator with default parameters to perform measurements for baseline study. A detailed

description of this model can be found in [43] [49]. Results from HIJING will be compared to the same obtained from AMPT SM to understand the effect of coalescence model of hadronization on the pion and proton triggered correlation at intermediate p_T .

2.4 Analysis Method

Two particle correlation is a widely used technique in high-energy physics for extracting the properties of the system produced in the ultra relativistically high energetic collisions. In the present analysis the correlation function is obtained among two sets of particles classified as *trigger* and *associated*. The p_T range of trigger and associated particles are $2.0 < p_T < 4.0$ GeV/ c and $1.0 < p_T < 4.0$ GeV/ c respectively and the correlation function has been constructed with a p_T ordering ($p_T^{\text{assoc}} < p_T^{\text{trigger}}$). The pseudo-rapidity of the particles are restricted within $-0.8 < \eta < 0.8$. A 2D correlation function is obtained as a function of the difference in azimuthal angle $\Delta\phi = \phi_{\text{trigger}} - \phi_{\text{associated}}$ and pseudo-rapidity $\Delta\eta = \eta_{\text{trigger}} - \eta_{\text{associated}}$. The same event correlation function is defined as $\frac{dN_{\text{same}}}{N_{\text{trigger}} d\Delta\eta d\Delta\phi}$, where N_{same} is the number of particles associated to triggers particles (N_{trigger}) that are taken from the same event. To correct for pair acceptance the same event correlation function is divided by mixed event correlation function $\alpha \frac{dN_{\text{mixed}}}{d\Delta\eta d\Delta\phi}$. The mixed event correlation function is constructed by correlating the trigger particles in one event to the associated particles from other events belonging to the same multiplicity event class. In case of data analysis, the mixed event correlation function is constructed on terms of both multiplicity and zvtx (for event generators, all the collisions take place at zvtx=0) and will be discussed in chapter 4. The factor α is used to normalize the mixed event to make it unity for pairs where both particles go into approximately the same direction ($|\Delta\eta| \approx 0$, $|\Delta\phi| \approx 0$).

Both p/π ratio and correlation analysis have been performed by dividing the entire minimum bias events into four multiplicity classes based on the total number of charged particles produced (with $p_T > 0.05$ GeV/ c) within $2.8 < \eta < 5.1$. This corresponds to the acceptance range of the ALICE VZERO-A detector in the Pb going direction in case of p-Pb collisions and used for multiplicity class determination by the ALICE collaboration [2],[3]. The multiplicity classes

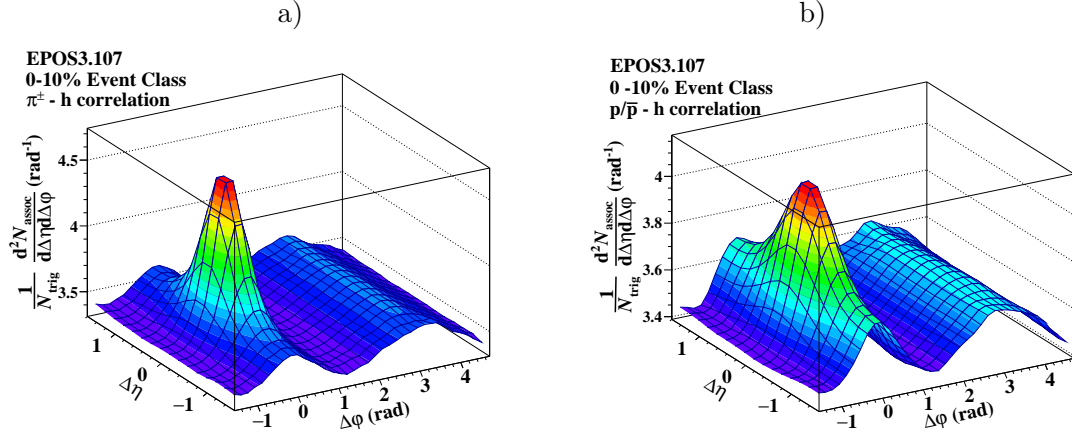


Figure 2.2: [Color online] Two particle $\Delta\eta$ - $\Delta\phi$ correlation function in 0-10 % event class of p-Pb collisions at $\sqrt{s_{NN}} = 5.02$ TeV from EPOS 3 with (a) pion and (b) proton as trigger particles.

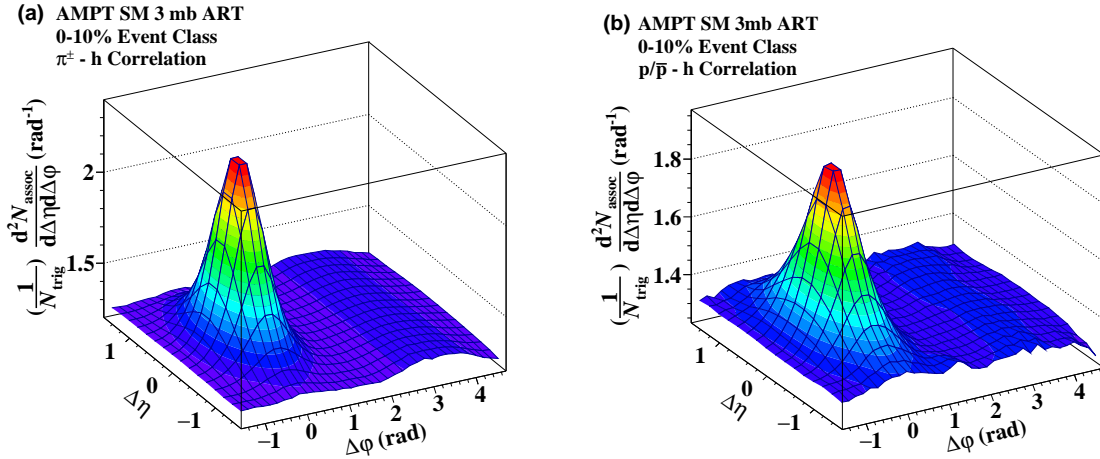


Figure 2.3: [Color online] Two Particle $\Delta\eta$ - $\Delta\phi$ correlation function in 0-10 % event class of p-Pb collisions at $\sqrt{s_{NN}} = 5.02$ TeV from AMPT SM (with ART) with (a) pion and (b) proton as trigger particles.

are denoted as 60-100%, 40-60%, 10-40%, 0-10% from the lowest to the highest multiplicity. Two particle correlation functions with proton and pion triggers in the 0-10% event class as obtained from EPOS 3 and AMPT string melting are given in Fig 2.2 and Fig 2.3. This analysis concentrates only on the near side ($|\Delta\phi| < \pi/2$) of the correlation function. The particles from

jet fragmentation are expected to be confined in a small angular region. To isolate the near side jet-like correlation, we need to subtract the modulation in $\Delta\phi$ arising out of the correlation with the event plane as represented by v_2 , v_3 or higher harmonics. In this analysis the flow modulated background is estimated from large $|\Delta\eta|$ ($|\Delta\eta| \geq 1.1$) and subtracted from the near side jet peak ($|\Delta\eta| < 1.1$) as it is done in [?].

The $\Delta\phi$ projected correlation functions for regions $|\Delta\eta| < 1.1$ (jet) and $|\Delta\eta| > 1.1$ (bulk) and

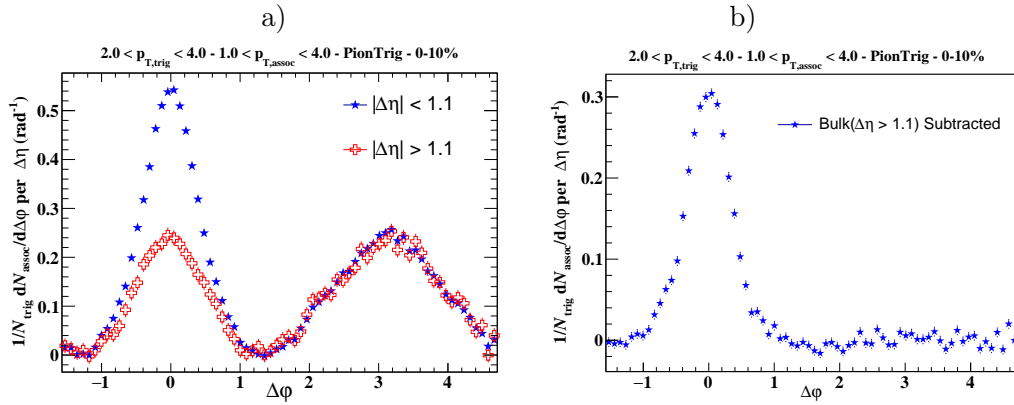


Figure 2.4: [Color online] (a) The $\Delta\phi$ projected correlation function for pion triggered correlation in 0-10% event class in EPOS 3 for two $\Delta\eta$ regions referred to as jet (blue) and bulk (red). (b) The $\Delta\phi$ projected correlation function after bulk subtraction as discussed in the text.

the background subtracted $\Delta\phi$ projected correlation function as obtained from EPOS 3 and AMPT are shown in Fig 2.4 and Fig 2.5. After bulk subtraction the event averaged near side jet like per trigger yield is calculated integrating the $\Delta\phi$ projection in the range $|\Delta\phi| < \pi/2$.

2.5 Results from EPOS3

In this analysis, two particle angular correlation measurements are performed by selecting the trigger particles (pions and protons) from an intermediate p_T range ($2.0 < p_T < 4.0$ GeV/ c), whereas, the associated particles have p_T in the range of $1.0 < p_T < 4.0$ GeV/ c . The intriguing feature of particle production at intermediate transverse momentum is the contribution from both hard and soft processes. In the ambit of EPOS model, particles originating from **corona**

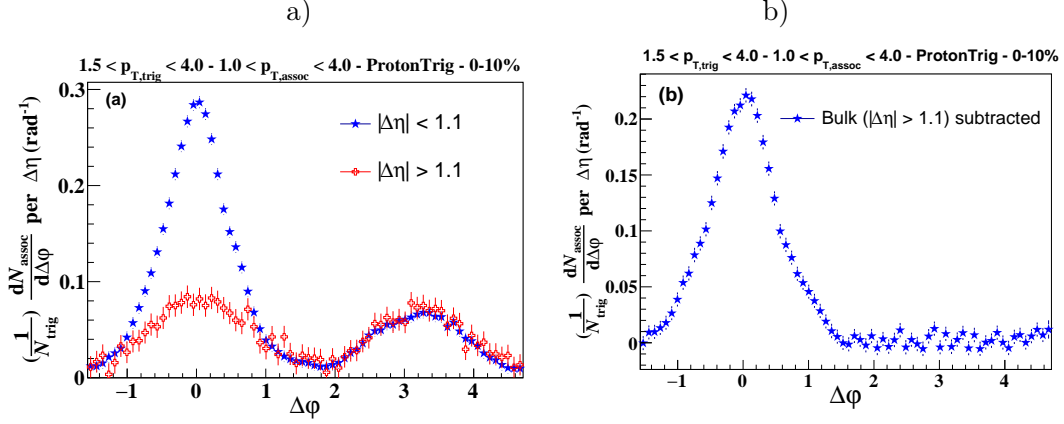


Figure 2.5: [Color online] (a) The $\Delta\phi$ projected correlation function for proton triggered correlation in 0-10% event class in AMPT SM for two $\Delta\eta$ regions referred to as jet (blue) and bulk (red). (b) The $\Delta\phi$ projected correlation function after bulk subtraction as discussed in the text.

are referred to as hard particles and those from the **core** are soft [13].

The two-dimensional correlation structure as obtained from the angular correlation measure-

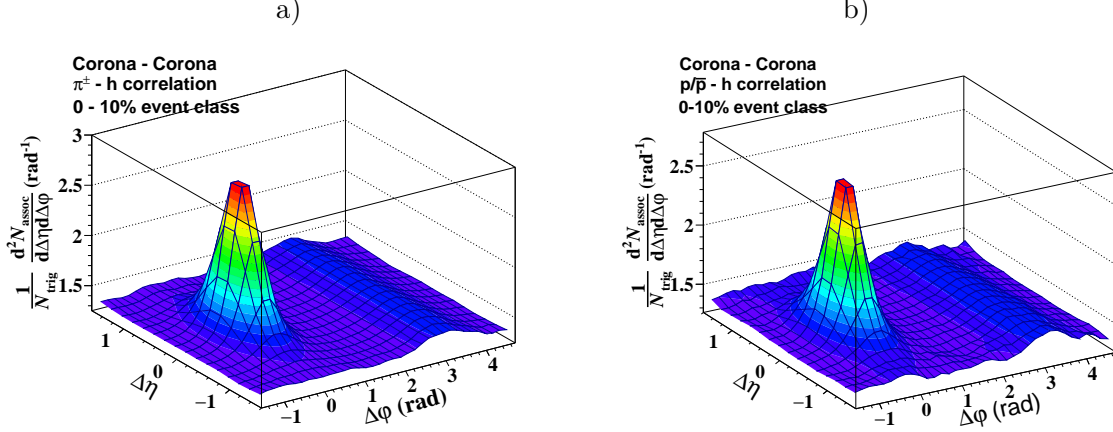


Figure 2.6: [Color online] Two particle $\Delta\eta$ - $\Delta\phi$ correlation function in 0-10 % event class of p-Pb collisions at $\sqrt{s_{NN}} = 5.02$ TeV in case of corona-corona correlation from EPOS 3 with (a) pion and (b) proton as trigger particles.

ments in p-Pb collisions at $\sqrt{s_{NN}} = 5.02$ TeV is shown in Fig 2.2. Particles originating from the core (soft particles) undergo hydrodynamical evolution and expected not to have correlated

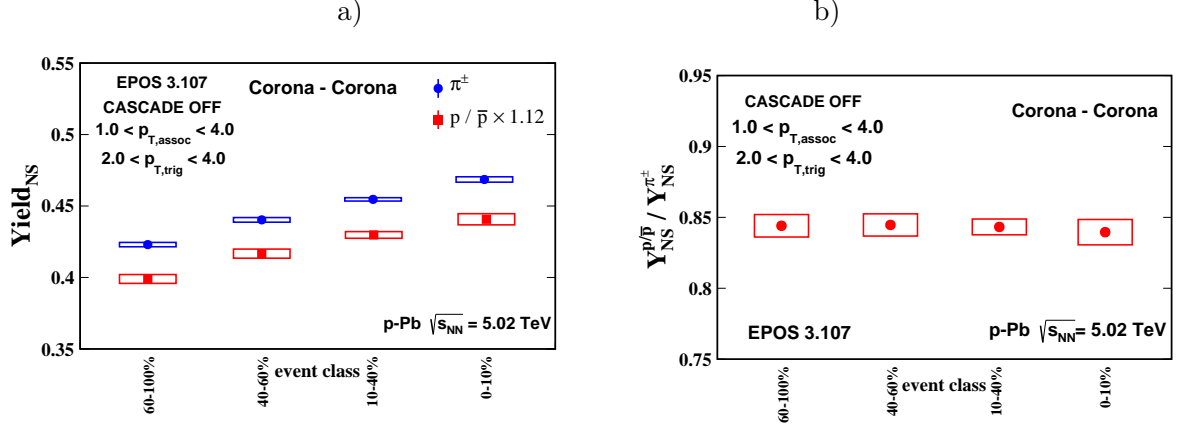


Figure 2.7: [Color online] (a) Multiplicity dependence of the near-side jet-like per trigger yield associated with pion and proton triggers in case of corona - corona correlation in p-Pb collisions at $\sqrt{s_{NN}} = 5.02$ TeV from EPOS 3.107 with hadronic cascade off. (b) Multiplicity dependence of the ratio of the near-side jet-like per trigger yield associated with proton and pion triggers in case of corona - corona correlation in p-Pb collisions at $\sqrt{s_{NN}} = 5.02$ TeV from EPOS 3.107 with hadronic cascade off.

partners beyond the "ridge" or flow like correlations. Thus bulk subtracted near side jet peak is dominated by the hard triggered (origin: corona) correlation. The bulk is estimated from the large $|\Delta\eta|$ ($|\Delta\eta| \geq 1.1$) and subtracted from the correlation function at small $|\Delta\eta|$ ($|\Delta\eta| < 1.1$) as already discussed in the analysis method section. The soft triggers having no small angle correlated hadrons in the bulk subtracted near side jet peak is expected to create a dilution in the per trigger jet-like yield.

To investigate in detail the role of core and corona particles in the trigger dilution effect, the multiplicity evolution of the hard triggered correlation (i.e. corona - corona correlation) has been studied. Particles, stemming out-of the corona only are chosen to construct 2D angular correlations (Fig 2.6) that show a prominent near-side jet peak over a nearly flat baseline. The multiplicity dependence of the near side jet yield (baseline subtracted) in corona - corona correlations are shown in Fig 2.7. Both the pion and proton triggered yields increase with multiplicity but the rate of increase has no trigger species dependence. The ratio of the proton to pion triggered yield is also shown in Fig 2.7. This ratio remains almost constant as a function of

multiplicity, showing no trigger dilution.

Now, in the calculation considering all (both core and corona) particles, there is a near side jet peak over the so-called ridge structure extended over a large $|\Delta\eta|$ as already shown in Fig 2.2. The bulk subtracted near side jet peak is formed by the hard triggered (corona - corona) correlation. But the correlation function is normalized by both soft and hard triggers and the soft triggers without small angle correlated hadrons in the bulk subtracted near side jet peak are expected to generate the trigger dilution effect. As we move from the lowest to highest multiplicity, the proportion of soft triggers increase and thus create a larger dilution in the higher multiplicity classes. The rate of dilution is associated with the rate of increase in the proportion of soft triggers which has a species dependence. In a hydro model like EPOS 3, radial flow pushes more protons than pions from lower to higher p_T ($2.0 < p_T < 4.0$ GeV/ c) creating a baryon to meson enhancement as shown in Fig 2.1. So, a larger rate of dilution is expected in proton triggered correlation compared to the pion triggered case.

In Fig 2.8(a) the multiplicity dependence of the bulk subtracted near side jet-like yield (per trigger) is shown. The pion triggered yield shows almost no variation with multiplicity whereas the proton triggered yield decreases gradually with increase in multiplicity. Comparison with Fig 2.7 shows that both pion and proton triggered yields get diluted with multiplicity but the proton triggered yield has a larger rate of dilution. The different trend in the multiplicity dependence of the pion and proton triggered yields can be attributed to the larger rate of increase of soft proton triggers (pushed by radial flow from lower to higher p_T) with multiplicity. In Fig.2.5(b) the multiplicity dependence of the ratio of proton to pion triggered yield is shown. A similar dilution pattern is observed from the lowest to highest multiplicity event classes with both hadronic cascade on and off (as shown in Fig 2.8 and Fig 2.9) - indicating hydrodynamics as a source of the trigger dilution observed here. The results obtained from corona-corona correlation only and considering all particles as shown in Fig 2.7 and Fig 2.8 conclude that the expected dilution comes only from the core. A similar study has been performed by the PHENIX [32] and STAR collaborations [31] in min-bias pp, d-Au and Au-Au collisions at $\sqrt{s_{NN}} = 200$ GeV. A hint of

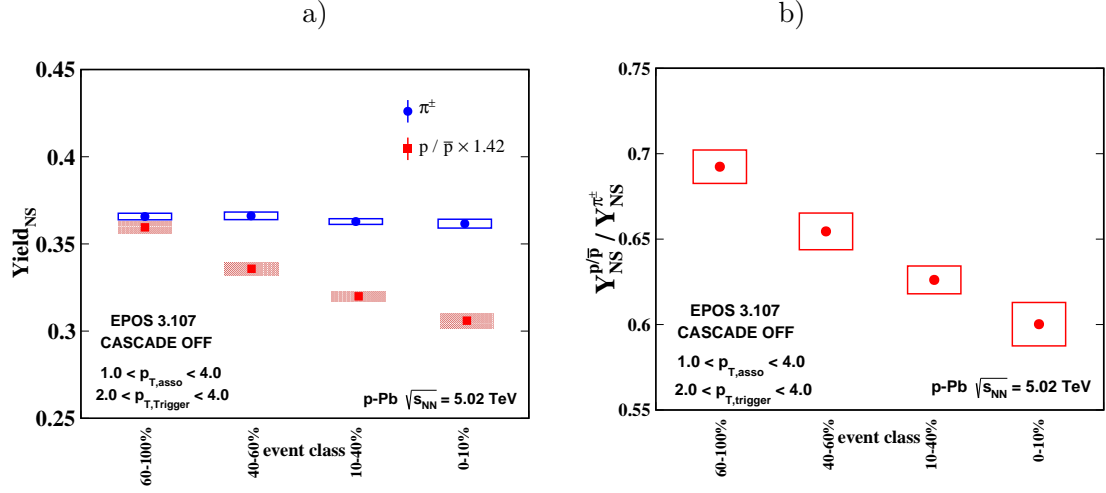


Figure 2.8: [Color online] (a) Multiplicity dependence of the near-side jet-like per trigger yield (bulk subtracted) associated with pion and proton triggers (particles from both core and corona are considered) in p-Pb collisions at $\sqrt{s_{NN}} = 5.02$ TeV from EPOS 3.107 without hadronic cascade. (b) Multiplicity dependence of the ratio of the near-side jet like per trigger yield (bulk subtracted) associated with proton and pion triggers (particles from both core and corona are considered) in p-Pb collisions at $\sqrt{s_{NN}} = 5.02$ TeV from EPOS 3.107 without hadronic cascade.

trigger dilution has been observed in the most central Au-Au collisions compared to the min-bias d-Au/ pp as shown in Fig 2.10. The pion triggered yield increases in the most central Au-Au collisions compared to the min-bias d-Au whereas, proton triggered yield remains almost unchanged or slightly reduced. The different trend in pion and proton triggered yields from min-bias d-Au to the most central Au-Au collisions has been argued to be a combined effect of competitive processes that include soft physics processes (coalescence model of hadronization and/or radial flow) and jet-medium interplay [31] [32]. A larger modification in the proton(non pion) triggered yield was expected as a larger fraction of proton triggers are predicted to be generated from gluon jets rather than quark jets compared to pion triggers [31]. Due to the difference in the colour charge, a larger medium induced energy loss by gluon jets is expected - resulting in higher jet like yields for proton (non pion) triggers as argued in [31]. However, lack of any such enhancement in data [31] has been attributed to the dominance of soft processes towards baryon production

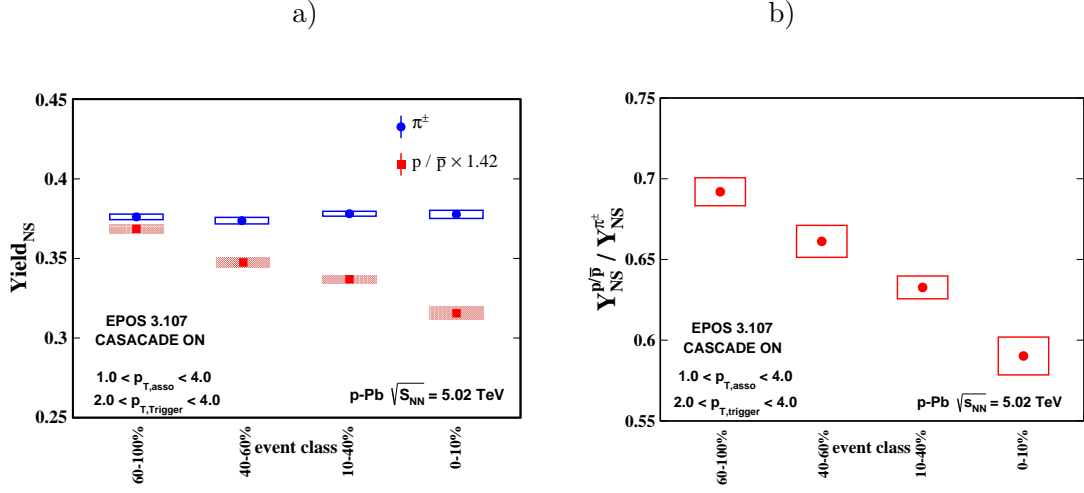


Figure 2.9: [Color online] (a) Multiplicity dependence of the near-side jet-like per trigger yield (bulk subtracted) associated with pion and proton triggers (particles from both core and corona are considered) in p-Pb collisions at $\sqrt{s_{NN}} = 5.02$ TeV from EPOS 3.107 with hadronic cascade on. (b) Multiplicity dependence of the ratio of the near-side jet like per trigger yield (bulk subtracted) associated with proton and pion triggers (particles from both core and corona are considered) in p-Pb collisions at $\sqrt{s_{NN}} = 5.02$ TeV from EPOS 3.107 with hadronic cascade on.

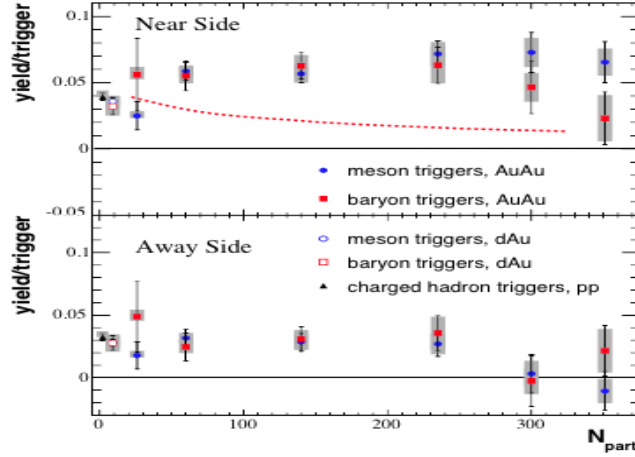


Figure 2.10: [Color online] N_{part} dependence of the near-side jet like yield associated with baryon and meson triggers in Au-Au collisions at $\sqrt{s_{NN}} = 200$ GeV [32] and its comparison with the minimum bias d-Au collisions at $\sqrt{s_{NN}} = 200$ GeV.

at intermediate p_T . It should be noted that in A-A collisions where jet quenching is prominent, the quenched energy is expected to manifest itself in terms of particles at low and intermediate p_T possibly affecting both jet and bulk in a way that is yet to be understood un-ambiguously. In small collision systems, like p-Pb, where medium induced modification of jets is observed to be less significant compared to that in the heavy ions [22] [14], a larger suppression in proton triggered yield (creating trigger dilution) can be dominantly associated with the presence of soft triggers at intermediate p_T created by soft processes without significant contribution from the jet-medium interplay.

In this study, it has been shown that a model (EPOS) having hydrodynamical flow can generate trigger dilution in small collision systems (p-Pb) at LHC energy. Therefore hydrodynamics can be taken as an alternative to other explanation like coalescence model of hadronization which has been argued to be one of the possible reasons for trigger dilution in [31] [32]. This observation puts a strong motivation for such a study by the LHC experiments as this observable may serve as an useful probe to investigate the presence of collective dynamics in small collision systems. Further comparison with other models like AMPT string melting (incorporates coalescence model of hadronization) and data at LHC energy will be essential to constrain different models aiming to explain the observed signatures of collective behaviours in small collision systems.

2.6 Results from AMPT

In this section, results from AMPT string melting version in p-Pb collisions at $\sqrt{s_{NN}} = 5.02$ TeV has been discussed. Again, the trigger particles are selected from the intermediate p_T range ($1.5 < p_T < 4.0$ GeV/ c) where the inclusive proton to pion enhancement has been observed in the string melting version of AMPT as shown in Fig 2.1. To understand the effect of coalescence on the per trigger yield, the result from the AMPT SM model has been compared with the HIJING output where coalescence model of hadronization is not implemented. In absence of significant jet-medium interplay in small collision systems like p-Pb, any modification in the pion and proton triggered jet-like yields compared to the HIJING case may be dominantly attributed to the

dynamics of quark coalescence responsible for inclusive proton to pion enhancement at intermediate p_T . The effect of hadronic cascade on this observable has been studied by performing the analysis with ART (hadronic cascade) on and off. Any possible deviation of the results from the A-A case [47] may also help to understand the possible effect of jet-medium interplay on the per trigger yield associated with identified triggers selected from intermediate p_T . In Fig 2.3 the 2D correlation function for pion and proton triggers in the highest multiplicity (0-10%) event class of p-Pb has been shown. The bulk subtracted near-side jet-like yield (per trigger) as obtained

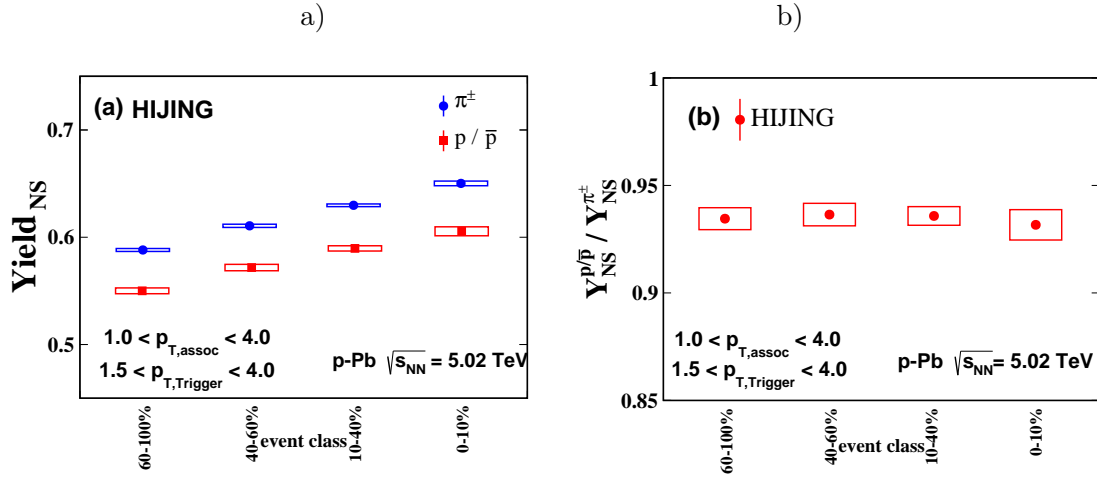


Figure 2.11: [Color online] (a) Multiplicity dependence of the near-side jet-like per trigger yield (bulk subtracted) associated with pion and proton triggers in p-Pb collisions at $\sqrt{s_{NN}} = 5.02$ TeV from HIJING. (b) Multiplicity dependence of the ratio of the near-side jet like per trigger yield (bulk subtracted) associated with proton and pion triggers.

from the HIJING model is shown in Fig 2.11(a). Both pion and proton triggered yields increase with multiplicity but the rate of increase has no trigger species dependence. The ratio of the proton to pion triggered yield is shown in Fig 2.11(b) and it shows no variation with multiplicity. This result is similar to the one obtained from EPOS corona-corona correlation shown in Fig 2.7 - indicating that the absence of radial flow and /coalescence model of hadronization is unable to produce the trigger dilution effect.

In Fig 2.12(a) the multiplicity evolution of the near-side bulk subtracted jet-like yield associ-

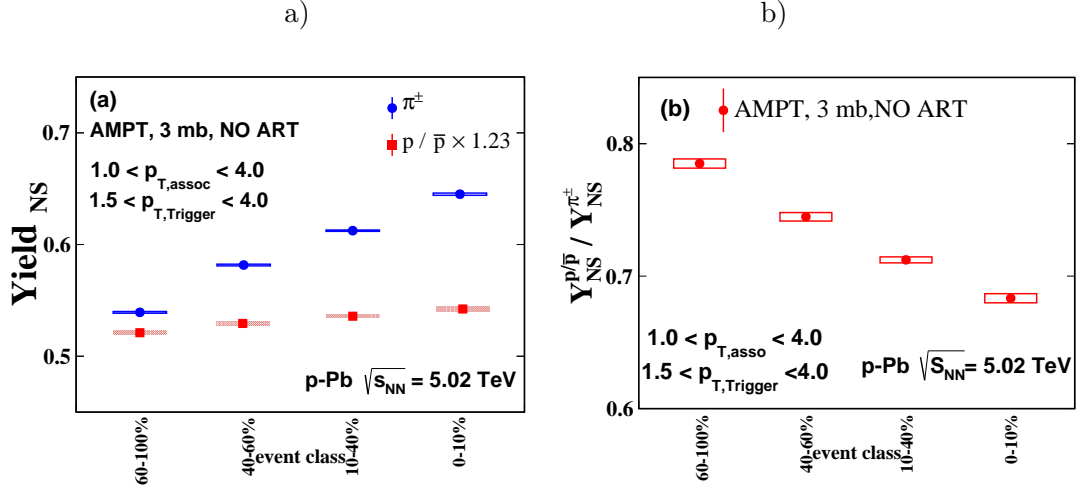


Figure 2.12: [Color online] (a) Multiplicity dependence of the near-side jet like per trigger yield (bulk subtracted) associated with pion and proton triggers in p-Pb collisions at $\sqrt{s_{NN}} = 5.02$ TeV from AMPT SM without hadronic cascade. (b) Multiplicity dependence of the ratio of the near-side jet like per trigger yield (bulk subtracted) associated with proton and pion triggers.

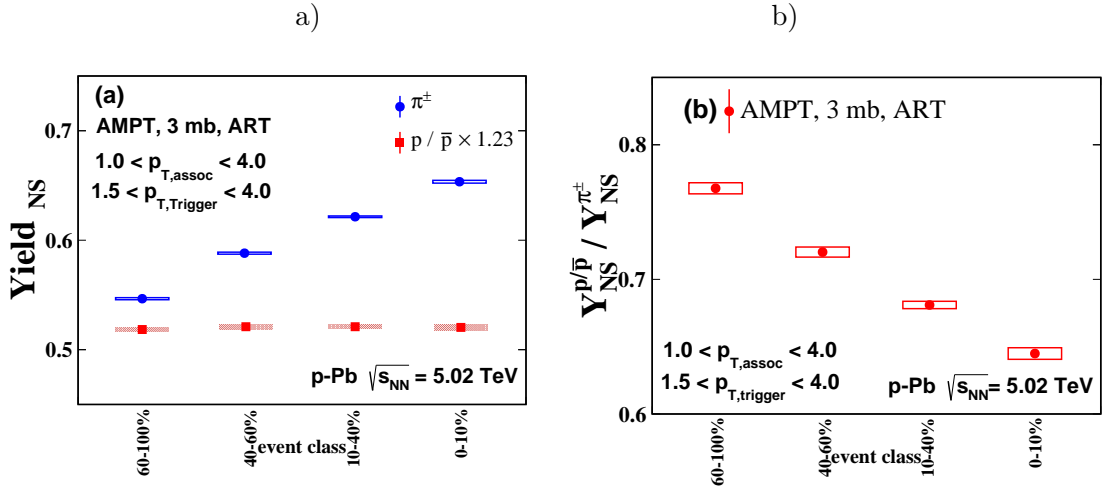


Figure 2.13: [Color online] (a) Multiplicity dependence of the near-side jet like per trigger yield (bulk subtracted) associated with pion and proton triggers in p-Pb collisions at $\sqrt{s_{NN}} = 5.02$ TeV from AMPT SM with hadronic cascade on. (b) Multiplicity dependence of the ratio of the near-side jet like per trigger yield (bulk subtracted) associated with proton and pion triggers.

ated with identified triggers is shown for the AMPT SM case without hadronic cascade. The pion triggered yield increases with multiplicity whereas the proton triggered yield shows a slower rate of increase compared to that of pions - creating trigger dilution as shown in Fig 2.12(b). This trend is quite different from the one obtained from the HIJING (Fig 2.11) and it can be attributed to the dynamics of coalescence implemented in the string melting version of AMPT. Also, this pattern is different from the one we have observed in Pb-Pb case [47] obtained from AMPT SM version. In that case the near-side jet-like pion and proton triggered yield initially increases with multiplicity/ N_{Part} and then the pion triggered yield shows a saturation whereas the proton triggered yield exhibits a gradual suppression [47] as shown in Fig 2.14. As a result the ratio of proton to pion triggered yield [47] decreases with multiplicity - creating trigger dilution. However, no such trigger species dependence of the near side jet-like yield has been

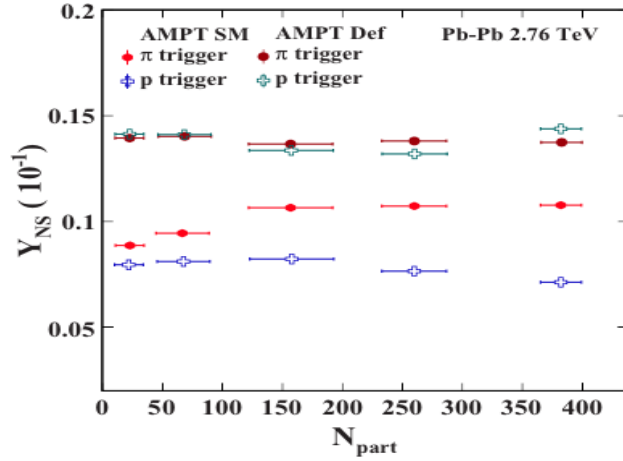


Figure 2.14: [Color online] Centrality dependence of the near-side yield from the background subtracted correlation function. The yields from default version of AMPT have been multiplied by 1.5 for better visualization [47].

observed for the default case as shown in Fig 2.14. In case of Pb-Pb [47], the trigger dilution may be due to the combined effect of competing processes that involve in medium energy loss of jets and quark recombination which creates inclusive proton to pion enhancement at intermediate p_T (trigger p_T region for this analysis). Proton production at intermediate p_T is more favored in the

recombination process and the particles created via quark coalescence are unlikely to have correlated partners in small angular region which is a characteristic of jet fragmentation. As a result, with increase in multiplicity, a relatively higher suppression in the proton triggered jet-like yield (bulk subtracted) is expected compared to pion triggered case as triggers are selected from the intermediate p_T range where inclusive proton to pion enhancement has been observed. Now, in case of heavy ion collisions where severe jet quenching is present [51], it will be hard to disentangle the effect of jet-medium interplay from soft physics (e.g coalescence model of hadronization and/or radial flow). In the context of the AMPT model, the jet modification takes place only via 2 to 2 elastic parton scatterings during ZPC. So, in small collision systems like p-Pb where the system is less dense compared to the Pb-Pb case, the medium induced modification of jets is expected to be less significant compared to heavy ions [51]. So, any difference in the trend of multiplicity evolution of pion and proton triggered yields compared to the HIJING results can be associated mainly with the presence of particles produced via coalescence model without significant contribution from the jet-medium interplay. The multiplicity evolution of the pion and proton triggered jet-like yields has been studied with hadronic cascade on and is shown in Fig 2.13 and it's comparison with the hadronic cascade off case (as shown in Fig 2.12) indicates that the dilution slightly increases with hadronic cascade on. Radial flow may be generated during hadronic cascade contributing to the inclusive proton to pion enhancement at intermediate p_T creating further dilution.

The effect of hydrodynamical flow on the yields associated with identified triggers at intermediate p_T has been investigated in detail in the previous section. While no or negligible multiplicity dependence was observed for the yield obtained from pion triggered correlations, the yield associated with proton triggers was seen to be suppressed gradually with increasing multiplicity - resulting in "trigger dilution" in EPOS [34]. The results obtained from AMPT has been compared with the same extracted from EPOS in Fig 2.15 and Fig 2.16. The ratio of yields associated with proton and pion triggered correlations suppress progressively as a function of event multiplicity in both models (Fig 2.16). However, in the similar kinematic ranges of trigger and associated

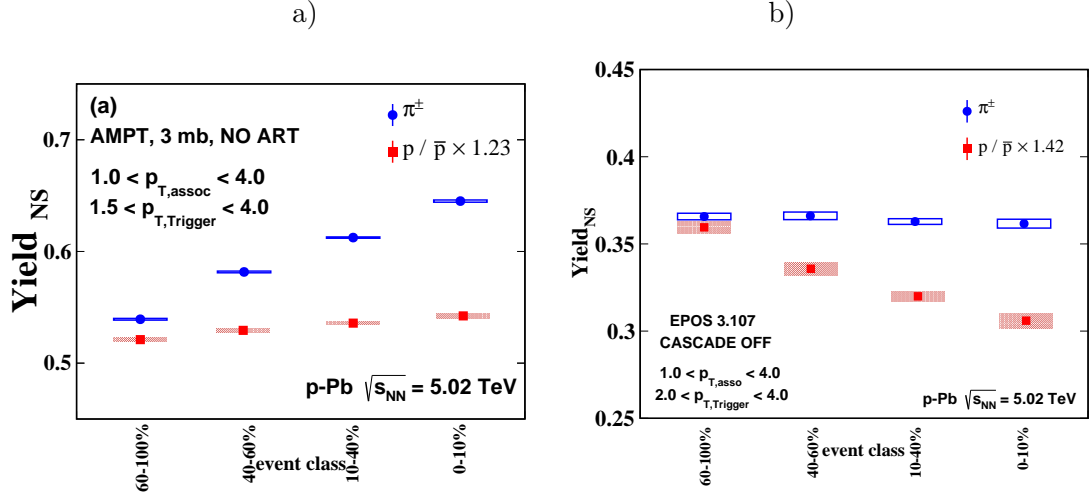


Figure 2.15: [Color online] (a) Multiplicity dependence of the near-side jet-like per trigger yield (bulk subtracted) associated with pion and proton triggers in p-Pb collisions at $\sqrt{s_{NN}} = 5.02$ TeV from (a) AMPT SM and (b) EPOS 3 without hadronic cascade.

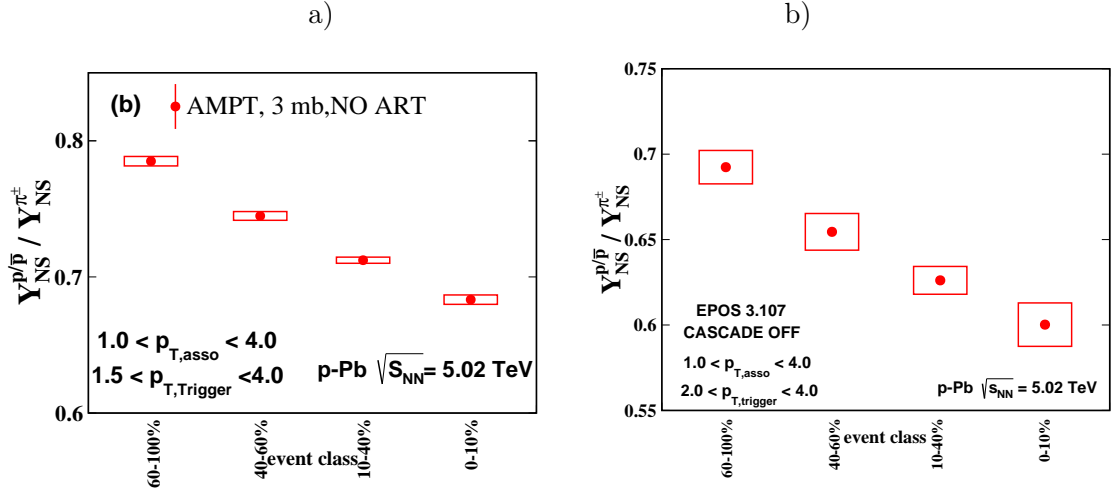


Figure 2.16: [Color online] Multiplicity dependence of the ratio of the near-side jet-like per trigger yield (bulk subtracted) associated with proton and pion triggers in p-Pb collisions at $\sqrt{s_{NN}} = 5.02$ TeV from (a) AMPT SM and (b) EPOS 3 without hadronic cascade.

particles, there is a stark difference in the multiplicity evolution of individual proton and pion triggered yields between AMPT and EPOS as shown in Fig 2.15. This suggests, although trigger

dilution can originate from both coalescence and radial flow, the response of the individual pion and proton triggered yields, studied as a function of multiplicity, is sensitive to the underlying dynamics or the physics processes involved. Thus, this observable can be used to probe whether the anomalous baryon enhancement at intermediate p_T is because of the momentum boost due to radial flow or a consequence of coalescence model of hadronization.

This work shows that the trigger dilution in small collision systems may serve as a useful probe to investigate the presence of coalescence mechanism as a hadronization scheme and radial flow at intermediate p_T compared to the heavy ion case where severe jet quenching affects the correlation pattern making it difficult to disentangle the effect of soft physics (coalescence model of hadronization, radial flow) from the jet-medium interplay. In chapter 4, The results obtained from the analysis of ALICE data for p-Pb collisions at 5.02 TeV will be compared with the model derived results to constrain the underlying dynamics of small collision systems in a more quantitative way.

Bibliography

- [1] CMS Collaboration, Phys. Lett. B 718 (2013) 795-814
- [2] B. Abelev et al. (ALICE Collaboration), Physics Letters B 719 (2013), pp. 29-41
- [3] B. Abelev et al. (ALICE Collaboration), Phys. Lett. B 726 (2013) 164-177
- [4] B. Abelev et al. (ALICE Collaboration), Phys. Rev. C 90 (2014) 054901
- [5] B. Abelev et al. (ALICE Collaboration), Phys. Lett. B 728 (2014) 25-38
- [6] A. Adare et al. (PHENIX Collaboration), Phys. Rev. Lett. 114, 192301 (2015)
- [7] CMS Collaboration, Phys. Lett. B 742 (2015) 200-224
- [8] J. D. Bjorken, Energy loss of energetic partons in QGP: possible extinction of high p_T jets in hadron-hadron collisions?, (1982). FERMILAB-PUB-82-059-THY.
- [9] K. Adcox et al., (PHENIX Collaboration), Phys. Rev. Lett. 88, 022301 (2002).
- [10] C. Adler et al., (STAR Collaboration), Phys. Rev. Lett. 89, 202301 (2002).
- [11] Oliver Busch for the ALICE Collaboration, Jets in Pb-Pb collisions at ALICE;
<https://doi.org/10.1051/epjconf/201713707005>
- [12] B. Abelev et al., (ALICE Collaboration), Phys. Rev. Lett. 110 (2013) 082302.
- [13] K. Werner et al., Phys. Rev. Lett. 112 (2014) 23, 232301.

- [14] K. Werner et al., Phys.Rev. C89 (2014) 6, 064903.
- [15] Guo-Liang Ma and Adam Bzdak, Phys. Lett. B 739 (2014) 209-213.
- [16] Adam Bzdak and Guo-Liang Ma, Phys. Rev. Lett. 113, 252301 (2014).
- [17] A. Bzdak, B. Schenke, P. Tribedy, and R. Venugopalan, (2013), Phys. Rev. C 87, 064906.
- [18] Liang He et al., Phys. Lett. B 753 (2016) 506-510.
- [19] Hanlin Li et al., arXiv:1601.05390 [nucl-th].
- [20] Hanlin Li et al., arXiv:1604.07387v1 [nucl-th].
- [21] D. Sarkar, S. Choudhury, S. Chattopadhyay; Phys. Rev. C 94, 044919 (2016)
- [22] B. Abelev et al. (ALICE Collaboration), Phys. Rev. Lett. 110, 082302 (2013)
- [23] S. S. Adler, et al. PHENIX Collaboration), Phys. Rev. C 69 (2004) 034909
- [24] B. Abelev et al. (ALICE Collaboration), Phys. Lett. B 736 (2014) 196-207
- [25] R. Fries, B. Muller, C. Nonaka, and S. Bass, Phys. Rev. Lett. 90 (2003) 202303.
- [26] V. Greco, C. Ko, and P. Levai, Phys. Rev. Lett. 90 (2003) 202302.
- [27] R. Hwa and C. B. Yang, Phys. Rev. C 70 (2004) 024904.
- [28] E. Shuryak and I. Zahed, (2013), hep-ph/1301.4470.
- [29] R. Fries, B. Muller, C. Nonaka, and S. Bass, Phys. Rev. Lett. 90 (2003) 202303.
- [30] V. Greco, C. Ko, and P. Levai, Phys. Rev. Lett. 90 (2003) 202302.
- [31] N. M. Abdelwahab et. al (STAR Collaboration) Phys. Lett. B 751 (2015) 233-240
- [32] S.S. Adler et. al (PHENIX Collaboration) Phys. Rev. C 71 (2005) 051902
- [33] D. Sarkar, S. Choudhury, S. Chattopadhyay; Physics Letters B 760 (2016) 763-768

- [34] D. Sarkar, S. Choudhury, S. Chattopadhyay; Physics Letters B 760 (2016) 763-768
- [35] K. Werner et al., Phys.Rev. C82 (2010) 044904.
- [36] H.J. Drescher et al., Phys.Rept. 350 (2001) 93-289
- [37] K. Werner, Phys.Rev.Lett. 98 (2007) 152301
- [38] Z. W. Lin et. al , Phys. Rev. C. 72 (2005) 064901.
- [39] D. Solanki et al.,Phys. Lett. B720 (2013) 352-357.
- [40] J. Xu and C. M. Ko , Phys. Rev. C83 (2011) 034904.
- [41] J. D. Orjuela, A. Adare, D. McGlinchey and J. L. Nagle, Phys. Rev. C 92, (2015), 054903.
- [42] Z. W. Lin and C. M. Ko , Phys. Rev. C. 65 (2002) 034904.
- [43] X. N. Wang and M. Gyulassy, Phys. Rev. D 44 (1991) 3501.
- [44] B. Zhang, Comput. Phys. Commun. 109 (1998) 193 .
- [45] B. A. Li and C. M. Ko, Phys. Rev. C 52 (1995) 2037 .
- [46] B. A. Li, A. T. Sustich, B. Zhang and C. M. Ko, Int. J. Mod. Phys. E, 10 (2001) 267-352.
- [47] S Choudhury, D. sarkar, S. Chattopadhyay; Phys. Rev. C 93, 054902 (2016)
- [48] B. Ablev et al. (ALICE Collaboration), Phys. Lett. B 741 (2015) 38-50
- [49] T. Sjostrand, Comput. Phys. Commun. 82(1994) 74 .
- [50] B. Ablev et al. (ALICE Collaboration), Phys. Lett. B 741 (2015) 38-50
- [51] Subrata Pal and Marcus Bleicher, Phys. Lett. B 709 (2012) 82-86.

Chapter 3

The ALICE Experiment at the LHC

3.1 Introduction

In this chapter, a brief overview on the Large Hadron Collider (LHC) will be followed by a detailed discussions of the ALICE detectors, with emphasis on the sub-detectors which are extensively used in the analysis (will be discussed in detail in the next chapter). A Large Ion Collider Experiment (ALICE) is located in one of the four interaction points of LHC as shown in Fig 3.1 and dedicated to the study of the matter produced in ultra-relativistic heavy ion collisions. It is believed that in such high energy heavy-ion collisions a strongly interacting partonic matter (namely sQGP) which is believed to be existed after few micro seconds of the Big Bang can be produced. However the results of pp and p-Pb collisions at LHC energies also indicate towards the possible creation of such matter in small collision systems where formation of sQGP is not intuitive. The data collected by the ALICE detector for different collision systems at LHC energies have been analyzed and comparison of the results provide a critical understanding of the matter produced in such ultra relativistic high energetic collisions.

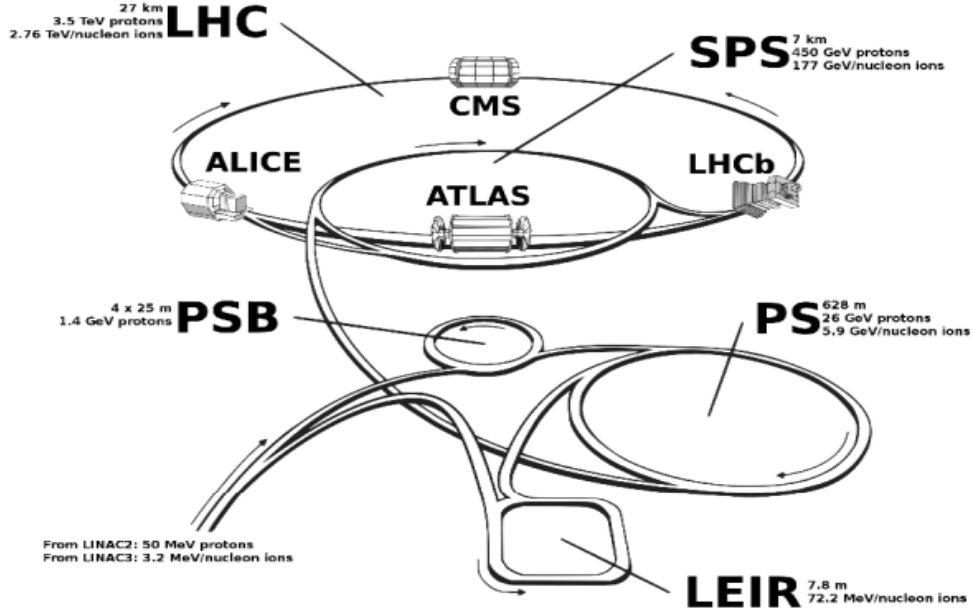


Figure 3.1: (Color online) Schematic view of the LHC acceleration stages and collision schemes [3]

3.2 The Large Hadron Collider (LHC)

The large Hadron Collider at CERN [1, 2] is the largest and the most powerful particle accelerator operating since 2009. It is placed at mean depth of 100 m (varying from 50-175 m) underground in a circular tunnel of 27 km and consist of two hadron synchrotrons capable of accelerating counter-rotating protons or ions and collide them at 4 intersection points as shown in Fig 3.1. Till 2014, pp collisons at $\sqrt{s} = 2.76, 7, 8$ TeV p-Pb collisions at $\sqrt{s_{NN}} = 5.02$ TeV and Pb-Pb collisions at $\sqrt{s_{NN}} = 2.76$ TeV were produced in LHC.

The protons are first accelerated at a linear accelerator, called LINAC2, and then injected into the booster ring at an energy of 50 MeV and it's energy is increased upto 1.4 GeV. The beam is further transferred to Proton Synchrotron (PS) which accelerates the beam to 25 GeV and subsequently the Super Proton Synchrotron (SPS) to accelerate upto 450 GeV. The protons from SPS are injected to LHC and further accelerated upto the desired beam energy.

In case of Pb-Pb or p-Pb collisions, the of Pb^{29+} -ions are produced from a highly-pure vaporized

sample of Lead and get accelerated upto 4.2 MeV/nucleon by passing through a linear accelerator called LINAC3. These ions are further stripped to produce Pb^{54+} by passing through a series of carbon foils. The bunch of Pb^{54+} -ions are further accelerated to 72 MeV per nucleon in Low Energy Ion Ring (LEIR). The beam bunches are further injected into the PS, to be accelerated upto 5.9 GeV/nucleon and then passed to the SPS. Pb^{54+} -ions are finally stripped to Pb^{82+} in the SPS and further accelerated to 177 GeV/nucleon. The Pb^{82+} ion beam is then sent to LHC for final acceleration.

The p-Pb run at $\sqrt{s_{NN}} = 5.02$ TeV

The analysis details of the p-Pb data sample recorded in 2013 at $\sqrt{s_{NN}} = 2.76$ TeV will be discussed in the next chapter. The energy of the proton beam was 4 TeV and for Pb beam it was 1.58 TeV per nucleon. The nucleon-nucleon centre-of-mass system was shifted in the direction of the proton beam with a rapidity of -0.465 with respect to the ALICE laboratory system (centre of the ALICE detector system is considered at $z=0$, the nominal interaction point). The integrated luminosity during the p-Pb run for the ALICE experiment was 32.84 nb^{-1} .

3.3 The ALICE Experiment

The ALICE (A Large Ion Collider Experiment) [4, 5] is a complex detector system at LHC dedicated towards the study the properties of the matter formed in the ultra-relativistic high energetic collisions. The ALICE is made of 17 sub-detectors placed at different pseudorapidity regions and can be categorized into 3 parts: central-barrel detectors, forward-detectors and the Muon Spectrometer. The central detectors are surrounded by a 0.5 T magnet and these are mainly used for the tracking and particle identification. The forward detectors are mainly used for triggering and/or centrality/multiplicity class estimation. The muon spectrometer is used for tracking muons and the PMD is used for identifying photons. The ALICE detector system weighs almost 10k tonnes having dimensions of $16 \times 16 \times 26 \text{ m}^3$. The schematic representation

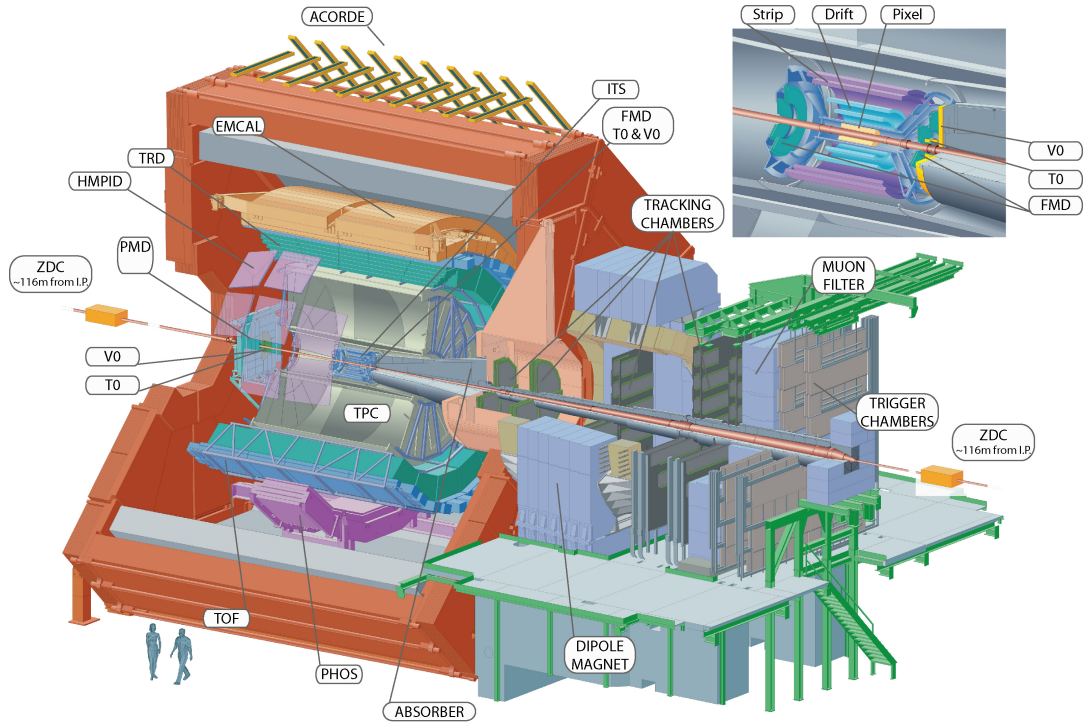


Figure 3.2: (Color online) Schematic view of the ALICE experiment, with its subdetectors. Photo Courtesy: CERN Document Server (ALICE-PHO-GEN-2012-001-12)

of the ALICE with all the sub detectors is shown in Fig 3.2. The origin of the detector system coincides with the nominal interaction point. The combination of all the sub detectors in ALICE can measure tracks with transverse momentum from $0.15 \text{ GeV}/c$ upto $100 \text{ GeV}/c$ and perform particle identification upto $20 \text{ GeV}/c$. For the analysis of the data collected in p-Pb collisions at 5.02 TeV (to be discussed in the next chapter), 3 central detectors (ITS and TPC, TOF) are used for vertex reconstruction, tracking and particle identification. Whereas, VZERO- A (forward detector) is used for multiplicity class estimation. All these 4 sub-detectors are discussed in this chapter. For a detailed description of all the detectors in ALICE, the reader is referred to [4, 5].

3.3.1 Inner Tracking System -ITS

The Inner Tracking System (ITS) [6] is located close to the interaction point and is used for estimation of the primary interaction vertex, tracking and particle identification of low momentum tracks. As shown in Fig 3.3, the entire ITS is composed of 6 cocentric sub detectors: 2 silicon pixel detectors (SPD), 2 silicon drift detectors (SDD) and 2 silicon strip detectors (SSD) and spanned from 3.9 cm to 43 cm in the transverse direction (radially outward). The pseudo-rapidity coverage of the entire ITS is $|\eta| < 0.9$ and it covers 2π in azimuth. ITS is also used to reconstruct the secondary vertices of heavy- quark decays (D and B mesons) and hyperons with a resolution of $100 \mu\text{m}$ in the transverse direction. The ITS along with other detectors (e.g. TPC) perform the tracking in ALICE and also serve the role of standalone tracker for very low momentum charged particles that are trapped or decay before reaching the Time Projection Chamber (TPC). The momentum resolution of ITS is 2% for pions having transverse momentum between 100 MeV/c and 3 GeV/c. Particle identification is also done in ITS via the measurement of specific energy loss (dE/dx) method mainly for low p_T particles. The material budget of this silicon based detector is low and it is less than 8% in terms of radiation length.

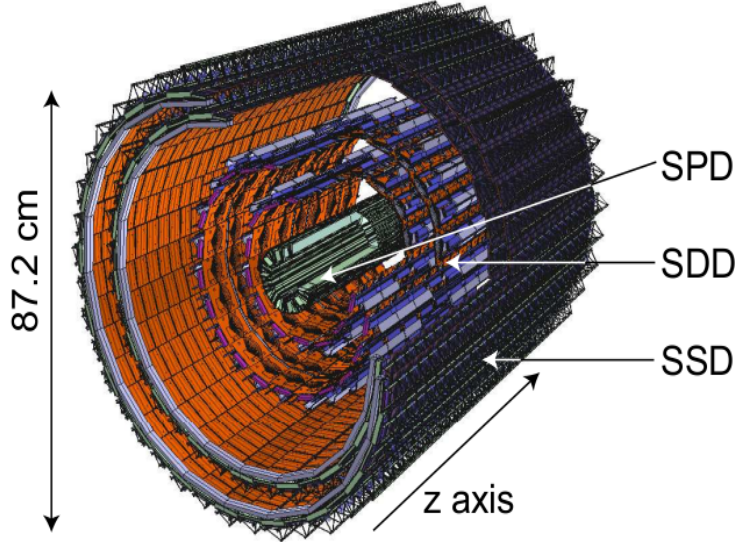


Figure 3.3: (Color online) A schematic view of ALICE-Inner Tracking Chamber with different sub-layers: SPD, SDD and SSD.

Silicon Pixel Detector :

The first two layers of ITS are made of pixel based silicon detectors, the SPD, which consist of silicon diodes with a thickness of $200\text{ }\mu\text{m}$. The 2-dimensional array of 256×160 finely segmented silicon pixels of size $50\text{ }\mu\text{m}$ ($r\phi$) by $425\text{ }\mu\text{m}$ (z) allow them to localize tracks with maximum spatial resolution of $12\text{ }\mu\text{m}$ in $r\phi$ and $100\text{ }\mu\text{m}$ in the z -direction. The finely granulated SPD contributes towards precise primary vertex measurement but can't perform particle identification due to lack of energy-loss information.

Silicon Drift Detector:

The SDD s are two intermediate layers of the ITS and located at radial distances of $r=15.0\text{ cm}$ and 23.9 cm from the beam pipe. Each SDD consists of a $300\text{ }\mu\text{m}$ -thick layer of homogeneous high-resistivity silicon and particularly used for particle identification using specific energy loss (dE/dx) of the tracks passing through the active volume of the detector. The position of the track-hits in the transverse direction is determined from the drift-time of electrons to the electrode with respect to the trigger-time and the z -position of the hits are obtained from the centroid of the charge accumulated in the anodes. SDD can measure a hit position with a resolution of $38\text{ }\mu\text{m}$ in $r\phi$ and $28\text{ }\mu\text{m}$ in z . SDD performs the particle identification along with the tracking measurement.

Silicon Strip Detectors:

The outermost layers of ITS are made of double-sided silicon strips placed at a radial distances of $r=38\text{ cm}$ and 43 cm respectively. SSD can perform hit reconstruction with a spatial resolution of $20\text{ }\mu\text{m}$ in $r\phi$ and $830\text{ }\mu\text{m}$ in z . It is also used for low momentum particle identification exploiting the energy loss (dE/dx) information in the detector volume.

3.3.2 Time Projection Chamber -TPC

The ALICE Time Projection Chamber (TPC) [7] is the most important central-barrel detector dedicated towards tracking and particle identification. The TPC is the largest gas detector in the world, with a volume of 90 m³ and it is located coaxially with beam-pipe and ITS with its inner radius located at 80 cm and the outer radius at approx 250 cm from the beam pipe. The length of the TPC is about 510 cm along the beam pipe and it covers a phase space of $|\eta| < 0.9$ and full range of azimuth. This is filled with a gas mixture of (Ne:CO₂ :: 90%:10%) to ensure low electron diffusion, small space charge effect and low material budget along with good momentum resolution, high rate handling capacity, minimal re-scattering and secondary particle generation. The electrode grid, placed at the center of the TPC produces a drift field of 100 kV towards the multi-wire proportional chambers (MWPC) at $z = \pm 2.5$ m and provide an axial uniform electric field of 400 V/cm. The charged particles ionize the gas while traversing through the active detector volume and the electrons liberated in the process of ionisation drift towards the end-plates (over a distance of 250 cm) at an average drift velocity of 2.7 cm/s. The

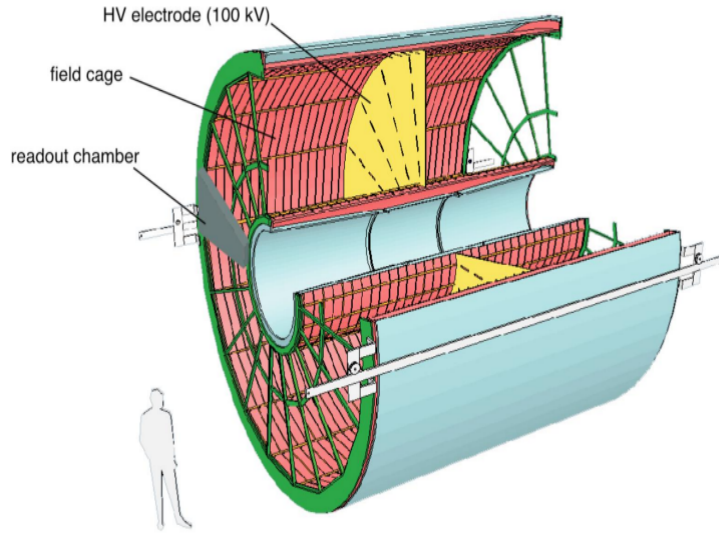


Figure 3.4: (Color online) Schematic view of the ALICE-TPC [8]

end-plates are equipped with 159 segmented anode read-out pads placed in MWPCs to collect

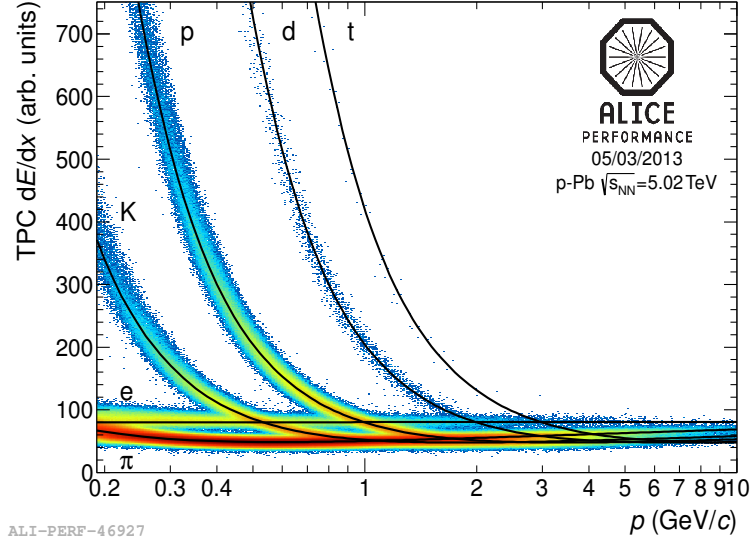


Figure 3.5: (Color online) $\frac{dE}{dx}$ versus momentum (p) curve in the TPC active volume for p-Pb collisions at $\sqrt{s_{NN}} = 5.02$ TeV. For each particle there is a distinctly separated band below $p_T < 1$ GeV/c which merges at higher p_T .

the electrons and therefore the maximum number of charged clusters for a track within the TPC active volume can be upto 159. The hit points on the anode-pads provide x-y positions of the tracks. The z-coordinates of the trajectory (along the beam-axis) are calculated from the arrival time of the signal at the anode plane relative to the collision time of the beams as obtained from the LHC-clock. The TPC can reconstruct tracks with a resolution of about 800-1100 μm in the transverse plane and 1100-1250 μm along the z-direction. In TPC, tracks with p_T from about 200 MeV/c to 100 GeV/c can be measured with a momentum resolution of 2.5%. For tracks with $p_T < 4.0$ GeV/c and with more than 140 clusters it reaches around 5.5%. The ALICE TPC has a long drift time (90 μs) which leads to the pile up of events in case of high luminosity runs and it becomes hard to disentangle the pileup events from the triggered event. The pile up is removed by determining and discriminating the vertices positions in the reconstruction phase. The specific energy loss $\langle dE/dx \rangle$ and momentum information as obtained from TPC (sometimes in combination with other central barrel detectors) are used to trace the mass of the

particles using the Bethe-Block formula given below [9, 10]:

$$\langle dE/dx \rangle = \frac{C_1}{\beta^2} [\ln(C_2 \beta^2 \gamma^2) - \beta^2 + C_3] \quad (3.1)$$

Parameters in the equations have their usual meanings. The $\langle dE/dx \rangle$ vs momentum curve as obtained from the TPC corresponding to different particle species in p-Pb collisions at $\sqrt{s_{NN}} = 5.02$ TeV is shown in Fig 3.5.

The number-of-sigma ($n\sigma^i$) deviation of the measured $\langle dE/dx \rangle$ response of each track from the standard Bethe-Block curve of a particular mass hypothesis is used for particle identification. Particle identification in ALICE will be discussed in detail in the next chapter.

$$n\sigma^i = \frac{\frac{dE}{dx} - \langle \frac{dE}{dx} \rangle^i}{\sigma^i}, i = \pi, k, p/\bar{p}. \quad (3.2)$$

The material budget of TPC is less than 11% in terms of radiation length. TPC along with other detectors (e.g ITS) also contributes towards primary vertex reconstruction of the events.

3.3.3 Time of Flight -TOF

The ALICE Time Of Flight (TOF) [11, 12] detector is another central barrel gaseous detector which uses Multi-gap Resistive-Plate Chambers (MRPC). The basic constituents of this TOF are 120 cm long 10-gap glass MRPC strips as shown in Fig 3.6. The TOF has a cylindrical shape with inner and outer radii located at 370 cm and 399 cm from the beam axis and it covers a full azimuth with an $|\eta|$ acceptance of 0.9 ($|\eta| < 0.9$). The active area of the detector is filled with a gas mixture: 90% Freon, 5% SF₆ and 5% Iso-butane. The results obtained from the test beam with 6 GeV/c pions show that MRPCs reach an efficiency level of 99.9% and time resolution is better than 40 ps at an voltage of ± 6 KV across the gas-gap. However, as the over-all resolution of the TOF also includes the jitter in the initial time (t_0) information available from the T0

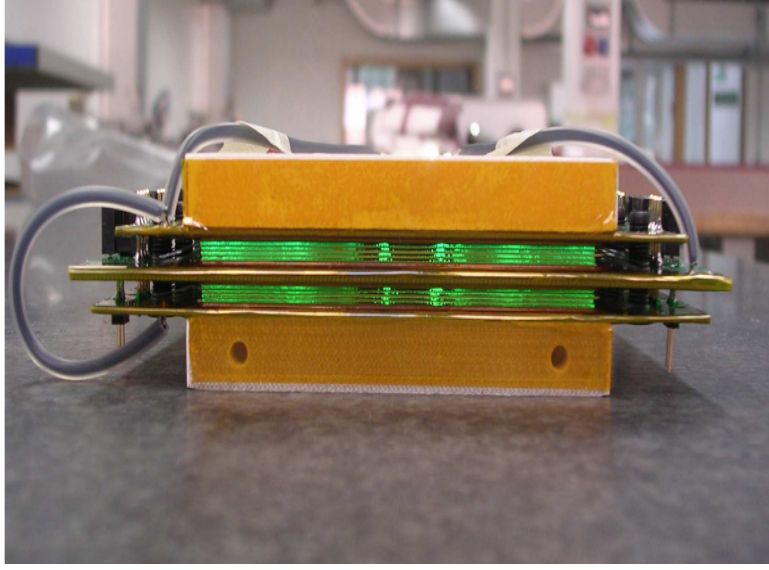


Figure 3.6: (Color online) Photograph of the 10-gap glass-MRPC used to fabricate ALICE-TOF [13].

detector, the overall time resolution of ALICE-TOF is given by: $\sigma_{TOF} = \sqrt{\sigma_{intrinsic}^2 + \sigma_{t0}^2}$. The Time-of-Flight measures the time (t) taken by a particle to traverse a known trajectory of length L . The two particles of unequal masses (m_1 and m_2) but having same momentum (p) will cover the same length L in a time difference of:

$$t_2 - t_1 = \frac{L}{2c} \left(\frac{m_1^2 c^2 - m_2^2 c^2}{p^2} \right) \quad (3.3)$$

This difference in the time-of-flight for two different masses is used to identify particles with different masses. The capability of TOF to effectively separate different particle species using $n\sigma$ method depends on the time difference ($t_2 - t_1$) and the intrinsic time resolution (δt) of the detector as:

$$\frac{t_2 - t_1}{\delta t} = n\sigma \quad (3.4)$$

The TOF has a time resolution of 80 ps and it can provide particle identification (PID) in the intermediate momentum range (from $p_T = 2 - 4$ GeV/c) with a 3σ π/K separation upto

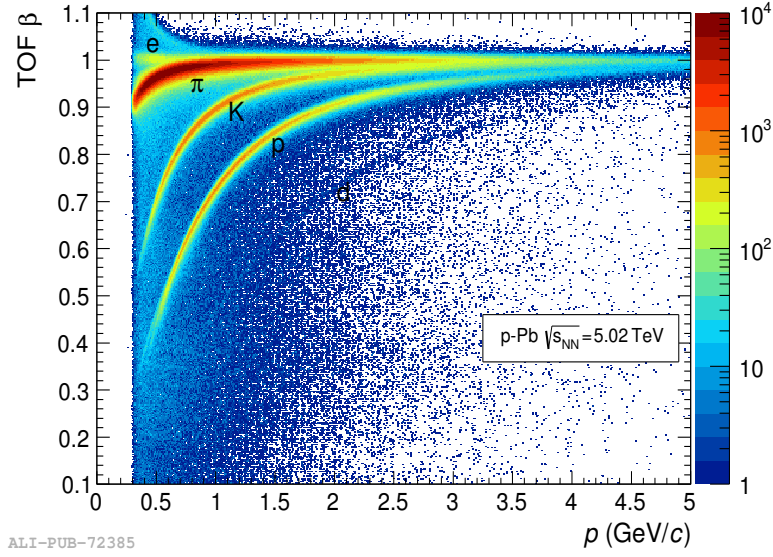


Figure 3.7: (Color online) TOF $\beta = v/c = L/tc$ distribution as measured by ALICE-TOF detector as a function of momentum in p-Pb collisions at $\sqrt{s_{NN}} = 5.02$ TeV.

2.5 GeV/c and K/p separation upto 4 GeV/c respectively. Combined with TPC and ITS, TOF contributes to vertex and track reconstruction and facilitate event by event identification of π^\pm , K and protons upto a momentum range of 4 GeV/c [14].

3.3.4 VZERO (V0)

The ALICE VZERO is a forward detector made of two arrays of plastic scintillator counters, called VZERO-A and VZERO-C [15, 16] and installed on either side of the ALICE interaction point ($z=0$), at +340 cm and -90 cm respectively. The VZERO-A covers the pseudorapidity range $2.8 \leq \eta \leq 5.1$ and VZERO-C covers $3.7 \leq \eta \leq -1.7$. Both detector has 4 rings and each ring is segmented into 8 sectors, making an overall 32 segmented counters. The information from VZERO detector is used for triggering, centrality estimation and backgrounds rejection. With a time resolution of about 1 ns, VZERO can identify beam-gas events that occurred outside of the nominal interaction region. The information of the energy deposited in the V0 scintillators is used to extract charged particle multiplicity in the detector coverage. It provides minimum-bias

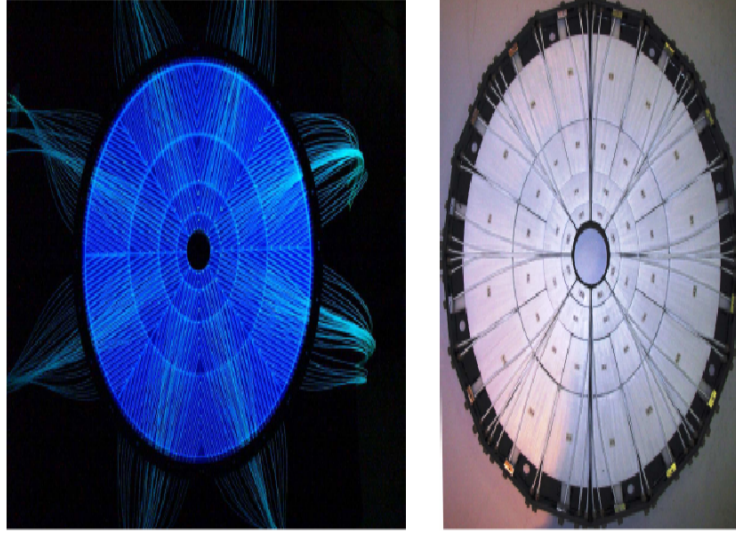


Figure 3.8: (Color online) V0 detector modules [17]

triggers for the central barrel detectors and the calibrated V0 signal amplitudes are used for centrality estimation (this will be discussed in the next chapter). With moderate granularity in the azimuthal direction (45°) VZERO detectors are also used for experimental estimation of event plane inclination.

3.4 The Forward Detectors

Other than VZERO there are other forward detectors in ALICE - pre-shower Photon Multiplicity Detector (PMD), silicon-based Forward Multiplicity Detector (FMD) quartz Cherenkov detector T0 and Zero Degree Calorimeter (ZDC).

The ALICE Forward Multiplicity Detector or FMD [16] is used to estimate charged particle multiplicity at forward rapidity. The pseudorapidity coverage of the FMD on either side of the interaction point is $-3.4 \leq \eta \leq -1.7$ and $1.7 \leq \eta \leq 5.0$, respectively and Combination of FMD and ITS allow charged particle counting over an extraordinarily large pseudorapidity range ($-3.4 \leq \eta \leq 5.0$). The FMD is made of 5 rings of silicon strip detectors placed around the beam-pipe.

The first 3 inner rings (FMD1i, FMD2i and FMD3i) contain 10 hexagonal silicon cells and the 2 outer rings (FMD2o and FMD3o) have 20 silicon sensors segmented into 2 sectors. Along with the multiplicity measurement at large forward rapidity, it is also used for independent and reliable measurement of event plane inclination.

The Photon Multiplicity Detector or PMD [18, 19] is designed to measure photons at the forward rapidity and its working principle is similar to that of a proportional counter. It is located at 3.67 m from the interaction point towards the A side of the ALICE and covers the pseudo-rapidity range of $2.3 < \eta < 3.9$ and full azimuth. The PMD consists of two planes, Charged Particle Veto (CPV) and Pre-Shower (PRE) with a Pb-converter placed between these two planes. To deliver high photon-conversion efficiency but low transverse shower spread, the thickness of the Pb-converter has been optimised. Each PMD plane has 24 modules and each module has 4608 honeycomb cells. The active volume of the detector is filled with Ar-CO₂ gas mixture in a proportion of 70:30 by weight.

The ALICE T0 [16] consists of two arrays (T0A and T0C) of Cherenkov counter placed asymmetrically with respect to the interaction point (IP). The T0A is installed at 3.75 m from the IP on the A-side of the ALICE and T0C at 7.27 m from the IP on the C-side of the ALICE. The T0 detectors can measure the start time of the collision with a precision of 25 ps and this time is also used as a start time for the TOF detector for the time-of-flight measurement of the particles.

The Zero Degree Calorimeter (ZDC) [20] is located at 114 m on either side of the interaction point and it consists of a hadronic and an electromagnetic calorimeter. The ZDC measures the energy deposited by the spectator nucleons and the amount of energy deposited in ZDCs is related to the spectator nucleon number. This information is used for centrality/multiplicity class estimation in nuclear collisions [21]. The hadronic ZDC is made of two tungsten-quartz neutron calorimeter (ZN) and two brass-quartz proton calorimeter (ZP). As the spectator protons are

deflected by the magnetic elements along the beam-line, the ZP is placed outside the beam-line on the side where positive particles are deflected.

3.5 Event Reconstruction - Vertexing and Tracking

- Vertex Determination:** In ALICE, the initial primary vertex reconstruction is done using the cluster information from first two layers in ITS (SPD). The pair of space points in first two layers of ITS is connected by a line and is named as tracklet. All the tracklets are propagated to the nominal interaction point (IP). The point which is close to IP and where most of the tracklets converge is considered as an initial estimation of the primary vertex. However, for final estimation of the primary vertex, instead of tracklets fully reconstructed global tracks from ITS and TPC are extrapolated and made to converge around the IP. As TPC is a gas detector with a long drift time ($90 \mu\text{s}$)- there is a possibility of pile up of events in case of high luminosity runs. In that case, this process of vertex reconstruction is repeated and at each iteration, clusters which have been already assigned to a vertex are discarded.
- Tracking:** A track while passing through the active volume of the detector produces a collection of hits or clusters and tracking is the technique of connecting these disjoint points in order to reconstruct the trajectory of the particles and extract its kinematics. The clusters in a detector provide information about the spatial location of the tracks, signal strength, signal time and their corresponding errors and is the main ingredient for tracking. In ALICE, the tracking is done via three stage inward-outward-inward scheme [22, 23]. In the first stage the outer most space- points of TPC (considered as seeds for the track-finding algorithm) are propagated in-ward and at each step the clusters nearest to the previous seed are considered as the seed for the next layer. Tracks having less

than 20 space-points (clusters) or missing more than 50% of the total clusters are rejected. The tracks which are reconstructed in the TPC are extrapolated to the outer layer of the ITS and further extended close to the primary vertex (to check the convergence of the tracks). For tracks which fail to reach TPC (very low momentum tracks), a stand-alone track reconstruction in the ITS is carried out using the tracklet information.

In the second stage, the Kalmann Filter [24] method is used to refit the clusters (obtained in the previous stage) in the outward direction (vertex to TPC). The track-length information and expected flight time of different tracks are estimated and stored for the particle identification purpose using TOF. Track clusters as obtained in ITS-TPC are matched with the clusters inside TOF (possible only for the tracks that reach TOF) and propagated further for track matching in EMCAL, PHOS and HMPID.

In the third stage, the Kalmann Filter procedure is repeated in outward-inward approach, starting from the TRD. Several track informations such as position, track-curvature, direction etc are estimated and stored for further use. The kinematic variables are estimated from the parameters obtained from the track-fitting within the outer radius of TPC only.

Bibliography

- [1] The CERN Large Hadron Collider : Accelerator and Experiments, Volume ?1, Breskin, Amos (ed.) and Voss, Rudiger (ed.) (CERN), 2009.
- [2] The CERN Large Hadron Collider : Accelerator and Experiments, Volume ?2, Breskin, Amos (ed.) and Voss, Rudiger (ed.) (CERN), 2009.
- [3] J. J. Goodson and R. McCarthy, *Search for Supersymmetry in States with Large Missing Transverse Momentum and Three Leptons including a Z-Boson*. PhD thesis, Stony Brook U., May, 2012. Presented 17 Apr 2012.
- [4] ALICE Collaboration, K. Aamodt et al., The ALICE experiment at the CERN LHC,? JINST 3 (2008) S08002.
- [5] ALICE Collaboration, B. B. Abelev et al., Performance of the ALICE Experiment at the CERN LHC,? Int. J. Mod. Phys. A29 (2014) 1430044, arXiv:1402.4476 [nucl-ex].
- [6] ALICE Inner Tracking System (ITS): Technical Design Report, CERN-LHCC-99-012, <http://edms.cern.ch/file/398932/1>.
- [7] ALICE Time Projection Chamber: Technical Design Report, CERN-LHCC-2000-001, <http://cdsweb.cern.ch/record/451098>.
- [8] Saikat Biswas (for the ALICE Collaboration), arXiv:1511.04988, 2015.

- [9] H. Bethe. Zur Theorie des Durchgangs schneller Korpuskularstrahlen durch Materie. *Annalen der Physik*, 397(3):325-400, (1930).
- [10] F. Bloch. Zur Bremsung rasch bewegter Teilchen beim Durchgang durch Materie. *Annalen der Physik*, 408(3):285-320, (1933).
- [11] ALICE Time-Of-Flight system (TOF): Technical Design Report, CERN-LHCC-2000-012, <http://cdsweb.cern.ch/record/430132>.
- [12] ALICE Time-Of-Flight system (TOF): addendum to the technical design report, CERN-LHCC-2002-016, <http://cdsweb.cern.ch/record/545834>
- [13] Roberto Preghenella thesis, CERN-THESIS-2009-206.
- [14] C. Lippmann, *Nuclear Instruments and Methods in Physics Research A* 666, 148-172 (2012).
- [15] E. Abbas et al. (ALICE Collaboration), *JINST* 8, P10016 (2013), arXiv:1306.3130.
- [16] ALICE forward detectors: FMD, T0 and V0: Technical Design Report, CERN-LHCC-2004-025, <http://cdsweb.cern.ch/record/781854>.
- [17] Chiara Bianchin thesis, CERN-THESIS-2012-033.
- [18] ALICE Photon Multiplicity Detector (PMD): Technical Design Report, CERN-LHCC-99-032, <http://cdsweb.cern.ch/record/451099>.
- [19] ALICE Photon Multiplicity Detector (PMD): addendum to the technical design report, CERN-LHCC-2003-038, <http://cdsweb.cern.ch/record/642177>.
- [20] ALICE Zero-Degree Calorimeter (ZDC): Technical Design Report, CERN-LHCC-99-005, <http://cdsweb.cern.ch/record/381433>.
- [21] B. Abelev et al. (ALICE Collaboration), *Phys. Rev. C* 88, 044909 (2013).
- [22] M. Ivanov, I. Belikov, P. Hristov, T. Kuhr and K. Safarik, *Nucl. Instr. and Meth. A* 566, 70 (2006).

- [23] Y. Belikov, M. Ivanov, K. Safarik and J. Bracinik, eConf C0303241, TULT011 (2003),
arXiv:physics/0306108.
- [24] Nucl. Instrum. Meth. A 262, 444-450 (1987).

Chapter 4

Two particle correlations with identified trigger particles in p-Pb collisions at $\sqrt{s_{NN}} = 5.02$ TeV (Data analysis in ALICE)

4.1 Introduction

In this chapter the details of the two particle correlation analysis with identified trigger particles in p-Pb collisions at $\sqrt{s_{NN}} = 5.02$ TeV have been discussed. In this analysis, pions and protons at intermediate transverse momentum ($2 < p_T < 4$ GeV/c) are considered as trigger particles and all charged hadrons with transverse momentum $1 < p_T < 4$ GeV/c are considered as associated particles. As shown in Fig.4.1, an inclusive baryon-to-meson enhancement has been observed at the intermediate p_T (trigger p_T) region in p-Pb collisions at 5.02 TeV similar to that observed in heavy ion collisions (Pb-Pb collisions at 2.76 TeV). The choice of the trigger p_T region ($2 < p_T < 4$ GeV/c) is of particular interest as it is believed to have contributions from both hard (fragmentation) and soft (hydrodynamics and/or coalescence model of hadronization) processes of particle

production. Using the two particle correlation technique, the multiplicity evolution of the pion- and proton-triggered jet-like yields has been studied to explore the underlying mechanisms of particle production in the intermediate p_T (trigger p_T) region.

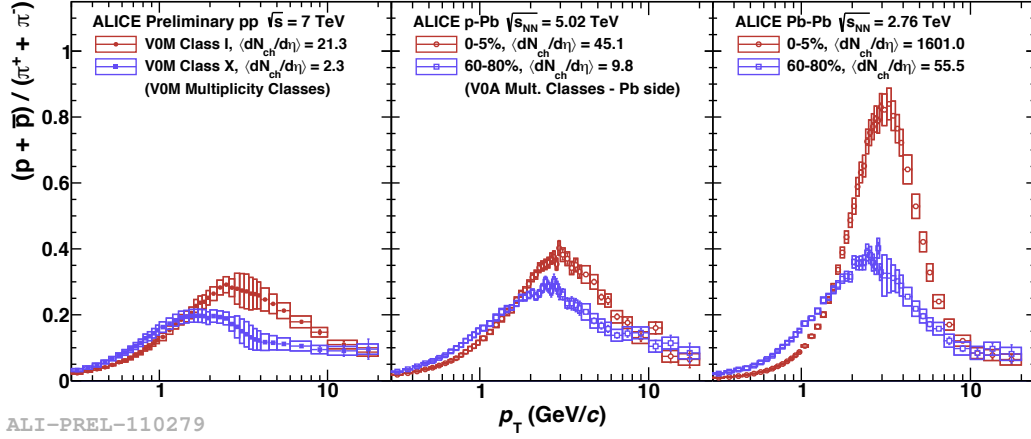


Figure 4.1: p_T -differential p/π ratio for different multiplicity classes/centralities in pp at 7 TeV (left panel), p-Pb at 5.02 TeV (central panel) and Pb-Pb at 2.76 TeV (right panel).

4.2 Datasets

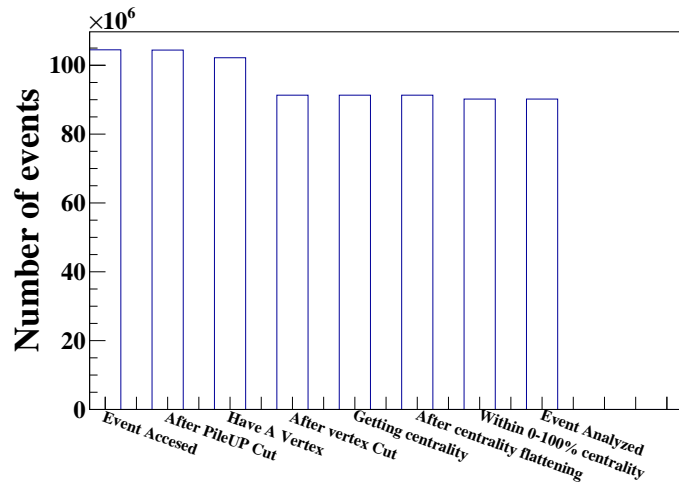
p-Pb $\sqrt{s_{NN}} = 5.02$ TeV

Around 120 million minimum bias p-Pb collision events have been recorded by ALICE in the period of January-February 2013. The raw data (also called as ESD or Event Summary Data) had been reconstructed and calibrated several times to ensure proper reconstruction of events and tracks and stored in AOD (Analysis Object Data) files. The AOD files are smaller in size and contain less (analysis specific) information compared to that in ESD - making it convenient to store and process for analysis. For this analysis, the AOD data (LHC13b Pass3, LHC13C Pass2) have been analyzed with the AliROOT software [1] using the ALICE analysis framework [2]. The detector acceptance, reconstruction efficiency are estimated from the Monte Carlo simulation. For this purpose, the particles produced in DPMJET (version 3.05) event generator [3, 4] are

passed through GEANT3 (version 3.21) [5] based detector simulation environment mimicking the detector configuration as in real data runs.

4.3 Event Selection

For this analysis, events that pass AliVEvent::kINT7 physics selection criteria are considered [6]. This is the minimum selection criteria to consider maximum number of inelastic collisions (i.e. minimum bias). This is implemented in both online (during data taking) and offline (during reconstruction) phases. The online stage accepts 99.2% of the total non-single-diffractive (NSD) events with a negligible contamination from single-diffractive (SD) and electromagnetic (EM) events [6]. This is done by requiring at least one beam-beam hit in a V0A channel (out of total 32 channels) and another hit in a V0C channels (out of total 32 channels). The offline selection is done via averaging cell-by-cell timing in V0A and V0C and applying a cut on these average times to select only those events which are compatible with beam-beam timing. In addition, another cut is applied by measuring the time of neutrons on the ZDC (on Pb-going direction) which should be compatible with the neutrons originating from beam-beam collisions. The offline selection criteria rejects 0.5-1.0% of the event sample selected online. The triggered



THIS THESIS

Figure 4.2: Number of events after each selection step.

events having reconstructed vertex within 10 cm of the nominal interaction point (at $z=0$) are considered for this analysis. The vertex reconstruction algorithm initially estimates its position using SPD space point information and further fitting it with the tracks reconstructed within the acceptance range of ITS and TPC ($|\eta| < 0.9$) [7]. The average position of the beam - beam interaction region and its distribution in a particular run are also used for this purpose. Around 90 M events are passed the event selection criteria and used for this analysis (as shown in Fig.4.2).

4.4 Multiplicity class selection

The determination of centrality (in terms of geometrical quantity like impact parameter " b " or number of participants (N_{part}) or number of binary nucleon nucleon collisions (N_{coll})) is highly non trivial in p-Pb collisions compared to the heavy ion collisions [8]. In case of heavy ion collisions (e.g. Pb-Pb collisions at 2.76 TeV), the distance between the centres of two Lorentz contracted nuclei in the transverse plane (namely impact parameter " b ") defines the centrality of the collision [9]. The Glauber model [10, 11] is used to derive the number of participants N_{part}

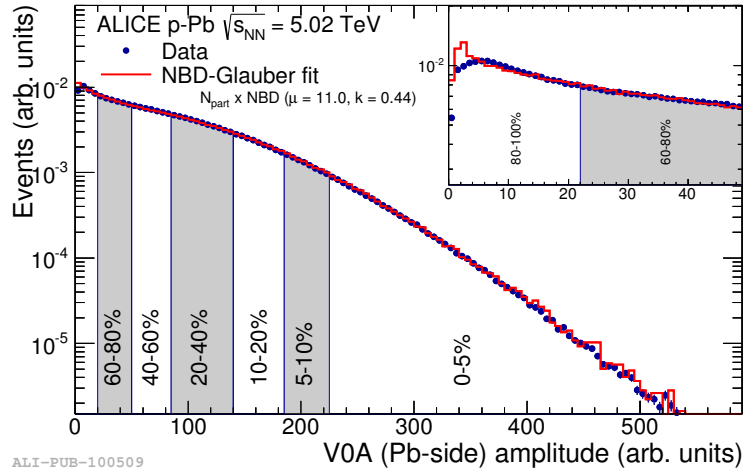


Figure 4.3: Distribution of the sum of amplitudes in the V0A hodoscopes (Pb-going direction for p-Pb collisions at 5.02 TeV), as well as the NBD-Glauber fit (explained in the text) of the data points. Figure taken from [8]

and the number of binary nucleon nucleon collisions N_{coll} from the impact parameter b . But

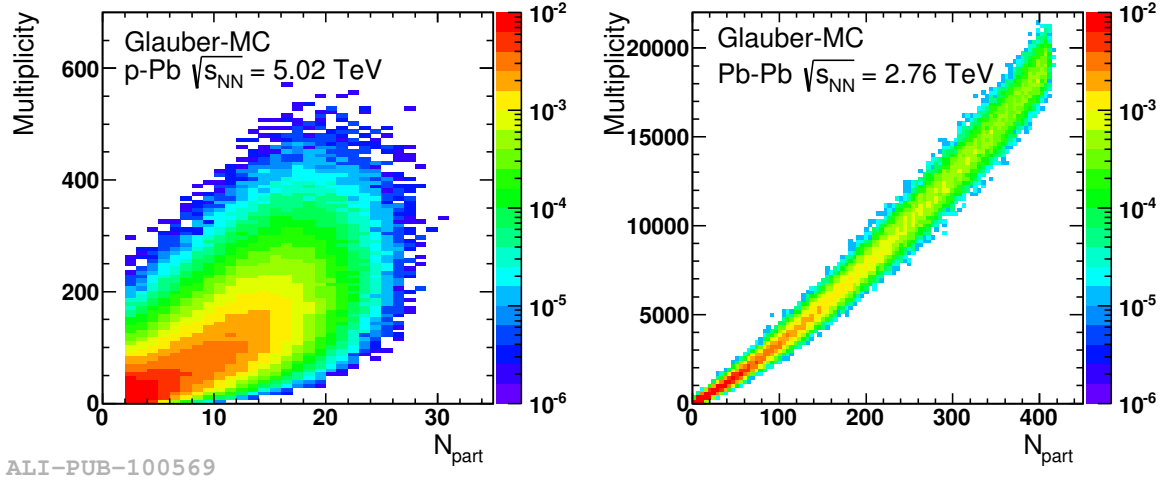


Figure 4.4: V0A multiplicity as a function of N_{part} from Glauber Monte Carlo for p-Pb collisions at 5.02 TeV (left) and Pb-Pb collisions at 2.76 TeV (right). Figure taken from [8].

N_{part} and N_{coll} are not directly measurable quantities whereas multiplicity or energy distribution are measured experimentally. In ALICE, the multiplicity classes are defined based on the amount of charge deposited within the acceptance range of different detectors (e.g. VZERO-A, VZERO-C, VZERO-M) and are termed as V0A, V0C or V0M multiplicity classes. The N_{part} and the N_{coll} are related to the measurable observables like energy or multiplicity distribution via some model [8]. As an example, the V0A charged particle multiplicity distribution which is used as centrality estimator in case of p-Pb collisions follows the Negative Binomial Distribution (NBD) and N_{part} can be estimated from the fitting of the multiplicity distribution with Glauber-NBD [8] as shown in Fig 4.3. But the estimation of geometric parameters (e.g. N_{part} or N_{coll}) from multiplicity or energy distribution (centrality estimator) works well only when the centrality estimator (multiplicity) varies monotonically as a function of N_{part} [12–16]. Now, in case of both Pb-Pb and p-Pb collisions, the average of multiplicity (centrality estimator) changes monotonically with N_{part} along with inherent fluctuations as shown in Fig 4.4 (using Glauber Monte Carlo) [8]. The Pb-Pb collisions at 2.76 TeV produce more energetic QCD matter compared to the p-Pb collisions at 5.02 TeV giving rise to a larger range in multiplicity and N_{part} . Whereas, compared to the total range in multiplicity and N_{part} , the fluctuations in those

quantities are much larger in p-Pb collisions compared to the Pb-Pb case. In [8], it is shown that such fluctuations originate from the fluctuations in the number of multiple parton-parton interactions. So, in p-Pb collisions a particular N_{part} corresponds to a large range of multiplicity and the selection of events on the basis of N_{part} will create a significant multiplicity bias in the sample [8]. For this reason, in case of p-Pb collisions the classification of events in terms of centrality (N_{part}) is non trivial and it is better to use the multiplicity itself to classify events into different classes. To study the multiplicity dependence of the per trigger yield associated with identified triggers, the selected events are divided into 5 event classes (percentile ranges) according to the charge counted in the VZERO detector(V0A,($2.8 < \eta < 5.1$)). The V0A detector is placed along the Pb going direction and therefore more sensitive to the fragmentation of the Pb nucleus in p-Pb collisions. The event classes are defined as "0-10%", "10-20%", "20-40%", "40-60%", "60-100%" from the highest to the lowest multiplicity - which is basically the fraction of the total analyzed event sample based on the cuts on total charge counted in the V0A detector [17].

4.5 Track Selection

In ALICE, the two tracking detectors - ITS and the TPC are used to reconstruct the particles via Kalman filter method [7]. Several sets of cuts on the different track parameters (e.g. number of hit pad-rows in the TPC, χ^2 per point of the momentum fit in the TPC, distance of closest approach (DCA) in longitudinal and transverse direction, ITS-refit etc) are used to ensure proper reconstruction of the tracks and minimum contamination from secondary particles and particles originating from beam-material interaction. In ALIROOT framework, a set of cuts on the track parameters are defined as "filterbits" and is identified with a number. This analysis is performed using the filterbit(768) which means:

a) p_T -dependent minimum number of TPC clusters: $N = 70 + 1.5 * p_T$ (GeV/c) for $p_T < 20$ GeV/c, $N=100$ for $p_T > 20$ GeV/c.

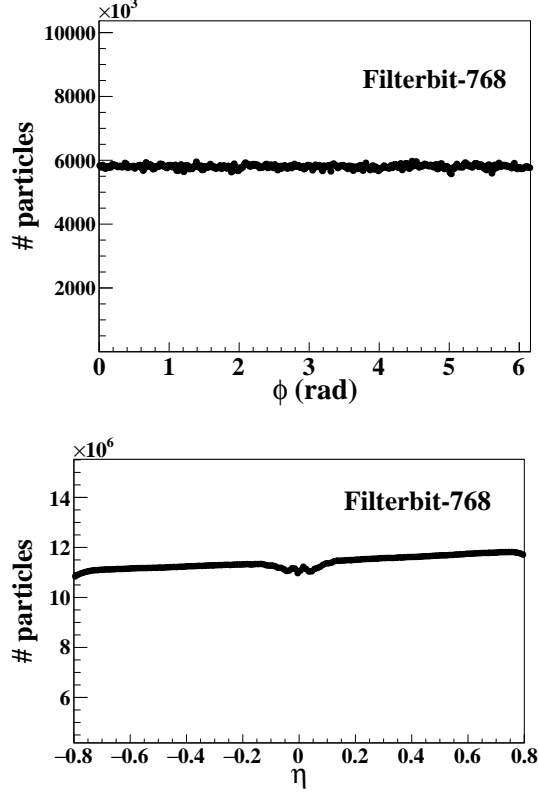


Figure 4.5: ϕ (top) and η (bottom) distribution of particles as obtained from filterbit 768.

- b) χ^2 per point of the momentum fit in the TPC is less than 4.
- c) Fraction of shared TPC clusters less than 0.4.
- d) χ^2 per point of the momentum fit in the ITS less than 36.
- e) DCA cuts : $D_{XY} < 2.4$ cm, $D_z < 3.2$ cm.

The ϕ and η distribution of particles (using filterbit 768) are shown in Fig.4.5. The tracks within $|\eta| < 0.8$ are considered to avoid lower tracking efficiency at the detector edges. Bit 32 (Global tracks with tight DCA cut - to reduce contamination from the secondaries) ,bit 16 (global tracks

with wide DCA cut) and 96 (global + SDD) are also considered for systematic studies. Trigger particles ($2 < p_T < 4$ GeV/c) are identified as pions and protons using both TPC and TOF (discussed in detail in section 4.7).

4.6 Correlation Function

Two particle correlation functions are constructed using the method described in chapter 2 and also discussed in [18]. This correlation function has been constructed for each event class for a certain range of trigger and associated p_T . For each multiplicity class, the correlation between pairs of triggers (identified as pions or protons) and associated charged hadrons is measured as a function of the azimuthal angle difference $\Delta\phi$ and pseudorapidity difference $\Delta\eta$.

$$\frac{d^2N}{d\Delta\phi d\Delta\eta}(\Delta\phi, \Delta\eta) = \frac{1}{N_{trig}} \frac{dN_{assoc}}{d\Delta\phi d\Delta\eta} = \frac{S(\Delta\phi, \Delta\eta)}{B(\Delta\phi, \Delta\eta)} \quad (4.1)$$

Where N_{assoc} is the number of particles associated to the trigger particles N_{trig} for a particular event class. In this analysis, p_T ordering ($p_{T,asso} < p_{T,trig}$) has been used to avoid double counting in case of overlapping p_T region of trigger and associated particles. The Signal

$$S(\Delta\phi, \Delta\eta) = \frac{1}{N_{trig}} \frac{d^2N^{same}}{d\Delta\phi d\Delta\eta} \quad (4.2)$$

is constructed by pairing the trigger particles with the associated particles from the same event. The background

$$B(\Delta\phi, \Delta\eta) = \alpha \frac{d^2N^{mixed}}{d\Delta\phi d\Delta\eta} \quad (4.3)$$

distribution corrects for pair acceptance and pair efficiency.

It is constructed by pairing the trigger particles from one event with the associated particles from other events which belong to the same multiplicity event class and also within the 2 cm wide z-vtx interval of the event from which the trigger particle is taken. In ideal case, the background distribution is normalized by a factor α such that it is unity at $(\Delta\eta, \Delta\phi) \sim (0,0)$ i.e. for the pairs

THIS THESIS

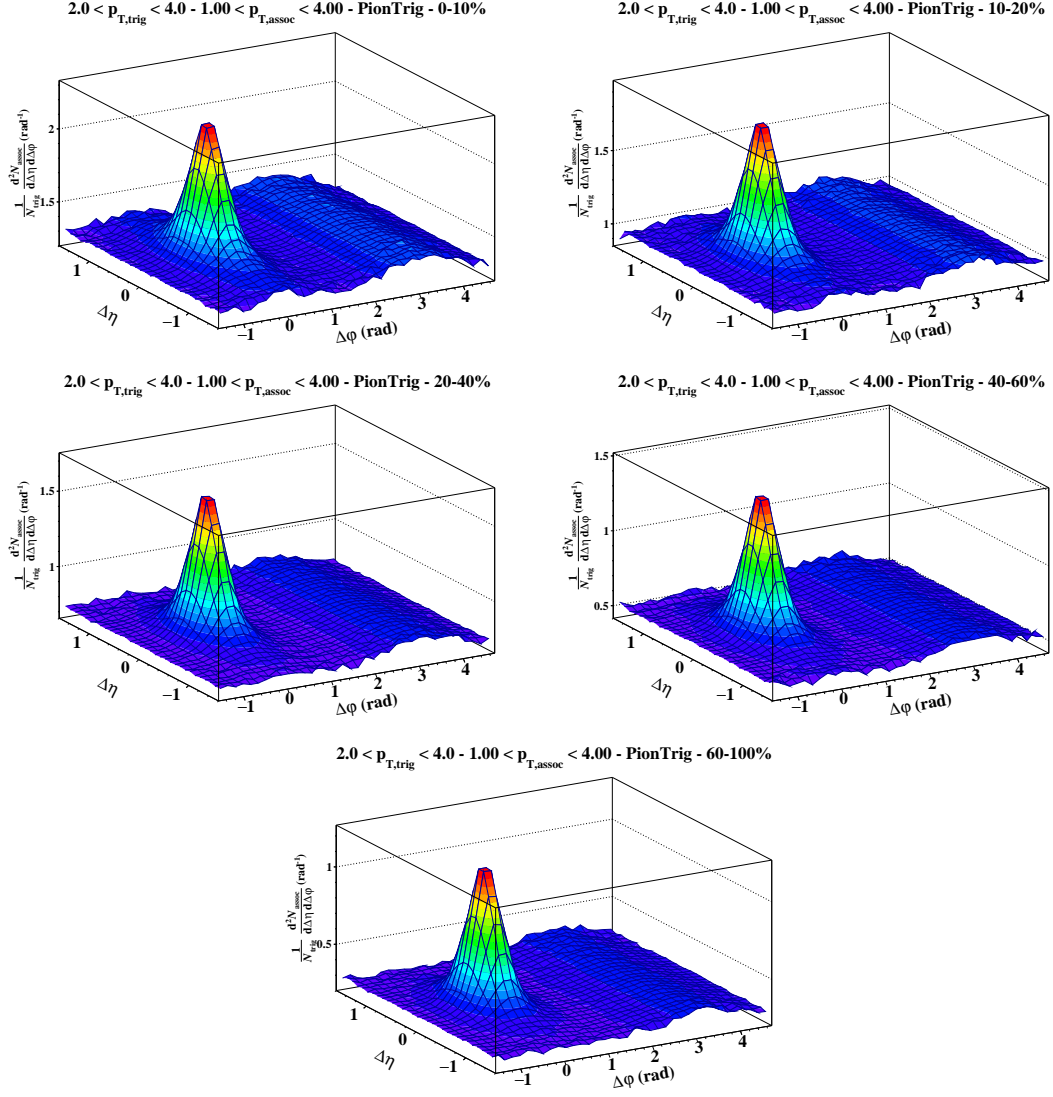


Figure 4.6: Pion triggered correlation functions (efficiency corrected) for five multiplicity classes used in this analysis.

THIS THESIS

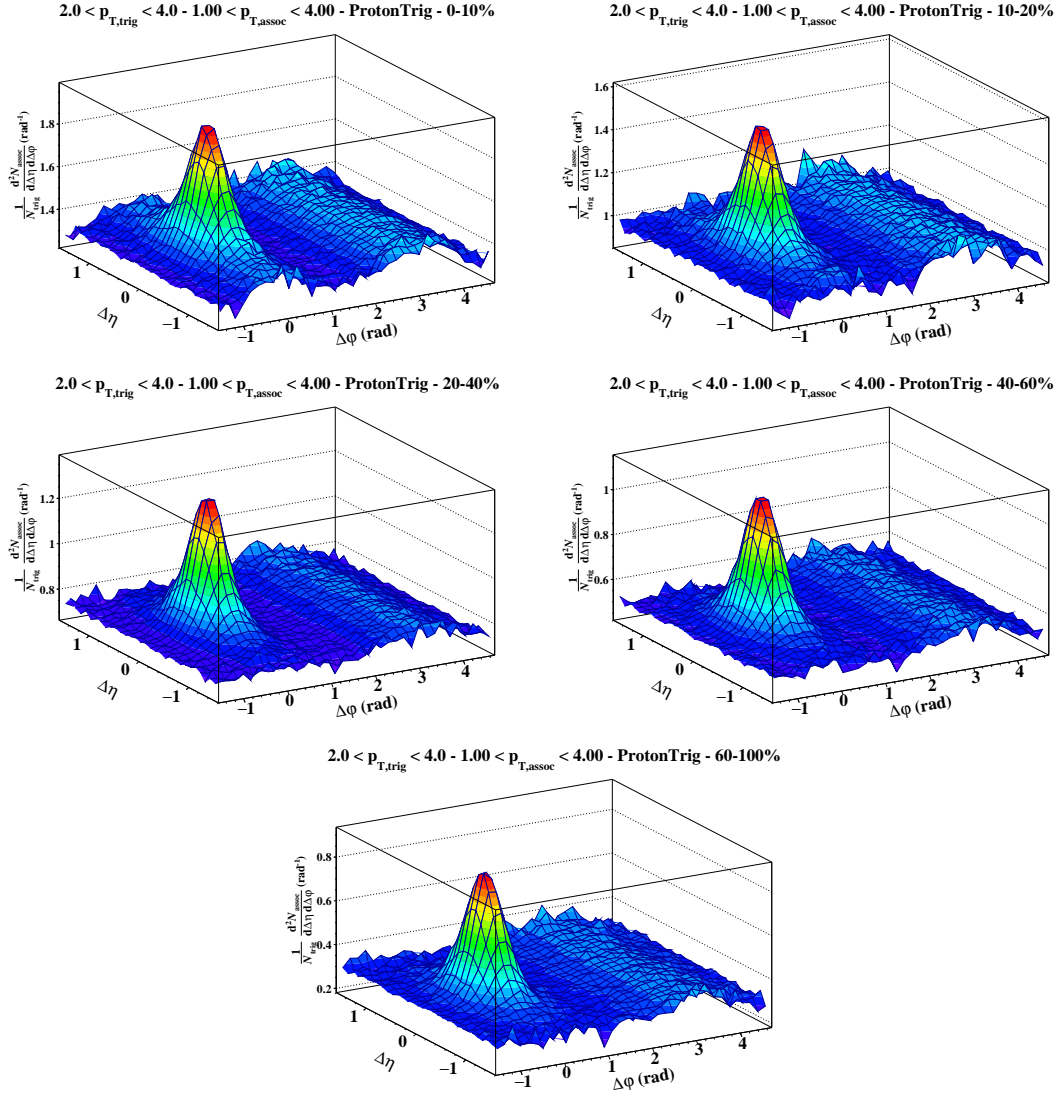


Figure 4.7: Proton triggered correlation functions (efficiency corrected) for five multiplicity classes used in this analysis.

where both particles are going approximately in the same direction (because if the trigger particle is within the detector acceptance, the associated particle is as well). But two tracks with similar momentum and shared clusters inside TPC (i.e spatially very close to each other) can be counted as one by the detector and this reduces the pair efficiency at small angles. This is known as track merging effect. This detector effect has been corrected by introducing a two-track efficiency cut which removes pairs which are spatially very close and potentially affected by this track merging effect. While pairing the trigger and associated particles to construct the signal and background distributions, only pairs that are separated by $|\Delta\eta| > 0.02$ and $|\Delta\phi_{min}^*| > 0.02$ are considered [19]. Where $\Delta\phi_{min}^*$ is the minimal azimuthal separation at the same radius between the two tracks within the active detector volume after taking into account the bending of the tracks due to the magnetic field [19]. As this cut is applied on the both same and mixed event distributions, the two-track effects are removed while taking the ratio between the same and mixed event distributions. This procedure corrects for the possible bias in the yield due to track merging effect of the pairs with small opening angles.

Now, this two-track efficiency cut generates a hole in the mixed event distribution (as shown in Fig. 4.8) and the background normalization factor can't be estimated from $(\Delta\eta, \Delta\phi) \sim (0,0)$. In this case the normalization factor is estimated by exploiting the flat $|\Delta\phi|$ distribution at $\Delta\eta \sim 0$ (see e.g. Figure 1 bottom right panel) by taking the average over that region. A small correction factor due to the finite bin size at $\Delta\eta \sim 0$ is also applied to α to take into account the fact that the top of the background function (i.e. bins at $\Delta\eta \sim 0$) is not a tip of a triangle rather is an integral over some range of the triangle. The pair acceptance and pair efficiency varies as a function of z-vtx. To take this into account the correlation function defined by Eqn 4.1 is constructed for each z-vtx interval. The final correlation function is the weighted average of the correlation functions over all z-vtx intervals [22].

Also, some wing structure has been found in the $\Delta\eta$ projection of the correlation function. To correct for that, the $\Delta\eta$ projection of the away side ($\pi/2 < \Delta\phi < 3\pi/2$) of the correlation function is fitted with a zero-degree-polynomial function and the ratio between the data and the

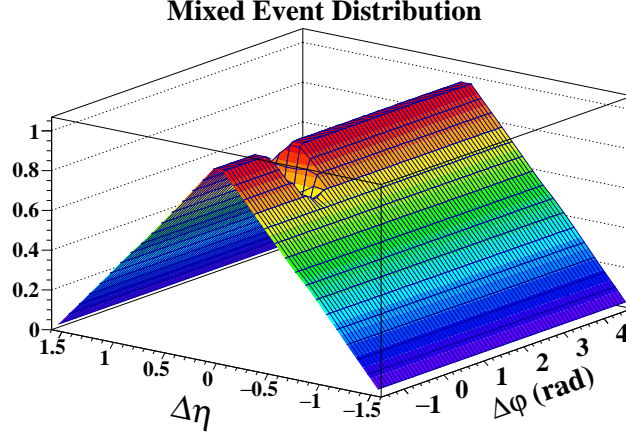


Figure 4.8: Normalized mixed event distribution function for trigger pions having $2.0 < p_T < 4.0$ GeV/c and unidentified associated particles having $1.0 < p_T < 4.0$ GeV/c in 0-10% multiplicity class of p-Pb collisions at $\sqrt{s_{NN}} = 5.02$ TeV (This Thesis).

fit value is used to correct the wing structure as described in [18],[20]. To reduce the effect of the decay products in the near side jet like peak, particle pairs which are likely to be generated from γ conversions or K_s^0 and $\Lambda(\bar{\Lambda})$ decay are removed by a cut on the invariant mass of the pairs (assuming the electron, pion or proton mass). The γ conversion pairs are removed by rejecting the pairs with invariant mass ($m_{inv} < 0.04$ GeV/ c^2) while the decay contribution from K_s^0 and $\Lambda(\bar{\Lambda})$ are reduced by removing pairs with invariant mass around their respective mass values with a tolerance of ± 0.02 GeV/ c^2 . The final correlation functions are corrected for efficiency and contamination which will be discussed in detail in another section. The efficiency corrected pion and proton triggered 2D correlation functions are shown in Fig. 4.6 and Fig. 4.7.

4.7 Particle Identification

For this analysis, particle identification for tracks having $2.0 < p_T < 4.0$ GeV/c is performed using the information obtained from both TPC (Time Projection Chamber) and TOF (Time of Flight). The performance plots of these two detectors for p-Pb collisions at 5.02 TeV are shown in Fig. 4.9. Tracks have been identified as pions and protons using combined (TPC+TOF) $n\sigma$ method (this method is similar to that mentioned in [17]). The variable $n\sigma$ can be defined

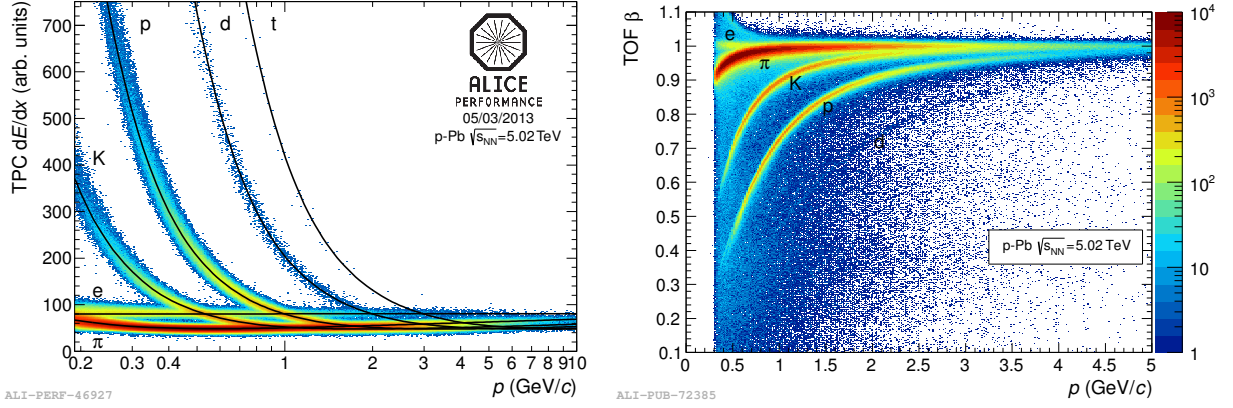


Figure 4.9: Left: Specific energy loss dE/dx in the tPC together with Bethe-Bloch curves for the different particle species. Right: TOF β (velocity) vs particle momentum (measured with TPC) curve.

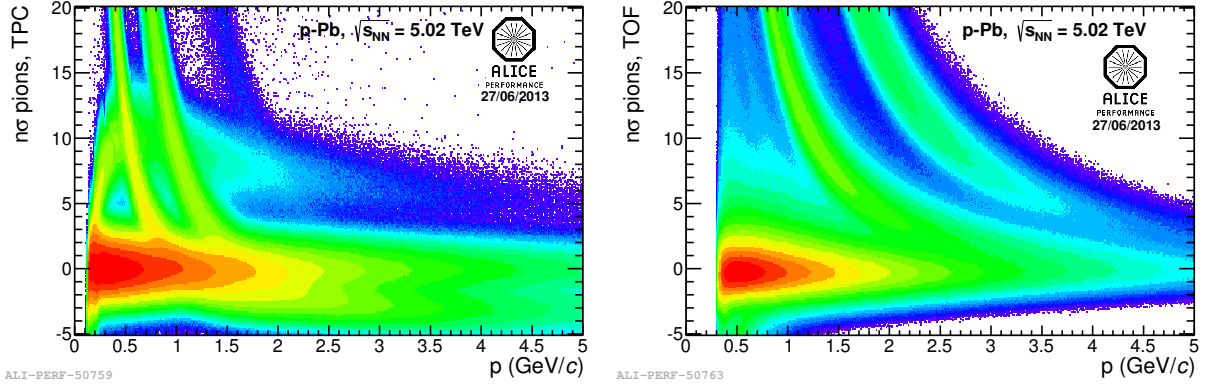


Figure 4.10: $n\sigma$ distribution for the different detectors in pion mass hypothesis for p-Pb collisions ($\sqrt{s_{NN}} = 5.02$ TeV) data sample.

separately for each detector. For TPC, it is defined as the number of standard deviation of a particular track's dE/dx value (experimentally measured) from the Bethe-Bloch expectation of a particular particle species like π , k or p, normalized by the detector resolution (σ) as shown in Eqn 4.4. In case of TOF, the similar definition of $n\sigma$ holds with the time-of-flight information from the detector depending upon the mass of the particle species (Eqn 4.5).

So, in case of TPC:

$$n\sigma_{\pi,k,p}^{TPC} = \frac{\frac{dE}{dx}_{\text{measured}} - \frac{dE_{\pi,k,p}}{dx}_{\text{expected}}}{\sigma_{\pi,k,p}} \quad (4.4)$$

In case of TOF:

$$n\sigma_{\pi,k,p}^{TOF} = \frac{t_{\text{measured}} - t_{\text{expected}}^{\pi,k,p}}{\sigma^{\pi,k,p}} \quad (4.5)$$

Now, From Fig. 4.9 it is clear that the separation between the different particle species bands decreases with increase in p_T and this variation is different for TPC compared to TOF. In TPC, the bands corresponding to different particle species start to merge around $p_T = 0.6-0.7$ GeV/c, whereas, in case of TOF the separation is good even for $p_T > 2.5$ GeV/c. But as the TOF is situated outside TPC, considering only TOF for particle identification reduces the efficiency as some of the tracks get trapped inside TPC and never make it to TOF. To optimize the efficiency and purity a combined (TPC+TOF) $n\sigma$ method has been developed and used for particle identification for tracks upto p_T 4.0 GeV/c [17]. The $n\sigma$ distributions for different detectors in pion mass hypothesis for p-Pb collisions at $\sqrt{s_{NN}} = 5.02$ TeV are shown in Fig.4.10. In this analysis the variable combined $n_{\sigma,PID}$ is defined as:

$$n_{\sigma,PID}^2 = n_{\sigma,TPC}^2 + n_{\sigma,TOF}^2 \quad (4.6)$$

For example $n_{\sigma,PID} = 3$ means a circular cut of radius 3 in $n_{\sigma,TPC}-n_{\sigma,TOF}$ plane around the mean position of the species to be identified. To illustrate the procedure the $n_{\sigma,TPC}-n_{\sigma,TOF}$ plot for pion mass hypothesis for $1.5 < p_T < 1.6$ GeV/c is shown in Fig. 4.11. With increase in p_T the separation between the mean position of different particle species decreases (as the bands for different particles start to merge in both TPC and TOF as shown in Fig. 4.9) and it leads to the possible overlap of the circles of radius 3 around the mean positions of different species. This creates misidentification of the particle species (e.g pions will be identified as kaons and vice versa) and affect the purity of the sample. This effect is measured as "misidentification rate" and will be discussed in the next section.

The cuts on $n_{\sigma,PID}$ used for this analysis:

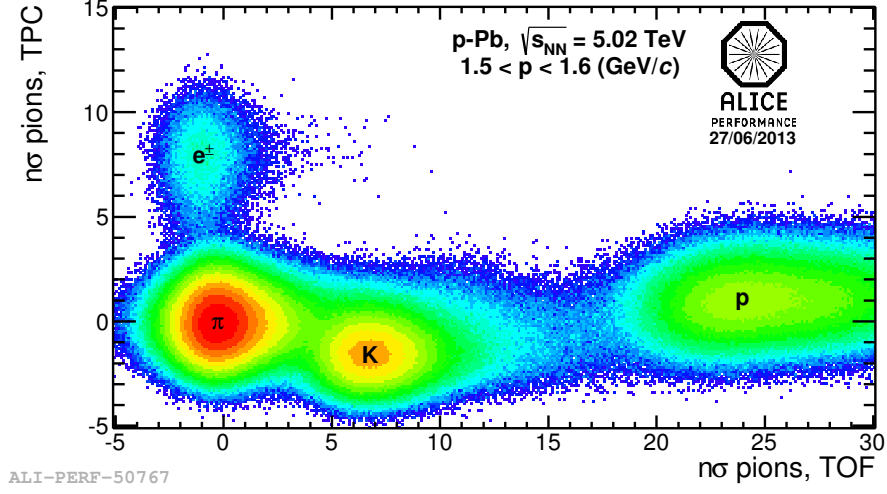


Figure 4.11: $n_{\sigma,TPC}$ - $n_{\sigma,TOF}$ plot for $1.5 < p_T < 1.6$ GeV/c in pion mass hypothesis for p-Pb collisions at $\sqrt{s_{NN}} = 5.02$ TeV .

$n_{\sigma,PID} = 3$ for tracks having $2.0 < p_T < 4.0$ GeV/c

For systematic checks this cut has been varied to:

$n_{\sigma,PID} = 2$ for tracks having $2.0 < p_T < 4.0$ GeV/c

AND

$n_{\sigma,PID} = 3$ for tracks having $2.0 < p_T < 4.0$ GeV/c (With exclusive NSigma cut)

Where exclusive Nsigma cut means all the tracks which are in the overlapped zone (i.e. in the overlapping zone of the two circles whose radius is defined by the $n_{\sigma,PID}$ around the mean positions of the PID species in TPC-TOF plane) are ignored for a better purity of the PID samples. In addition, The resolution of TOF gets worse in low multiplicity events and that effect is evaluated by removing the events with start time defined by the T0Fill. The differences between different PID configurations discussed here are considered as systematic uncertainty to the final result.

4.7.1 Misidentification rate

During particle identification, some tracks will be misidentified (e.g some pions are identified as kaons and vice versa and also true for other particle species) and will affect the purity of

the sample. This happens due to the overlap of circles of radius defined by $n_{\sigma, PID}$ cut in the TPC-TOF plane around different particle species. This misidentification rate is extracted from MC using the *TunedOnData* option switched **ON** in *PIDResponse* task [21]. Now, the Monte

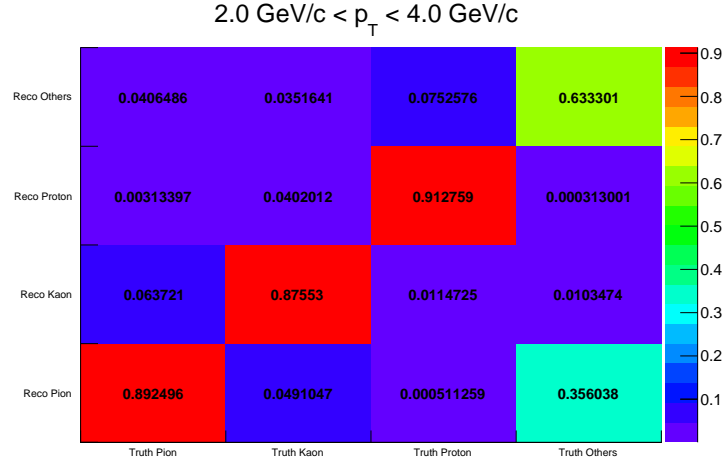


Figure 4.12: Misidentification rate for $2.0 < p_T < 4.0 \text{ GeV/C}$ for p-Pb collisions at $\sqrt{s_{NN}} = 5.02 \text{ TeV}$ (using DPMJET) (This Thesis).

Carlo (MC) production can't reproduce all the features present in the real data due to different reasons as imperfect simulation at microlevel, inadequate knowledge of the material budget, geometry alignment effects etc. But for a reliable PID method an accurate description of the detector response is necessary. As an example, for TPC the η dependence of the dE/dx signal, position of dE/dx crossing between the species as observed in the data are not reproduced in MC production. So, in the *TunedOnData* option the PID parameterisations of expected signals are extracted from data and used instead of using the parameterisations directly generated by the MC [21]. The misidentification fractions for each species are reported in Fig.4.12 for ($2.0 < p_T < 4.0 \text{ GeV/c}$). As the particle ratios in Data and MC are different, the values mentioned in the figures are normalized to the MC (i.e. the sum of each column is 1) to make it independent of relative particle yields in MC [17]. The diagonal terms represent the PID efficiency of the species from MC. The non diagonal values represent the misidentification rate (i.e. the fraction of species "A" identified as species "B" by the particle identification method). In this analysis, the effect

of the misidentification on the final observables (per trigger yields and their ratios) are studied using different PID cuts including the stringent one (with lower $n_{\sigma, PID}$ value and with exclusive NSigma PID option ON) and the effect has been included as systematic uncertainty.

4.8 Analysis and Corrections

This analysis is done in the p_T region ($1.0 < p_T < 4.0$ GeV/ c) and particle identification is done for trigger particles only i.e. for the tracks having $p_T > 2.0$ GeV/ c ($2.0 < p_T < 4.0$ GeV/ c). Particle identification method has been discussed in the previous section. To correct for detector

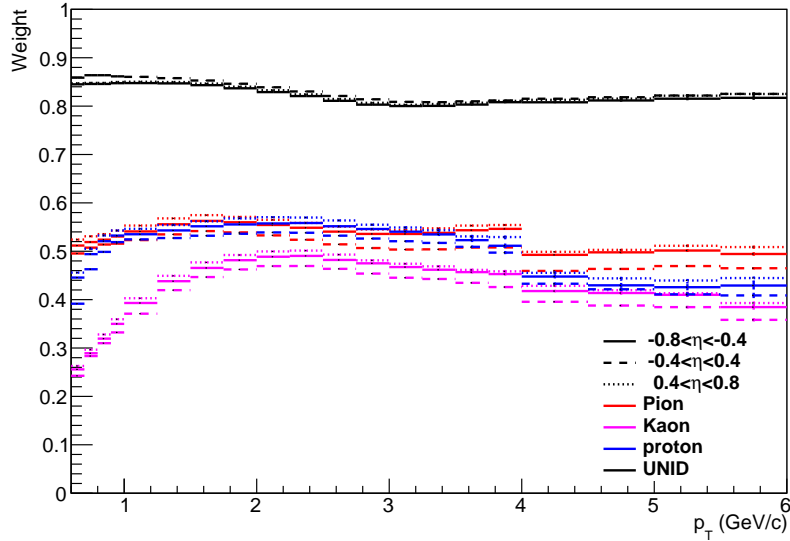


Figure 4.13: The correction factor(defined in Eq. 4.7) as a function of p_T for different η ranges and particle species (This Thesis).

acceptance, reconstruction efficiency and contamination by secondary particles, each track(both trigger and associated) is weighted with a correction factor as a function of η , p_t , Z_{vtx} and multiplicity (though the correction factor does not have any significant dependence on multiplicity). For identified particles this correction factor also includes the TOF matching efficiency and the particle identification efficiency [17]. The correction factor is defined as (determined using the

Monte Carlo sample):

$$w = \frac{\text{MC reconstructed tracks}(\text{ID}_{\text{MC}} = \text{ID}_{\text{Detector}})}{\text{MC generated primaries}} \quad (4.7)$$

The correction factors are extracted from MC samples with *TunedOnData* option switched **ON** in *PIDResponse* task. The correction factor(defined in Eq. 4.7) is plotted as a function of p_T in Fig. 4.13 for pions, kaons protons and hadrons for different η intervals.

4.9 Bulk Subtraction Procedure

The main goal of this analysis is to extract the near side ($-\pi/2 < \Delta\phi < \pi/2$) jetlike per trigger yield associated with pion and proton triggers at intermediate p_T ($2.0 < p_T < 4.0$ GeV/c). Now, the near side jet peak is located around $(\Delta\eta, \Delta\phi) \sim (0, 0)$ and the long range correlation at large $|\Delta\eta|$ contains the bulk/ridge structure as shown in Fig.4.7. Assuming the ridge to be $|\Delta\eta|$ independent, the bulk contribution is measured from large $|\Delta\eta|$ ($|\Delta\eta| > 1.2$) and subtracted from the short range correlation structure ($|\Delta\eta| < 1.2$) as it is done in [20]. The $\Delta\phi$ projected correlation functions for regions $|\Delta\eta| < 1.2$ (jet) and $|\Delta\eta| > 1.2$ (bulk) are shown in Fig.4.14. The background subtracted $\Delta\phi$ projections are shown in Fig.4.15.

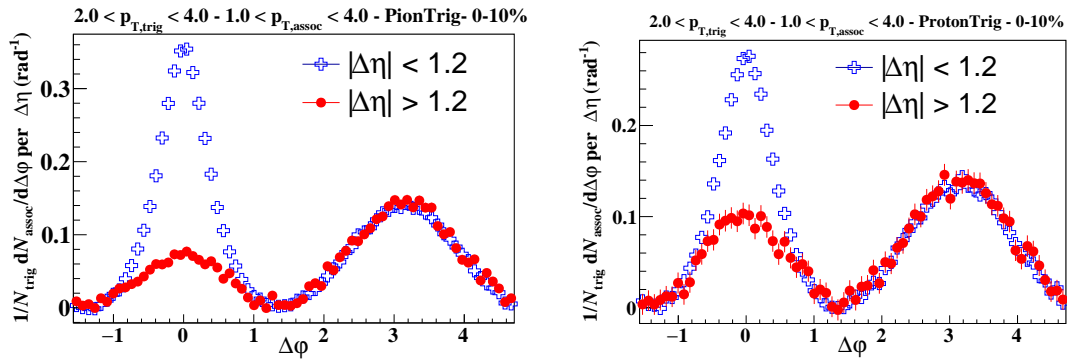


Figure 4.14: $\Delta\phi$ distributions of the jet ($|\Delta\eta| < 1.2$) and bulk ($|\Delta\eta| > 1.2$) region for pion triggered (left) and proton triggered (right) correlation function in 0-10% V0A multiplicity class (This Thesis).

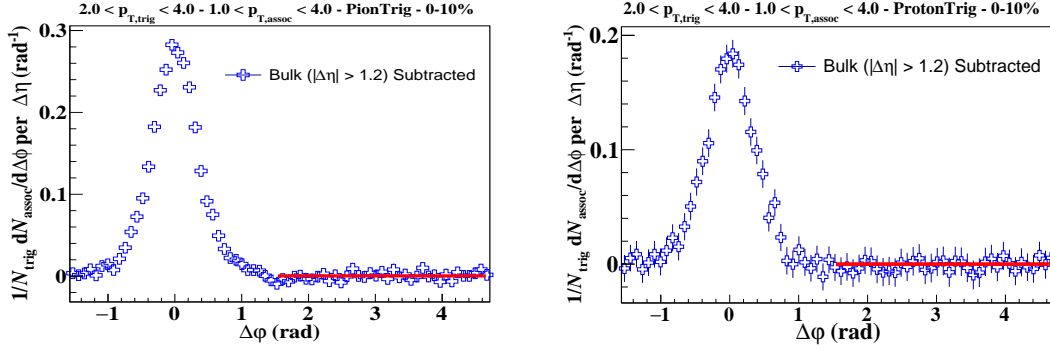


Figure 4.15: The bulk subtracted $\Delta\phi$ distributions for pion triggered (left) and proton triggered (right) correlation functions in 0-10% V0A multiplicity class. The flattish away side is fitted with zero-degree-polynomial function for residual baseline determination (This Thesis).

4.10 YIELD DETERMINATION

To calculate the near side ($-\pi/2 < \Delta\phi < \pi/2$) jet-like yield from the bulk subtracted 1D projections of the correlation functions as shown in Fig.4.15, both zero yield at minimum (ZYAM) and fitting (2 gaussians + flat baseline) methods are used.

In the ZYAM bin counting method, the histograms are integrated (bin contents are added) above a minimum value, in which the yield is set to zero [20]. The advantage of this method is that there is no need to make any assumption on the shape of the jet-peak and it reduces the systematic uncertainty associated with the yield determination. Now, due to subtraction of the long range correlation ($|\Delta\eta| > 1.2$) from the short range one ($|\Delta\eta| < 1.2$), the baseline is expected to be zero. But as the detector efficiencies are estimated from simulation which is not exact as reality, a small residual baseline may be present. After long range subtraction, the residual baseline is estimated for each multiplicity class from the flattish away side either as a weighted average of the correlated yields or by fitting the nearly flat away side with a zero degree polynomial function as shown in Fig.4.15. The residual baseline is further subtracted from the bulk subtracted near side jet peak prior to the final yield determination. The difference between the yields obtained using two different methods of residual baseline subtraction is found to be negligible. Also, as the away side peak is slightly wider than the near side [20], the near side yield has been evaluated

within $|\Delta\varphi| < 1.48$. This range has been varied from 1.47 to 1.49 and the effect on the yield has been found to be negligible. Furthermore, the near side region of the 1-D $\Delta\varphi$ distribution is fitted with two Gaussians and a constant term. One of the Gaussians has a narrow width to fit the peak region and the other one has relatively broader width for the tail region. The functional form is presented below:

$$f(\Delta\varphi) = C + A_1 e^{-\left(\frac{\Delta\varphi}{2\sigma_1}\right)^2} + A_2 e^{-\left(\frac{\Delta\varphi}{2\sigma_2}\right)^2} \quad (\sigma_2 > \sigma_1) \quad (4.8)$$

The $\Delta\varphi$ projection (1D) of pion and proton triggered correlation functions fitted with 2 gaussians and a constant baseline in 0-10% multiplicity class are shown in Fig.4.16 and the chi2/NDF values are shown in Fig 4.16. The ZYAM bin counting method results will be presented as the final

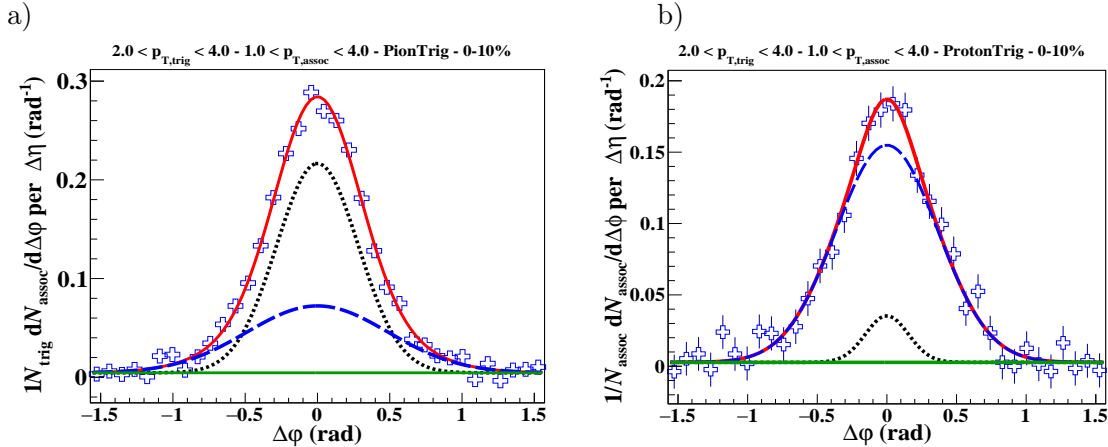


Figure 4.16: a) Pion triggered and b) proton triggered correlation function ($\Delta\phi$ projection) fitted with 2 gaussians and a flat baseline in 0-10% V0A multiplicity class (This Thesis).

one and the differences in the yields with respect to results obtained from the fit method will be included in the systematics. As ZYAM method doesn't make any assumption on the shape of the near side jet peak, it is more reliable than the fit method as discussed in [20]. Now, in case where bulk is not subtracted, the baseline is not zero by default. So, in that case the baseline is estimated from the zone between near side and away side correlation structure ($1.05 < |\Delta\phi| < 1.22$) in the long range ($|\Delta\eta| > 1.2$) of the correlation function [20]. Then this baseline

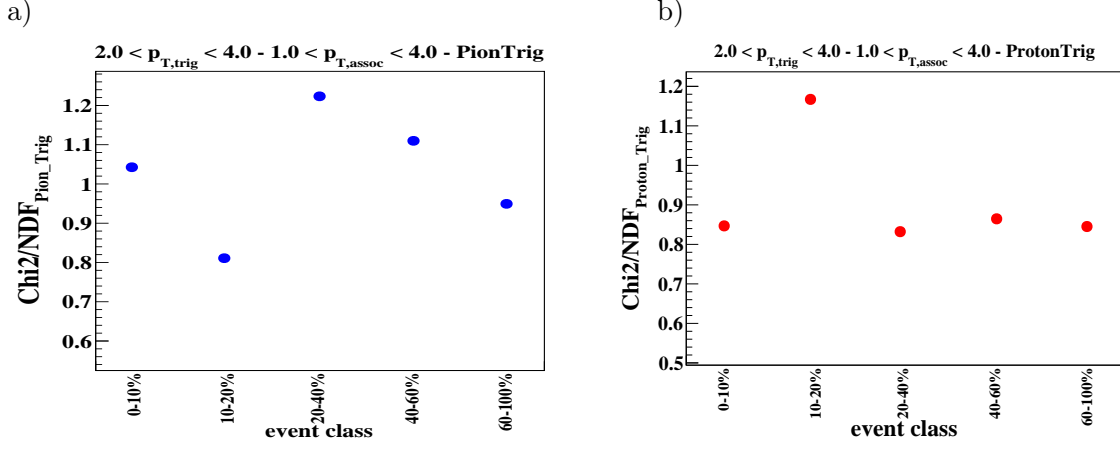


Figure 4.17: χ^2/Ndf values of 1-D fit to a) pion and b) proton triggered correlation function for different multiplicity classes (This Thesis).

is subtracted from the near side jet peak and jet-like yields are determined using the methods described above.

4.11 Systematics

The systematic uncertainties estimated from different sources are found to be multiplicity independent in case of small collision systems like p-Pb in previous analyses [17, 18, 20]. In this analysis, the near side jet-like yield is determined after bulk (estimated from $|\Delta\eta| > 1.2$) is subtracted from the short range correlation ($|\Delta\eta| < 1.2$). Now, as the η range is restricted upto $|\Delta\eta| < 0.8$, the bulk is actually estimated only from 4 $|\Delta\eta|$ bins ($1.2 < |\Delta\eta| < 1.6$) on both sides of the near side jet peak. The statistical fluctuations in the bulk may play a role in the yield determination as different systematic cuts may change the sample size and also the fluctuations in the bulk region, specially for the proton triggered correlation. For that reason, we have divided the entire analyzed sample into two V0A multiplicity classes (0-40% and 40-100%) to reduce the effect of statistical fluctuations in the bulk during systematic uncertainty determination. The different sources contributing to the systematic uncertainty are discussed below.

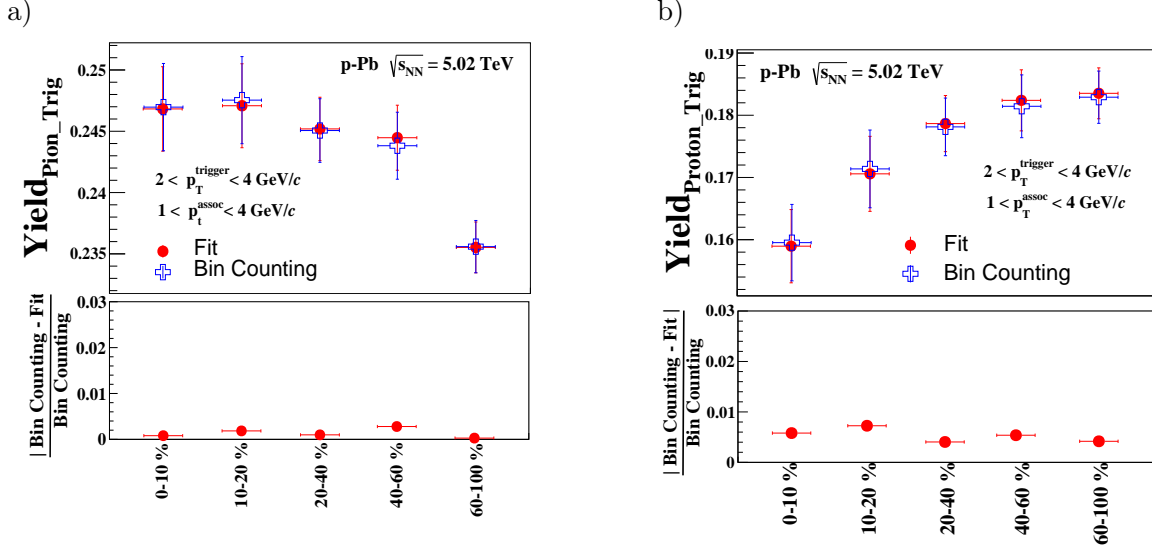


Figure 4.18: Near side yield associated with a) pion and b) proton triggered correlation calculated from bin counting and fit. The lower panel shows the relative difference w.r.t to bin counting method in both cases (This Thesis).

4.11.1 ZYAM procedure vs Fit

The near-side jet-like yields are estimated with bin counting and fitting method (constant baseline + 2 gaussians) as described earlier. The difference between the results as shown in Fig. 4.18 is considered for systematic uncertainty and it is found to be less than 1% for both pion and proton triggered yields.

4.11.2 Tracking efficiency

The tracking efficiency is calculated using the Monte-Carlo production (generator level) passing through GEANT simulated detector environment. But the simulated detector environment is not exactly same as reality and this leads to an uncertainty in the tracking efficiency. Also, this discrepancy depends on the set of cuts applied for track reconstruction. This analysis considers tracks having ($1.0 < p_T < 4.0$ GeV/c) and an overall 3% uncertainty in the tracking efficiency is used, as mentioned in [22].

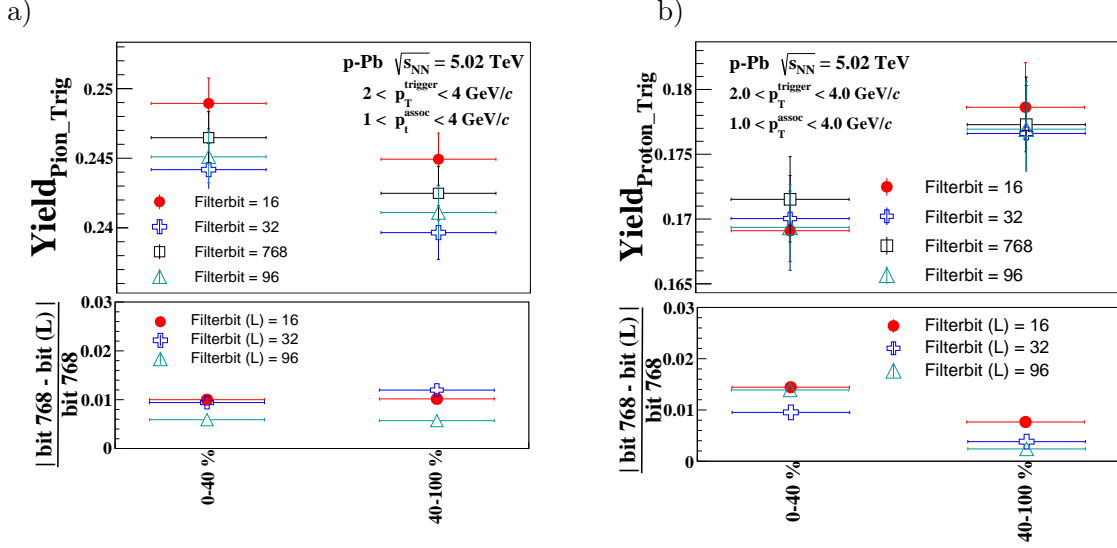


Figure 4.19: Near side yields of a) pion and b) proton triggered correlation in 0-40% and 40-100% VOA multiplicity classes for different track selection cuts. The lower panel shows the relative difference w.r.t default track cut (Filterbit- 768 which is discussed in detail in section 4.5) (This Thesis).

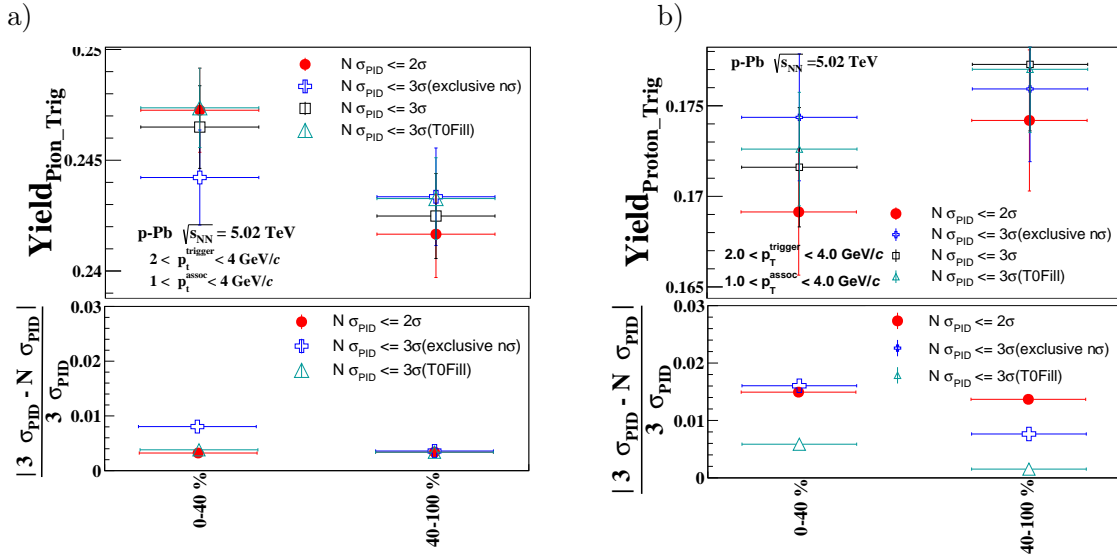


Figure 4.20: Near side yields of a) pion and b) proton triggered correlation in 0-40% and 40-100% VOA multiplicity classes for different PID selection cuts. The lower panel shows the relative difference w.r.t default 3σ PID cut (This Thesis).

4.11.3 Track selection

Different sets of track cuts (defined by different filterbits) are used to study the uncertainty associated with the track selection criteria. For this analysis the default filterbit is 768 and its meaning has been discussed in section 5. The analysis is then repeated for different filterbits. Fig 4.19 shows the near side yield associated with pion and proton triggers for different filterbits. The uncertainty due to different track selections is less than 2%.

4.11.4 PID selection

Different sets of $N\sigma$ cuts are used to estimate uncertainty due of PID selection criteria as already discussed in section 6. Now with change in $N\sigma$ values, the purity of the PID sample changes which further affects the final observable. Figure 4.20 demonstrates the near-side yield for different values of $N\sigma$, as indicated by the legends in the figure. The effect of different PID selections is found to be 1% for pion triggered yields whereas it is 2% for proton triggered case.

4.11.5 DCA cut variation

The effect of contamination from weak decays of $\Lambda/\bar{\Lambda}$ (decaying into proton and pion) is studied by repeating the entire analysis with filterbit 16 (global tracks with wide DCA cut) for different DCA-cut values like 3, 5, 7 σ [17]. The 7 σ cut is considered as default one and the difference between the yield at 7 σ and other values is considered as systematic uncertainty on the yields. For a stringent DCA cut (e.g. 3 σ) the probability for contamination from weak decay is lesser compared to the wider DCA (7 σ) cut. The near side yields from pion and proton triggered correlations are extracted for each DCA-cut mentioned above and the results are reported in Fig.4.21. It is seen that the effect is negligible for the pion triggered yields whereas, the effect is less than 1% for the proton triggered yields.

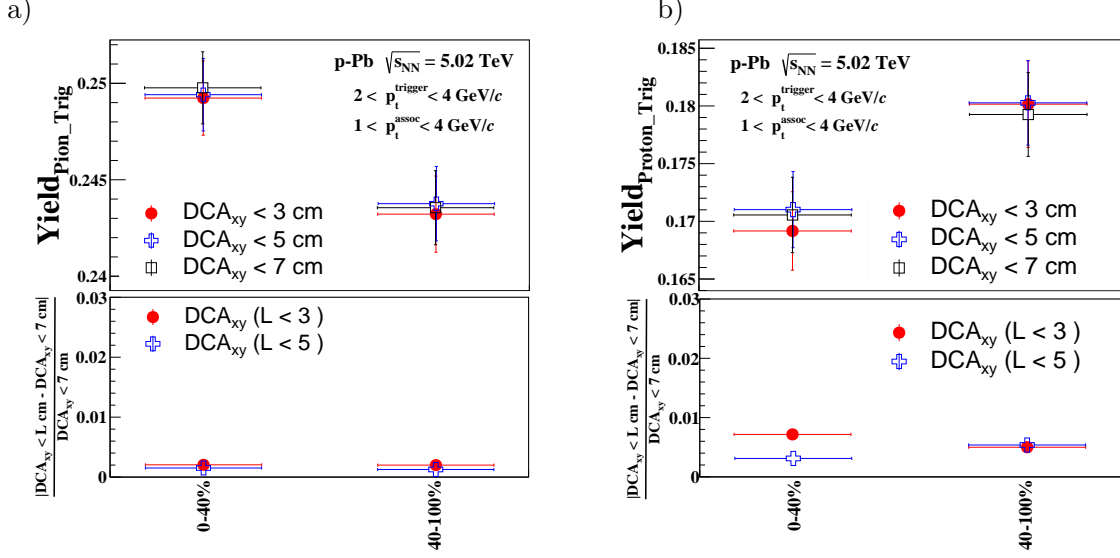


Figure 4.21: Near side yields of a) pion and b) proton triggered correlation in 0-40% and 40-100% V0A multiplicity classes for different DCA cut values. The lower panel shows the relative difference w.r.t default 7σ DCA cut (This Thesis).

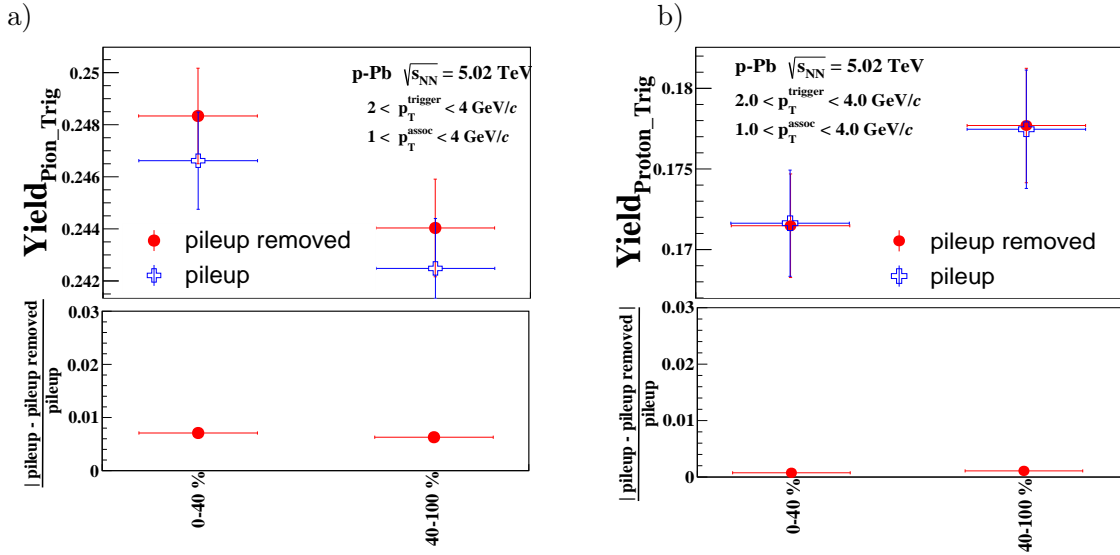


Figure 4.22: Near side yields of a) pion and b) proton triggered correlation in 0-40% and 40-100% V0A multiplicity classes with and without pile up correction. The lower panel shows the relative difference w.r.t without correction (This Thesis).

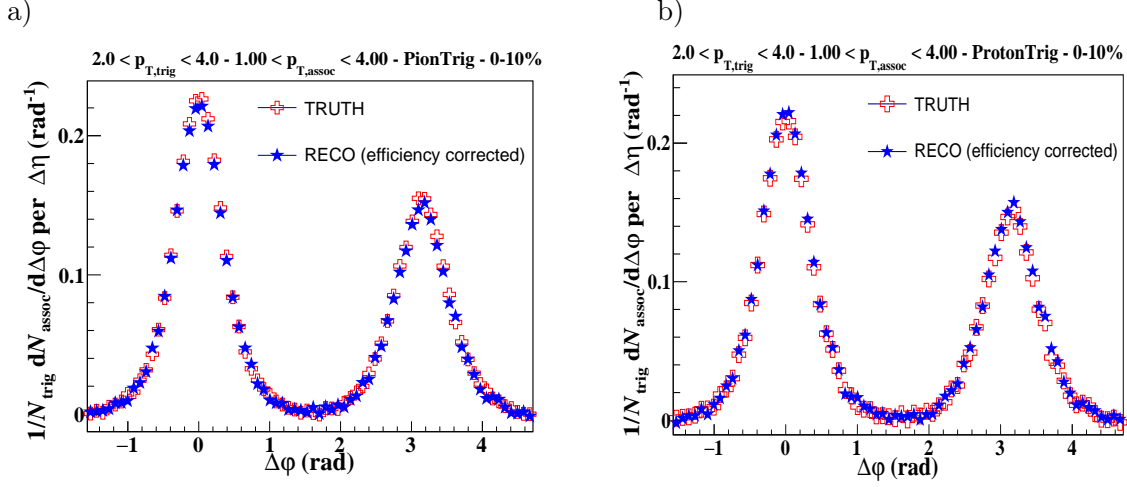


Figure 4.23: $\Delta\phi$ distribution of the MC TRUTH and MC RECO (efficiency corrected) a) pion and b) proton triggered correlation function in 0-10% V0A multiplicity class (This Thesis).

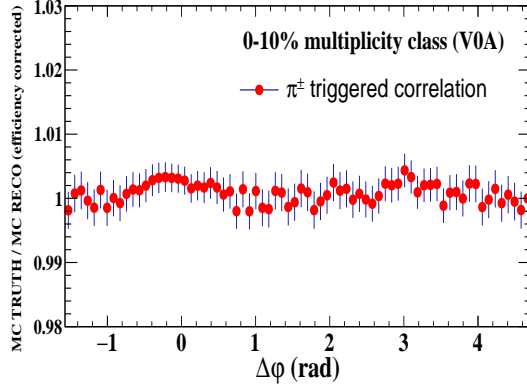
4.11.6 Pile-up

The effect of pile up (which can affect the TPC reconstructed data) has been studied using the multi-vertexer method. In this method, the vertexes are being classified with different "BCid" (bunch crossing identification number) using the TOF reconstructed tracks. The tracks having the same "BCid" number correspond to a particular vertex. For an event with more than one vertex, vertexes which are constructed using less than 5 tracks (contributors) are rejected. The discrepancy due to pile-up rejection is estimated by calculating the near side yield with and without default pile up rejection cuts as implemented within the analysis framework. The effect is less than 1% as shown in Fig 4.22.

4.11.7 MC-closure

To validate the reliability of the correction factors and correction procedure, the reconstructed MC events are corrected with the correction/ weight factors calculated from Eqn 4.7 and compared with the results calculated at the generator level without incorporating any detector effect or reconstruction algorithms. If the correction scheme is appropriate and weight factors are properly extracted, correlation functions derived from the reconstructed MC after corrections,

a)



b)

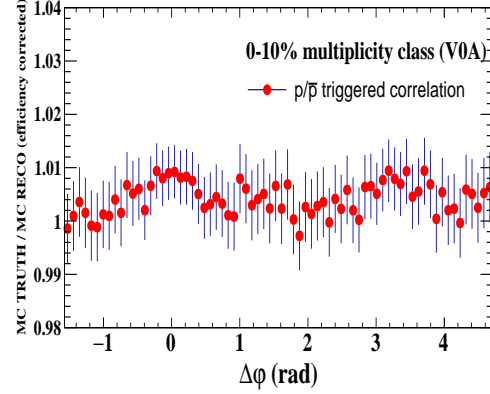


Figure 4.24: Ratio of $\Delta\varphi$ distribution of the MC TRUTH and MC RECO (efficiency corrected) a) pion and b) proton triggered correlation function in 0-10% V0A multiplicity class (This Thesis).

source	Near side yield π	Near side yield p/\bar{p}	ratio of yields(proton/pion)
Bin counting vs fit	1%	1%	negl.
Baseline Est.	negl.	negl.	negl.
Track Selection.	2%	2%	negl.
Tracking Eff.	3%	3%	negl.
PID Selection	1%	2%	1%
DCA cut variation	negl.	1%	1%
Pile-up	1%	negl	1%
MC-closure	negl.	negl	negl
Total (added in quadrature)	4%	4%	2%

Table 4.1: Summary of Systematics

and the generated MC (truth) should have a perfect agreement. The $\Delta\varphi$ projection of the MC truth and efficiency corrected reconstructed correlation functions and their ratio as shown in Fig 4.23 and Fig 4.24 show negligible difference between the two, therefore validating the correction procedure.

The contributions from all the sources of systematic uncertainties are listed in Table 4.1. The total uncertainty in the individual pion and proton triggered yields is 4% whereas for the ratio of proton to pion triggered yield it is 2% (as some sources of the systematic uncertainties get cancelled for the ratio).

4.12 Results and Discussion

In Fig 4.25, the multiplicity evolution of the pion and proton triggered near side jet-like yield with and without bulk subtraction is shown. For the un-subtracted case, both pion and proton triggered yields are increasing with multiplicity. But for the bulk subtracted case, the pion triggered yield shows almost no variation with multiplicity whereas the proton triggered yield decreases gradually with increase in multiplicity as shown in Fig 4.26(a). As a result, in the bulk subtracted case the ratio of proton to pion triggered jet-like yield (Fig 4.26(b)) decreases with multiplicity, creating trigger dilution [23, 24]. The trigger particles are selected from the intermediate p_T region where the inclusive proton to pion enhancement has been observed in p-Pb collisions at 5.02 TeV as shown in Fig.4.1(middle one). This enhancement can be explained in terms of coalescence model of hadronization and or radial flow [25, 26]. Particles pushed from lower to higher p_T by radial flow or produced via coalescence model of hadronization ("soft particles") are expected not to have short range collimated jet-like correlation beyond the expected flow (ridge) like correlation. Therefore the bulk/flow subtracted near-side jet peak is dominated by the hard triggered (jet) correlation only. As detectors can't distinguish between particles originating from hard and soft processes - the correlation functions are normalized by both hard and soft triggers and the soft triggers without any jet-like correlated partners in the bulk subtracted jet peak are expected to cause the "trigger dilution" effect in the per trigger jet-like yield [23, 24] [25, 26].

Now, soft processes like coalescence and/or radial flow favor proton production over the pion at intermediate p_T creating proton to pion enhancement. So, the rate of increase of the soft protons is more compared to the soft pions with multiplicity in the trigger p_T region. Thus once bulk(ridge) is subtracted, the baryon-triggered jet like yield is expected to get suppressed more compared to the pion triggered one from low to high multiplicity event classes commonly referred to as "trigger dilution" [23, 24] [25, 26] and that pattern has been observed in the data as shown in Fig 4.26.

In case of heavy ion collisions where severe jet quenching is present, the quenched energy is

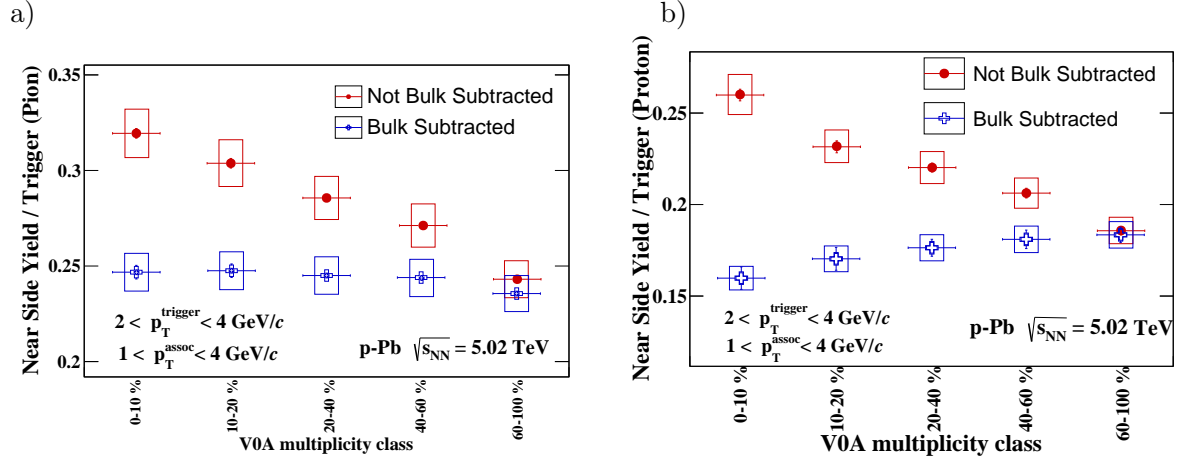


Figure 4.25: Near side yields of a) pion and b) proton triggered correlation for different multiplicity classes of p-Pb collisions at 5.02 TeV, with and without bulk subtraction (This Thesis).

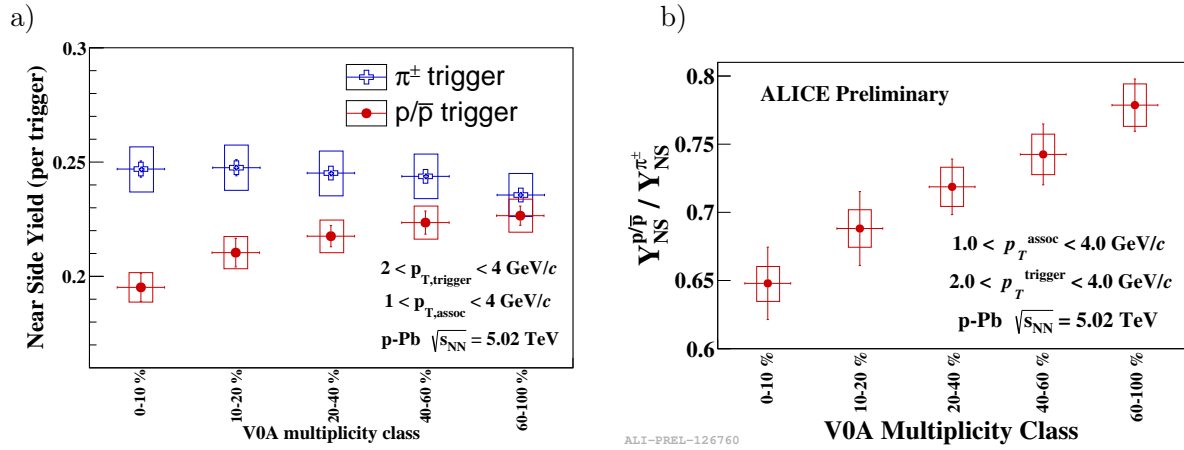


Figure 4.26: a) Near side yields of pion and proton triggered correlation for different V0A multiplicity classes of p-Pb collisions at 5.02 TeV, with bulk subtraction (This Thesis). b) Ratio of the near side jet-like yields associated with proton and pion triggers.

expected to manifest itself in terms of particles at low and intermediate p_T possibly affecting both jet and bulk in a way which is yet to be understood unambiguously making it difficult to disentangle the effect of soft physics (coalescence model of hadronization, radial flow) from the jet-medium interplay [23, 24]. Now, in the absence of jet quenching, trigger dilution can be used as a probe for soft physics in small collision systems (e.g p-Pb collisions). Also, Multiplicity evolution of the pion- and proton-triggered near side jet-like yields can provide insight on the particle production mechanism at intermediate p_T . For a better understanding, we have compared the

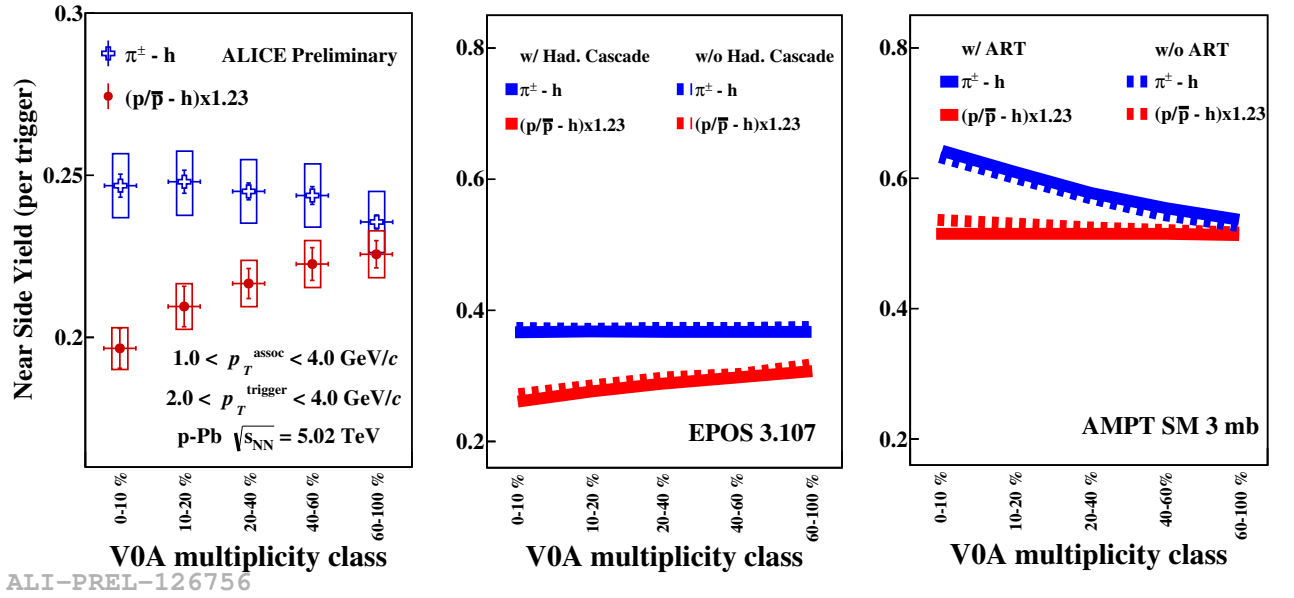


Figure 4.27: Near side yield from pion and proton triggered correlation in DATA (left), EPOS 3 (middle) and AMPT string melting (right).

data result with model based study using EPOS 3.107 (3+1 D hydro model) and AMPT string melting (incorporates coalescence model of hadronization) [25, 26]. As shown in Fig 4.27, none of the models can explain the data but EPOS3 can qualitatively reproduce the multiplicity evolution of the individual yields whereas the AMPT shows a pattern completely different from what we observe in the data - indicating radial flow as a possible source of trigger dilution in p-Pb collisions at $\sqrt{s_{NN}} = 5.02 \text{ TeV}$.

Bibliography

- [1] Aliroot reference guide. <http://aliroot-docs.web.cern.ch/aliroot-docs/>.

- [2] ALICE Collaboration, M. Zimmermann, The ALICE analysis train system, J. Phys. Conf. Ser. 608 no. 1, (2015) 012019, arXiv:1502.06381 [hep-ex].

- [3] S. Roesler, R. Engel, and J. Ranft, The Monte Carlo event generator DPMJET-III, in Advanced Monte Carlo for radiation physics, particle transport simulation and applications. Proceedings, Conference, MC2000, Lisbon, Portugal, October 23-26, 2000, pp. 1033-1038. 2000. arXiv:hep-ph/0012252 [hep-ph]. <http://www-public.slac.stanford.edu/sciDoc/docMeta.aspx?slacPubNumber=SLAC-PUB-8740>.

- [4] A. Capella, U. Sukhatme, C.-I. Tan, and J. Tran Thanh Van, Dual parton model, Phys. Rept. 236 (1994) 225-329.

- [5] R. Brun, F. Carminati, and S. Giani, GEANT Detector Description and Simulation Tool,.

- [6] ALICE Collaboration, B. Abelev et al., Pseudorapidity density of charged particles in p + Pb collisions at $\sqrt{s_{NN}} = 5.02$ TeV, Phys. Rev. Lett. 110 no. 3, (2013) 032301,

arXiv:1210.3615 [nucl-ex].

- [7] ALICE Collaboration, B. B. Abelev et al., Performance of the ALICE Experiment at the CERN LHC, Int. J. Mod. Phys. A29 (2014) 1430044, arXiv:1402.4476 [nucl-ex].
- [8] ALICE Collaboration, J. Adam et al., Centrality dependence of particle production in p-Pb collisions at $\sqrt{s_{NN}} = 5.02$ TeV, Phys. Rev. C91 no. 6, (2015) 064905, arXiv:1412.6828 [nucl-ex].
- [9] ALICE Collaboration, B. Abelev et al., Centrality determination of Pb-Pb collisions at $\sqrt{s_{NN}} = 2.76$ TeV with ALICE, Phys. Rev. C88 no. 4, (2013) 044909, arXiv:1301.4361 [nucl-ex].
- [10] R. Glauber, Lectures in Theoretical Physics. WE Brittin and LG Dunham, New York: Interscience, 1959.
- [11] M. L. Miller, K. Reygers, S. J. Sanders, and P. Steinberg, Glauber modeling in high energy nuclear collisions, Ann. Rev. Nucl. Part. Sci. 57 (2007) 205-243, arXiv:nucl-ex/0701025 [nucl-ex].
- [12] J. E. Elias, W. Busza, C. Halliwell, D. Luckey, P. Swartz, L. Votta, and C. Young, An Experimental Study of Multiparticle Production in Hadron - Nucleus Interactions at High-Energy, Phys. Rev. D22 (1980) 13.

- [13] PHOBOS Collaboration, B. B. Back et al., Scaling of charged particle production in d-Au collisions at $\sqrt{S_{NN}} = 200$ GeV, Phys. Rev. C72 (2005) 031901, arXiv:nucl-ex/0409021 [nucl-ex].
- [14] PHENIX Collaboration, A. Adare et al., Phys. Rev. C90 no. 3, (2014) 034902, arXiv:1310.4793 [nucl-ex].
- [15] STAR Collaboration, J. Adams et al., Evidence from d + Au measurements for final state suppression of high p_T hadrons in Au+Au collisions at RHIC, Phys. Rev. Lett. 91 (2003) 072304, arXiv:nucl-ex/0306024 [nucl-ex].
- [16] ALICE Collaboration, B. Abelev et al., Pseudorapidity density of charged particles in p + Pb collisions at $\sqrt{S_{NN}} = 5.02$ TeV, Phys. Rev. Lett. 110 no. 3, (2013) 032301, arXiv:1210.3615 [nucl-ex].
- [17] <https://aliceinfo.cern.ch/Notes/node/183>:Long-range angular correlations of π , K, p in pPb collisions at $\sqrt{S_{NN}} = 5.02$ TeV
- [18] <https://aliceinfo.cern.ch/Notes/node/147>:Long-range angular correlations on the near and away side in p-Pb collisions at $\sqrt{S_{NN}} = 5.02$ TeV
- [19] J. Gramling, <https://indico.cern.ch/materialDisplay.py-contribId=36-sessionId=6-materialId=slides-confId=142700>
- [20] <https://aliceinfo.cern.ch/Notes/node/230>:Minijets analysis with two-particle correlations

in p-Pb collisions at $\sqrt{s_{NN}} = 5.02$ TeV

[21] <https://twiki.cern.ch/twiki/bin/view/ALICE/PIDInAnalysis>

[22] ALICE Collaboration, B. Abelev et al., Multiplicity dependence of pion, kaon, proton and lambda production in p-Pb collisions at $\sqrt{s_{NN}} = 5.02$ TeV, arXiv:1307.6796 [nucl-ex].

[23] N. M. Abdelwahab et. al (STAR Collaboration) Phys. Lett. B 751 (2015) 233-240

[24] S.S. Adler et. al (PHENIX Collaboration) Phys. Rev. C 71 (2005) 051902

[25] D. Sarkar, S. Choudhury, S. Chattopdhyay. Phys. Lett. B 760 (2016) 763-768

[26] D. Sarkar, S. Choudhury, S. Chattopdhyay. Phys. Rev. C 94, 044909 (2016)

Chapter 5

Investigating the radial flow like effects in pp collisions at $\sqrt{s} = 7$ TeV using two particle correlations with identified triggers

5.1 Introduction

The observation of collective-like behaviors in pp collisions at LHC energy can be qualitatively explained by both hydro based models (e.g. EPOS 3) and other mechanisms like multi-parton interactions (MPI) with color reconnection (CR) as implemented in PYTHIA 8 - making it difficult to pinpoint the underlying mechanism responsible for the observed flow like effects in high multiplicity pp collisions. In this chapter, using the two particle correlation technique, it has been demonstrated that the multiplicity evolution of the near side jet-like yield associated with pion and proton triggers selected from intermediate p_T (where inclusive baryon to meson enhancement has been observed) can disentangle the effect of hydrodynamical flow from the effect of MPI based color reconnection in a straightforward way.

Like p-Pb, radial flow like effects on spectra [1–4], ridge like structures [5] [6], mass ordering of $\langle v_2 \rangle$ [7] [8], strangeness enhancement [9], [10] has been observed in pp collisions at LHC energy and it has triggered the debate about the presence of hydro like collectivity in small collision systems. These collective like behaviors were initially observed in heavy ion collisions [11–14] and attributed to the hydrodynamical evolution of a strongly interacting system. But for the applicability of hydrodynamics, thermalization of the system is an essential prerequisite for which the mean free path of the constituents has to be smaller than the system size. This is not so obvious for small collision systems making hydrodynamical modelling of small systems debatable [15]. Also, the absence of jet quenching in p-Pb collisions at LHC energy [16] as already discussed in chapter 2 further indicates that the medium may be transparent to the hard-QCD processes and other mechanisms may be responsible for the observed flow like signatures in small systems. Though hydrodynamical models can explain the observed flow like signatures in pp and p-Pb collisions at LHC energy [17] [18–20], other mechanisms like incoherent parton scattering with coalescence model of hadronization in AMPT [21–23], multi parton interactions (MPI) with color reconnection in PYTHIA [24, 25] can also reasonably explain the collective like signatures in small systems. In a recent work, it has also been demonstrated that the combination of the event by event initial gluon distribution by IP-Glasma and the Lund string fragmentation as implemented in PYTHIA can also generate the hydro like signatures in pp collisions at LHC energy[26].

Now, two completely different physics mechanisms as implemented in EPOS 3 (3+1 D event by event hydrodynamical model) and PYTHIA 8 (with color reconnection) can qualitatively generate the radial flow like effects in terms of observables like hardening of spectra with multiplicity, mass dependence of mean p_T vs multiplicity, baryon to meson enhancement at intermediate p_T [20] [24, 25] etc. So, it would be useful to find an observable whose response towards these two mechanisms is completely different and can be used to disentangle the effect of one from the other to explore the origin of flow like effects in pp collisions at LHC energy. The effect of hydrodynamical flow on the per-trigger yields associated with pion and proton triggers at intermediate

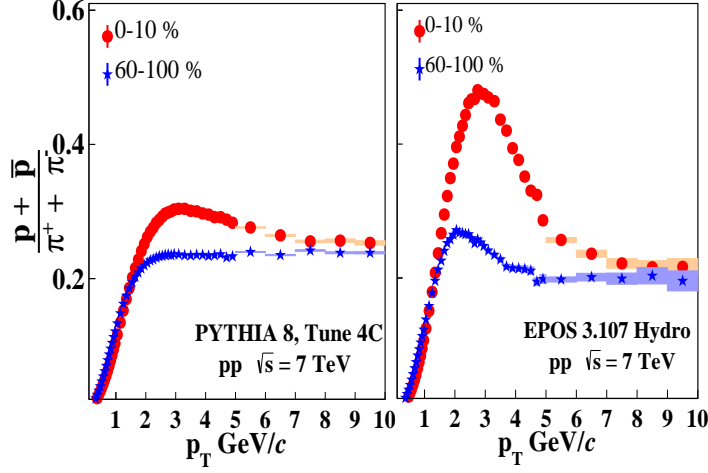


Figure 5.1: [Color online] Inclusive proton over pion ratio as obtained from PYTHIA 8 (left) and EPOS 3 (right) in 0-10% and 60-100% event classes of pp collisions at $\sqrt{s} = 7$ TeV.

p_T has been discussed in detail in chapter 2 using the EPOS 3 model for p-Pb collisions at $\sqrt{s_{NN}} = 5.02$ TeV and the results are published in [27]. The pion and proton triggers were selected from intermediate p_T ($2.0 < p_T < 4.0$ GeV/c) where the inclusive proton to pion enhancement has been observed [27] and can be explained in terms of radial flow in the context of EPOS 3. Particles undergoing hydrodynamical evolution (originating from the "core" in EPOS 3) are expected not to have correlated partners in the bulk subtracted near side jet peak - creating dilution in the per trigger jet-like yield [27]. As the radial flow pushes massive hadrons more compared to the lighter ones, a larger rate of dilution with multiplicity is expected in the proton triggered correlation compared to the pion triggered case - an effect commonly known as "trigger dilution" [27–29].

In PYTHIA 8, color reconnection (CR) generates the proton to pion enhancement in pp collisions at 7 TeV at intermediate p_T [24] as shown in Fig 5.1 and this is qualitatively similar to the pattern generated by EPOS 3. By construction, the hard and soft components of the interaction

are strongly coupled in the color reconnection (CR) mechanism and it plays the crucial role in generating the radial flow like signatures in high multiplicity pp collisions at LHC energy [25]. In [25] it has also been demonstrated that the blast wave model [30] fits the spectra in low multiplicity pp events having jets with $p_T^{jet} > 5 \text{ GeV}/c$ compared to the events without any jet selection [25]. In high multiplicity pp events, the blast wave model [30] can describe the spectra only when the CR mechanism is included and the fitting gets better with increasing p_T^{jet} [25]. This indicates that the jet is playing crucial role in originating the flow like effects in PYTHIA 8. In this work, It is shown that the correlation with identified triggers selected from intermediate p_T can disentangle the effect of hydrodynamics from the effect of CR mechanism in PYTHIA 8 in a simple way without involving any jet reconstruction or fitting of the spectra as discussed in [25].

5.2 The EPOS 3 model

Basic features of this model has already been discussed in the previous chapters and details can be found in [20] [31] [32] [33].

5.3 The PYTHIA 8 model

PYTHIA is a multi parton interaction [34] based event generator for pp collisions. In PYTHIA, each collision is described by leading-order p-QCD calculations, initial and final state parton radiation, multiple parton-parton interactions (MPI), beam remnants and Lund string fragmentation model of hadronization [25]. The MPI can reasonably explain the multiplicity distribution and correlation between transverse sphericity with multiplicity in pp collisions at LHC energy. However, in order to explain the hydro like behavior as observed in pp collisions at LHC energy, the color reconnection mechanism [35] is required. In this mechanism, final partons from independent hard scatterings are color connected to generate a transverse boost [24]. This effect is more prominent for events with several partonic scatterings as it generates a large transverse

boost mimicking the radial flow like effect in hydrodynamics. Though the origin of this boost like effect in the CR mechanism is completely different compared to that of hydrodynamics, this can explain the hardening of spectra with multiplicity, inclusive baryon to meson enhancement at intermediate p_T , mean p_T vs multiplicity and its mass dependence as observed in the pp collisions at LHC energy [20] [24].

5.4 Analysis Method

The two particle correlation technique used in this chapter is already discussed in detail in chapter 2 and also in [27]. The p_T range of trigger and associated particles are $2.0 < p_T < 4.0$ GeV/ c and $0.5 < p_T < 4.0$ GeV/ c respectively and the correlation function has been constructed with a p_T ordering ($p_T^{assoc} < p_T^{trigger}$). The pseudo-rapidity of the particles are restricted within $-0.8 < \eta < 0.8$.

Both p/ π ratio and correlation analysis have been performed by dividing the entire minimum

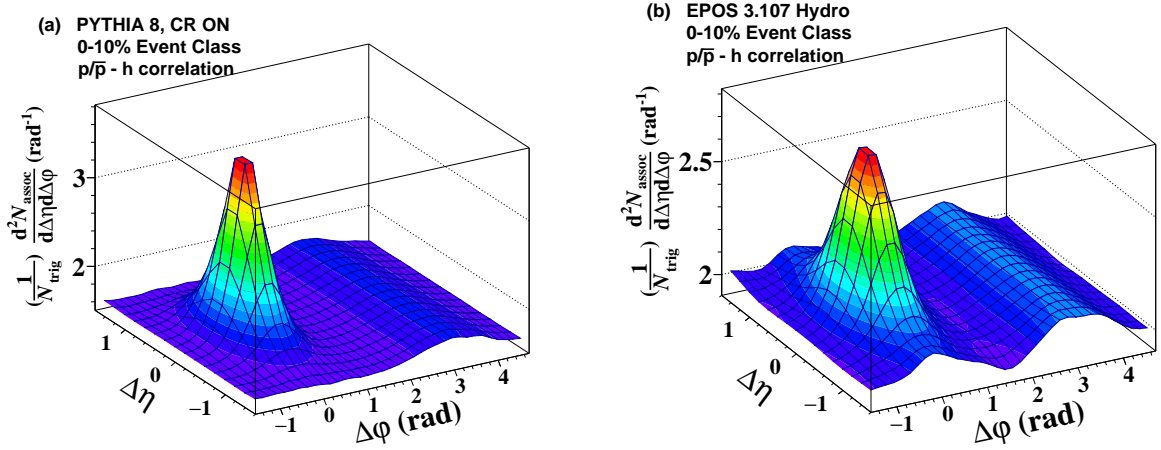


Figure 5.2: [Color online] Two particle $\Delta\eta$ - $\Delta\phi$ correlation function in 0-10 % event class of pp collisions at $\sqrt{s} = 7$ TeV with proton as trigger particles from (a) PYTHIA 8 and (b) EPOS 3.

bias events into four multiplicity classes based on the total number of charged particles produced (with $p_T > 0.05$ GeV/ c) within $2.8 < \eta < 5.1$ or $-3.7 < \eta < -1.7$. This corresponds to the acceptance range of ALICE VZERO-A and VZERO-C detector and used for multiplicity class

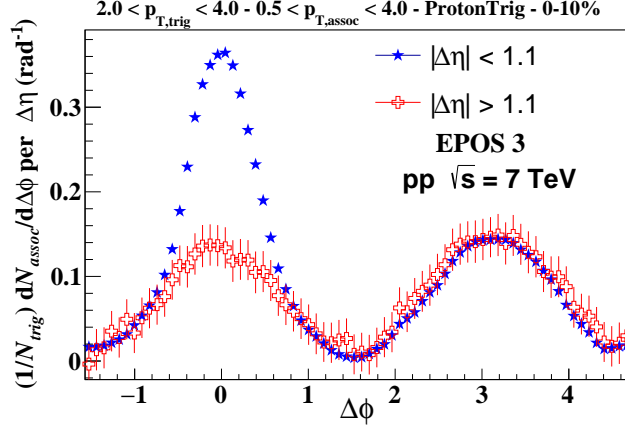


Figure 5.3: [Color online] The $\Delta\phi$ projected correlation function for two $\Delta\eta$ regions referred to as jet (blue) and bulk (red).

determination by the ALICE collaboration [36]. The multiplicity classes are denoted as 60-100%, 40-60%, 10-40%, 0-10% from the lowest to the highest multiplicity. Two particle correlation functions with proton triggers as obtained from PYTHIA 8 and EPOS 3 in the 0-10% event class are given in Fig 5.2.

This analysis concentrates only on the near side ($|\Delta\phi| < \pi/2$) of the correlation function. The particles from jet fragmentation are expected to be confined in a small angular region. The flow modulated background is estimated from large $|\Delta\eta|$ ($|\Delta\eta| \geq 1.1$) and subtracted from the near side jet peak ($|\Delta\eta| < 1.1$) as it is done in [27] [37]. The $\Delta\phi$ projected correlation functions for regions $|\Delta\eta| < 1.1$ (jet) and $|\Delta\eta| > 1.1$ (bulk) are shown in Fig 5.3. The background subtracted $\Delta\phi$ projected correlation function is shown in Fig 5.4. After bulk subtraction the event averaged near-side jet-like per trigger yield is calculated by integrating the $\Delta\phi$ projection in the range $|\Delta\phi| < \pi/2$.

5.5 Results and Discussion

In this work, the multiplicity evolution of the bulk subtracted near-side jet-like per trigger yield associated with pion and proton triggers in pp collisions at $\sqrt{s} = 7$ TeV has been studied. The

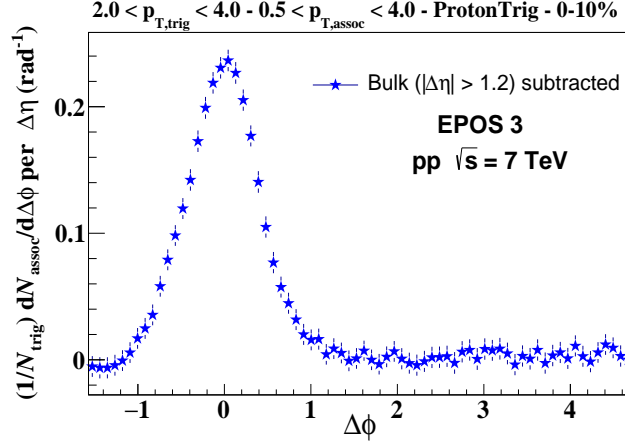


Figure 5.4: [Color online] The $\Delta\phi$ projected correlation function after bulk subtraction as discussed in the text.

trigger particles are selected from the intermediate p_T range ($2.0 < p_T < 4.0$ GeV/ c) where the inclusive proton to pion enhancement has been observed in data [3] and can be qualitatively explained by both hydrodynamics (EPOS 3) and MPI based color reconnection (PYTHIA 8) as shown in Fig 5.1.

In Chapter 2 it has been shown that in case of corona-corona (jet-like) correlation in EPOS 3 [27], the pion and proton triggered jet-like yields increase with multiplicity but the rate of increase has no trigger species dependence - showing no trigger dilution. Now, in the calculation considering all (both core and corona) particles [27], the bulk subtracted near side jet peak contains the hard triggered (corona - corona) correlation only. But the correlation function is normalized by both hard and soft triggers and the soft triggers (originating from "core") generate the trigger dilution effect [27] in the per trigger jet-like yield. Now, a similar pattern of "trigger dilution" has also been observed in pp collisions at $\sqrt{s} = 7$ TeV using EPOS 3 data. In Fig. 5.5(a) the multiplicity dependence of the bulk subtracted near side jet-like yield (per trigger) as calculated from EPOS 3 is shown. Both pion and proton triggered yield decrease with multiplicity but the proton triggered yield exhibits a larger rate of suppression, creating trigger dilution as shown in Fig 5.5(b). Radial flow pushes more protons than pions from lower to higher p_T and the

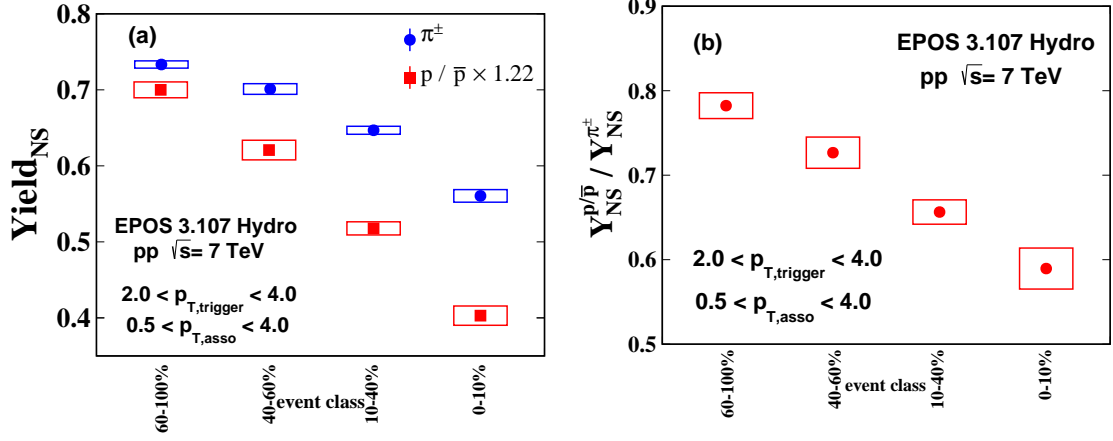


Figure 5.5: [Color online] a) Multiplicity dependence of the near-side jet-like per trigger yield (bulk subtracted) associated with proton and pion triggers in pp collisions at $\sqrt{s} = 7$ TeV from EPOS 3.107. b) Multiplicity dependence of the ratio of the proton to pion triggered yield in pp collisions at $\sqrt{s} = 7$ TeV from EPOS 3.107.

particles originating from the core are unlikely to have correlated partners in the bulk subtracted near side jet peak which is a characteristic of the jet fragmentation. As a result, with increase in multiplicity, a relatively higher suppression in the proton triggered jet-like yield (bulk subtracted) is expected compared to the pion triggered case as triggers are selected from the intermediate p_T range where inclusive proton to pion enhancement has been observed [27].

In small collision systems like pp or p-Pb, trigger dilution can be used as a probe to detect the presence of hydrodynamical flow in the system [27] compared to the heavy ion case where severe jet quenching affects the correlation pattern making it difficult to disentangle the effect of soft physics (e.g. radial flow) from the jet-medium interplay [28, 29]. Now, color reconnection in PYTHIA 8 [20] [24] can also qualitatively explain the hydro like behaviors as observed in data [3]. As, both EPOS 3 and PYTHIA 8 can generate the inclusive proton to pion enhancement at intermediate p_T , it would be interesting to check whether the response of the multiplicity evolution of the near side jet-like yield associated with identified triggers at intermediate p_T can disentangle the effect of hydrodynamical flow from color reconnection or not.

The multiplicity dependence of the bulk subtracted near side jet-like yield (per trigger) as

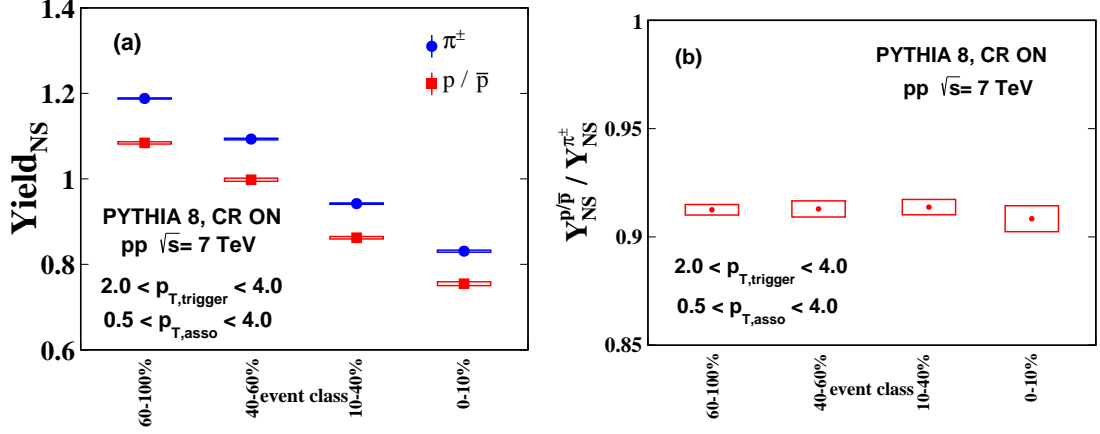


Figure 5.6: [Color online]a) Multiplicity dependence of the near-side jet-like per trigger yield (bulk subtracted) associated with proton and pion triggers in pp collisions at $\sqrt{s} = 7$ TeV from PYTHIA 8 (CR on). b) Multiplicity dependence of the ratio of the proton to pion triggered yield in pp collisions at $\sqrt{s} = 7$ TeV from PYTHIA 8 (CR on).

obtained from PYTHIA 8 is shown in Fig 5.6(a). Both pion and proton triggered jet-like yields decrease with multiplicity but the rate of decrease has no trigger species dependence - showing no trigger dilution as shown in Fig 5.6(b). Color reconnection is unable to produce any trigger species dependence of the near side jet-like yields associated with pion and proton triggers selected from intermediate p_T where inclusive baryon to meson enhancement has been observed. This implies that the trigger dilution is not necessarily associated with inclusive proton to pion enhancement at intermediate p_T , rather, it depends on the underlying physics mechanism that generates the baryon enhancement at the inclusive level. In EPOS 3, the baryon enhancement is due to radial flow and it generates trigger dilution, whereas, the CR mechanism in PYTHIA 8 can generate radial flow like effect at the inclusive spectra level but unable to produce any trigger dilution effect. Thus, this observable can serve the purpose of disentangling the real hydrodynamical effect as implemented in EPOS 3 from color reconnection in PYTHIA 8 which can mimic the flow like patterns in pp collisions in terms of some observables mentioned earlier [20] [24]. This method is

much easier and straightforward compared to the one described in [25] as it doesn't involve any jet reconstruction or fitting of the spectra with blast wave parametrization. Further comparison with the data analyzed in the way proposed in this paper will be necessary to understand the underlying mechanism responsible for the observed flow like patterns in high multiplicity pp collisions at LHC energy.

Bibliography

- [1] B. Abelev et al. (ALICE Collaboration), Phys. Lett. B 728 (2014) 25-38
- [2] B. Abelev et al. (ALICE Collaboration), Phys. Lett. B 760 (2016) 720-735
- [3] Identified particle production in pp collisions at 7 and 13 TeV measured with ALICE.
(Rafael Derradi De Souza on behalf of the ALICE Collaboration, SQM2016)
<https://indico.cern.ch/event/403913/contributions/2142003/>
- [4] CMS Collaboration, arXiv:1605.06699
- [5] CMS Collaboration, Phys. Lett. B 718 (2013) 795-814
- [6] B. Abelev et al. (ALICE Collaboration), Physics Letters B 719 (2013), pp. 29-41
- [7] B. Abelev et al. (ALICE Collaboration), Phys. Lett. B 726 (2013) 164-177
- [8] CMS Collaboration, Phys. Lett. B 765 (2017) 193-220
- [9] J. Adam, et al., (ALICE Collaboration), arXiv:1606.07424.
- [10] J. Adam, et al., (ALICE Collaboration), Phys. Lett. B 758 (2016) 389-401
- [11] R. Bala, I. Bautista, J. Bielcikova, A. Ortiz, Heavy-ion physics at the LHC: Review of Run I results, Int. J. Mod. Phys. E25 (2016) 1642006. arXiv:1605.03939, doi:10.1142/S0218301316420064.
- [12] B. Abelev et al. (ALICE Collaboration), Phys. Rev. Lett. 736 (2014), 196-207

- [13] S. S. Adler, et al. PHENIX Collaboration), Phys. Rev. C 69 (2004) 034909
- [14] B. Ablev et al. (ALICE Collaboration), Phys. Lett. B 736 (2014) 196-207
- [15] A. Bzdak, B. Schenke, P. Tribedy, and R. Venugopalan, (2013), Phys. Rev. C 87, 064906.
- [16] J. Adam, et al., (ALICE Collaboration), Phys. Lett. B 749 (2015) 68-81
- [17] P. Bozek, W. Broniowski, G. Torrieri, Phys. Rev. Lett. 111 (2013) 172303
- [18] K. Werner, Iu. Karpenko, T. Pierog., Phys.Rev.Lett. 106 (2011) 122004.
- [19] K. Werner et al., Phys.Rev.Lett. 112 (2014) 23, 232301.
- [20] K. Werner et al., Phys.Rev. C89 (2014) 6, 064903.
- [21] Guo-Liang Ma and Adam Bzdak, Phys. Lett. B 739 (2014) 209-213
- [22] Adam Bzdak and Guo-Liang Ma, Phys. Rev. Lett. 113, 252301(2014)
- [23] D. Sarkar, S. Choudhury, S. Chattopadhyay, Phys. Rev. C 94, 044919 (2016)
- [24] A. Ortiz et al., Phys. Rev. Lett. 111, 042001 (2013).
- [25] A. Ortiz, G. Bencedi, H. Bello, arxiv: 1608.04784.
- [26] B. Schenke, S. Schlichting, P. Tribedy, R. Venugopalan, Phys. Rev. Lett. 117, 162301 (2016)
- [27] D. Sarkar, S. Choudhury, S. Chattopadhyay, Physics Letters B 760 (2016) 763-768
- [28] S.S. Adler et. al (PHENIX Collaboration) Phys. Rev. C 71 (2005) 051902
- [29] N. M. Abdelwahab et. al (STAR Collaboration) Phys. Lett. B 751 (2015) 233-240
- [30] E. Schnedermann, J. Sollfrank, U. W. Heinz, Phys. Rev. C48 (1993) 2462-2475.
- [31] K. Werner et al., Phys.Rev. C82 (2010) 044904.
- [32] H.J. Drescher et al., Phys.Rept. 350 (2001) 93-289

- [33] K. Werner, Phys.Rev.Lett. 98 (2007) 152301
- [34] T Sjostrand, M. van Zijl, Phys. Rev. D 36 (1987) 2019-2041.
- [35] T Sjostrand et al., Comput. Phys. Commun. 191 (2015) 159-177, arXiv:1410.3012.
- [36] B. Abelev et al. (ALICE Collaboration), Phys. Lett. B 727 (2013) 371-380
- [37] B. Abelev et al. (ALICE Collaboration), Phys. Lett. B 741 (2015) 38-50
- [38] E. Shuryak and I. Zahed, (2013), hep-ph/1301.4470.

Chapter 6

Ridge from jet-medium interaction in p-Pb collisions at $\sqrt{s_{NN}} = 5.02$ TeV

6.1 Introduction

In this chapter the effect of the jet-medium interplay (as implemented in EPOS 3) on the ridge like structure observed in high multiplicity p-Pb collisions at $\sqrt{s_{NN}} = 5.02$ TeV has been investigated. EPOS 3 takes into account hydrodynamically expanding bulk matter, jets and the jet-medium interaction. The basis of this model is multiple scatterings where each scattering finally produces flux tube / string. In the higher multiplicity event classes where the flux tube/string density is higher, there is a finite probability that the strings will pick up quarks and antiquarks (or diquarks) from the bulk (core) for flux tube breaking to produce jet hadrons (corona) instead of producing them via usual Schwinger mechanism. This will eventually create a correlation between core and corona and also influence the corona-corona correlation as the corona particles containing quarks and antiquarks (or diquarks) from the bulk also carry the fluid information. The relative contributions of the core-core, core-corona, corona-core and corona-corona correlations towards the ridge in the high and low multiplicity p-Pb collisions at $\sqrt{s_{NN}} = 5.02$ TeV has been studied. The multiplicity evolution of the ridge in all the cases is

also reported.

Two-particle angular correlation measurements in p-Pb [1], pp [2] and d-Au [3] collisions have revealed existence of azimuthal correlations extended to large pseudorapidity separation $|\Delta\eta|$ popularly known as "ridge". In heavy-ion collisions, such long-range structures along $|\Delta\eta|$ have been attributed to the collective emission of particles representing the initial anisotropy in the over-lap geometry of the colliding nuclei. Several other observations, like, mass-ordering of the elliptic flow coefficient (v_2) of identified particles [4], quark-scaling of v_2 [5] and baryon-to-meson enhancement at intermediate p_T [6] suggest similarity between the systems formed in small and heavy-ion collisions. It has been argued that the angular-correlations in small systems are dominated by jet-like processes. However, the emergence of the near side ridge in high-multiplicity event classes of small collision systems (pp and p-Pb) [2] [4] still lacks un-ambiguous understanding. Several theoretical propositions have been made based on correlated emission from glasma flux tubes (CGC approach) [7], collective flow due to hydro-dynamical effects [8] [9] or incoherent parton scatterings [10] [11], but no general agreement could be reached. EPOS 3 creates significant ridge like structure in the higher multiplicity classes of pp [9] and p-Pb [8] collisions at LHC energy and it has been discussed in terms of hydrodynamical evolution of the medium as the ridge structure vanishes in case the hydro evolution is switched off [9]. This indicates that the hydrodynamical evolution as implemented in EPOS 3 is the key ingredient to create the ridge structure in high multiplicity classes of small collision systems. Our work shows that in the context of EPOS 3, ridge in the higher multiplicity classes of p-Pb collisions has non zero contribution from the fluid-jet interaction [12].

EPOS 3 is a 3+1D event by event hydro model based on flux tube initial conditions [13] [14]. The basis of this model is multiple scatterings where each scattering consists of a hard elementary scattering plus initial state radiation - commonly referred as a parton ladder or pomeron. In this formalism each ladder may be considered as a longitudinal colour field which can be treated as a relativistic string. After multiple scatterings the final state partonic system consists of mainly longitudinal colour flux tubes carrying transverse momentum of the hard scattered partons in

the transverse direction- known as kinks in the string language. Depending on the energy of the string segments and local string density, the high density areas form the "core"(containing string segments more than a critical value per unit area in given transverse slices) and the low density area form the "corona" [15]. The strings in the core thermalize and then undergo hydrodynamical expansion and finally hadronize to form the bulk part of the system. In the low density region, the flux tubes (strings) eventually expand and finally break via the production of quark-antiquark or diquark-antidiquark pairs following Schwinger mechanism responsible for production of jet hadrons (corona) in EPOS. But in the high multiplicity event classes where the density of the string segments is higher because of many elementary scatterings, the strings cannot decay indepenedently following Schwinger mechanism only. After initial scatterings, the produced flux tubes / strings initially form a "matter" which eventually constitute both bulk and jets based on the energy loss by them. As mentioned in [12] three possibilities can occur:

a) String segments without sufficient energy to escape the matter will evolve hydrodynamically and finally hadronize to produce the bulk (core).

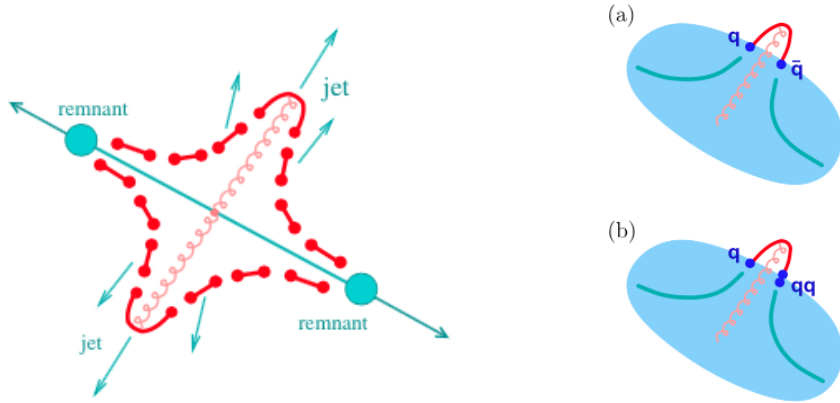


Figure 6.1: [Color online] Left: Flux tube breaking via $q\bar{q}$ production, which screens the color field (Schwinger mechanism). Right: Escaping string segment, getting its endpoint partons from the fluid. We show the case of a quark and an antiquark (a) and of a quark and a diquark (b). The rest of the string dissolves in matter. [12]

b) High energetic string segments will escape the matter and hadronize following Schwinger mechanism producing jet hadrons or corona.

c) Some string segments are produced inside the matter or at the surface but have enough energy to escape. These segments may pick up quark, antiquark, diquark or antidiquark needed for the flux tube breaking from the fluid (bulk) with properties (momentum, flavor) determined by the fluid [12] rather than the Schwinger mechanism. This scenario is illustrated in Fig 6.1. The produced jet hadrons are composed of a high p_T string segment originating from the initial hard process and di(quarks) from the fluid carrying fluid properties including transverse fluid velocity. As a result, these jet hadrons appear at relatively higher p_T than the jet hadrons produced via usual Schwinger mechanism only and also provide information about the fluid [12]. As baryons carry higher number of quarks compared to mesons, they will have larger momentum push from the fluid-jet interaction contributing to the inclusive baryon to meson enhancement at intermediate p_T as observed in Pb-Pb collisions at $\sqrt{s_{NN}} = 2.76$ TeV [12]. It has also been shown in [12] that this effect is more pronounced in the higher multiplicity classes of Pb-Pb collisions at $\sqrt{s_{NN}} = 2.76$ TeV where the transverse size of the system is higher increasing the probability of fluid-jet interaction.

A similar baryon to meson enhancement was also observed in p-Pb collisions at $\sqrt{s_{NN}} = 5.02$ TeV and EPOS 3 can qualitatively generate the pattern [13]. The jet hadrons carrying fluid properties (produced via formalism (c)) are expected to be correlated with the bulk part of the system. Therefore except from core-core, core-corona and corona-core correlations are expected. Also, it would be interesting to look at the corona-corona correlations at higher multiplicity event class where a larger fraction of corona particles are expected to be formed inside the matter [12] and carry fluid properties compared to the lower multiplicity event classes.

In this work, the two-particle correlation technique has been adopted to investigate the multiplicity evolution of the near-side ridge with triggers ($2.0 < p_T < 4.0$ GeV/ c) and associated particles ($1.0 < p_T < 4.0$ GeV/ c) from intermediate p_T in p-Pb collisions at 5.02 TeV. p_T ranges

of trigger and associated particles are chosen in the region where the ridge structure has been prominently observed in the experimental results [1]. An inclusive baryon to meson enhancement has also been observed in this p_T range in p-Pb collisions at 5.02 TeV [?]. In this analysis, the ridge is defined by $|\Delta\eta|$ separation ($|\Delta\eta| \geq 1.2$) in the near side ($|\Delta\phi| < \pi/2$) of the correlation function as it is done in [16]. The multiplicity evolution of the ridges in core-core, core-corona, corona-core and corona-corona correlations has been studied. The relative contribution of the core-core (pure hydrodynamical origin), core-corona and corona-core (fluid-jet interaction) and corona-corona correlations towards the "total" ridge in the high and low multiplicity event classes of p-Pb collisions has also been investigated.

6.2 Analysis Method

The two particle correlation function has been constructed in the same way as it has already been discussed in chapter 2. The p_T range of trigger and associated particles are $2.0 < p_T < 4.0$ GeV/ c and $1.0 < p_T < 4.0$ GeV/ c respectively and the correlation function has been constructed with a p_T ordering ($p_T^{\text{assoc}} < p_T^{\text{trigger}}$). The pseudo-rapidity of the particles are restricted within $-0.8 < \eta < 0.8$. This analysis has been performed by dividing the entire minimum bias events into different multiplicity classes based on the total amount of charged particles produced (with $p_T > 0.05$ GeV/ c) within $2.8 < \eta < 5.1$. This corresponds to the acceptance range of ALICE VZERO-A detector in the Pb going direction in case of p-Pb collisions and used for multiplicity class determination by the ALICE collaboration [1],[4]. The multiplicity classes are denoted as 60-100%, 40-60%, 20-40%, 0-20% from the lowest to the highest multiplicity. Two particle correlation functions in case of core-core, core-corona, corona-core and corona-corona correlations in the 0-20% multiplicity class are shown in Fig 6.2. This analysis concentrates only on the near side ($|\Delta\phi| < \pi/2$) of the correlation function. The particles from jet fragmentation are expected to be confined in a small angular region- so the ridge is estimated from large $|\Delta\eta|$ ($|\Delta\eta| \geq 1.2$) as it is done in [16]. The pedestal subtracted ridge structures from the highest (0-20%) and the lowest (60-100%) multiplicity classes are compared in Fig 6.3. The pedestal is determined from

the $\Delta\phi$ projection (for $|\Delta\eta| \geq 1.2$) with the zero yield at minimum (ZYAM) assumption and estimated as an average of the 8 (out of 36) lowest $\Delta\phi$ points [17].

6.3 Results and Discussion

In this analysis the trigger ($2.0 < p_T < 4.0$ GeV/ c) and associated ($1.0 < p_T < 4.0$ GeV/ c) particles are selected from intermediate p_T range where particles from both hard (origin: corona) and soft (origin: core) processes are present [13]. In the highest multiplicity event class (0-20%) where the core contribution and so the fluid-jet interaction are significant, the 2D correlation structure for core-core, core-corona, corona-core and corona-corona correlations are shown in Fig 6.2. The near side "ridge"(elongated structure along $|\Delta\eta|$) is present in all the cases. In case of core-core correlation (i.e both trigger and associated particles are from core), the ridge is purely from hydrodynamical origin and it increases with multiplicity as shown in Fig 6.3(a), where the ridge contribution from 60-100% and 0-20% event classes are compared. The ridge structure is also observed in core-corona and corona-core correlations and shown in Fig 6.2(b) and Fig 6.2(c) for 0-20% event class. The origin of ridge in these two cases is the fluid-jet interaction. The jet hadrons (corona) produced inside or at the surface of the bulk via flux tube breaking using partons from the bulk (core) [12] carry fluid information and eventually correlated with the bulk part of the system - creating the correlation between core and corona. The probability of fluid-jet interaction increases with increase in multiplicity / system size as more jet hadrons (corona) are expected to be produced using partons from the bulk (core) [12]. The multiplicity evolution of the ridge originating from the fluid-jet interaction (core-corona and corona-core correlations) is shown in Fig 6.3(b) and 6.3(c) and the ridge contribution increases with increase in multiplicity.

The ridge is also present in the corona-corona correlation in both 60-100% and 0-20% event class as shown in Fig 6.3(d). In the lowest multiplicity class this may be dominantly due to the flux tube initial condition. Flux tubes are extended upto many units of space time rapidity as they extend from projectile to target remnants [12] and therefore may contribute to the ridge like structure. The contribution from the fluid-jet interaction is expected to be more prominent

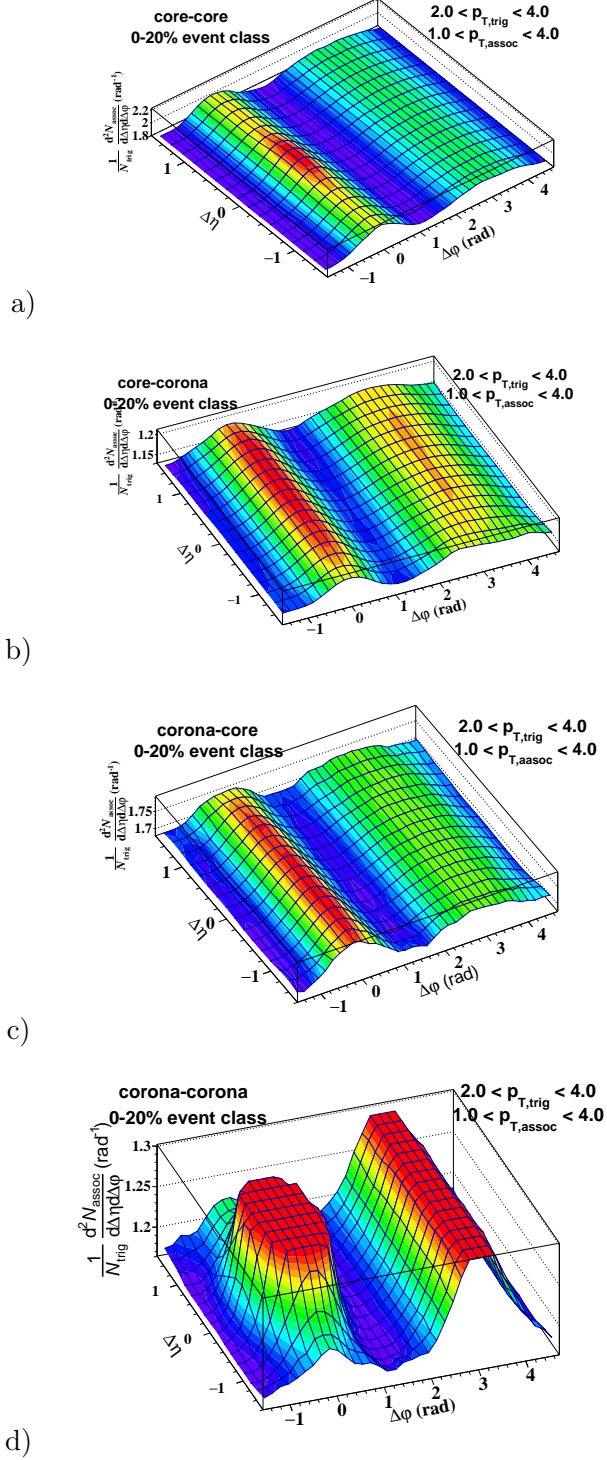


Figure 6.2: [Color online] Two Particle $\Delta\eta$ - $\Delta\phi$ correlation function in the 0-20 % event class of p-Pb collisions at $\sqrt{s_{NN}} = 5.02$ TeV from EPOS 3 for a) core-core , b) core-corona, c) corona-core, d) corona-corona correlations

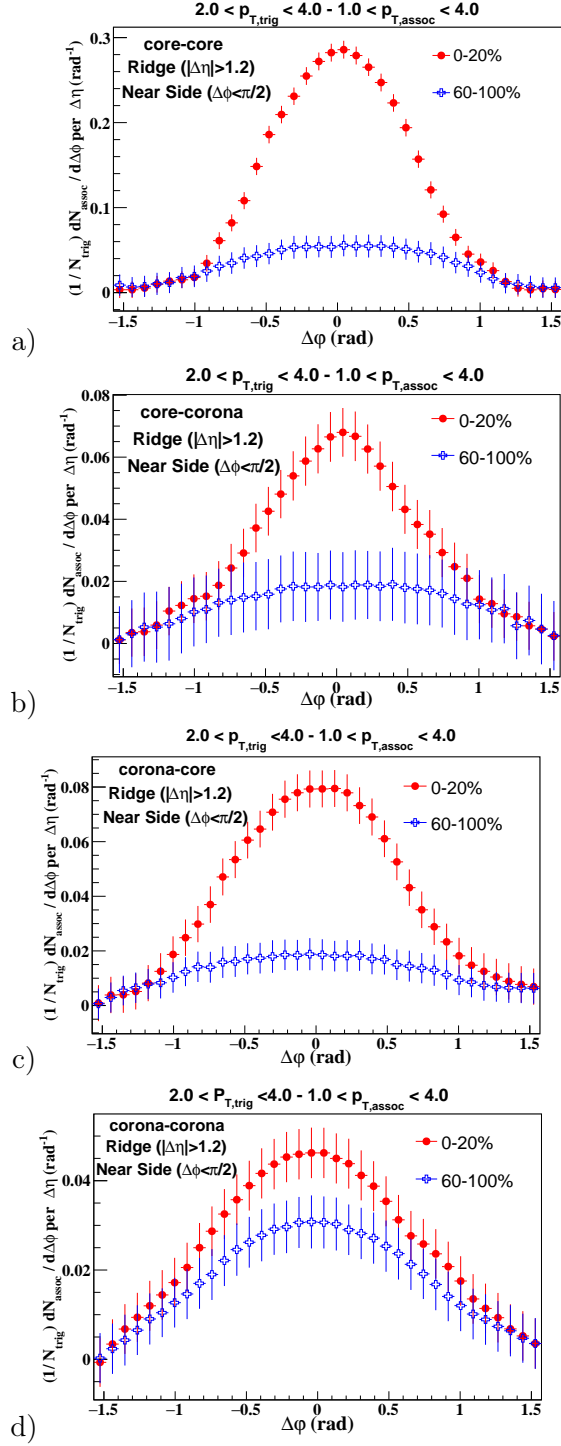


Figure 6.3: [Color online] Multiplicity dependence of the near-side ridge (pedestal subtracted) obtained from a) core-core , b) core-corona, c) corona-core, d) corona-corona correlations. In each case ridges from 0-20% and 60-100% event class have been compared.

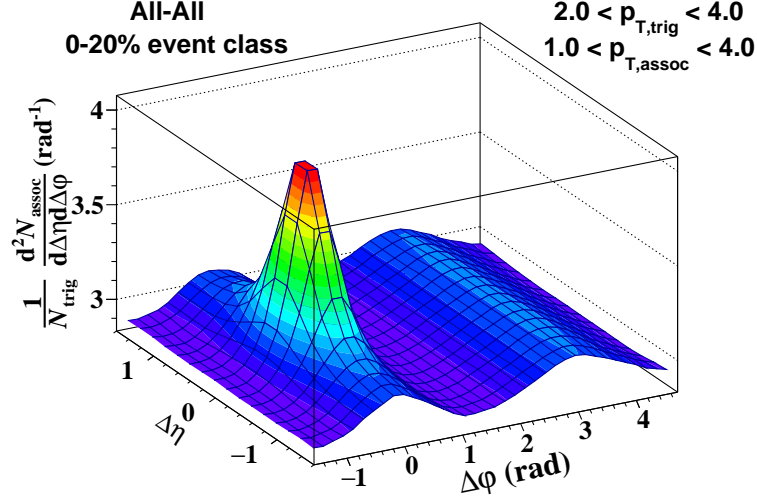


Figure 6.4: [Color online] Two Particle $\Delta\eta$ - $\Delta\phi$ correlation function in the 0-20 % event class of p-Pb collisions at $\sqrt{s_{NN}} = 5.02$ TeV from EPOS 3 considering all particles from core and corona.

in the highest multiplicity class as more jet hadrons carry the fluid properties and the ridge is found to be slightly enhanced compared to the lowest multiplicity class as shown in Fig 6.3(d). The 2D correlation structure obtained from the correlation analysis considering all particles from core and corona in the 0-20% event class is shown in Fig 6.4 and the ridge structure extracted from this correlation function is shown in Fig 6.5. It is mentioned as "All-All" in both cases. The relative contribution of the ridges from different origins towards the total ("All-All") ridge in the 0-20% multiplicity class is shown in Fig 6.5 and it is obtained by normalizing the core and corona triggered correlations (shown in Fig 3) by total (core+corona) number of trigger particles in the trigger p_T region. In the 0-20% event class, there are around 68% particles originating from corona and the rest 32% are from core compared to the 77% corona and 23% core in the 60-100% event class in the trigger p_T region ($2.0 < p_T < 4.0$ GeV/ c). So, due to normalization of the core and corona triggered correlations (shown in Fig 6.3) by all (corona+core) triggers, the core triggered correlations are diluted by 68% whereas the corona triggered correlations by 32% in the 0-20% event class. The relative contribution of core and corona (core : corona)

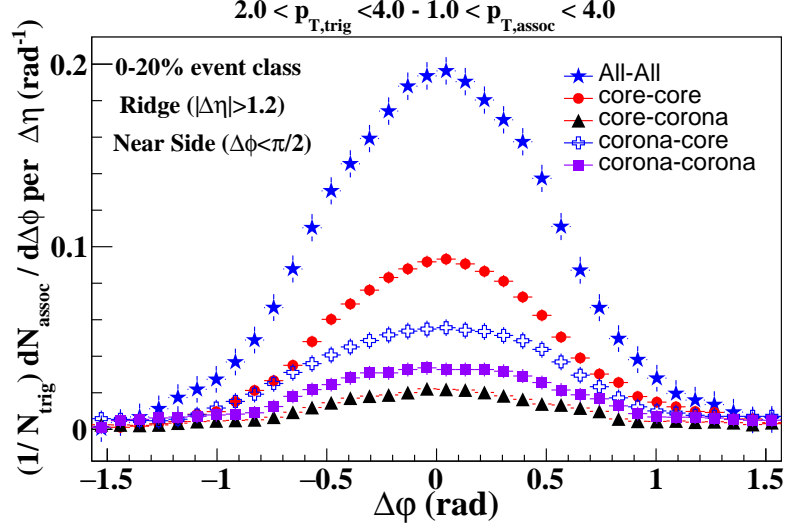


Figure 6.5: [Color online] Relative contribution of ridges from different origins towards the total ridge in the 0-20% event class of p-Pb collisions at $\sqrt{s_{NN}} = 5.02$ TeV.

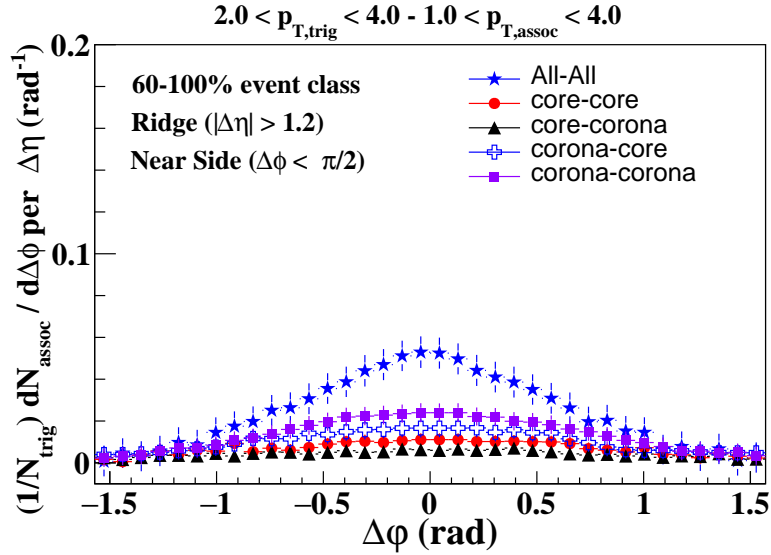


Figure 6.6: [Color online] Relative contribution of ridges from different origins towards the total ridge in the 60-100% event class of p-Pb collisions at $\sqrt{s_{NN}} = 5.02$ TeV.

in the associated p_T region ($1.0 < p_T < 4.0$ GeV/ c) changes from (37% : 63%) in 60-100% event class to (56% : 44%) in 0-20% event class. From Fig 6.5 it is clear that though the hydrodynamical evolution of the system (core-core correlations) contributes maximum to the total ("All-All") ridge, a non zero contribution from the fluid-jet interaction is also present in the high multiplicity class of p-Pb collisions. In Fig 6.6, it has been shown that in 60-100% event class, the total ridge ("All-All") is much smaller than the same in 0-20% event class and it is mainly dominated by the corona triggered correlations (corona-corona and corona-core) compared to the core triggered ones (core-core and core-corona). This indicates that the effect of core towards ridge structure reduces with decrease in multiplicity and the corona triggered correlations play an important role in the lower multiplicity classes of p-Pb collisions. This work shows that in the context of EPOS 3 - which takes into account hydrodynamically expanding bulk matter, jets and the interaction between the two, the ridge has nonzero contribution from the fluid-jet interaction. As the probability of producing jet hadrons inside or at the surface of the high density of core increases with the multiplicity/system size [12], the ridge contribution from fluid-jet interaction increases with increase in multiplicity as shown in Fig 6.3. The jet hadrons carrying fluid information play an important role as they are correlated with the bulk part of the system and contributing to the ridge structure. Further study with identified particles may be helpful to understand the chemical composition of the ridge in the p-Pb collisions at LHC energy.

Bibliography

- [1] B. Abelev et al. (ALICE Collaboration), Physics Letters B 719 (2013), pp. 29-41
- [2] CMS Collaboration, Phys. Lett. B 718 (2013) 795-814
- [3] A. Adare et al. (PHENIX Collaboration) , Phys. Rev. Lett. 114, 192301 (2015)
- [4] B. Abelev et al. (ALICE Collaboration), Phys. Lett. B 726 (2013) 164-177
- [5] CMS Collaboration, Phys. Lett. B 742 (2015) 200-224
- [6] B. Abelev et al. (ALICE Collaboration), Phys. Lett. B 728 (2014) 25-38
- [7] Kevin Dusling and Raju Venugopalan, Phys. Rev. D 87 (2013), 094034
- [8] K. Werner et al., Phys.Rev.Lett. 112 (2014) 23, 232301.
- [9] K. Werner, Iu. Karpenko, T. Pierog., Phys.Rev.Lett. 106 (2011) 122004.
- [10] Guo-Liang Ma and Adam Bzdak, Phys. Lett. B 739 (2014) 209-213
- [11] Adam Bzdak and Guo-Liang Ma, Phys. Rev. Lett. 113, 252301(2014)
- [12] K. Werner, Phys. Rev. Lett. 109, 102301 (2012)
- [13] K. Werner et al., Phys.Rev. C89 (2014) 6, 064903.
- [14] K. Werner et al., Phys.Rev. C82 (2010) 044904.
- [15] K. Werner, Phys.Rev.Lett. 98 (2007) 152301

- [16] B. Ablev et al. (ALICE Collaboration), Phys. Lett. B 741 (2015) 38-50
- [17] K. Aamodt et al. (ALICE Collaboration), Phys. Rev. Lett. 108, 092301

Chapter 7

Investigating the role of partonic and hadronic dynamics in mass splitting of elliptic anisotropy in p-Pb collisions at $\sqrt{s_{NN}} = 5.02$ TeV using a multi phase transport model (AMPT)

7.1 Introduction

Wealth of data collected during the decades of operation of RHIC and a first few years of LHC provide compelling evidence that a strongly coupled and nearly perfect fluid of quarks and gluons are produced in Pb-Pb/Au-Au collisions at ultra-relativistic energies. A manifestly evident signature for the formation of such a matter is the collective motion (flow) of the final state particles. A large azimuthal anisotropy in the momentum space has been regarded as one of the most definitive and strong indication of such collective behaviour and has been argued

to be a consequence of collective expansion of the system that starts with an initial azimuthal anisotropy in the coordinate space. This interpretation was initially applicable to heavy-ion collisions as large system size and high density were considered to be mandatory for the creation of a thermalized deconfined medium. Elliptic anisotropy, long-range ridge structures, mass ordering of v_2 , baryon to meson enhancement at intermediate p_T etc, which were once attributed to the hydro-dynamical evolution of a strongly interacting system of large dimensions found to be challenged when analogous measurements in small collision systems produced similar outcome [1–6]. Even hydro-based models [7], [8], [9] found to be in reasonable agreement with experimental results indicating that local thermal equilibration might be achieved even for small system size. In [10], [11] it is shown that microscopic transport models (AMPT) are also capable of generating similar effects in small collision systems through in-coherent parton scattering with a nominal scattering cross-section. The system evolving in transport model is relatively less dense [12] compared to the system evolving in near hydro limit where large number of collisions among the constituents generate the pressure gradient and the hydro like collectivity. In [12] it has been shown that anisotropic escape mechanism of partons is the dominant source of flow (v_2) generation in AMPT. Recent studies [13] also indicate that mass-splitting of v_2^{hadron} in AMPT originates from the dynamics of coalescence [14] and hadronic re-scattering during the evolution of the system and not necessarily associated with the collectivity in the system. In this chapter, the possible role of partonic and hadronic dynamics in the generation of mass ordering of v_2^{hadron} in AMPT has been investigated in detail. Events generated from the default and string-melting versions of AMPT for different scattering cross-sections have been analysed to calculate elliptic flow of partons and hadrons as a function of event-activity (multiplicity). Although anisotropic flow in AMPT is dominantly from the escape mechanism but its qualitative features exhibit striking similarity with collective response of the medium. This study based on the AMPT (SM version) generated data for p-Pb collisions at $\sqrt{s_{NN}} = 5.02$ TeV suggests that the parton cascade coupled with dynamics of coalescence [14], [15], [16] can generate mass ordering of v_2^{hadron} at the partonic level without hadronic interactions. Also, hadronic interactions alone can generate

mass ordering of v_2^{hadron} without any contribution from the partonic phase and therefore the total effect has a contribution from both partonic and hadronic level.

7.2 The AMPT Model

The AMPT [17–20] model has already been discussed in chapter 2. In this chapter, the effect of partonic interactions (namely Zhang Parton Cascade (ZPC) [21]) on the partonic and hadronic v_2 has been investigated using two parton scattering cross sections: a) cross section - 0 mb (ZPC off) and b) cross section - 3 mb (ZPC on). The effect of hadronization on the hadronic v_2 has been studied using default (hadronization via Lund string fragmentation [22, 23]) and string melting (hadronization via coalescence of partons) version of AMPT. After hadronization the v_2 of hadrons is determined with and without hadronic rescatterings which is modelled by A Relativistic Transport model (ART) [24].

7.3 v_2 extraction

The anisotropic emission of charged particles can be quantitatively characterised in terms of the co-efficients in the Fourier expansion of the azimuthal dependence in the invariant yield relative to the reaction plane angle [25]:

$$E \frac{d^3N}{dp^3} = \frac{1}{2\pi} \frac{d^2N}{p_T dp_T dy} \left(1 + \sum_1^n 2v_n \cos(n(\phi - \psi_R)) \right) \quad (7.1)$$

Where ϕ is the azimuthal angle in the Lab-frame and ψ_R is the reaction plane angle. The second term in the expansion, v_2 , is known as elliptic flow and can be simply obtained by $\langle\langle \cos(2(\phi - \psi_R)) \rangle\rangle$. The angular brackets stands for the statistical average over many events. Under the experimental conditions reaction plane ψ_R can not be determined directly hence new methods have been improvised to calculate v_2 independent of the reaction plane angle. The azimuthal correlations among two or multi particles [26–28] is found to be an useful tool to

reconstruct v_n coefficients. Thus one can calculate v_2 from two-particle azimuthal correlations as [29]:

$$\langle\langle e^{i2(\phi_i-\phi_j)} \rangle\rangle = \langle v_2^2 \rangle + \delta_n \quad (7.2)$$

δ_n in the above equation is the “non-flow” contribution to the two particle correlation. In the high multiplicity events this calculation may be computationally intensive due to large number of 2-particle combinations. To counter computational inefficiency, a revision to this method was suggested called as Q-cumulant method [29, 30]. In this approach, 2-particle correlations are expressed in terms of flow vectors or Q-vectors mathematically represented as:

$$Q_2 = \sum_1^M e^{i2\phi_i} \quad (7.3)$$

Summation runs over all particles usually called as reference particles (RP). The genuine 2-particle azimuthal correlations can be obtained by separating the diagonal and the off-diagonal terms in $|Q_2|^2$ as:

$$|Q_2|^2 = M + \sum' e^{i2(\phi_i-\phi_j)} \quad (7.4)$$

Thus the average 2-particle azimuthal correlations over all reference particles (RP) in a single event can be calculated using:

$$\langle 2 \rangle = \frac{|Q_2|^2 - M}{M(M-1)} \quad (7.5)$$

$\langle \rangle$ represents particle average in a single event. Finally the 2-particle cumulant ($c_2\{2\}$) and integrated flow ($V_2\{2\}$) can be obtained averaging over all particles over all events:

$$c_2\{2\} = \langle\langle 2 \rangle\rangle, V_2\{2\} = \sqrt{\langle\langle 2 \rangle\rangle} \quad (7.6)$$

$\langle\langle \rangle\rangle$ indicates both particle and event average.

v_2 obtained in this method is prone to contaminations from non-flow effects like decay of resonances, jet induced correlations etc. To suppress these additional correlations, which are generally

short range, an optimum $\Delta\eta$ gap can be introduced between reference particles (RP) [31]. This can be achieved by dividing an event into two sub events, A and B , separated by $\Delta\eta$ gap. Hence the Eq (7.5) is modified as :

$$\langle 2 \rangle_{\Delta\eta} = \frac{Q_2^A \cdot Q_2^B}{M_A \cdot M_B} \quad (7.7)$$

Where Q_2^A, Q_2^B are flow vectors corresponding to the sub-events A and B , and M_A, M_B are the multiplicities of the reference particles in each sub-event. Having calculated integrated flow ($V_2\{2\}$) one can extract differential flow of Particles of Interest (POI's) using the analogous technique. In sub-event Q-cumulant method, differential flow of particles can be expressed as:

$$\langle 2'_{\Delta\eta} \rangle = \frac{p_{2,A} \cdot Q_2^B}{m_{p,A} \cdot M_B} \quad (7.8)$$

Where $m_{p,A}$ is the number and p_2 is the Q-vector of the particles of interest (POI's) whose differential flow calculation is intended . To avoid overlap in the pseudorapidity range among POI's and RP's they are taken from different sub-events. Finally, differential flow is calculated via:

$$v_2\{p_T\} = \frac{\langle 2'_{\Delta\eta} \rangle}{V_2\{2\}} \quad (7.9)$$

In this work, all freezeout partons / final state hadrons produced within the pseudorapidity range of $|\eta| < 1.0$ are considered. Each event is divided into two sub-events with a pseudo-rapidity separation among the freezeout partons / final state hadrons of $(|\Delta\eta|) > 0.4$ at least.

This analysis (extraction of v_2^{parton} and v_2^{hadron}) has been performed by dividing the entire minimum bias events into four multiplicity classes based on the total number of charged particles produced (with $p_T > 0.05$ GeV/c) within $2.8 < \eta < 5.1$. This is the acceptance range of ALICE VZERO-A detector in the Pb going direction in case of p-Pb collisions and has been used for multiplicity class determination by the ALICE collaboration [1],[2]. The multiplicity classes are denoted as 60-100%, 40-60%, 20-40%, 0-20% from the lowest to the highest multiplicity.

7.4 Results and Discussion

In this work, the multiplicity evolution of the elliptic flow for freezeout partons (v_2^{parton}) and hadrons (v_2^{hadron}) in p-Pb collisions at $\sqrt{s_{NN}} = 5.02$ TeV has been studied. The effect of partonic interactions via Zhang's parton cascade (ZPC) and different hadronization mechanisms (Lund string fragmentation (LSF) in default and coalescence in string melting version of AMPT) on mass splitting of v_2^{hadron} has been investigated. The effect of hadronic interactions on the mass splitting of v_2^{hadron} has also been reported.

In Fig 7.1 the multiplicity evolution of the elliptic flow of freezeout partons (v_2^{parton}) is shown

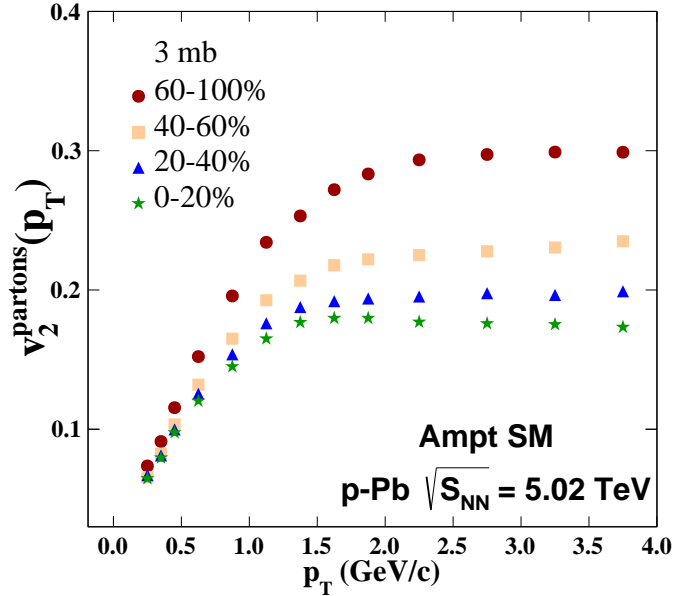


Figure 7.1: [Color online] Multiplicity dependence of p_T -differential v_2^{parton} in p-Pb collisions at $\sqrt{s_{NN}} = 5.02$ TeV from AMPT-SM with parton scattering cross-section of 3 mb.

with ZPC on (scattering cross section of 3 mb). The v_2^{parton} decreases with increase in multiplicity. In AMPT the freezeout partons exhibit space momentum correlations largely due to the escape mechanism [12] and the escape probability of a freezeout parton depends on its position and momentum at the freezeout point. The escape probability of these freezeout partons may be

affected by the phase space distribution of the surrounding partons that depends on the initial geometry of the system - influencing the preferential escape direction of the partons along the shorter axis. In the lowest multiplicity class (60-100%) of p-Pb collisions where the partonic interactions are less significant, the non flow effects [32] and escape mechanism [12] generate larger v_2^{parton} compared to the higher multiplicity classes where v_2^{parton} has additional contribution from the space-momentum correlation generated during partonic interactions during ZPC.

In Fig 7.2 the coordinate space distributions of the freezeout partons in a single event are shown

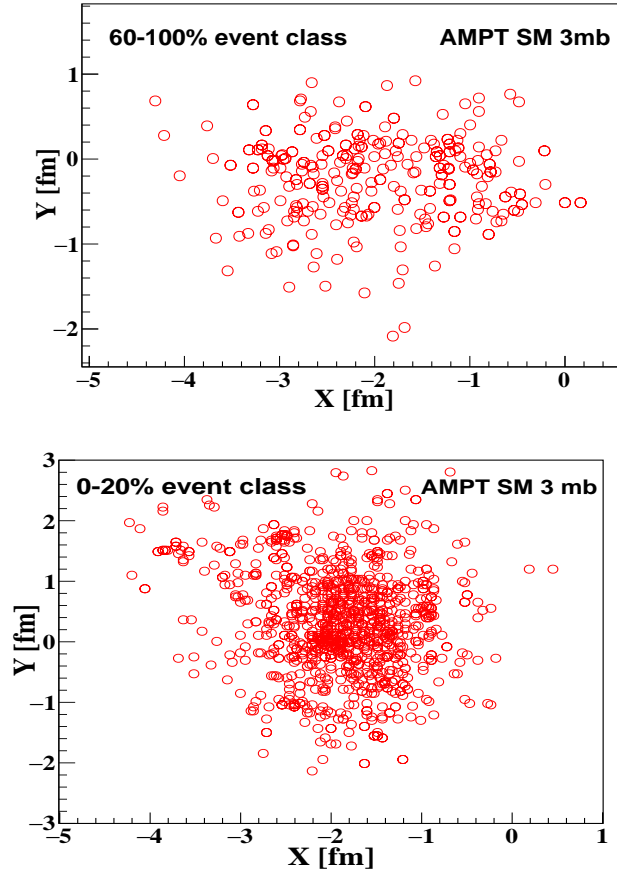


Figure 7.2: [Color online] Coordinate space distribution of freezeout partons in a single event in a) 60-100% (top) and b) 0-20% (bottom) event class of p-Pb collisions at $\sqrt{s_{NN}} = 5.02$ TeV.

for the highest(0-20%) and lowest (60-100%) multiplicity classes. The high density of partons in

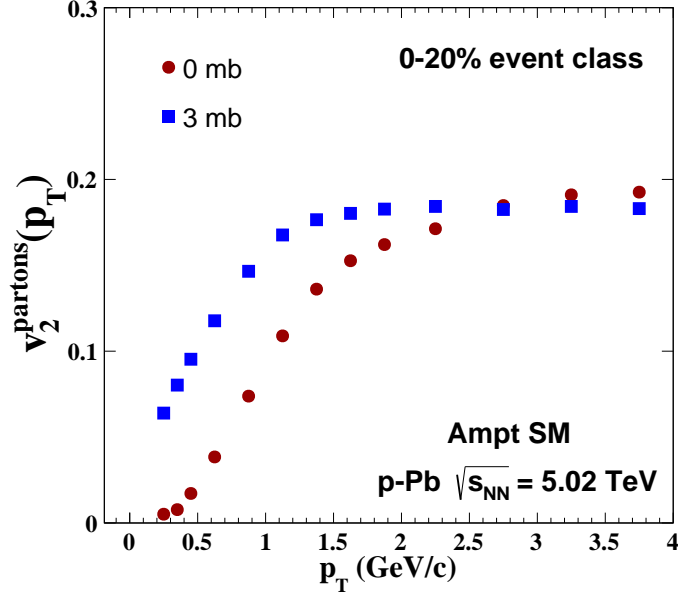


Figure 7.3: [Color online] v_2^{parton} plotted as a function of p_T in the highest multiplicity event class (0-20%) of p-Pb collisions at $\sqrt{s_{NN}} = 5.02$ TeV for parton scattering cross-section of 0 mb (red) and 3 mb (blue) from AMPT-SM version.

the highest multiplicity class possibly reduces the non flow effects and escape probability of the freezeout partons, thus reducing the v_2^{parton} compared to the lowest multiplicity class as shown in Fig 7.1. It indicates that even though the collective contribution to the v_2^{parton} increases in the higher multiplicity classes due to larger number of collisions among partons, the total v_2 goes down as the escape probability of the partons and non flow effects decrease with increase in multiplicity. In Fig 7.3 the p_T dependence of v_2^{parton} for ZPC ON (scattering cross section of 3 mb) and OFF (scattering cross section of 0 mb) in SM version of AMPT is shown for the highest multiplicity event class. In ZPC off case, the v_2^{parton} is solely due to non flow effects [32] as there is no partonic interaction present. Whereas, in ZPC on case the escape mechanism and hydro like collectivity generated through partonic interactions contribute towards the observed v_2^{parton} . In both cases the v_2^{parton} is approximately linear at low p_T and it saturates at higher p_T .

In this work we have also investigated the effect of different hadronization mechanisms (with

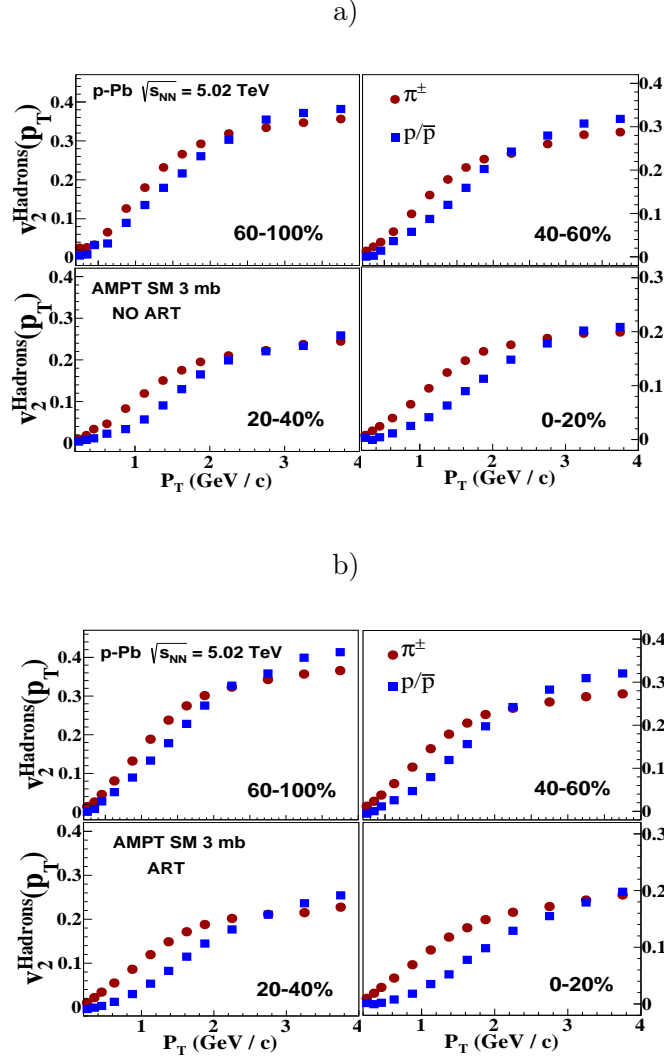
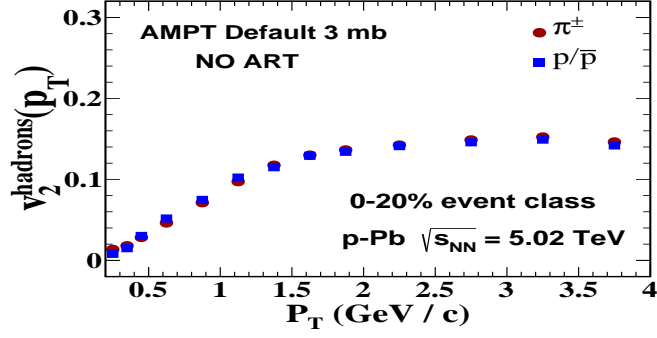


Figure 7.4: [Color online] Multiplicity evolution of $v_2(p_T)$ of pion and proton for 3 mb parton scattering cross-section in p-Pb collisions at $\sqrt{s} = 5.02$ TeV (a) without hadronic-rescattering (NO ART) and (b) with hadronic-rescattering ON (ART).

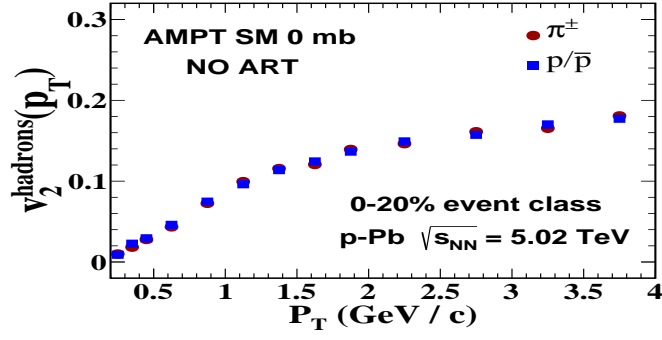
and without ZPC) on the mass splitting of v_2^{hadron} , which was believed to be a characteristic signature of hydro like collectivity. A recent study has shown that the mass ordering can be generated from the dynamics of the coalescence [14] in AMPT even when parton azimuthal directions are randomized [13]. In Fig 7.4 the multiplicity evolution of the mass splitting of v_2^{hadron} in the string melting (SM) version of AMPT for ZPC on (with and without hadronic scattering

$\langle \text{ART} \rangle$) is shown. In case of ZPC on, the mass splitting is evident even in the lowest multiplicity event class and this splitting increases with increase in multiplicity whereas, the value of v_2^{hadron} decreases. As the number of collisions suffered by a parton increases with multiplicity, the collective contribution to the elliptic anisotropy increases resulting in more prominent mass splitting. However, if ZPC is turned off, the coalescence model of hadronization is unable to produce any mass splitting of v_2^{hadron} even in the highest multiplicity event class as shown in Fig 7.5(b) (*AMPT SM 0 mb*). In ZPC off case the v_2^{parton} is solely due to non flow effects [32] (as the escape mechanism is due to non zero partonic scattering cross section) and its p_T dependence is similar to the ZPC on case as shown in Fig 7.3. Due to linearity of v_2^{parton} at low p_T , if constituent quarks p_T and v_2 simply add to hadronic p_T and v_2 then baryon and meson v_2 should coincide with each other and there would be no mass splitting at low p_T [13]. Now, even though the linearity of v_2^{parton} at low p_T is present in both ZPC on and off cases - after coalescence it is only the ZPC on case where mass splitting of v_2^{hadron} is observed even in the lowest multiplicity event class as shown in Fig 7.4. Whereas, no mass splitting is observed in ZPC off case (Fig 7.5(b)) even in the highest multiplicity class. The parton cascade changes the initial phase space distribution of the partons. So during coalescence after ZPC, the constituent parton p_T may have a spread in momentum for a given hadron p_T and v_2^{parton} do not add up arithmetically to hadron v_2 because of finite opening angles or kinematics [13]. The dynamics of coalescence [14] among these constituent partons (having a spread in their momentum and finite opening angles) is considered to be the source of mass splitting of v_2^{hadron} at low p_T in AMPT [13] before any hadronic scatterings take place. Now, parton cascade creates space-momentum correlation. Whereas, in [13] it is argued that the dynamics of coalescence can generate the mass ordering in the azimuth-randomized version of AMPT where the parton space-momentum correlation is destroyed by randomizing parton azimuthal directions. In that case also the initial phase space distribution of the partons are modified by ZPC followed by randomizing the outgoing parton azimuthal directions after each parton-parton scattering [12] [13] and then the dynamics of coalescence creates the mass ordering of v_2^{hadron} even in the absence of any event plane correlation.

a)



b)



c)

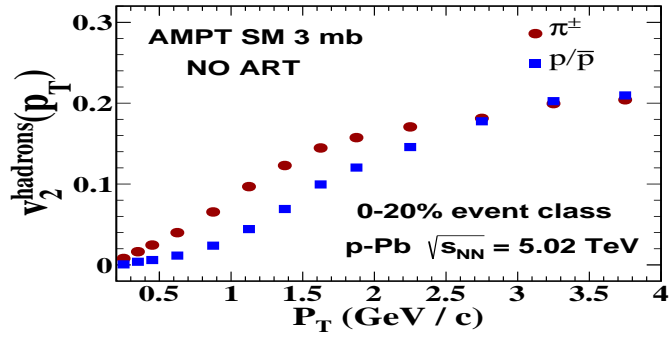


Figure 7.5: [Color online] $v_2(p_T)$ of pion and proton for most central (0-20%) event class in p-Pb collision at $\sqrt{s_{NN}} = 5.02$ TeV for different configurations: a) Default 3 mb without ART , b) 0 mb String Melting without ART and c) 3 mb String Melting without ART .

To study further, we repeated our analysis with default version of AMPT keeping ZPC on and without hadronic scattering. In Fig 7.5, the comparison between 3 configurations - *default 3 mb* (ZPC + Lund string fragmentation (LSF)) , *SM 0 mb* (No ZPC + coalescence (SM)) and *SM 3 mb* (ZPC + coalescence (SM)) have been shown for the highest multiplicity event class. No mass splitting is observed for both *default 3 mb* (Fig 5(a)) and *SM 0 mb* Fig(5(b)) case. This suggests that the parton cascade (ZPC) combined with lund string fragmentation and coalescence without parton cascade are unable to produce any mass splitting of v_2^{hadron} without hadronic scattering- confirming that both ZPC and coalescence model of hadronization at the partonic level (Fig 7.4 and Fig 7.5(c)) are the sources of the observed mass splitting of v_2^{hadron} .

The mass splitting is found to be slightly enhanced under the influence of hadronic interactions

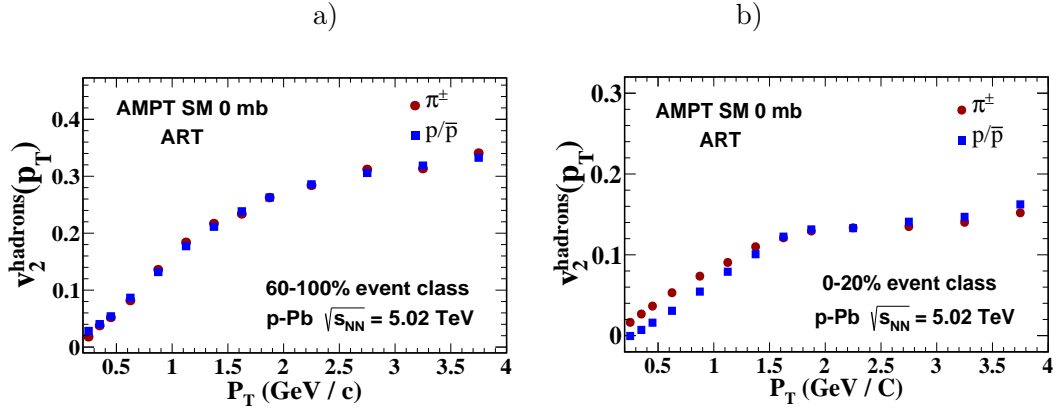


Figure 7.6: [Color online] $v_2(p_T)$ of pion and proton in a) 60-100% (left) and b) 0-20% (right) event class of p-Pb collisions at $\sqrt{s_{NN}} = 5.02$ TeV in string melting version of AMPT with ART on and ZPC off.

mainly in the highest multiplicity event class as shown in Fig 7.4. To study the effect of hadronic scattering alone, the analysis has been repeated with hadronic scattering (ART) only with partonic scattering turned off in SM version of AMPT. In the lowest multiplicity (60-100%) class, no mass splitting of v_2^{hadron} is observed as shown in Fig 7.6(a). But, in the highest multiplicity class (0-20%), as shown in Fig 7.6(b), a clear mass splitting is observed at lower p_T . This indicates that with the increase in hadronic density, contribution from hadronic interactions towards

mass splitting increases significantly, which may play a major role in case of heavy ions. This measurement is in agreement with the observations made in [13] and [32].

This study based on the AMPT model suggests that in small collision system like p-Pb, dynamics of coalescence can generate the mass splitting of v_2^{hadron} even in the lowest multiplicity class of p-Pb collisions in absence of any hadronic scattering, provided partonic interactions are allowed prior to hadronization via coalescence mechanism. Also, in Fig 7.6 it is shown that hadronic scattering alone can generate the mass splitting of v_2^{hadron} in the high multiplicity class of p-Pb collisions consistent with the observations reported in [13] and [32]. These results indicate that the mass ordering of v_2^{hadron} in AMPT can originate independently from both partonic (ZPC+coalescence) and hadronic (ART) phases. The partonic contribution can generate this effect even in the lowest multiplicity class of p-Pb collisions (Fig 7.4) where the system is expected to be far away from the ideal hydro limit [13]. Whereas, interactions at both partonic and hadronic phases can generate the mass ordering in the higher multiplicity classes (Fig 7.4 and 7.6). This suggest that the mass splitting of v_2^{hadron} is not uniquely associated with the hydrodynamical evolution of the partonic phase (QGP), produced in relativistic high energy collisions.

Bibliography

- [1] B. Abelev et al. (ALICE Collaboration), Physics Letters B 719 (2013), pp. 29-41
- [2] B. Abelev et al. (ALICE Collaboration), Phys. Lett. B 726 (2013) 164-177
- [3] B. Abelev et al. (ALICE Collaboration), Phys. Rev. C 90 (2014) 054901
- [4] B. Abelev et al. (ALICE Collaboration), Phys. Lett. B 728 (2014) 25-38
- [5] CMS Collaboration, Phys. Lett. B 718 (2013) 795-814
- [6] A. Adare et al. (PHENIX Collaboration) , Phys. Rev. Lett. 114, 192301 (2015)
- [7] K. Werner et al., Phys.Rev.Lett. 112 (2014) 23, 232301.
- [8] K. Werner, Iu. Karpenko, T. Pierog., Phys.Rev.Lett. 106 (2011) 122004.
- [9] K. Werner et al., Phys.Rev. C89 (2014) 6, 064903.
- [10] Guo-Liang Ma and Adam Bzdak, Phys. Lett. B 739 (2014) 209-213
- [11] Adam Bzdak and Guo-Liang Ma, Phys. Rev. Lett. 113, 252301(2014)
- [12] Liang He, Terrence Edmonds, Zi-Wei Lin, Feng Liu, Denes Molnar, Fuqiang Wang, Phys. Lett. B 753 (2016) 506-510
- [13] Hanlin Li, Liang He, Zi-Wei Lin, Denes Molnar, Fuqiang Wang, Wei Xie, arXiv:1604.07387v1 [nucl-th]

- [14] Z.-W. Lin, J. Phys. G38, 075002(2011)
- [15] R. Fries, B. Muller, C. Nonaka, and S. Bass, Phys. Rev. Lett. 90 (2003) 202303.
- [16] V. Greco, C. Ko, and P. Levai, Phys. Rev. Lett. 90 (2003) 202302.
- [17] Z.-W. Lin, C.M. Ko, B.-A. Li, B. Zhang, S. Pal, Phys. Rev. **C 72**, 064901 (2005).
- [18] Z.W. Lin *et al.*, Phys. Rev. **C 64**, 011902 (2001).
- [19] B. Zhang *et al.*, Phys. Rev. **C 61**, 067901 (2000).
- [20] X.-N. Wang, M. Gyulassy, Phys. Rev. **D 44**, 3501 (1991).
- [21] B. Zhang, Comput. Phys. Commun. 109, (1998) 193.
- [22] B. Andersson, G. Gustafson and B. Soderberg, Z. Phys. C 20, 317 (1983).
- [23] B. Andersson, G. Gustafson, G. Ingelman and T. Sjostrand, Phys. Rept. 97 , 31 (1983).
- [24] B. A. Li and C. M. Ko, Phys. Rev. C 52, (1995) 2037.
- [25] S. Voloshin and Y. Zhang, Z. Phys. C 70, 665 (1996).
- [26] S. Wang *et al.*, Phys. Rev. C 44, 1091 (1991) .
- [27] P. Danielewicz and G. Odyniec, Phys. Lett. B 157, 146 (1985) .
- [28] A. M. Poskanzer and S. A. Voloshin, Phys. Rev. C 58, 1671 (1998) .
- [29] Ante Bilandzic, Raimond Snellings and Sergei Voloshin, Phys. Rev. C 83, 044913 (2011) .
- [30] A. Bilandzic *et al.*, Phys. Rev. C 89, 064904 (2014) .
- [31] Y. Zhou [ALICE Collaboration], arXiv:1407.7677 [nucl-ex]
- [32] Y. Zhou *et al.*, Phys. Rev. C 91, 064908 (2015) .

Chapter 8

Summary and Outlook

In this thesis, the presence of collectivity in small collision systems (pp and p-Pb collisions at LHC energies) has been investigated by using a measure of correlations with identified triggers at intermediate p_T where the inclusive proton to pion enhancement has been observed [1]. This enhancement is similar to the one already observed in the heavy-ion collisions at RHIC and LHC energies where it has been described in terms of radial flow and/or coalescence model of hadronization [2, 3] - indicating the presence of soft physics in the system. Now, applicability of the hydrodynamical scenario to pp and p-Pb [4–6] systems is in contradiction with the basic idea of hydrodynamics, i.e., the mean free path of partons must be smaller than the size of the system [7]. In this work, we report both model based calculations and results obtained from the data analysis in ALICE regarding recent measurements of the near-side jet-like yields obtained from the angular correlation measurement with pions and protons as trigger particles and unidentified charged hadrons as associated particles at intermediate transverse momentum (p_T). Events generated by the string melting version of a multiphase transport model (AMPT) and 3+1 D event by event hydrodynamical model (EPOS 3) are analyzed to calculate the near-side jetlike yields associated with pion and proton triggers in p-Pb collisions at 5.02 TeV [8, 9]. The multiplicity evolution of the trigger species dependence of jet-like yields, obtained from AMPT, found to be completely different from the same when extracted from the hydrodynamical model (EPOS 3).

In [11], it has been shown that the jet-medium interaction in heavy ion collisions can contribute towards the observed baryon enhancement in the A-A collisions and it is hard to disentangle the effect of jet-medium interplay from the soft physics (e.g coalescence and/or radial flow). But, in small collision systems where the jet-medium interaction has been found to be negligible, trigger species dependence of the associated jet-like yield may be attributed dominantly to the dynamics of quark coalescence and/or radial flow.

The data taken by the ALICE collaboration for p-Pb collisions at $\sqrt{s_{NN}} = 5.02$ TeV has been analyzed and proton triggered jet-like yield has been found to decrease gradually with multiplicity whereas the pion triggered jet-like yield remains almost constant. EPOS 3 (3+1D event-by-event hydro model) and AMPT with string melting (incorporates coalescence model of hadronization) can not reproduce the data quantitatively. But, EPOS 3 can qualitatively mimic the multiplicity evolution of the pion- and proton-triggered jet-like yields - indicating radial flow as a possible source of the observed trigger dilution in p-Pb collisions at $\sqrt{s_{NN}} = 5.02$ TeV. Analogous measurements in Au-Au collisions at RHIC energy have shown a hint of dilution in proton-triggered correlation [2, 3] at its highest multiplicity suggesting that the soft physics processes in p-Pb and heavy ion collisions may have a qualitative similarity. But as severe jet quenching is present in case of heavy ion collisions and that can contribute towards the baryon enhancement at intermediate p_T , the interpretation of that result in terms of the soft physics (coalescence and/or radial flow) only is not that straight forward [10]. In the absence of jet quenching, trigger dilution can be used as a probe for soft physics in small collision systems. Multiplicity evolution of the pion- and proton-triggered near-side jet-like yields can also provide information about the particle production mechanism at intermediate p_T [8, 9].

Now the similar collective like behaviors has also been observed in pp collisions at 7 TeV and can be qualitatively explained by both hydro based models (e.g. EPOS 3) and other mechanisms like multi-parton interactions (MPI) with color reconnection (CR) as implemented in PYTHIA 8 - making it difficult to pinpoint the underlying mechanism responsible for the observed flow like effects in high multiplicity pp collisions. In this thesis, using the two particle correlation

technique, it has been demonstrated that the multiplicity evolution of the near-side jet-like yield associated with pion and proton triggers selected from intermediate p_T (where inclusive baryon to meson enhancement has been observed) can disentangle the effect of hydrodynamical flow from the effect of MPI based color reconnection in a straightforward way. Both EPOS 3 and PYTHIA 8 (with color reconnection) can qualitatively generate the observed baryon to meson enhancement at intermediate p_T . In EPOS 3, the proton triggered yield decreases at a larger rate with multiplicity compared to the pion triggered case creating trigger dilution. However, no such trigger species dependence of the near-side jet-like yield has been observed in case of PYTHIA 8 which indicates that inclusive baryon to meson enhancement at intermediate p_T does not necessarily lead to the trigger dilution effect. Thus, this observable can be used as an useful tool to disentangle the real hydrodynamical effects from color reconnection in small collision systems where hydrodynamical collectivity is not so intuitive. The comparison of these model derived results with the results obtained from data will provide insight on the underlying mechanisms responsible for the collective like behaviors observed in pp collisions at 7 TeV.

Also, the effect of the jet-medium interplay (as implemented in the EPOS 3 model) on the ridge like structure observed in high-multiplicity p-Pb collisions at $\sqrt{s_{NN}} = 5.02$ TeV has been investigated [12]. EPOS 3 takes into account hydrodynamically expanding bulk matter, jets and the jet-medium interaction. The basis of this model is multiple scatterings where each scattering finally produces flux tubes (strings). In the higher multiplicity event classes where the density of flux-tubes (strings) is higher, there is a finite probability that the strings will pick up quarks and antiquarks (or diquarks) from the bulk (core) for flux-tube breaking to produce jet hadrons (corona) instead of producing them via the usual Schwinger mechanism. This will eventually create a correlation between core and corona and also influence the corona-corona correlation because the corona particles containing quarks and antiquarks (or diquarks) from the bulk also carry the fluid information. The relative contributions of the core-core, core-corona, corona-core, and corona-corona correlations toward the ridge in high- and low-multiplicity p-Pb collisions at 5.02 TeV has been shown using the data generated by EPOS 3. The multiplicity evolution of the

ridges in all the cases has also been reported. It has been shown that the core triggered correlations play the dominant role in the higher multiplicity classes of p-Pb collisions however, in the lower multiplicity classes, the corona triggered correlations have dominant contribution towards the total ridge.

In this thesis, we have also discussed the mass ordering of v_2 as observed in p-Pb collisions at 5.02 TeV in the context of AMPT model [13]. The mass ordering of v_2^{hadron} is regarded as one of the key signatures of collective behaviour in ultra relativistic heavy ion collisions. This observation has been found to be in compliance with the hydrodynamical response of a strongly interacting system to the initial spatial anisotropy. Flow coefficients measured with identified particles in p-Pb/d-Au collisions have shown similar mass-splitting of v_2^{hadron} indicating towards the presence of collective dynamics in small collision systems. Arguably, small size in the overlap geometry of such colliding systems may not be suitable for hydrodynamical treatment that demands an early thermalization. Studies based on a multi phase transport model suggests that elliptic or triangular anisotropy is primarily due to escape mechanism of partons rather than hydro like collectivity and mass ordering of v_2^{hadron} can be generated from coalescence dynamics as implemented in string melting version of AMPT even when parton azimuthal directions are randomized. In this work, studies have been performed on p-Pb collisions at $\sqrt{s_{NN}} = 5.02$ TeV using AMPT model which has been found to explain the elliptic and triangular flow in such a system where escape mechanism is the dominant source of flow generation. We report that the mass splitting of v_2^{hadron} can originate independently both at the partonic and hadronic level in the string melting version of the AMPT model and not uniquely associated with the formation and corresponding hydrodynamical evolution of the partonic phase (QGP) in relativistic high energy collisions.

In short, this thesis work concentrates on the understanding of the collective like behaviours in small collision systems (pp and p-Pb) at LHC energies and also propose a way to probe the origin of those. Different model studies have been performed to study the experimentally observed collective signatures (e.g. ridge, flow (v_2), mass ordering of v_2) in small systems. Also,

the multiplicity evolution of the near-side jet-like yields (as obtained from different model based studies and data analysis) has been shown as a potential observable to probe the presence of soft physics in small collision systems. More studies on the data available for pp and p-Pb collision systems at different LHC energies will be essential to understand the origin of collective like effects and constrain different models aiming to explain those patterns.

Bibliography

- [1] Identified particle production in pp collisions at 7 and 13 TeV measured with ALICE.
(Rafael Derradi De Souza on behalf of the ALICE Collaboration, SQM2016)
<https://indico.cern.ch/event/403913/contributions/2142003/>
- [2] N. M. Abdelwahab et. al (STAR Collaboration) Phys. Lett. B 751 (2015) 233-240
- [3] S.S. Adler et. al (PHENIX Collaboration) Phys. Rev. C 71 (2005) 051902
- [4] E. Cuautle and G. Paic?, J. Phys. G 35, 075103 (2008).
- [5] P. Bozek, Eur. Phys. J. C 71, 1530 (2011).
- [6] I. Bautista, L. Cunqueiro, J. D. de Deus, and C. Pajares, J. Phys. G 37, 015103 (2010).
- [7] A. Ortiz et al., Phys. Rev. Lett. 111, 042001 (2013).
- [8] Debojit Sarkar, Subikash Choudhury, Subhasis Chattopadhyay; Physics Letters B 760 (2016) 763-768
- [9] Debojit Sarkar, Subikash Choudhury, Subhasis Chattopadhyay; Physics Letters B 760 (2016) 763-768
- [10] Debojit Sarkar, Subikash Choudhury, Subhasis Chattopadhyay; Phys. Rev. C 93, 054902 (2016)
- [11] K. Werner, Phys. Rev. Lett. 109, 102301 (2012).

- [12] Debojit Sarkar, Subhasis Chattopadhyay; Phys. Rev. C 95, 044906 (2017)
- [13] Debojit Sarkar, Subikash Choudhury, Subhasis Chattopadhyay; Phys. Rev. C 94, 044919 (2016)